

Histopathological and Ultrastructural Characterization of Equine Hoof Shape Deformities

By

Ramzi Al–Agele

BVSc, High Dip, MSc

Thesis submitted to the University of Nottingham for the degree of Doctor of Philosophy

Division of Comparative Medicine

School of Veterinary Medicine and Science

The University of Nottingham

January 2018

Abstract

Satisfactory investigations of the equine foot appear to be limited by the histo-morphological complexity of internal hoof structures. Foot lameness is considered to be one of the most debilitating pathological diseases in the horse. In most species, foot lameness is traditionally linked to hoof deformity, and a set of molecular events have been defined in relation to the disease. The differential capsular growth rate is essential in order to understand the aetiology of hoof distortions. It is now well established that keratinocyte progenitor cells grow from the papillae and not from the lamellae. The importance of hoof material synthesis, and therefore the underlying cell proliferation from the papillae, in the pathology of laminitis has been underlined in different species. Despite this knowledge, it remains unclear how cell proliferation itself is involved in this pathology. So far, there is controversy regarding the incidence of foot lameness in horses, as it is unclear whether it is foot lameness that triggers hoof distortions or *vice-versa*. In addition, very little scientific evidence exists to prove either point; this requires a deeper understanding of the physical biology and biomechanics of the hoof given that the horse stands on its hooves. It is remarkable that very little physics has been introduced to enhance our understanding of the disease. In order to develop a better understanding of foot lameness, we aim to provide a model of foot lameness encompassing anatomy, cell biology and physics to help reveal new evidence for evaluating the incidence of pathological changes within internal structures of the animal's foot. It is anticipated that the results found will aid in bridging this gap in knowledge.

Fifty-four equine hooves were collected and categorized based upon their morphology, and tissue sections were harvested from the periople, coronary and proximal part of lamellae. Markers of progenecity (p63), cell proliferation (PCNA, Ki-67) and differentiation (K14, K10) were used to assess the hoof growth rate in coronary regions using immunohistochemistry (PCNA, Ki-67, p63) and immunofluorescence (p63 and K14). For assessing the involvement of physical forces in hoof growth, the Micro CT-scans of individual foot were analysed to highlight differences in the ultrastructure of the feet, for example differences in dorsal curvature between different foot samples.

The results presented in this study confirm previous findings, add evidence that a high percentage of Ki-67 and p63 positive cells are found in the proximal part of the papillae, and seem to contribute to hoof deformities. This evidence might be attributed to physical growth forces present in the proximal part of the hoof whereby the change in cell size might contribute to force generation, tissue remodelling (i.e. cornification) and hoof deformities.

As hoof distortion can result from uncontrolled epidermal basal cell proliferation from the epidermal papillae. A model of cultured keratinocytes under different stresses such as stretch, hydrostatic pressure and/or low oxygen conditions. This revealed that these stresses together with low oxygen conditions stimulate cell differentiation, and upregulate keratin levels. Consequently, this leading to changes in their morphology and cell surface area. Together these results suggests that cell culture, growth, passage and physical or biological treatments have improved our knowledge of natural cell stimulation and aid our understanding of how equine progenitor keratinocytes (EPKs) would hypothetically respond to external stimuli other than biological ones.

The results presented regarding physical forces showed that there is a strong correlation between the dorsal hoof curvature and the level of Ki-67 and p63 abundance at the dermal papillae. In addition, K14 and TUNEL apoptotic cells localized along the dermal papillae in the coronary hoof region were also found in 'dished' hooves. Specifically, when the hoof curvature is positive (i.e. for the 'dished' hoof) there is an increase in the mitotic index shown by Ki-67 and p63 expression in the quarter regions compared to the dorsal one. Negative hoof curvatures (i.e. having a claw-like shape), however, did not shown any correlation with Ki-67 and p63 expression in any tissue type, except for K14 expression levels in the dorsal and quarter regions. These outcomes demonstrated that the two proteins (p63 and Ki-67) participate in hoof growth, and very probably to the differential growth of the hoof capsule as observed in chronic laminitis. This is probably through a contribution of sustained level of epidermal basal cell proliferation. In conclusion, the morphometric data of the change in cell size and the localisation of proliferation cells on the proximal part of papillae provide evidence on the way of hoof morphogenesis. These were confirmed with behaviour of cultured keratinocytes under different stresses. Additionally, the difference in the proliferation rates between the dorsal, quarter regions of the hoof wall are connected to hoof curvatures. The data gives new insights into the physical biology of the normal versus pathologically affected equine feet, and bovine and ovine feet in the future, providing new information for potential treatment(s). Consequently, this research aims to bridge gaps across scientific fields to ameliorate our understanding of the equine foot. However, further studies need to be carried out in order to understand the pathways of cellular response at the coronary region.

Declaration

I declare that the work in this dissertation was carried out in accordance with the regulations of the University of Nottingham.

The work is original and has not been submitted for any other degree at the University of Nottingham or elsewhere.

Name: Ramzi Al-Agele
Signature:
Date:

Conferences, Posters and Oral Presentations:

1. Ramzi Al-Agele, Emily Paul, Catrin Rutland and Cyril Rauch. An investigation of causes and outcomes of hoof growth rate and their relation to equine hoof conformation. 8th Meeting of Young Generation of Veterinary Anatomists (YGVA), Poznan, Poland 15th – 17th July 2015.

2. Ramzi Al-Agele. Physical biology of equine hoof growth. Early Careers Presentation Day; Oral Presentation, in Veterinary Medicine and Science; 15th of December 2015.

3. Ramzi Al-Agele, Catrin Rutland and Cyril Rauch. An evaluation of equine cultured keratinocyte differentiation under low oxygen and high oxygen conditions and related gene expression. Proceedings of the 31st Conference of the European Association of Veterinary Anatomists Vienna, Austria 27th -30th July 2016.

4. Working on a Physical Biology paper: Physics of nail conditions: why will horses always do better at the "pointe" technique than ballet dancers? Ramzi Al-Agele, Emily Paul, Tom Ryan, Craig Sturrock, John Burford, Michael Drakopoulos, Robert C. Atwood, Nghia T. Vo, Paula Williams, Catrin S. Rutland and, Cyril Rauch.

5. Working on a second paper of a Physical Biology paper: On the Growth and Form of Hooves. Ramzi Al-Agele, Emily Paul, Sophie Taylor, Charlotte Watson, Tom Ryan, Craig Sturrock, Michael Drakopoulos, Robert C. Atwood, Catrin S. Rutland, Nicola Menzies-Gow, Edd Knowles, Jonathan Elliot, Patricia Harris and, Cyril Rauch1*.

Acknowledgements

I am very grateful to my supervisors, Dr. Cyril Rauch and Dr. Catrin Rutland for their scientific supervision and unwavering support. I am also thankful their guidance through my PhD, their invaluable advice and comments for this thesis. I consider working with them both have been one of the extreme privileges of my professional scientific life.

I am also would like to express my genuine gratefulness to all staff members, who in various ways assisted me throughout my study. The technical staff in the dissection. Emily Paul for all her help with hoof collection and preparation, and for her hard working in analysis the data of CT scan images. Special thanks for the professional technician Aziza Alibhai for her help and support during the first year. Tom Ryan, the most motivating farrier there ever was and a practitioner with very long experience in the profession. Professor Pat Harris for the interesting in equine laminitis discussions, and Waltham Pet Nutrition. Special thanks to friends and colleagues, I have had very beautiful moments during my hard work of study and I give thanks for their help and support in and outside of work.

I wish to express my deepest thankfulness to my beloved mother, sisters and relatives and family in Iraq for their motivation and inspiration through my career. I also wish to express genuine love and thankfulness to my wife Ansam, sons Yousif, Ghafor and Ahmmed for their longanimity and help throughout my PhD. Finally, I am genuinely grateful to the Iraqi culture attaché in London for their support overseas and particularly to the Iraqi government's Ministry of Higher Education and Scientific Research for providing me with an Overseas Scholarship.

List of Abbreviations

Akt	A serine-threonine-protein kinase
BM	Basement membrane
bp	Base pair
BSA	Bovine serum albumin
˚C	Degree Celsius
CT	Computed tomography
cDNA	Complementary deoxyribonucleic Acid
DAB	3,3́-Diaminobenzidine
DAPI	4’,6–Diamidino–2–phenylindole
DMEM	Dulbecco’s Modified Eagle’s Medium
DMSO	Dimethyl sulfoxide
DNA	Deoxyribonucleic acid
DPX	Distyrene, plasticizer, xylene
dNTPs	Deoxynucleotide phosphates
EDTA	Ethylenediaminetetraacetic acid
FI	Florescent intensity
FCS	Fetal calf serum
EPKs	Equine progenitor keratinocytes
GAPDH	Glyceraldehyde 3-phosphate dehydrogenase
g	Gram
H&E	Hematoxylin and eosin
HCl	Hydrochloric acid
HEPES	4-(2-hydroxyethyl)-1-piperazineethanesulfonic acid
HIF-1ά	Hypoxic-inducible factor -1alpha
HP	Hydrostatic pressure
HRP	Horseradish peroxidase
hr	Hour(s)
IF	Intermediate filaments
K	Keratin (s)
kDa	Kilodaltons
kV	Kilovolts
L	Litre

min	Minute(s)
ml	Millilitre
mm	Millimetre
mm^2	Square millimetre
mM	Millimolar
mRNA	Messenger Ribonucleic acid
ng	Nanogram
P	Passage (s)
Pa	Pascal
PBS	Phosphate Buffer Saline
PCR	Polymerase Chain Reaction
PCNA	Proliferating cell nuclear antigen
pH	Potential of hydrogen
PI3K	Phosphoinositide 3-kinase
PVDF	Polyvinylidene Fluoride
RNA	Ribonucleic acid
RNase	Ribonuclease
RT–PCR	Reverse transcriptase Polymerase Chain Reaction
sec	Second(s)
SDS	Sodium dodecyl sulfate
TAE	Tris–acetate–EDTA
TBS	Tris Buffered Saline
TEMED	N,N,N´,N´-tetramethylethane-1,2-diamine
TBST	Tris-buffered saline tween-20
U	Unit(s)
W	Watt
w/v	Weight per volume
µg	Microgram
µM	Micromolar
µl	Microlitre
µm	Micrometre
$µm^2$	Square micrometre

List of Contents

1 Introduction 2

1.1 Foot lameness 2

1.1.1 Foot lameness in ungulate (farm animals) 2

1.2 Hoof anatomy 10

1.2.1 Foot vasculature 11

1.2.1.1 Arterial supply 11

1.2.1.2 Venous supply 14

1.3 Hoof growth and distortion 15

1.3.1 Microstructure of the hoof wall 19

1.3.1.1 The lamellae 20

1.3.2 Hoof keratin 23

1.4 Interactions between the hoof capsule and the distal phalanx 26

1.5 Pathological changes of the hoof suspensory apparatus 27

1.6 Capsular shape and morphological changes in the laminar junction 30

1.7 Laminitis 32

1.7.1 Lamellar wedge 37

1.8 Elements of physics in relation to the equine foot 38

1.9 The link between hoof morphology and residual stresses 40

1.10 Modelling the set of forces in a growing hoof 42

1.10.1 The Growth force 42

1.10.2 The Adhesion force 43

1.10.3 Gravity 46

1.11 Hypothesis 47

1.12 Aims 47

1.13 Objectives 48

1.13.1 Research plan 49

2 Chapter 2 52

2.1 Materials and methods 53

2.2 Collection of hoof samples 53

2.3 Sample processing for histology 55

2.3.1 Tissue sectioning 55

2.3.2 Haematoxylin and Eosin (H&E) staining 55

2.3.3 PAS stain 56

2.3.4 Masson's trichrome stain 57

2.4 Immunohistochemistry 58

2.4.1 Spatial localisation of PCNA 58

2.4.2 Spatial localisation of Ki-67 59

2.4.3 Spatial localisation of p63 61

2.5 Statistical analysis 62

2.5.1 H&E 62

2.5.2 Measuring hoof wall thickness and comparison with H&E data 63

2.5.3 Change in cell size 67

2.6 PAS 69

2.7 Counting cells of proliferation PCNA, Ki-67 & stem p63 69

2.8 Immunofluorescence for coronary hoof sections 70

2.9 Apoptosis 72

2.10 Isolation of epidermal cells from equine hoof at coronary papillae 74

2.11 Immunofluorescence on culture keratinocytes 77

2.12 Osteogenesis differentiation 80

2.13 The role of insulin in culture keratinocytes 82

2.14 Mechanical cell stretching 83

2.14.1 Estimation of strain application at the centre of the 'flexcell' culture 85

2.15 Hydrostatic pressure 87

2.16 Culturing EPKs under low oxygen conditions 89

2.17 RNA extraction and quantification 89

2.17.1 RNA extraction 89

2.17.2 Reverse transcription and first strand synthesis of RNA samples 91

2.17.3 PCR 92

2.17.4 Agarose gel electrophoresis 93

2.17.5 Quantification of target gene mRNA levels 94

2.18 Proteins extraction, quantification, and Western blotting 96

2.18.1 Proteins extraction 96

2.18.2 Protein Quantification 97

2.18.3 Polyacrylamide gel preparation for protein electrophoresis 98

2.18.4 Protein transfer 100

2.18.5 Western blot 101

2.18.6 ECL detection 102

2.18.7 Image acquisition with imager 102

2.19 Measuring hoof angle 103

3 Chapter 3 107

3.1 Introduction 108

3.2 Hypothesis 112

3.3 Aims and objectives 113

3.4 Results 114

3.4.1 Analysis hoof shape 114

3.4.2 Haematoxylin and Eosin (H&E) staining 115

3.4.2.1 Changes in cell size of tubular and intertubular horn 122

3.4.2.2 Epithelial thickness of coronary region 128

3.4.3 PAS 132

3.4.4 Masson's trichrome stain 134

3.4.5 Immunohistochemistry 137

3.4.5.1 Assessment p63 +ve cells along the dermal papillae 137

3.4.5.2 Assessment Ki-67 +ve cells along the dermal papillae 140

3.4.5.3 Assessment apoptotic TUNEL positive cells along the papillae. 142

3.5 Discussion 144

3.5.1 Conclusions 152

4 Chapter 4 153

4.1 Introduction 154

4.2 Hypothesis 162

4.3 Aim and objectives 162

4.4 Results 164

4.4.1 Phenotypic characterisation of cultured progenitor keratinocytes 164

4.4.2 Immunostaining of cultured EPKs spheres 169

4.4.3 The role of blebbistatin on the spreading of EPKs 170

4.4.4 Assessment of the influence of blebbistatin on cytoskeletal EPKs 171

4.4.5 Expression and localization of inhibition myosin isoforms in EPKs 173

4.4.6 Assessment of EPKs pluripotency during cell passages 175

4.4.7 Osteogenesis of EPKs 179

4.4.8 The influence of hydrostatic pressure on EPKs 181

4.4.9 Stretch cultured EPKs 187

4.4.9.1 Stretch of EPKs after incubation for 24hrs with blebbistatin ...187

4.4.9.2 Stretch of EPKs incubated with blebbistatin 192

4.4.9.3 Stretch of EPKs without blebbistatin 196

4.4.10 Stretch of EPKs after 10 days of culture 198

4.4.11 EKPs assessment under different oxygen levels 203

4.4.11.1 Assessment the level of gene expression under 5% O_2 209

4.4.12 Assessment the impact of insulin on culture EPKs 212

4.4.12.1 Assessment the PI3k/Akt pathway in cultured keratinocytes treated with Insulin 215

4.5 Discussion 216

4.5.1 Conclusions 224

5 Chapter 5 226

5.1 Introduction 227

5.1.1 Hoof growth 227

5.1.1.1 Growth rate of hoof wall 227

5.2 Hypothesis 232

5.3 Aim and objectives 233

5.4 Results 234

5.4.1 Evaluation of staining patterns of PCNA proliferating cells 234

5.4.2 Assessment of the expression of Ki-67 proliferation antibody 237

5.4.3 Assessment the localization of stem progenitor keratinocytes p63 242

5.4.4 Variation between the percentage of p63 and Ki-67 +ve cells 248

5.4.5 Expression of K14 and p63 in epithelial coronary papillae 249

5.4.6 Assessment of apoptosis at the dermal coronary region 253

5.4.7 The influence of the degree of hoof curvature on epithelium thickness 255

5.5 Discussion 257

5.5.1 Conclusion 260

6 Chapter 6 261

6.1 General discussion 262

6.2 Summary of integrated key findings 275

6.2.1 Conclusion and future work 279

6.2.2 Future work 280

7 References 281

8 Appendices 314

8.1 An example of equine feet images 314

8.2 Experimental design 316

8.3 Collagenase digest 317

8.4 The efficiency of the primers 318

8.5 Relation between hydrostatic pressure and oxygen concentration 320

8.6 Specificity of antibody 325

List of Figures

Figure 1-1: Schematic drawing showing transferring limb foot lameness 6
Figure 1-2: Schematic drawing illustrating an arched or misshapen coronary band 7
Figure 1-3: Schematic showing (A) normal radiological spaces in comparison with abnormal ones (B+C) 9
Figure 1-4: Schematic drawing of a sagittal section of equine hoof 11
Figure 1-5: Diagram of micro CT image illustration vascularisation of equine foot 12
Figure 1-6: Schematic drawing showing the dermal papillae and their layers 16
Figure 1-7: Sagittal section of equine foot showing coronary dermal papillae 17
Figure 1-8: Schematic drawing showing dorsolateral view of the equine hoof capsule 20
Figure 1-9: Photomicrographs show normal lamellae 21
Figure 1-10: Schematic showing application of forces linked to weight bearing 22
Figure 1-11: Schematic diagram of the cornifying keratinocytes 25
Figure 1-12: Schematic illustrates the regulatory functions of keratins 26
Figure 1-13: Photographs illustrating the suspensory apparatus of distal phalanx 28
Figure 1-14: Schematic drawing illustrate hoof capsule in different chronic conditions 29
Figure 1-15: Schematic drawing illustrating the connection between the distal phalanx 30
Figure 1-16: The different developmental stages of laminitis 33
Figure 1-17: The anatomical displacement (indicated by *) of the distal phalanx 38
Figure 1-18: Schematic drawing illustrating the stresses applied on the hoof wall 41
Figure 1-19: Schematic drawing illustrating the main proliferation sites 43
Figure 1-20: Dissection of a hoof capsule 44
Figure 1-21: Photos showing variations in growth forces in the equine hoof 45
Figure 1-22: Equine hoof photographs show large and small angles 46
Figure 2-1: Schematic illustrating the epithelial thickness calculation 63
Figure 2-2: The process for hoof wall thickness calculation by CT scan 65
Figure 2-3: Schematic showing the link between hoof wall and coronary thickness 66
Figure 2-4: Determination of cell size calculation along the dermal papillae 68
Figure 2-5: Schematic illustrating the isolation of progenitor keratinocytes 76
Figure 2-6: Schematic showing measurement fluorescence intensity of EPKs 80
Figure 2-7: Schematic showing culturing cells in mechanically active environment 84
Figure 2-8: Schematic showing calculation of stretch loading on cultured EPKs 86
Figure 2-9: Schematic illustrating hydrostatic pressure applied on culturing cells 88
Figure 2-10: An example on optimisation the concentration of K14 protein loading 99
Figure 2-11: The process for hoof angle calculation 103
Figure 2-12: Schematic illustrating the process hoof curvature calculation 105
Figure 3-1: Equine foot show a distinct curvature in the dorsal hoof wall 114
Figure 3-2: H&E stained coronary hoof tissue 116
Figure 3-3: Graph and photomicrograph stitched showing the number of papillae 117

Figure 3-4: Photomicrograph stitched images and graph show dermal papillae diameter . 119
Figure 3-5: H&E stained photomicrographs illustrate intertubular epidermal layers 121
Figure 3-6: Photomicrographs represent appearance different papillae..... 122
Figure 3-7: The cell size changes in the interpapillary epidermal cells..... 125
Figure 3-8: The cell size changes lining dermal papillae..... 127
Figure 3-9: Epithelial coronary thickness 129
Figure 3-10: Schematic diagram showing wall and coronary tissue thickness 131
Figure 3-11: Photomicrograph of PAS stained hoof tissue. 132
Figure 3-12: PAS stained photomicrograph of dermal papillae..... 133
Figure 3-13: PAS stained photomicrograph and graph showing BM thickness. 133
Figure 3-14: Masson's Trichrome stained photomicrographs at dermal papillae..... 135
Figure 3-15: Photomicroscope images illustrating the collagen bundles at dermal tissues.. 136
Figure 3-16: The frequency of p63 +ve cells plotted against papillae length..... 139
Figure 3-17: The Ki-67 +ve cells plotted against papillae length..... 141
Figure 3-18: The TUNEL +ve cells plotted against papillae length..... 143
Figure 4-1: Schematic diagram illustrating the stages of epidermal skin epithelization..... 157
Figure 4-2 : Schematic diagram illustrates cells response for biomechanical stimuli 160
Figure 4-3: Schematic diagram showing the area of interest for isolation EPKs..... 164
Figure 4-4: Sphere development in equine progenitor keratinocytes (EPKs)..... 166
Figure 4-5: Growing and expansion of equine progenitor keratinocytes (EPKs) 167
Figure 4-6: Epidermosphere showing the source of EPKs increase growth..... 168
Figure 4-7: Epidermosphere identification with immunofluorescence staining 169
Figure 4-8: Cytoskeletal organization of the contractile system in EPKs treated with bleb. 171
Figure 4-9: Cell marker expression in EPKs in control and treated with bleb. 172
Figure 4-10: Graphs showing statistical analysis of EPKs treated or not with bleb. 173
Figure 4-11: Structural organization of the microfilaments in cells treated with bleb..... 174
Figure 4-12: CD44 and K14 expression in EPKs during cell passages 175
Figure 4-13: Ki-67 and K14 expression in EPKs during cell passages..... 176
Figure 4-14: Quantification of CD44, K14 and Ki-67 after EPKs passages 177
Figure 4-15: Immunofluorescence staining of F-Actin in EPKs during cell passages 178
Figure 4-16: Photos and photomicrographs show osteogenesis of EPKs..... 180
Figure 4-17: The impact of HP on Ki-67 and K14 expression levels..... 183
Figure 4-18: Immunofluorescence showing HP effect on actin filaments..... 184
Figure 4-19: Quantification the impact of HP on the expression of Ki-67, K14 185
Figure 4-20: The impact of HP on K14 and K10 expression levels 186
Figure 4-21: The impact of stretch force after incubated 24hrs with blebbistatin 188
Figure 4-22: Quantification the expression of K14 and K10 under mechanical stretch 189
Figure 4-23: The impact of stretch force on the Ki-67/K14, after being treated 24h with bleb. 191
Figure 4-24: Quantification of the impact of stretch force on CD44 protein expression..... 192

Figure 4-25: The impact of stretch force on Ki-67 and K14 expression levels 193
Figure 4-26: Quantification of Ki-67, K14 and K10 expression under stretch force 194
Figure 4-27: The impact of stretch force on F-actin in EPKs incubated with blebbistatin.. 195
Figure 4-28: The impact of stretch force in the absence of blebbistatin 196
Figure 4-29: Quantification of Ki-67 and K14 expression under mechanical stretch 197
Figure 4-30: The impact of stretch force on Ki-67 and K14 after 10 days culture 198
Figure 4-31: The impact of stretch force on K10 and K14 after 10 days culture..... 199
Figure 4-32: The impact of stretch force on F-Actin filaments after 10 days culture 199
Figure 4-33: Quantification of Ki-67, K14 and K10 under stretch, after 10 days culture ... 201
Figure 4-34: Quantification of K14 and CD44 protein under stretch after 10 days culture 202
Figure 4-35: The impact of low oxygen levels on HIF-1α and K10 expression 203
Figure 4-36: The impact of low oxygen levels on HIF-1α and Ki-67 expression..... 204
Figure 4-37: The impact of low oxygen levels on K14 and Ki-67 expression 204
Figure 4-38: The impact of low oxygen levels on K14 and K10 expression 205
Figure 4-39: The impact of low oxygen levels on CD44 and K14 expression 205
Figure 4-40: Quantification of HIF-1α, Ki-67, K10/K14 expression levels under low O_2 207
Figure 4-41: Quantification CD44 expression under 1% O_2 208
Figure 4-42: Quantification K14 protein expression under 1% and 5% O_2 209
Figure 4-43: PCR products of amplification K14 gene from EPKs 210
Figure 4-44: Quantification of gene expression levels under 5% O_2 conditions..... 211
Figure 4-45: The impact of Insulin on Ki-67 and K14 expression levels 213
Figure 4-46: The impact of different insulin doses on the expression of Ki-67 and K14..... 214
Figure 4-47: Quantification Akt protein pathway when treated with 1µg/ml insulin 215
Figure 5-1: Schematic diagram illustrating the physical stimulus on the coronary region . 231
Figure 5-2: Photomicrographs of PCNA stained sections..... 235
Figure 5-3: Localisation of PCNA +ve cells in coronary epidermis of equine foot 236
Figure 5-4: The percentage of PCNA in relation to hoof angle 237
Figure 5-5: Localisation of Ki-67 +ve cells in the epithelium of coronary papillae and skin 238
Figure 5-6: The correlation between expression of Ki-67 and hoof angle 239
Figure 5-7: Correlation between the expression of Ki-67 and hoof curvature..... 240
Figure 5-8: Percentage of Ki-67 +ve cells plotted against hoof curvature 241
Figure 5-9: Percentage of Ki-67 +ve cells plotted against distal phalanx curvature..... 242
Figure 5-10: Expression of p63 in the epithelium of coronary papillae 243
Figure 5-11: The correlation between expression of p63 and hoof angle..... 243
Figure 5-12: Correlation between the expression of p63 and hoof curvature 245
Figure 5-13: Percentage of p63 +ve cells plotted against hoof curvature 246
Figure 5-14: Percentage of p63 +ve cells plotted against hoof curvature at heel region 247
Figure 5-15: Percentage of p63 +ve cells plotted against distal phalanx curvature 247
Figure 5-16: Difference between Ki-67 and p63 antibodies 248
Figure 5-17: Expression of p63 and K14 in equine hoof papillae. 249

Figure 5-18: Expression of epithelial cell marker K14 in equine hoof papillae 250
Figure 5-19: Correlation between K14 expression and hoof curvature..... 251
Figure 5-20: The ratio of K14 expression to Ki-67 +ve cells against hoof curvature..... 252
Figure 5-21: The ratio of K14 expression to p63 +ve cells plotted against hoof curvature .. 252
Figure 5-22: Apoptotic TUNEL positive cells 253
Figure 5-23: Percentage of TUNEL +ve cells plotted against hoof curvature..... 254
Figure 5-24: The ratio of Ki-67 or p63 to TUNEL +ve cells plotted against hoof curvature 255
Figure 5-25: The ratio of epithelial thickness plotted against hoof curvature 256
Figure 6-1: Schematic drawing shows the hoof growth and distortion..... 278
Figure 8-1: Photographs of equine feet..... 315
Figure 8-2: Standard cure calculation of equine keratinocytes genes copy number 319
Figure 8-3: Schematic diagram showing the calculation of oxygen concentration 325

List of Tables

Table 1-1: Foot lameness scoring..... 6
Table 2-1: The source of hoof collection 53
Table 2-2: Primary antibodies used in immunofluorescence protocol..... 78
Table 2-3: Second primary antibodies were used in immunofluorescence protocol 78
Table 2-4: Elastic modulus (Y) of living cells in culture conditions measured using atomic force microscopy (AFM). 85
Table 2-5: Table showing the calculation of hydrostatic pressure loading on cultured equine hoof keratinocytes..... 88
Table 2-6: Primers used for qPCR amplification of the ten segments equine keratinocytes gene, whereas GAPDH and β-Actin are housekeeping genes 92
Table 2-7: Table showing the final concentration of constituents used in PCR reaction 93
Table 2-8: The volume and final concentrations used in running qPCR protocol ... 95
Table 2-9: Primary antibodies used for Western blot 101
Table 2-10: Secondary antibodies used for Western blot..... 101
Table 3-1: Characteristics of data analysis for cell volumes at a distance from basement membrane (n=3)..... 124
Table 5-1: Ki-67 and p63 proliferation technique 248

Chapter 1

Introduction

1 Introduction

1.1 Foot lameness

1.1.1 Foot lameness in ungulate (farm animals)

Foot lameness is a physical impairment of a limb that has a negative effect on the freedom of movement of the animal (Archer et al., 2010, Whitton, 2016). It is accompanied by clinical signs linked to a disturbance of locomotion that is related to hoof pathologies that can be caused by infection, environmental and/or genetic causes (O'Callaghan, 2002, Weishaupt, 2008). Foot lameness can also manifest in pain and foot lesions that, in turn, lead to an abnormal gait (Green et al., 2002, Bicalho and Oikonomou, 2013) with undesirable consequences on performance (Mülling et al., 2006) and welfare (Broster et al., 2009). This disruption in gait originates from involuntary and voluntary exertions to diminish the level of discomfort and/or pain that are the result of damage or injury of ligaments, muscles, nerves or integument (O'Callaghan, 2002, Whitton, 2016), or could be due to asymmetric and/or uneven feet promoting the development of foot lameness (Wiggers et al., 2015).

Virtually all ungulate animals can be affected by foot lameness (Murray et al. 1996, Winter, 2008, Ross and Dyson, 2010, Christodoulopoulos, 2009). However, our knowledge concerning the aetiology of the condition is often related to the economic implications of the animal in our society (Archer et al., 2010, Bicalho and Oikonomou, 2013). For this reason, a brief introduction has highlighted the foot lameness in cattle and sheep as an example to the economical and societal importance of foot lameness. Foot lameness is classified into acute and chronic types depending on the severity of lesions and the time requirement for healing, if

healing is possible (Vermunt, 1992). Several different types of lesions can cause foot lameness. For example, the majority of foot lameness in cattle is triggered by any one of four different diseases of the foot which are, by order of clinical importance: sole haemorrhage/sole ulceration; white line disease; digital dermatitis; and interdigital necrobacillosis (Hedges et al., 2001, Chesterton et al., 2008, Archer et al., 2010). Amory et al. (2008) determined that together, sole ulcer/sole ulceration and white line diseases account for 58% of lesions, and digital dermatitis, and interdigital necrobacillosis for 8% of lesions. These lesions often concern the rear feet (Lethbridge, 2009) and present the most important financial and welfare problems faced by the dairy industry (O'Callaghan, 2002), as they are responsible for a drop in reproductive efficacy, a decrease in milk production, and increased culling rates (Murray et al. 1996, Bicalho and Oikonomou, 2013). Some authors such as Clarkson et al. (1996) estimated that the UK prevalence of foot lameness ranged from 38-55 cases for every 100 cows per year. These relatively high figures were also found by others, including Hedges et al. (2001) with an incidence rate of 68% and Lethbridge (2009) with an incidence rate of 35%. Attention has also been drawn to the significance of foot lameness in sheep and goats from both welfare and economic standings as most of these foot lameness cases involve similar lesions as those caused by footrot (Clifton and Green, 2016), interdigital dermatitis and contagious ovine digital dermatitis (Winter, 2008). These lesions, for example footrot and interdigital dermatitis represent most common causes of foot lameness in sheep in the UK, causing about 80% of foot lameness (Kaler and Green, 2008). Economically, in the United Kingdom, Nieuwhof and Bishop (2005) estimated that the financial cost of foot lameness in the sheep industry is about £24m annually. British dairy goats have

extra complications, which include causing hoof separation, increase in growth rate of claws, sole abscess and footrot (Hill et al., 1997) as well as cracks and erosions on the bulbs of the heel that expand beside the internal hoof wall (Christodoulopoulos, 2009). Although male goats are more affected (85%) than females (67.3%), the hind limbs seem to be the focus of foot lameness in goats (62.4% of foot lameness cases) as is observed in cattle (Nonga et al., 2009).

Similarly, in horses, foot lameness is a significant and predominant medical disorder which accounts for about to $1 billion in losses annually for the equine industry in the United States of America (Seitzinger et al., 2000, Moorman et al., 2013). In the UK, the maintenance of each horse is estimated to cost about £2660 annually and much of this in the treatment of foot lameness (Uprichard et al., 2014). Foot lameness in the horse is the most prevalent and frequent medical issue, affecting about 11% of the general equine population in the UK (Cross, 2011), and this percent increased significantly in 2012 to 18.6% (Ireland et al., 2012) due to for instance ,foot balance, shoeing and triming. Some subpopulations however, seem to be more affected than others as for example it is estimated that nearly 33% of dressage horses in the UK suffer from foot lameness (Murray et al., 2010). The clinical diagnosis of foot lameness in the equine population is subdivided into scores ranging from 0 to 5 depending on the degree of the condition (Table 1-1), with 5 being the worst outcome (Wagner, 2010).

Lame horses adapt their gait to compensate for the pain originating from damaged tissues or foot lesions (Uhlir et al., 1997, Weishaupt et al., 2004, Whitton, 2016). Accordingly, foot lameness is considered to be one of the most common signs of kinetic disorder affecting the musculoskeletal system (Whitton, 2016). Thus, horses attempt to manage foot lameness by numerous mechanisms, all directed at

unloading the affected limb (Alvarez, 2007). The methods of compensatory forces for loading limbs have been explained by Weishaupt et al. (2004), who demonstrated that lame horses exhibited a decrease in the overall vertical impulse per stride, a lessening of the impulse in the lame diagonal posture level, and a reduction of the loading rate by the rise of the stance period, all of these helping to diminish the pressure on the foot (Maliye and Marshall, 2016). The most symmetric compensatory actions are detected in the vertical displacement and quickening of the head in front limbs foot lameness (Keegan et al., 2001). As forelimb foot lameness is more common than hind limb foot lameness (Keegan et al., 2010), it has been suggested that conformations of the distal limbs may have a substantial impact in the development of front and rear limbs foot lameness (Wiggers et al., 2015). The relatively high prevalence of forelimb foot lameness (Keegan et al., 2010) which reaches to more than 75% of equine foot lameness being found in a forelimb particularly in Thoroughbred horses and 40% in Standardbred racehorses (Malikides et al., 2007). This may be explained by that fact that the centre of gravity of the horse is closer to the front limbs than the rear limbs, as the loading ratio is spread approximately 60% forelimbs: 40% hind limbs (Ross and Dyson, 2010). Uhlir et al. (1997) showed that horses with severe foot lameness in the front limb display an untrue foot lameness in the contralateral rear limb, whereas horses with a real rear limb foot lameness exhibit an incorrect foot lameness in the ipsilateral front limb. This indicates that the site of the lame limb may be assumed from the spreading of two foot lameness on a diagonal axis (Figure 1-1). In addition, Landman et al. (2004) defined the severity of foot lameness grades between 0 and 5 as described in Table 1-1.

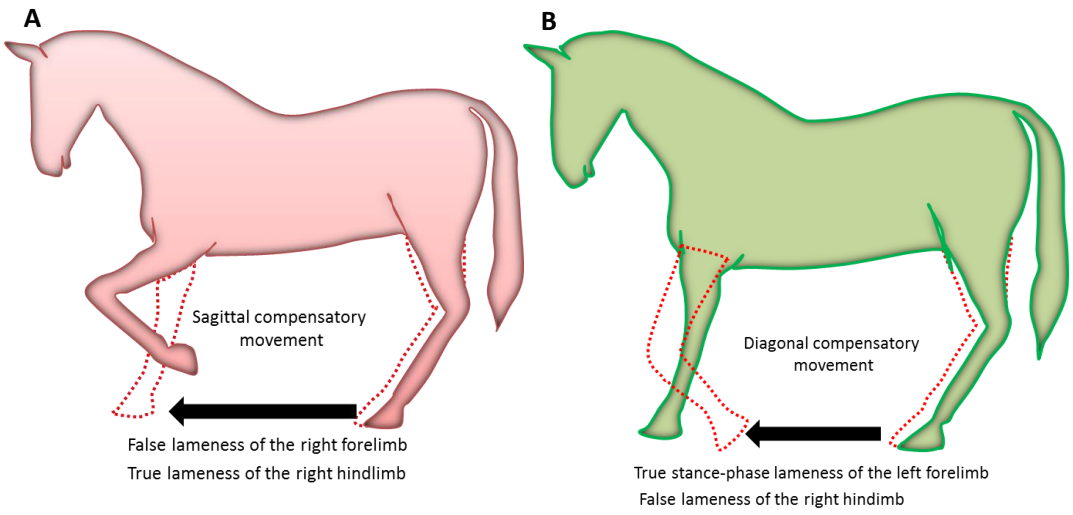


Figure 1-1: Schematic drawing showing transferring limb foot lameness

This illustrates A) lame horse transfer from true rear limb lameness (dashed red line), B) lame horse movement from true front limb lameness. Figure modified from (Uhlir et al., 1997).

Table 1-1: Foot lameness scoring

This is adapted from the American Association of Equine Practitioners (Landman et al., 2004)

Score	Description of lameness severity	Additional explanation
0	Foot lameness is not tangible at any conditions	–
1	Clinical signs of foot lameness are difficult to observe	Not consistently apparent during circling and weight carrying
2	It is difficult to observe lame horses during a walk or trot in a straight line	Consistently apparent at some conditions, for example weight carrying, circling inclines
3	Observing lame horses during a trot and under all circumstances	Consistently observable
4	Clinical signs of foot lameness are obvious	Marked nodding, hitching or shortened stride
5	There is minimal weight bearing in motion or during rest	Inability to walk or move

Although the aetiology of equine foot lameness is still an active research area, recent efforts have also tried to determine whether the hoof shape is a disposing factor for foot lameness-causing lesions. The investigation of variations between foot lameness and non-foot lameness affected horses by Dyson et al. (2011b), demonstrated that the angle between the capsular wall and the ground is larger in the lame horse with an enlarged heel, curved or misshapen coronary band (Figure 1-2) diverging growth lines can occur, and that the tubular horns differ from non-lame horses. It was suggested that hereditary influences and trimming are factors contributing to the asymmetrical shape of the hoof (French and Pollitt, 2004a, Kummer et al., 2006).

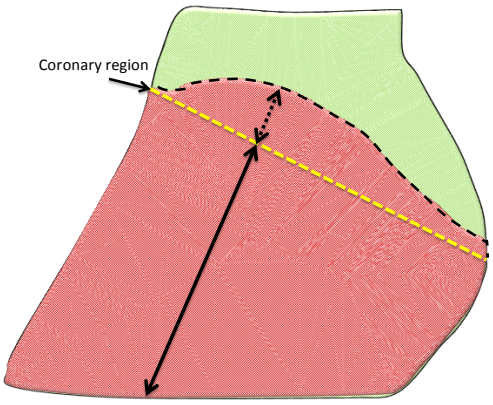


Figure 1-2: Schematic drawing illustrating an arched or misshapen coronary band

This figure shows a concave line occurs clearly on the coronary band (shown in yellow). Figure adapted from (Dyson et al., 2011b).

In chronic foot lameness, the hoof capsule of the lame foot can be more distorted than in the non-lame one (Holroyd et al., 2013a), as a result of altered loading forces applied to the hoof, hence affecting the shape of the hoof and the internal structures of the foot (Ryan, 2013, Drumond et al., 2016). These variations in the shape of the capsule are triggered by biological sources causing autolysis of the collagen fibres connecting the epithelium to the bone (Ross and Dyson, 2010).

The role of these fibres is to support and suspend the weight of the horse via the distal phalanx, as well as to maintain the shape of the capsule constant (Mungall and Pollitt, 1999, Pollitt, 2016). Another cause that could lead to hoof distortion is the ability of the foot to produce keratinous material proximally (Daradka and Pollitt, 2004). A subtle change in the structural and functional components of the hoof wall which is produced by an alteration of the microvascular system in the corium could change the amount of keratinous tissue (Mülling and Greenough, 2006). A number of chronic foot lameness states can be related to sheared heels causing palmar foot pain and hoof deviation (Whitton, 2016). Sheared heels are considered as one of the main causes of foot lameness in the equine species, which results from an abnormal stride and persistent uneven weight bearing (O'Grady and Castelijns, 2011). This leads to higher soft tissue strains that predispose the hoof capsule to deformation (O'Grady, 2012).

To date, very little information exists on how distortion of the hoof capsule affects the biomechanical performance of the foot and how such an effect translates into the correlation between conformation and foot lameness. Most studies have focused on the diagnostic method and treatment of specific foot lameness conditions. Conversely, few of them are based on a prospective analysis for evaluating the risk factors which could lead to foot lameness problems. Ross and Dyson (2010) found that the foot conformation can relate to the score of foot lameness through walking or foot stride measurements, and it has also been suggested that the conformation of the equine foot can be a predisposing factor for foot lameness (Holroyd et al., 2013a), although evidences that proves this is limited (Parks, 2003, Holroyd et al., 2013a). The hoof conformation seems to be a two way process whereby the hoof shape is a key factor in foot lameness (Holroyd

et al., 2013b, Whitton, 2016) and foot deformation can arise as a consequence of foot lameness (Holroyd et al., 2013a). However, and as mentioned above, there has been little evidence showing that malformation is one of the predisposing factors for foot soreness and foot lameness. Dyson et al. (2011a) drew attention to the fact that, despite the differences in the shape of the distal phalanx between horses is mainly associated with changes in the direction of the dorsal hoof wall (Figure 1-3). For example, constant shoeing has an impact on the way in which the hoof grows and can, over time; result in a different foot conformation/capsular shape, which can have an effect on foot lameness (Van Heel et al., 2006, Baxter, 2011).

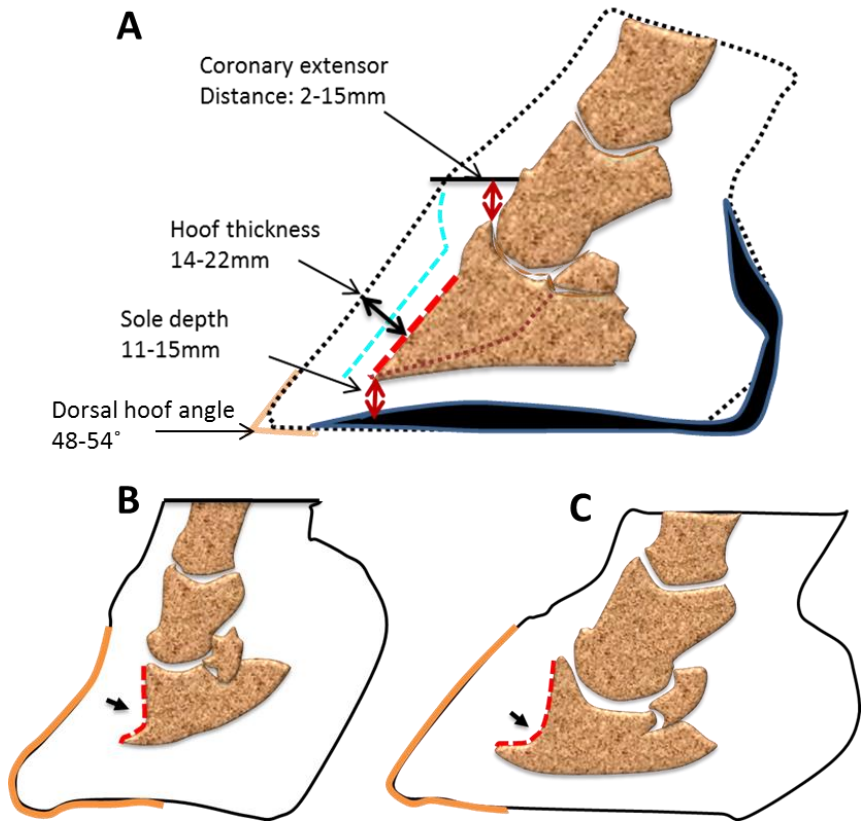


Figure 1-3: Schematic showing (A) normal radiological spaces in comparison with abnormal ones (B+C)

A) Shows the normal ratios between the parietal surface of the distal phalanx and the inner surface of the hoof wall in the front feet of horses. In radiographic images (B+C), black arrows show where the clear divergence occurs on the dorsal surface (red line) of the distal phalanx, these are consequently affected on the angle of solar margin and is also markedly increased and changing the hoof capsule. Figure adapted from (Sherlock and Parks, 2013).

According to Johnston and Back (2006) the conformation of the hoof wall has a direct relationship with the loading of the lower limb, protecting its optimal balance. Therefore, the geometrical tendency of the foot components determines the capacity of internal structures to sustain a loading balance through the weight-bearing phase of the stride cycle (Thomason, 1998, Thomason et al., 2002). In fact, it seems that the symmetrical orientation of the hoof segments determines the loading of internal structures throughout the weight bearing of the stride cycle (Sherlock and Parks, 2013). Thus, the hoof conformation of a particular foot is associated with the unbalanced cyclical loading, and sustaining an adequate balance of stresses can prevent internal tissue damage of the foot's constituents to reduce the occurrence of foot lameness (Johnston and Back, 2006).

So far, there has been very little published research help to improve our scientific knowledge regarding hoof distortion. This knowledge could be important in understanding the connection between mechanical imperfections and tissue responses or vice versa, leading ultimately to improved early diagnosis and treatments of foot lameness.

1.2 Hoof anatomy

Understanding the basic anatomy of the horse hoof is essential in order to further investigate the structures involved. The distal extremities of the domestic mammal are encased inside a keratinised capsule (Bragulla et al., 2007), which composes the hoof capsule of ungulates and the claw of carnivores (Konig et al., 2007). This insensitive horny structure encloses the distal part of the second phalanx, the distal phalanx and the navicular bone, in addition to connective tissues including,

for example, the distal interphalangeal joint, medial and lateral hoof cartilage, with the terminal end of the deep digital flexor tendon and navicular bursa (Bragulla et al., 2007, Budras and Sack, 2012, Stewart, 2013, Pollitt, 2010). These structures are connected to each other in order to provide a coherent and resilient structure within the foot (Davies et al., 2007) (Figure 1-4).

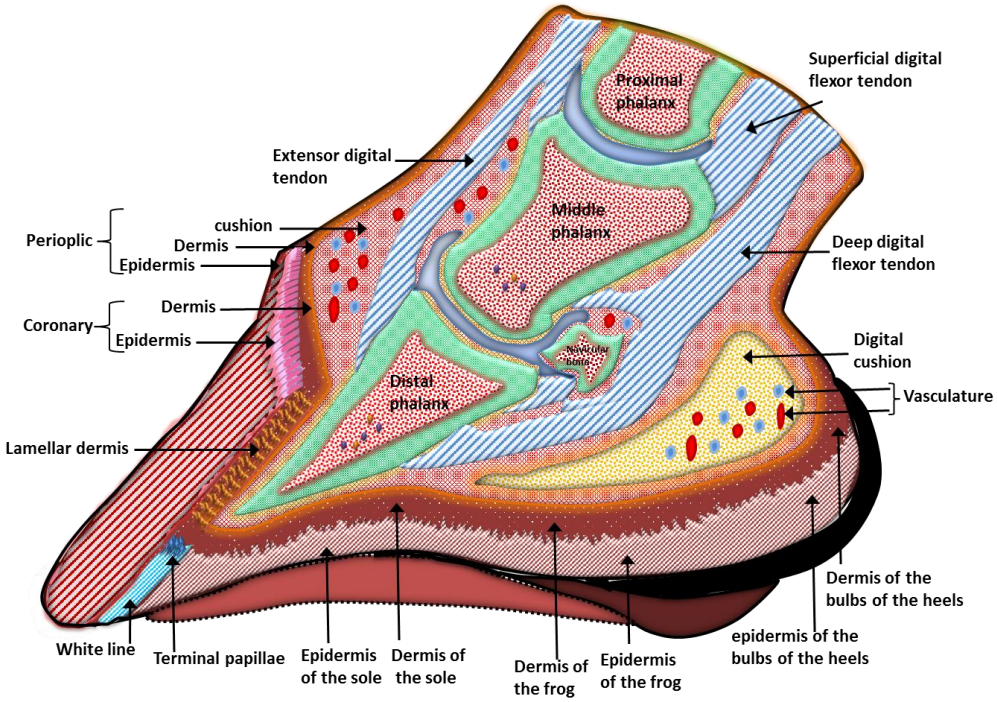


Figure 1-4: Schematic drawing of a sagittal section of equine hoof

Schematic diagram illustrates the entire structure of the horse hoof. Figure adapted from (Budras et al., 2003).

1.2.1 Foot vasculature

The vasculature of the hoof is described for both the arterial and venous supply (Sections 1.2.1.1 and 1.2.1.2 respectively).

1.2.1.1 Arterial supply

The vascular blood supply of the hoof originates from the common palmar digital artery and the dorsometatarsal artery, these main branches giving rise to medial

and lateral palmar/planter digital arteries (Figure 1-5) (Pollitt, 2010, Baxter, 2011). In the hind limb, the small planter common digital arteries contribute to form the digital arteries. At the level of second phalanx, there are branches nourishing to the heel bulbs and coronary region (Bragulla et al., 2007).

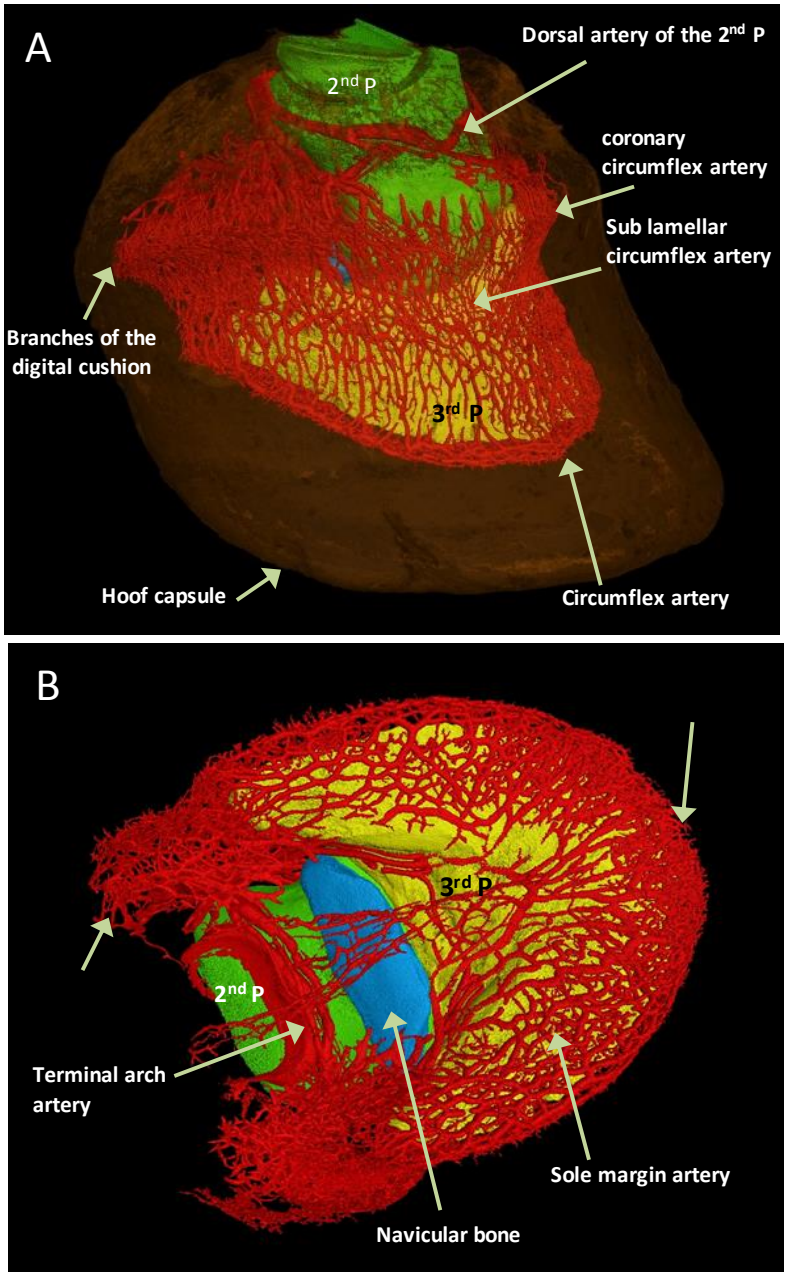


Figure 1-5: Diagram of micro CT image illustration vascularisation of equine foot

CT scan images showing the three dimensional reconstruction of arterial supply of equine foot. A) Shows arteries distributed throughout the dorsal surface of the distal phalanx and anastomoses located proximally with vessels of the coronet and distally forming the circumflex artery. B) Represents the arteries distributed in the sole margin. CT image of hoof study reconstructed by Dr Craig Sturrock and the information obtained from Budras et al. (2003).

The vascular arteries of the dermis are divided into three independent arterial blood supplies: the dorsal coronary corium; the palmar/planter portion of the coronary corium and laminar corium; and the dorsal laminar corium and solar corium, as the blood flow is reversely directed from the distal part to the proximal part within the dermal lamina (Baxter, 2011). The terminal branches of the blood supply enter the distal phalanx from the medial and lateral aspects and then form several anastomoses within the bone to make the terminal arch. At this arch, there are 8 to 10 blood vessels emerging distally to nourish the sole margin (Bragulla et al., 2007). This is a highly important organization of blood vessels in equine feet as the terminal arch and its branches are protected by the bony canal that can be altered in chronic laminitis, leading to ischemia and a decrease in the growth rate of the corium (Floyd and Mansmann, 2007).

The capillary network of the equine digit is complex due to the fact that the dorsal and palmar parts of the foot have different blood supplies and drainage routes (Konig et al., 2007). For instance, the blood vessels of the dorsal lamella pass through the distal phalanx and the blood supply of these portions is directed from the distal to the proximal way, while the palmar lamella is from the proximal circumflex to dorsal lamella (Collins et al., 2004).

Thus, haemorrhage from the sublamellar circulation can result in the rotation of the distal phalanx, as in the founder (Hood et al., 1993, Floyd and Mansmann, 2007, Orsini, 2011). Consequently, the blood vessels of the equine foot are predisposed to local vasoconstriction and the development of ischemic disease as the arteries from the plexus have thicker walls with small lumens and are unable to auto-regulate the volume variations that are involved in contraction of smooth muscle as well encompassing arteriovenous shunts (Hood et al., 1993).

1.2.1.2 Venous supply

The equine hoof veins are divided into three groups depending on their location: wall dermis veins which are separated into proximal and distal regions; coronary dermis veins; and frog and sole dermis veins (Bragulla et al., 2007). The dermal lamella is drained by: the coronary vein; the independent superficial vein; the proximal branch of the caudal hoof vein and; the circumflex vein. The toe and quarters are drained via the circumflex vein (Mishra and Leach, 1983, Konig et al., 2007). There are three interconnected areas such as venous plexuses without valves: the dorsal venous plexus on the dermal lamella; the palmar/planter plexus on the dermal sole and the cartilages of distal phalanx; and the coronary venous plexus in the coronary cushion. These anastomoses are drained by the medial and lateral digital veins (Pollitt, 2004a).

An additional feature of the blood circulation of the equine foot is the anastomoses of arteries and veins, which are, blood vessels forming shunts (Pollitt, 2004a). Each dermal papilla in the periople, coronary band, frog, sole and terminal papillae contain a meshwork of anastomosing arteriovenous vessels located at the base of the papillae (Baxter, 2011). These anastomoses are able to withdraw approximately 50% of the whole limb blood flow, and thus can be involved in ischemia due to blood flow diversion (Pollitt and Blake-Caddel, 1991). This could explain the relationship between laminitis and ischemia (Stewart, 2013).

1.3 Hoof growth and distortion

The development of the claw or hoof appears as the result of a morphological conglomeration resulting from the growth of the capsular wall at the end of the digits (Alibardi, 2009, Ethier et al., 2010). The capsular wall is produced throughout the life of the animal (Daradka and Pollitt, 2004). The frequent renewal of the hoof wall occurs at the coronary dermis, where germinal epidermal cells divide to create a population of keratin-producing cells (Pollitt, 1998, Daradka and Pollitt, 2004). The horny material of the hoof wall is generated by the differentiation of the epidermal cells that are accountable for the production of keratin and are, for this reason, called keratinocytes (Pollitt, 1998, Eurell and Frappier, 2013). Therefore, cornification - or the formation of horn- involves in the synthesis and exocytosis of intercellular cementing material (keratin), as well as the apoptosis of keratinocytes once the cement has formed (Tomlinson et al., 2004).

The hoof capsule is configured by the stratum corneum, which is composed of the perioplic epidermis, the coronary epidermis, and the lamellar epidermis, respectively (Bowker, 2003). Bertram and Gosline (1987) demonstrated that the structure of the hoof wall is made up of tubules organized in rows parallel to the outer surface of the hoof wall, and that they extend from the proximal dermal papillae to the distal ground surface (Lancaster et al., 2013). Each papilla is situated in a hollow structure at the surface of the epithelium (Bragulla, 2003, Konig et al., 2007). These hollow-centred tubes are composed of fibres that are organized in a vertical helix shape (Bragulla, 2003), curving around the tubules' axes, and exhibiting an irregular spiral trend between the different layers

composing the stratum (Bragulla and Hirschberg, 2003). In between the hollow-centred tubes, the hoof wall is produced by the proximal basal epidermal cells, which are located between the dermal papillae (Daradka and Pollitt, 2004) (Figure 1-6). These cells have a broad, flattened shape, with the longest axis being perpendicular to the orientated tubules (Banks, 1993). The dermo-epidermal junction, (the connection between the distal phalanx and the hoof capsule), varies considerably within and across species (Bragulla and Hirschberg, 2003).

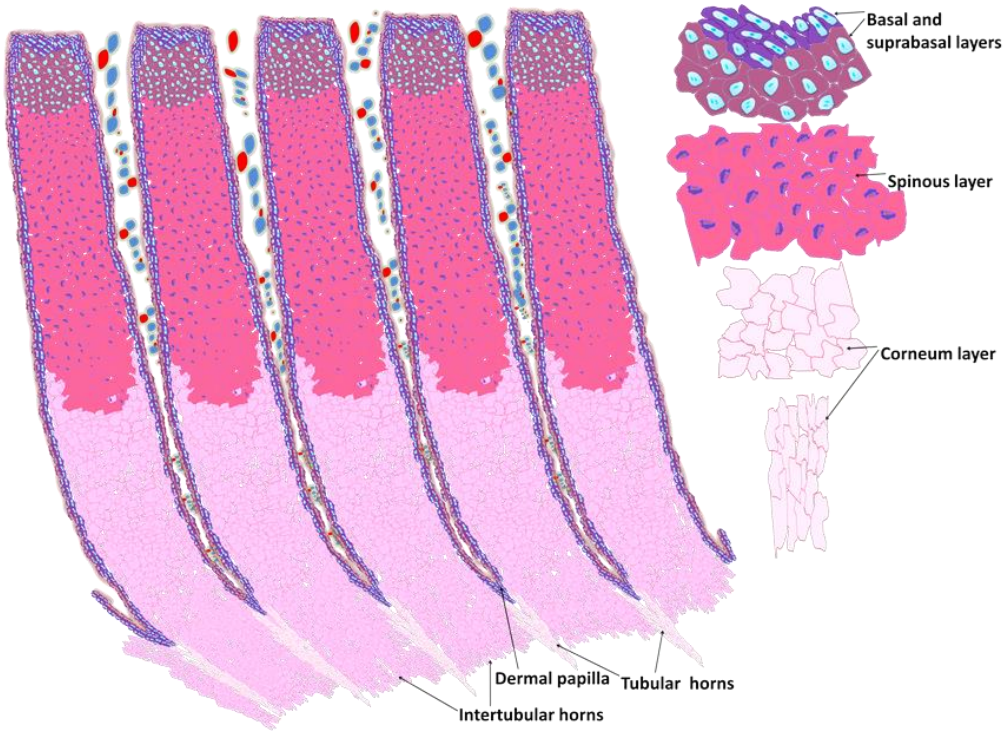


Figure 1-6: Schematic drawing showing the dermal papillae and their layers

Figure adapted from the current study illustrated the layers generating the stratum medium of hoof wall in particularly changes in the shape and size of keratinocytes in coronary region (red/blue represent the blood vasculature).

Such variations in the dimension and shape of the papillae and lamellae seem to play a key role in the mechanical support of the hoof capsule (Bragulla, 2003) (Figure 1-7). The dermal layer under the hoof wall forms longitudinal folds, which form the primary and secondary dermal lamellae that are perpendicular to the capsule (Bragulla, 2003, Eurell and Frappier, 2013).

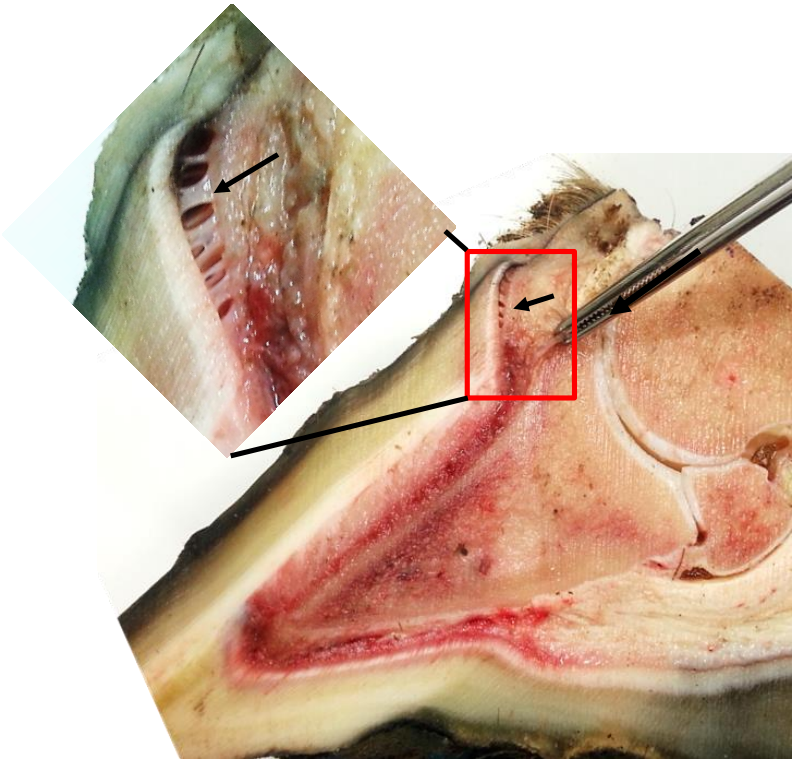


Figure 1-7: Sagittal section of equine foot showing coronary dermal papillae

Diagram illustrates the coronary band (red rectangle), and their roles in hoof growth throughout the formation tubular and intertubular horn via dermal papillae (black arrow). Image obtained from study.

Hoof capsule growth is related to mitotic activity at the germinal layer of the epidermal cells of the periople and coronet (Bragulla, 2003). The hoof wall grows at a rate of about 0.1-1mm per day across species (Vermunt and Greenough, 1995, Parks, 2003, Harrison et al., 2007), estimated, in horse ranged from 0.19-0.28 mm/day (Glade and Salzman, 1985).

Movement within the hoof is enabled by the sequential binding-unbinding of specific adhesive units (for example hemi-desmosomes) between the hoof and the secondary epidermal lamellae (Pollitt and Collins, 2013). The adhesive force between the dermal and epidermal lamellae is provided naturally by the area available for adhesion. Aside of adhesion, the overall mechanical properties, for example the thickness of the hoof capsule, is related to the proportion of

keratinization, which occurs in layers from the papillae and along the abaxial axis of the hoof, and develops along the proximo-distal axis (Bragulla, 2003).

The capsular growth rate is essential in understanding the aetiology of hoof distortion. It is now well established that keratinocyte progenitor cells grow from the papillae and not from the lamellae (Bragulla, 2003), implying that the capsular wall has to slide in a continuous fashion on the lamellae in the proximo-distal direction (Bragulla and Hirschberg, 2003, Bragulla, 2003, Pollitt, 2004a). This evidence was highlighted by Pollitt (2010) who demonstrated that the main sites for cell replication are at the level of the coronary band or coronet – in the papillae and proximal lamellae. The importance of hoof cell synthesis, and therefore cell proliferation, in the pathology of laminitis has been underlined in different species (Vermunt and Greenough, 1994, Daradka and Pollitt, 2004), however, it remains unclear how cell proliferation itself is involved in this pathology. Indeed, in the equine species, throughout chronic laminitis, there is a decrease in the proliferation index of epidermal cells from the coronary tissue (Jones et al., 2004, Carter et al., 2010a, Carter et al., 2011). This result may contrast with the greater proliferation measured of the same cells at the early stages of the disease course, for example less than 10 days prior to the onset of the disease as described by Kuwano et al. (2002). It is interesting to note, however, that MacCallum et al. (2002) found increased cellular proliferation in the hooves of cows which were becoming lame. These results suggested that an augmented rate of keratinisation could be a critical part of the defence mechanism against laminitis. Although growth rate, mechanical morphology and hoof wall are well recognized to be important in the pathology of laminitis (Bowker, 2003), the connection between all of these components is missing.

1.3.1 Microstructure of the hoof wall

The hoof capsule consists of two regions: the wall (lamina) and the base of the surface (*facies solearis*) (Budras et al., 2003). The wall is formed by the periople, coronet and wall layers (external, middle and internal layers) while the base surface is formed by the sole segment and the footpad of ungulates (Budras et al., 2003, Pollitt, 2004a). The size and distribution of these two segments differ considerably between animal species (Bragulla et al., 2007). The structural element of the hoof wall is the horny material which is formed from a α-keratin, a fibrous, structural protein present in claws, hooves, nails, horns and hair (Tombolato et al., 2010). This keratinous substance is composed of tubular structures made from dead keratinocytes (Eurell and Frappier, 2013). The tubules descend parallel to the distal phalanx, from the proximal to distal ends of the hoof (Kasapi and Gosline, 1999, Pollitt, 2004a). These tubular horns are produced by the highly modified layer of epidermal cells attached to the dermal papillae (Bragulla and Hirschberg, 2003). The density and size of these tubules vary between the inner and outer regions of hoof wall (Reilly et al., 1998a), as the tubules are more concentrated in the outer layer compared to the inner layer of the hoof (Lancaster et al., 2013). Similarly, their shape change from larger and rounder in the inner part of the wall to ones that are smaller and oval near the outer surface (Stewart, 2013). In addition, Lancaster et al. (2013) reported that there are regional differences in the concentration of tubules between the lateral and medial aspect of the hoof wall. The stratum medium/middle layer is manifested by a high density of tubular and intertubular horny materials (Pollitt, 2010). This tubular structure enables hoof to transmit ground concussion and load

bearing forces to the appendicular skeletal system (Bowker, 2003). The inner surface of the hoof wall contains a lamellar structure ranging from 2–5µm in thickness, and is assembled in such a way that the tubules intersperse between the lamellae (Tombolato et al., 2010). Accordingly, the capsular wall is organized by three contributory layers (Figure 1-8) as follows: the stratum externum, also termed the periople; the stratum medium, also called the coronet; and the stratum lamellatum, with the alternative name internum (Bragulla and Hirschberg, 2003, Pollitt, 2004a, Budras and Sack, 2012, Stewart, 2013).

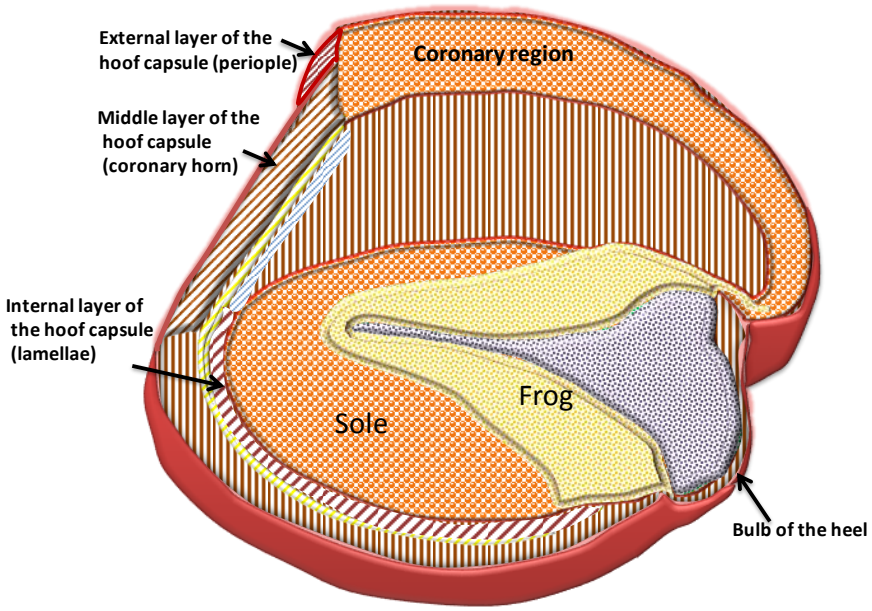


Figure 1-8: Schematic drawing showing dorsolateral view of the equine hoof capsule

Schematic diagram illustrates the layers of hoof wall and the regions of ground surface which contain the frog, sole, bar and bulb of the heel. Figure adapted from (Bragulla, 2003).

1.3.1.1 The lamellae

The orientations of epidermal lamellae are arranged from the proximal to the distal portion of the inner surface of the equine hoof and interface with corium lamella (Pollitt and Collins, 2013). The lamellae of the hoof wall are composed of primary, and a subset of secondary keratinized epidermal lamellae (Eurell and

Frappier, 2013). These structural lamellae are interdigitated with special expansions, i.e. the primary and secondary dermal lamellae (Pollitt, 2004a) (Figure 1-9). There are around 550-600 primary epidermal lamellae in each hoof, and each lamella has 150-200 secondary epidermal lamellae on its external surface (Pollitt, 2004a).

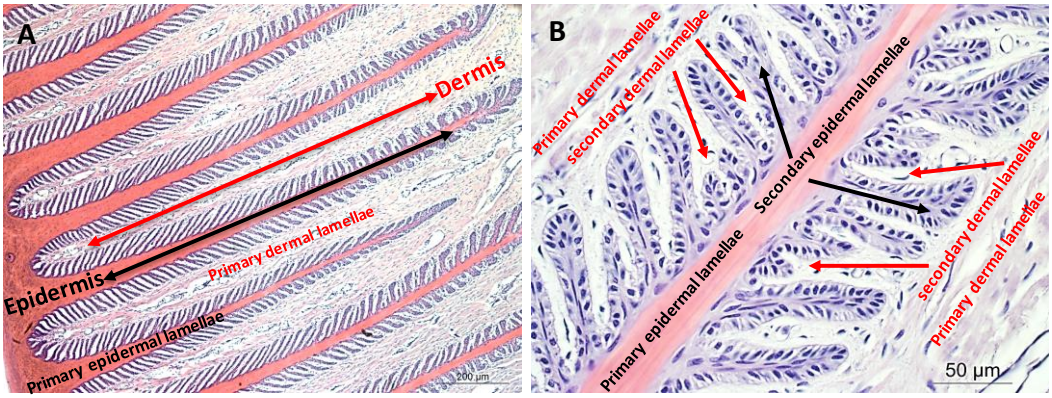


Figure 1-9: Photomicrographs show normal lamellae

A, B) H&E stained images showing structural lamellae and their interconnection between the primary and secondary dermal lamellae with primary and secondary epidermal lamellae. Image (A) scale bar represents 200µm and image (B) 50µm. Images obtained from study and source of information from (Eurell and Frappier, 2013).

Morphologically, epidermal lamellae may have different dimensions and shapes around the perimeter of the capsular wall, which appear to be associated with the conformation of the hoof and the stresses enforced on these laminae (Bowker, 2003). The hoof capsule consists of three layers: the externum, medium, and internum layers (Parks, 2003), which are formed from modified epidermal tissue organised in both laminar and tubular architecture (Lancaster et al., 2013). The dermal lamellae are a highly vascularised connective tissue that comprises capillaries, venules and arteriovenous anastomoses with a large nerve supply (Engiles, 2010).

The variations of pathological changes regarding the hoof wall are the result of a number of causes leading to the failure of the hoof-lamellar interface and rotation of the distal phalanx (Pollitt, 2004b, Collins et al., 2010) due to, for example, too strong loads on the foot (Ramsey et al., 2011). This mechanical cause is thought to be implicated in the variation of hooves shape with time (Douglas, 1998, Faramarzi et al., 2011). Inflammation and destruction of the hoof-lamellar interface, for instance laminitis, is one of the most debilitating pathological condition affecting the equine foot (Loftus et al., 2009, Pollitt, 2010, Wylie et al., 2011, Belknap and Geor, 2017), which is thought to be a major reason for decreasing optimal performance of the athletics horse (Trotter, 2004, Bentley et al., 2007). The lamellar connection between the distal phalanx and the inner hoof wall acts by absorbing energy for weight bearing forces (Pollitt, 2004a, Ramsey et al., 2011) (Figure 1-10).

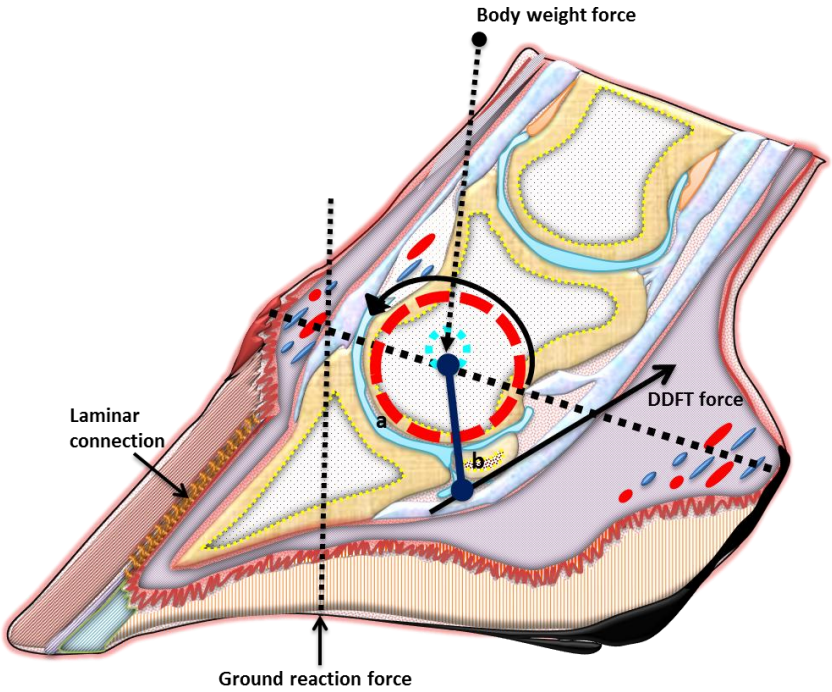


Figure 1-10: Schematic showing application of forces linked to weight bearing

Schematic diagram illustrates the complexity of the hoof shape and its connection proposes that specifically how it deforms throughout movement depending on the loads that is compressed through the axil of bones into the hoof, (a) coffin joint, (b) navicular bone, (DDFT) deep digital flexor tendon. This figure adapted from (Floyd and Mansmann, 2007, Ramsey, 2011).

The functional engagement of the lamellae appears as a resilient attachment between two comparatively inflexible structures: the hoof wall and the distal phalanx (Redden, 2003). Studies have shown that losing the stability of the basement membrane of the hoof-lamellar interface leads to the first stage in lamellar failure, which occurs before the full onset of laminitis (Visser and Pollitt, 2011).

1.3.2 Hoof keratin

Keratinocytes from the hoof wall produce specific proteins, called keratins (Bertram and Gosline, 1987) that are non-soluble proteins present particularly in the epithelial tissues. There are two types of keratin, α-helices and β-pleated sheets keratins which, when assembled, contain either a high level of sulphur bonds providing their hardness as for instance in hair, feathers, nails and hoof walls or a low level of sulphur bonds to make soft tissues such as skin, cuticle and the periople (Bragulla and Homberger, 2009, McKittrick et al., 2012). What triggers the amount of sulphur bounds remains unclear however (Bragulla and Homberger, 2009).

The mechanical traits of the capsular wall are essentially based on the keratinocyte cells and their geometric organization (Bertram and Gosline, 1987, Eurell and Frappier, 2013). Once the keratinocytes have lost their contact with the basement membrane, they start the differentiation process to produce particular keratins such as K1 and K10 (Bragulla and Homberger, 2009). Cornifying keratinocytes in cornifying epithelium undergo apoptosis to become the corneocytes in the upper corneum layer (Bragulla and Homberger, 2009) (Figure 1-11).

There have been an increasing number of keratin proteins detected in the hoof epidermal lamella. There are 30 keratin proteins besides vimentin, desmin, peripherin, internexin, 2 laminin filament proteins and 6 microtubule proteins (Carter et al., 2010b, Pinto, 2012). In line with this complex organization it was suggested that the level or type of keratin expressions could be involved in equine laminitis (Collins et al., 2010, Pinto, 2012). The keratins are placed at interfaces between tissue segments, and therefore can be exposed to biophysical stresses (Pekny and Lane, 2007). An experiment consisting of stretching keratinocytes was examined by Nishimura et al. (2009) who demonstrated that as a response there is a decrease in the number of growing epidermal cells, which seems to promote the overexpression of the suprabasal keratins (Goermar et al., 1993). More recently, and in the same field, Yano et al. (2004) demonstrated that mechanical stretching can stimulate the proliferation rate of human keratinocytes. This mechanism may contribute to a change in the expression of keratins (Yano et al., 2004). The first layer of epidermis that connects with the basement membrane expresses two predominant keratins K5 (type II contains basic or neutral with high molecular weight proteins) and K14 (type I includes acidic with low molecular weight proteins) (Porter and Lane, 2003, Bragulla and Homberger, 2009).

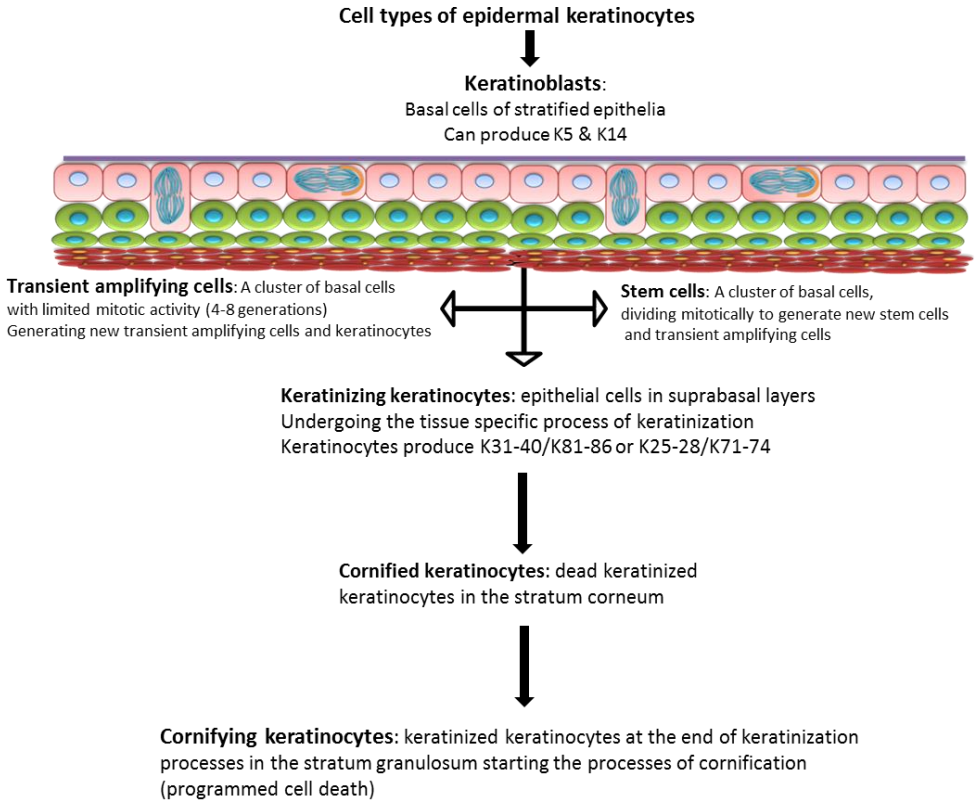


Figure 1-11: Schematic diagram of the cornifying keratinocytes

Schematic illustration of the basal layer of stratified epithelium consisting of keratinoblasts such as stem cells and transient amplifying cells in addition to undifferentiated keratinocytes. As these cells divide, they move upwards, start to differentiate and produce adequate keratin levels in order to become cornified. Figure adapted from (Bragulla and Homberger, 2009).

Some studies have investigated the pivotal role of keratin proteins in regulating the response to cell proliferation signals, and stated their capability to change the mitotic activity of epidermal cells (Figure 1-12). This can be controlled through a complex pattern of phosphorylation and molecular assemblies (Magin et al., 2007, Gu and Coulombe, 2007). Bragulla and Homberger (2009) reported a correlation between the expression of K14 and the mitotic activity and the level of pluripotency of epidermal basal layer. K14 (acidic) keratin and K5 (basic), keratins are produced together in the basal cells of stratified epithelium only in proliferating cells but not in differentiating cells (Byrne et al., 1994). Therefore, K14 is considered to be an essential component of stratified epithelium (Porter et al., 2000, Bragulla and Homberger, 2009).

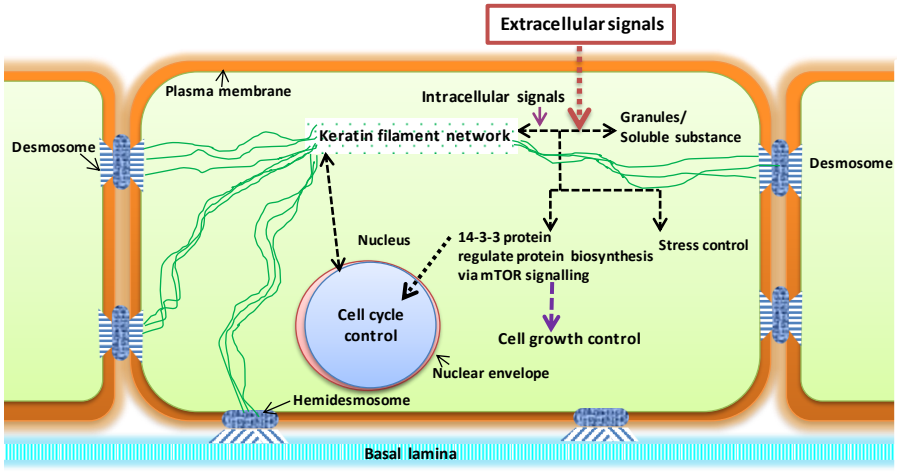


Figure 1-12: Schematic illustrates the regulatory functions of keratins

Illustration representing the mechanism by which keratin filaments are involved in the integrity of epidermal cells. Figure adapted from (Magin et al., 2007).

1.4 Interactions between the hoof capsule and the distal phalanx

The external morphology of the hoof capsule is indirectly associated with the function and shape of the internal segments of the hoof (Moleman et al., 2006). Despite the fact that studies have documented the role of sequels linked to mechanical stresses on the hoof wall (Hinterhofer et al., 2000, Hinterhofer et al., 2006, Thomason et al., 2002), very little work concerning the relationship between the shape of distal phalanx and the changes in hoof capsule (Cruz et al., 2006, Dyson et al., 2011a), has been published. It has, however, been observed that, although the hoof capsule appears intact, subclinical changes may occur at the level of the internal structures of the equine foot (Lancaster, 2011). How these subclinical changes impact the equine foot over time is unclear but given the hoof lamellar adhesion, any impact on this adhesion may change the capsular shape over time (Hampson et al., 2013). In this scenario, alteration of the shape of the hoof could have serious consequences on the distal phalanx (Dyson et al., 2011a),

for example altering its shape in response to weight loading (Thomason et al., 1992, Cruz et al., 2006).

Dyson et al. (2011a) have drew attention to the fact that, despite differences in the orientation of the distal phalanx between horses, mainly associated with changes in direction of the dished solar border, the morphology of the distal phalanx is unaffected by the external features of the hoof capsule. It is worth noting here that hoof shape can be altered when trimming and shoeing are considered (Van Heel et al., 2006). The impact of trimming/shoeing on the hoof capsule shape has been explained by Johnston and Back (2006) where they demonstrated that the formation of the hoof wall is physically connected to the loading of the lower limb, thus protecting its optimal balance on the ground (Ramsey et al., 2013). Therefore, the geometrical tendency of the foot components determines the ability of the internal structures to respond to loading through the bearing phase of the stride cycle (Gunnarsson et al., 2017).

1.5 Pathological changes of the hoof suspensory apparatus

The distal phalanx is attached within the hoof capsule through the suspensory apparatus (Pollitt and Collins, 2016), which connects the entire parietal surface of the distal phalanx to the lamellar structures of the internal hoof wall (Pollitt, 2010) (Figure 1-13). Preliminary work on equine lamellar connection was undertaken by Douglas et al. (1998) who found that this attachment provides the mechanism by which the weight is transferred between the distal phalanx and the epidermal laminae of the hoof wall. This connection, or attachment, has a substantial role in the biomechanics of healthy foot performance, and may lead to foot lameness if damaged (Johnston and Back, 2006).

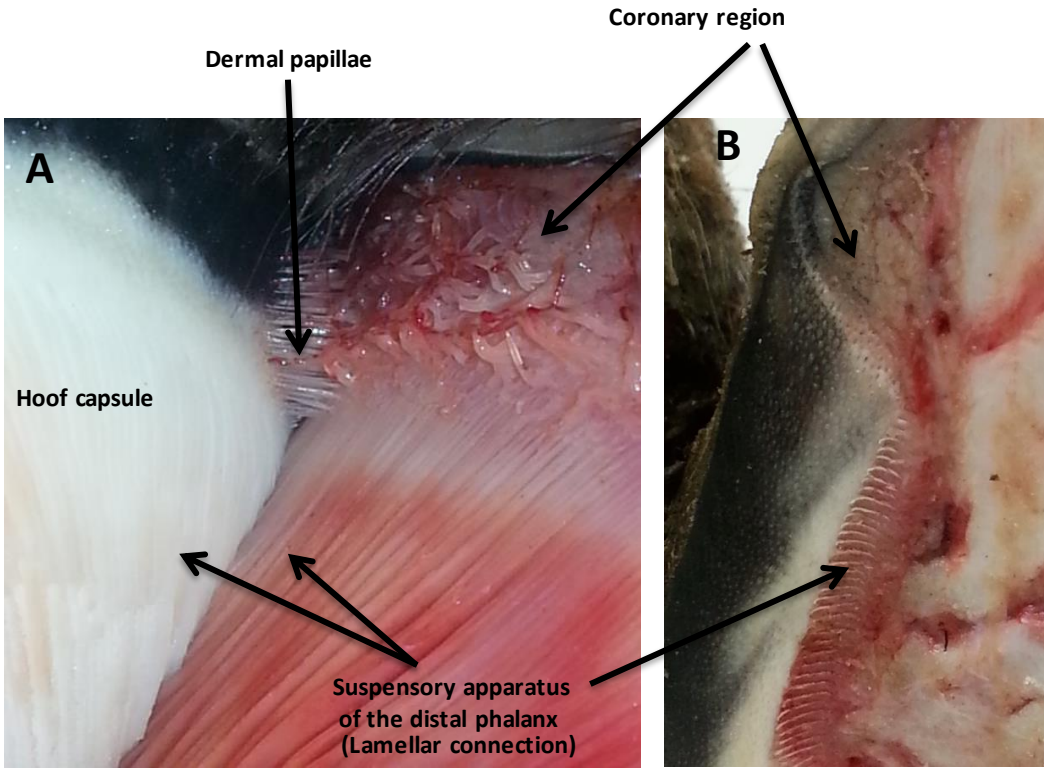


Figure 1-13: Photographs illustrating the suspensory apparatus of distal phalanx

A, B) equine hoof images were dissected showing the connection between the inner surface of hoof capsule white colour and the partial surface of distal phalanx representing the suspensory apparatus of equine foot. Image obtained from study.

Indeed, the failure of the connection between the epidermal laminae and the underlying basement membrane of the dermal lamellae would weaken the suspensory apparatus of the distal phalanx (Eades, 2010). Unsurprisingly, changes in the basement membrane of the suspensory tissue have been suggested to signal the first step of laminar failure (Visser and Pollitt, 2011). While Kyaw-Tanner and Pollitt (2004) reported that lesions in the basement membrane appear before any clinical signs of foot lameness. The dislocation of the distal phalanx, followed by its rotation, applies pressure, first on the sole at the palmar border of the distal phalanx and, secondly, on the coronet or upper area of the lamellae by the extensor process of the distal phalanx (Redden, 2003). These deflections lead to impaired blood flow into the basal layers of the hoof wall (Hood et al., 1993), and

can lead to an inhibition of the growth rate of the hoof capsule, affecting its shape over time and induced osteolysis of bone trabeculae in chronic stages (Engiles et al., 2015). A number of hoof shapes can arise from this chronic condition, including sheared heels, crushed heels, club foot, long-dished toe, and high-heel foot (Redden, 2003, Dyson et al., 2011b) (Figure 1-14). One of these chronic condition is the lamellar wedge that develops alongside laminitis, and that is an anatomical displacement of the distal phalanx within the hoof capsule (Carter et al., 2010b), is a direct consequence of the failure of the suspensory apparatus of the distal phalanx (Collins et al., 2010). However, the molecular events involved in the lamellar wedge condition are broadly unknown (Bragulla and Hirschberg, 2003).

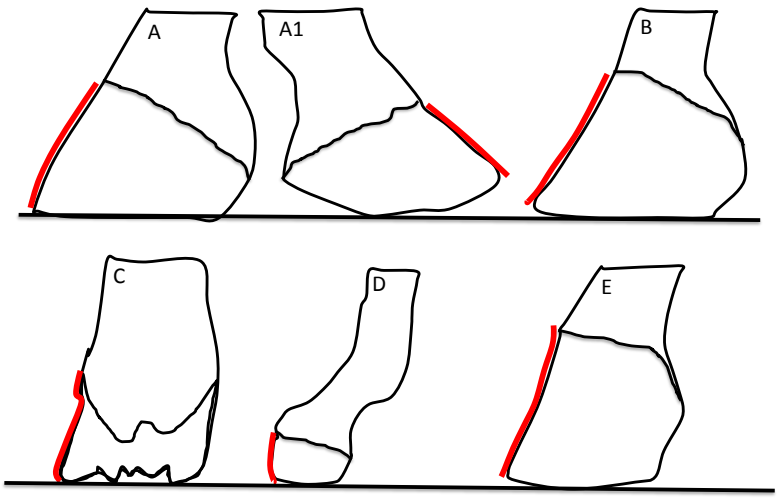


Figure 1-14: Schematic drawing illustrate hoof capsule in different chronic conditions

Different chronic conditions of hoof capsule (red line). (A, A1), crushed heels; (B) long-dished toe; (C), sheared heels; (D), club foot; (E), high-heel foot. This is adapted from (Kaneps and Turner, 2004, Dyson et al., 2011b).

Inflammation of the lamellae occurs primarily at the lamina corium in the area between the distal phalanx and the capsular wall, and particularly at the junction between the dermis and epidermis of the lamellae (Engiles, 2010).

In due course, and when complete, this destruction pulls the distal phalanx away from the hoof capsule, because of the pulling action of the deep digital flexor tendon which is attached on the ventral surface of the distal phalanx (Redden, 2003). The suspensory apparatus is therefore weakened in this case.

1.6 Capsular shape and morphological changes in the laminar junction

The laminar junction within the hoof wall absorbs, indirectly, the ground reaction stress that is applied on the equine foot (Gustås et al., 2001, Faramarzi, 2014) (Figure 1-15). Previous studies have highlighted the connection of hoof shape to the pattern of laminar morphology (Thomason et al., 2005, Thomason et al., 2008). The laminar function as a weight bearing tissue and can show various architectures in relation to the mechanical effort imposed on to them. For example, increasing the length and bifurcation of secondary epidermal lamellae contribute to mechanical efforts on the suspensory apparatus of distal phalanx (Sarratt and Hood, 2005, Davies et al., 2007).

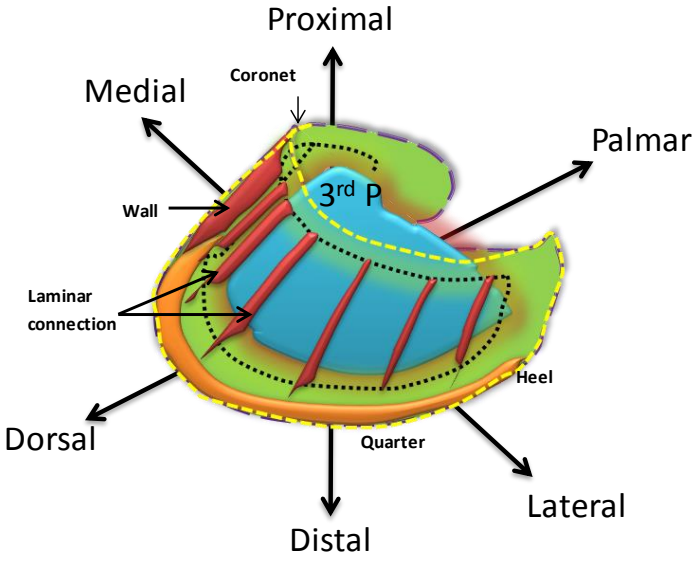


Figure 1-15: Schematic drawing illustrating the connection between the distal phalanx

Schematic adapted from (Thomason et al., 2005).

Although, damaged lamellae lead to altered hoof shape, the mechanical loads applied on the hoof can also change the shape and structure of the hoof wall (Ramsey et al., 2013). Consequently, a change in the lamellae morphology can be related to the adaptive function of the hoof under loading (Faramarzi et al., 2009). In line with this evidence is the fact that it was shown that the primary epidermal lamellae have the capability of remodelling in response to stress being applied to the regions of the hoof wall (Bowker, 2003, Faramarzi, 2011).

In the normal hoof, the population and density of the primary epidermal lamellae are diverse around the hoof perimeter and it is likely that such variation could also result from an adaptation to normal physical stress (Barreto-Vianna et al., 2013). Douglas and Thomason (2000) reported that the rapid changes in spacing, orientation and curvature of the lamellae can result in losing the physical support across the area of laminar attachment with the entire hoof wall. This demonstrates that there is a relationship between the mechanical behaviour of hoof capsule and laminar morphology, which seems to be the equine hoof structurally adapting for its mechanical function (Thomason et al., 2005). It would appear that this wide range of modifications is a reflection of the extrinsic shape of the hoof throughout its development; thereby the inner structures modified their structures and shapes (Engiles et al., 2015). However, further investigation is essential in order to understand the effect and extent of frequent strain on biomechanical traits and laminar morphology (Faramarzi, 2014).

1.7 Laminitis

Hoof pathologies exist across different species, including bovine and ovine species, often leading to a loss of productivity with important economic loss for the dairy/meat industries (Mülling et al., 2006, Schöpke et al., 2013). It has been estimated that around 25% of cattle in the UK, in addition to the rest of the EU, may be affected by laminitis, with a cost of more than €1 Billion per year (Mordak and Anthony, 2007). A survey including 113,000 horses stated a prevalence of 7.1% of laminitis in the UK (Hinckley and Henderson, 1996). While a prevalence of 20.1% was reported by Katz (2004). Similarly, in the USA estimated over 15% of horses were afflicted by laminitis throughout their life with a cost $13M annually (Moore and Jenne, 2010).

In all species, laminitis is traditionally linked to hoof deformity (Vermunt and Greenough, 1994, Engiles et al., 2015). This pathology has different biological causes involving systematic, metabolic and/or endocrinopathic disorders (Karikoski et al., 2011, Karikoski et al., 2015, Johnson, 2017), or physical cause involving the loading pattern of the feet (Pollitt and Visser, 2010).

Laminitis is a catastrophic and destructive disease of the equine foot with a multifactorial and complicated pathogenesis (Engiles, 2010, Belknap and Geor, 2017). Patho-anatomical changes in laminitis include the dislocation of the close attachments between the distal phalanx and the inner surface of hoof wall lamellae leading to severe pain and sinking of the axial skeleton (founder) (Redden, 2003, Lima et al., 2016). There is a significant relationship between the grade of foot lameness and the severity of the pathological changes in the lamellar tissues in

laminitis (Engiles et al., 2015). The progression of equine laminitis is divided into three phases; developmental, acute and chronic (Pollitt, 2004b) (Figure 1-16).

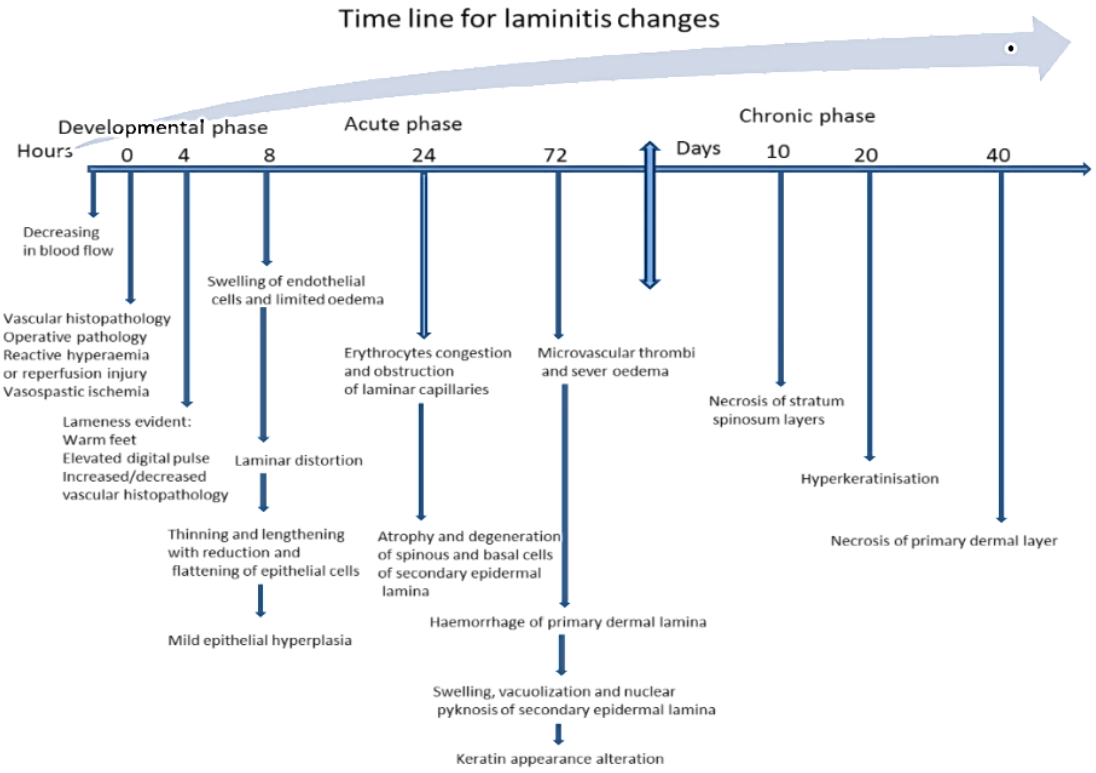


Figure 1-16: The different developmental stages of laminitis

Figure updated from (Hood et al., 1993).

The first stage is the developmental phase, which occurs within the period of time between the onset of histopathological variations occurring in the lamina and the first clinical signs of foot lameness (Moore et al., 2004). This stage lasts between 8-12hrs in the case of black walnut laminitis, and up to about 40hrs in the case of grain impaction laminitis (Pollitt, 2004b). Microscopically, this first stage is accompanied by a disorganisation of the basement membrane associated with an increase in metalloproteinase activity located (Noschka et al., 2009b, Kyaw-Tanner and Pollitt, 2004, De Laat et al., 2011a).

Basal cells of the lamellar tissue lose their shape and become more elongated and, as a result, the secondary epidermal lamellae appear pointed rather than club-shaped (Floyd and Mansmann, 2007). During in this stage, changes in cellular adhesion between the lamellae and the hoof wall determines the development into either acute or chronic laminitis (Carter et al., 2010a).

The second phase (acute) is attributed to the start of any clinical signs such as foot lameness and foot pain and can end within 72hrs, when the third phase (chronic) may begin if there is evidence of distal phalanx rotation (Pollitt, 2004b). Although laminitis can have different causes such as systemic inflammation, sepsis, equine metabolic syndrome (McGowan, 2010) and mechanical overload, research has indicated that they all lead to the disconnection between the basal epidermal lamellar cells and the basement membrane of the lamellar dermis (Eades, 2010, Heymering, 2010, Lima et al., 2016). Three theories exist explaining each the hemodynamic process leading to ischemia in acute laminitis (Bailey et al., 2004). The first one assumes that the digital vasoconstricted vessels, causing oedema, are associated with the development of microvascular thrombi, resulting in ischemia and severe pain (Moore et al., 2004). The second assumption emphasizes that ischemic necrosis with severe pain arises as the blood is redirected from the dermal connective tissue leading to a drop in oxygen levels in the epidermal tissue of the lamina (Hood et al., 1993). The third theory suggests that acute laminitis occurs due to an inappropriate stimulus or reaction of the vascular smooth muscle of the digit, resulting in a constant contraction. Thus creates varying grades of digital ischemia (Hood et al., 1993, Hinckley et al., 1996, Eades et al., 2002), and this vascular dysfunction is associated with endocrinopathic laminitis (Morgan et al., 2016).

The histomorphological structures of the interdigitation between the external surface of the distal phalanx and the lamellae of the interior hoof capsule are fundamental to keeping the distal phalanx in its position (Pollitt and Collins, 2016). Any failure in this connection produces soreness and distinctive foot lameness (Pollitt, 2004b, De Laat et al., 2013a). The biomechanical permanence of the equine digit depends mainly on the integrity of the basement membrane (Pollitt, 1994, Pollitt and Collins, 2016). Therefore, any degeneration in the basement membrane and malfunction of its interdigitation to the basal epidermal cells is sufficient for the initial histopathological actions to occur in acute laminitis (Pollitt, 1996, Visser and Pollitt, 2011). The basement membranes are made of type IV collagen while the main non-collagenous protein is laminin (LeBleu et al., 2007). Therefore, laminin-1 and collagen IV play significant roles in the dermo-epidermal attachment (Pollitt, 2004a). Johnson et al. (2000) showed that circulatory levels of collagen IV increased in cases of naturally occurring laminitis, and that this is certainly related to the activity of matrix metalloproteinase (MMP) enzymes (Kyaw-Tanner et al., 2008). Finally, at the cell level, another feature of acute laminitis is the augmentation in the number of apoptotic epidermal basal cells identified in the epithelial lamellae (Faleiros et al., 2004). Another laminitic phase, termed the sub-acute phase, can follow the acute phase when the displacement of the distal phalanx has not occurred (Moore et al., 2004). In this case, the animal improves progressively until there is very little or no clinical or morphological sign of laminitis or dislocation of the distal phalanx (Parks and O'Grady, 2003).

The third laminitic phase is known as the chronic phase, which can be considered after 72hrs with clinical symptoms ranging from permanent, slight foot lameness, continuous foot pain, and excessive disintegration of lamellar attachments, recumbence, capsular wall distortion and sloughing of the hooves (Pollitt, 2004b, Stewart, 2013, Belknap and Geor, 2017). There are three characteristic features which appear as a consequence of hoof collapse and the displacement of the distal phalanx which are: the rotation of the dorsal wall; the rotation on the mediolateral side; and sinking of the distal phalanx (Parks and O'Grady, 2003, Orsini et al., 2010, Bras, 2011). These features can appear independently or concurrently.

The sinking of the distal phalanx, or fatal founder syndrome (Bras, 2011), this condition can develop within 2-3 days following the onset of the first clinical signs of the sub-acute phase. it is also associated with severe pain and a characteristic gait due to complete separation of the distal phalanx (Parks, 2016). In this scenario, there is a palpable depression just proximal and around the circumference of the coronet (Parks and O'Grady, 2003). The severity of the case depends on to whether the anatomical features of laminitis can be compensated or not. Indeed, compensation may occur in cases where the distal phalanx does not show excessive displacement or rotation (Bras, 2011). This type of compensation can occur naturally, when horses/ponies change their gait, posture, or weight-bearing ability to remove of the stress applied on the hoof-lamellar interface (Morrison, 2010). Some features remain visible over time, including diverging the growth lines from the dorsal to the lateral/medial parts on the dorsal hoof wall, and a resulting change in contact angle between the hoof and the ground (Stewart, 2013).

1.7.1 Lamellar wedge

In chronically laminitic horses, the lamellar wedge appears as an abnormal horny mass, that is formed between the inner hoof wall and the epidermal lamellae, and is linked to the slight rotation of the distal phalanx (Kuwano et al., 2002, Pollitt, 2004b). This structure develops as a result of the impaired connection between the dermis and the epidermis (Pollitt and Collins, 2016). The normal biomechanical performance of the foot is affected by the lamellar wedge and leads to additional soreness and functional disability of the affected horses foot, particularly distortion in hoof capsule and distal phalanx (Engiles et al., 2015). In addition to locomotor dysfunction, abnormal keratinous tissue produced in the lamellae wedge tends to imitate the nature and magnitude of the hoof-lamellar interface for recovery of the affected foot (Collins et al., 2010). The separation of the distal phalanx inside the capsular wall can change the sole shape to become convex rather than be concave, due to differential growth of the proximal hoof wall portion (Pollitt, 2004b). The structural and physical appearance of this abnormal keratinized material is comparable to the white line tissue, and which is proposed to be an ectopic white line (O'grady, 2011). It was therefore thought that a large quantity of the ectopic white line could be able ultimately to prohibit the straight and normal growth of the hoof capsule (Kuwano et al., 2002) (Figure 1-17).

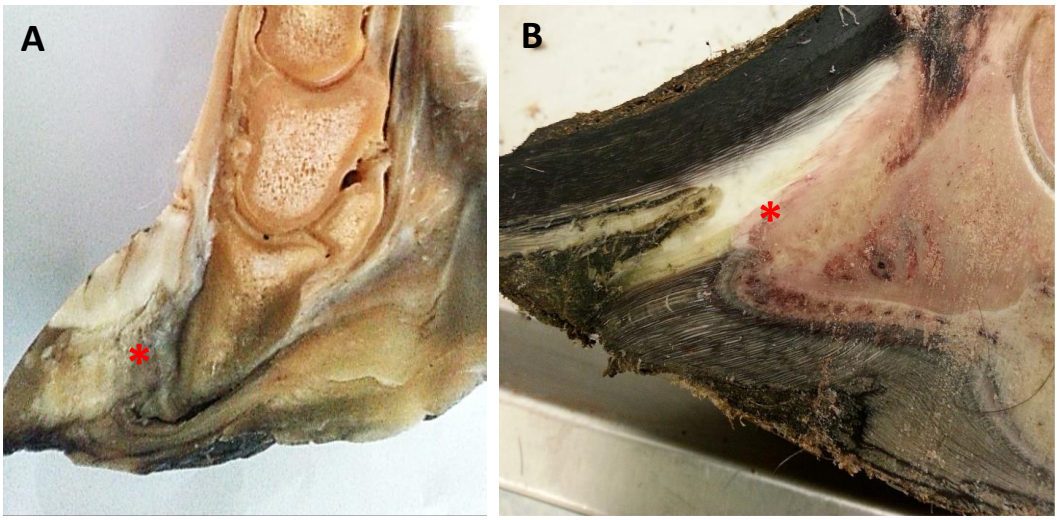


Figure 1-17: The anatomical displacement (indicated by *) of the distal phalanx

(A, B) Longitudinal section of two laminitic feet shows lamellae wedge inside the hoof capsule indicates (*) abnormal tissue, which changed the shape of hoof capsule. Images obtained from study, but source information includes (Kuwano et al., 2002, Collins et al., 2010).

1.8 Elements of physics in relation to the equine foot

Biomechanical stimulations on various regions of the hoof capsule can result in the development of conditions in the lower limb of equine feet (Ramsey et al., 2013). These pathological conditions are dependent on the age of the animal since the hoof capsule can also adapt its shape to some level of stress preventing hereby damage or injury of hoof segments (Johnston and Back, 2006). One study by Franck et al. (2006) evaluated the elastic modulus (the ratio of stress to strain along the loading direction) of the bovine the claw allowing an estimation of the firmness and the stiffness of the dorsal, abaxial and bulb horn wall. Results demonstrated that the elasticity of the bulb horn is greater than the capsular wall horn and that the dorsal wall is stiffer than the abaxial wall. Salo et al. (2010) reported that the modelled capsular wall stresses are higher in the middle section of the hoof wall, and lower around the coronary groove and the distal hoof wall.

Douglas et al. (1996) found that the elasticity of the equine dorsal superficial wall was higher in comparison to that the lower values at the dorsal inner wall, while the quarters having intermediate values. The difference in rigidity between the dorsal surface and inner walls proves that the equine hoof capsule is relatively inflexible at the level of the outer surface compared to the inner wall. Similar results were obtained in the quarters where analogous changes in rigidity through the capsule wall are measured (Ryan, 2013, Jansová et al., 2015). However, the decreased wall thickness at the quarters in comparison with the dorsal wall revealed that, practically, the quarters are less stiff than the dorsal wall (the stiffness is proportional to a power value of the wall thickness) (Thieme et al., 2015). Finally, the capsular wall being thinner at the quarters may facilitate the abrasion of both medial and lateral sides, which happens through weight-bearing (Douglas et al., 1996, Redden, 2003).

Additionally, Thomason et al. (2005) found that lower mechanical loads were present at the distal part of the laminar junction were as higher loads were present at the mid and proximal part levels. Geometrical analysis suggested that the stress applied to the dorsal lamellar tissue is a function of the contact angle between the hoof and the ground as well as on the elastic energy storage (Ramsey et al., 2011, Ramsey et al., 2012, Ramsey et al., 2013).

In general, most biomechanical works are focused on a static capsular wall without any insight into the impact hoof growth on hoof biomechanics (Thomason et al., 2002, Ramsey et al., 2013). However, we propose that understanding the stress components of a growing hoof are more in line with the natural impacts that can have physical or chemical stimuli on hoof shape.

1.9 The link between hoof morphology and residual stresses

The hoof capsule acts as a mediator between the animal and its surrounding environment, as well as a first line of defence against biomechanical, biochemical and microbiological challenges (Mordak and Anthony, 2007). The hoof capsule of the equine foot, as with most biological structures, varies in shape between animals (Bragulla and Hirschberg, 2003). The hoof shape can change during specific periods where trimming, weight bearing, growth and erosion take place (Hood et al., 2001). These variations are correlated to ecological reasons, including the firmness, abrasiveness, or humidity of the ground (Faramarzi et al., 2009, Ramsey et al., 2012). Investigations into the relationship between the distal parts of the equine foot, the residual stresses applied to the hoof, as well as its shape, have illustrated a way by which hoof shape can change (Bellenzani et al., 2012). It has previously been demonstrated that a reduced perfusion of the capillary beds in the dorsal coronary and lamellar areas can lead to the distortion of the capsular wall, such as it appears in chronically laminitic horses (Hood et al., 1993). As the distal phalanx rotates, the dorsal coronary dermis is compressed, resulting in low oxygen of the coronary tissues, which may be accountable for a reduced growth rate of the dorsal hoof wall (Moore et al., 2004, Morgan et al., 2016). An increase in the perfusion of the solar and toe areas may cause chronic inflammation in these areas (Ritmeester et al., 1998). As a result, the hoof morphology can change slightly due to the mechanical interactions between foot components (Thomason et al., 2004). This is possibly resulted from residual stresses visible through the attitude of the horse's strides (Johnston and Back, 2006). Accordingly, biomechanical loading can challenge the tissues of the foot (Ramsey et al., 2013) (Figure 1-18).

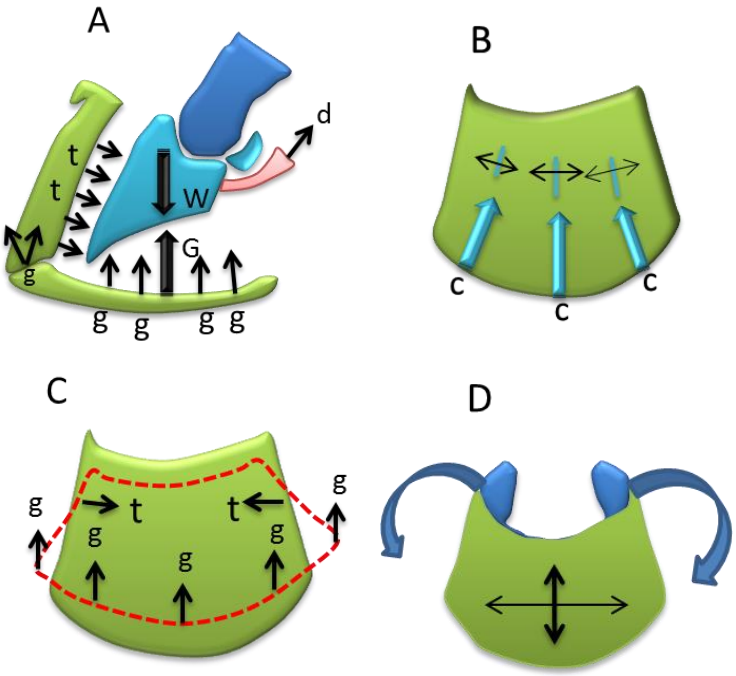


Figure 1-18: Schematic drawing illustrating the stresses applied on the hoof wall

Schematic diagram show (A) application of forces between the hoof wall and bones ("g" is the ground reaction on the hoof border, "G" is the ground reaction on the sole, "W" is the weight, "t" is the laminar tension and "d", is the digital flexor stresses applied on the distal phalanx; (B) stress applied on the anterior wall. C) Shows influence of internally directed tensile stress "t" and constituents of ground reaction force **"**g"**;** while (D) resulting movement of the heel during strides. Figure adapted from (Thomason et al., 1992).

Therefore, consideration of biochemical and biophysical mechanisms present in the equine foot could provide some prospects for early diagnostic of foot lameness (Johnston and Back, 2006). The mechanical stress during foot concussion on the ground is greater in the caudal region than in the cranial region because of the vertical stress component being distributed unevenly above the whole external surface of the hoof wall and the sole (Thomason and Peterson, 2008). It seems, therefore, that the heels and the quarters take an eminent proportion of the stress in absorbing concussion and upholding bodyweight (Barrey, 1990). This concept was highlighted in a study by Hood et al. (2001) which pointed to the connection that exists between the deformability of the ground surface and physical loading of the equine foot.

From the literature, it is obvious that studies have been carried out on the pathology and biomechanics of the equine foot and on the different aspects that impact its function. Despite these studies, very little research has been devoted to understanding how the hoof shape is related to hoof growth in relation to its physical connection on the ground.

1.10 Modelling the set of forces in a growing hoof

If one considers the hoof capsule as a planar surface, there are three forces present. The adhesion force that connects the lamellae to the capsule, the growth force that originates from the coronary papillae and; the ground reaction force to the weight (which is related to the mass of the animal via the gravity constant).

1.10.1 The Growth force

The growth force acts in a direction led by proliferation of the germinal epidermal cells in the coronary band that line the papillae, creating a downward force by the generation of new cells and development of the tubular and intertubular hoof horn (Bragulla, 2003, Pollitt, 2004a, Daradka and Pollitt, 2004, Budras et al., 2012). Figure 1-19 illustrates the proliferation of the basal epidermal cells lining the dermal papillae and the progression and division of the daughter cells from this region. This is correlated with density of dermal papillae per mm^2, as with high papillary density leads to generate more horny material (Harrison et al., 2007).

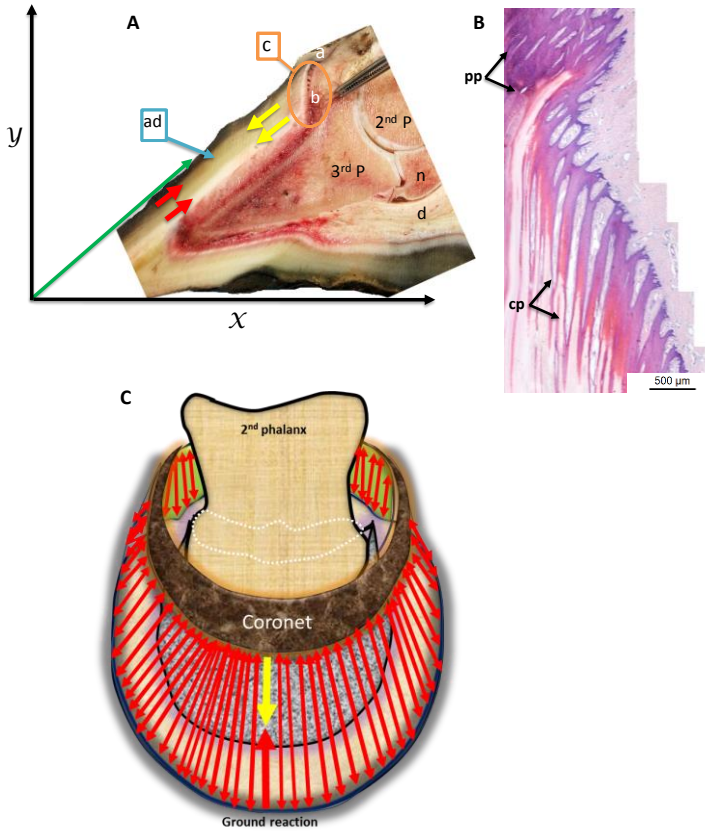


Figure 1-19: Schematic drawing illustrating the main proliferation sites

Yellow arrows signify the orientation of the growth force from the coronary band; ad, show the conflicting adhesive force. (a) Periople, (b) coronary papillae, (c) this region highlights the main proliferation zone, (2^{nd} P) second phalanx, (3^{rd} P) third phalanx, (n) navicular bone, (d) deep digital flexor tendon. B) Photomicrograph illustrating the dermal papilla at the periople and the coronet, pp) perioplic papillae and (cp) coronary papillae stained with H&E. C) Illustrates the forces direction at the coronary region. Images obtained from study. Scale bar represents 500µm.

1.10.2 The Adhesion force

As the horny hoof capsule grows distally from the coronary region, the adhesive force attaching the hoof wall to the distal phalanx and underlying tissue resists this growth, producing a force in the opposite direction (Figure 1-20). This is a factor, which is significant when determining the growth rate of the hoof wall. The adhesive force represents the structures and molecules between the dermal and epidermal layer that are necessary to attach the horny capsule to the underlying tissues, and also allow movement along a stationary surface (Rauch and Cherkaoui-Rbati, 2014) (Figure 1-20).

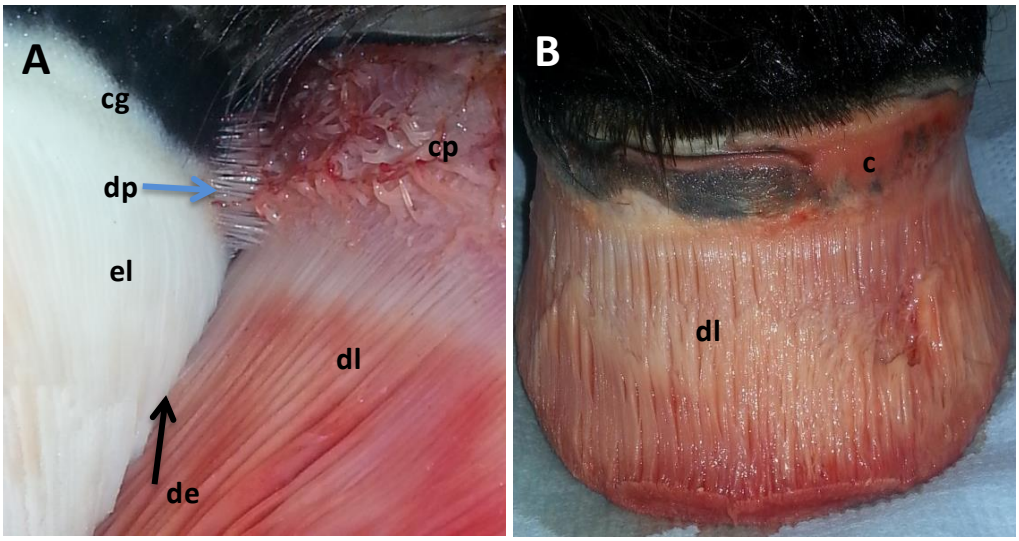


Figure 1-20: Dissection of a hoof capsule.

A) Hoof capsule appears separated at the dermoepidermal interface (de); orientation of the primary epidermal lamellae (el) is highlighted. The epidermal lamellae (el) appear white in colour after separation from dermal lamellae (dl); coronary papillae (cp) show the direction of dermal papillae (dp) inside the coronary groove (cg), blue arrow show where the papillae attached to the hoof capsule prior to dissection. B) Hoof appears without a capsular wall, (c) coronary region. Images obtained from study.

It is worth noting that the magnitude of the adhesion force is higher when the surface area between the lamellae and the hoof capsule is also high (Pollitt, 1998, Pollitt, 2010). That is to say that the adhesion force acting on the dorsal part has a higher magnitude than the same adhesion force on the quarter. Simply and assuming a constant growth force from the coronet, if it was possible to divide the hoof in several unconnected longitudinal slabs, the most dorsal slab should grow more slowly than the most medial/lateral ones (Rauch and Cherkaoui-Rbati, 2014). This highlights the presence of residual stress inside the hoof as the later grows normally. These residual stresses are important to shape the hoof capsule over a long period of time as the hoof capsule, has a physical material, tries to minimize the stresses (Ryan, 2013) (Figure 1-21).

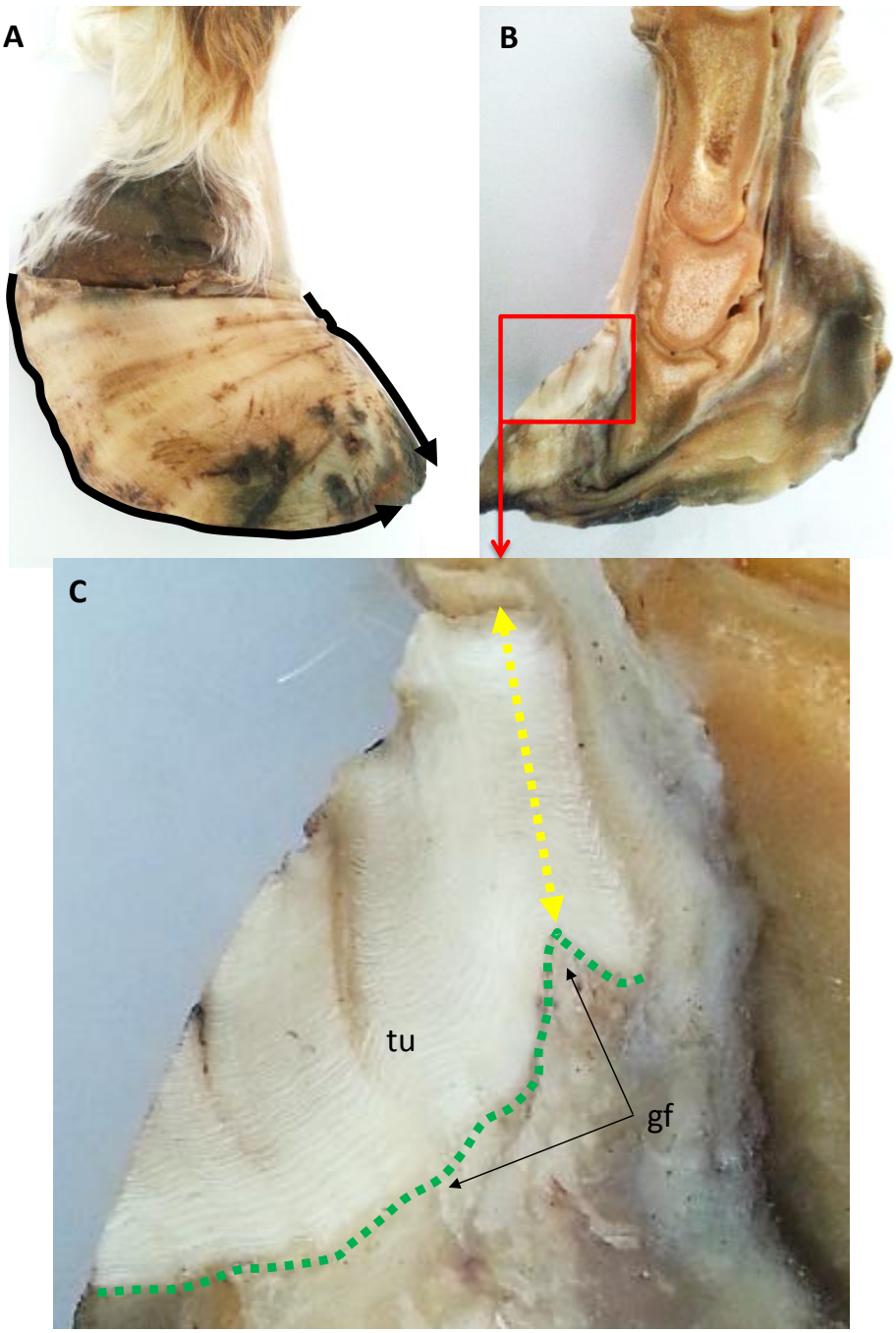


Figure 1-21: Photos showing variations in growth forces in the equine hoof

A) Shows the long curved black arrow on the quarter is longer than the arrow on the dorsal surface of the hoof capsule; B, C show the change that occurs in the direction of the growth force (gf) which leads to a change in the orientation of the tubular horn (tu) which appears from the outside as a growth line (yellow arrow).

1.10.3 Gravity

The ground reaction force associated with gravity comes as a force that has the same direction as the adhesion force, for example oppose the growth force – but whose amplitude varies as a function of the contact angle between the hoof and the ground (Thomason et al., 1992). As every foot is different, it is difficult to assess the impact of this force. However, we can already suggest that when the angle is small the impact of this force should be minimal and the converse is also true (Rauch and Cherkaoui-Rbati, 2014) (Figure 1-22).

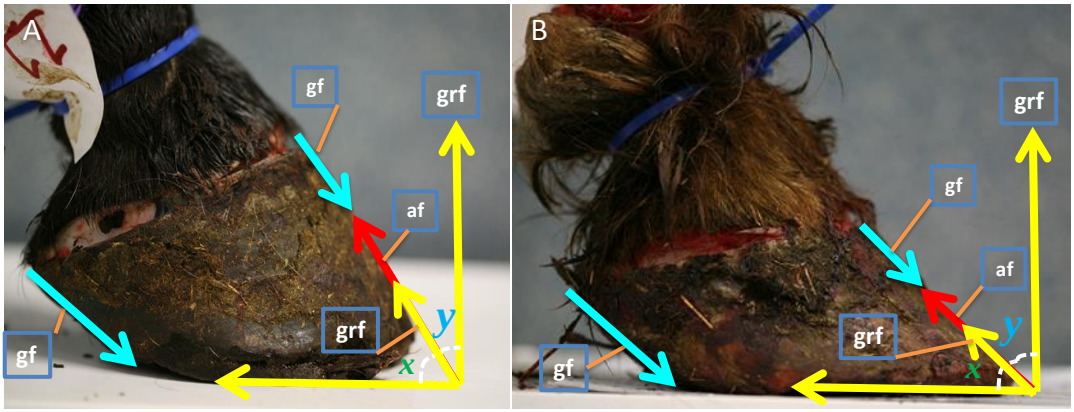


Figure 1-22: Equine hoof photographs show large and small angles

A) Shows a large contact angle (61.7˚) of a horse hoof, note (gf) is a growth force; (af) adhesive force; (grf) ground force or gravity force;. B) Shows a small contact angle (34.3˚) with the projection of forces that are different due to the shape of the hoof as it has concave shape. '*x*' represents the angle between the dorsal surface and the ground while '*y*' shows the angle between the dorsal surface and the ground reaction force.

It is possible, that the algebraic sum of these forces along the growth axis that will have an impact on the hoof shape (Thomason et al., 2002, Ramsey et al., 2013). In order to relate the physics to the biology, one needs to measure exactly the proliferation index from the coronet and relate such proliferation to the different physical parameters affecting hoof shape.

1.11 Hypothesis

Recent efforts have tried to determine whether the hoof shape is a disposing factor to foot lameness-causing lesions. The physical forces borne from the hoof's contact with the ground may have a significant effect on the hoof growth rate. This, where other predisposing factors might coexist, could result in the distortion of the hoof capsule, affecting the biomechanical performance of the foot and underlining the correlation between hoof conformation and foot lameness.

The overarching hypothesis for this work is that hoof shape will have a significant effect on hoof growth, altered proliferation rates, and patterns. In addition, a set of hypotheses were constructed within each experimental chapter in order to define the individual experiments and work plan.

1.12 Aims

The comprehension of the pathophysiology and progression of hoof distortions is incomplete, and this limits the efforts to prevent and treat devastating diseases, such as foot lameness and laminitis, successfully. Scientific investigation is proceeding at a phenomenal pace, shedding light on the pathophysiologic events involved in laminitis. Although extensive studies have been carried out on laminitis and biomechanical variations of the equine hoof, no study has been reported on the relationship between hoof shape and growth rate and its impact on foot lameness. It is possible that the interconnection between the hoof capsule and the growth rate, with regard to the orientation of the distal phalanx, is key. This study aims to uncover how histological, gross morphological and physical forces act within and upon the equine hoof to influence hoof shape. These aims will be

investigated using a number of methods, including immunohistochemistry (cell proliferation and apoptosis), tissue composition (basement membrane thickness and composition, and collagen distribution), gross morphological differences in whole foot, bone/hoof curvature measurements and angles (micro-CT imaging) and biophysics techniques using culture progenitor keratinocytes to incorporate an interdisciplinary information regarding hoof growth. In general, the aims of this thesis were to study the mechanisms involved in the overgrowth rate of the hoof capsule with a particular concentrate on the impact of hoof lameness/laminitis.

1.13 Objectives

The objectives of this project were:

1- To compare cell proliferation, keratin production and cell apoptosis of the epidermal papilla cells using immunohistochemical methods. This was performed by labelling proliferation, stem progenitor and apoptotic cells in differing hoof types.

2- To measure histological features of hoof tissue, including basement membrane thickness and collagen levels in differing hoof types, cell size changes along the length of dermal papillae.

3- To measure hoof contact angles, hoof and bone curvatures using the micro CT-scan.

4- To assess the behaviour of equine progenitor keratinocytes under different physical or chemical stresses that might have an effect on their proliferation capability and hoof growth. This was performed by

measuring the cell proliferation/differentiation using immunofluorescence and Western blot. Additionally, the pluripotency of progenitor keratinocytes after isolation and purification was assessed, subjected to differentiated media, and differentiation measured using Alizarin red stain.

1.13.1 Research plan

In order to achieve the objectives above the experiments were divided into 3 experimental chapters. Chapter 3 investigated how the hoof grows from the coronary region, chapter 4 examined the behaviour of isolated progenitor keratinocytes lining the dermal papillae, and chapter 5 studied the biophysics of hoof growth. The three chapters included the following techniques and analysis:

A. The experiments undertaken in chapter 3 to investigate hoof growth included:

1. Counting the number of dermal papillae
2. Measuring the diameter of dermal papillae
3. Measuring the changes in cell size lining and inter papillary space
4. Measuring the epithelial and hoof wall thicknesses
5. Measuring and assessing the basement membrane zone and the amount of collagen fibres attached to the basement membrane
6. Measuring the frequency of stem p63 +ve cells against the papillae length
7. Measuring the frequency of proliferation Ki-67 +ve cells against the papillae length
8. Measuring the frequency of TUNEL apoptotic +ve cells against the papillae length

B. The experiments undertaken in chapter 4 investigated the cell behaviour under different stresses including:

1. Assessment of the influence of blebbistatin on cytoskeletal element EPKs
2. Assessment of pluripotency during cell passages and the transdifferentiability of EPKs
3. Assessment of the influence of hydrostatic pressure on EPKs
4. Assessment of the influence of stretch of EPKs after incubation for 24hrs with blebbistatin
5. Assessment of the influence stretch of EPKs incubated with blebbistatin
6. Assessment of the influence stretch of EPKs without blebbistatin
7. Assessment of the influence of stretch of cultured keratinocytes after 10 days of culture
8. Assessment of culture keratinocytes under different levels of oxygen 1% , 3% and 5% O_2
9. Assessment of gene expression under 5% O_2
10. Assessment of the impact of insulin on equine hoof culture keratinocytes
11. Assessment of the PI3k/Akt pathway in cultured keratinocytes treated with Insulin

C. The experiments undertaken in chapter 5 investigated the physical biology of hoof growth including:

1. Evaluation of staining patterns of +ve cells
2. Assessment of the percentage of proliferation markers PCNA and Ki-67 +ve cells, and stem cell progenitor keratinocytes p63
3. Assessment of the variation between the percentage p63 and Ki-67 +ve cells
4. Assessment of the expression of epithelial cell marker K14 in equine hoof papillae
5. Comparisons between Ki-67 and K14 expression levels and the hoof curvatures
6. Comparisons between p63 and K14 expression levels and the hoof curvatures
7. Assessment of TUNEL apoptotic +ve cells at the dermal coronary region
8. Assessment of the correlation between the ratio of Ki-67 or p63 to TUNEL positive cells
9. Assessment of the influence of the degree of hoof curvature on epithelium thickness
10. Measuring the contact hoof angle, CT scan hoof curvature and distal phalanx bone curvature

Chapter 2

General Materials and Methods

2.1 Materials and methods

2.2 Collection of hoof samples

Equine hooves were collected from Tauton slaughterhouse in Bristol and from the F. Drury and Sons Ltd Swindon slaughterhouse. Ethical permission was given by The School of Veterinary Medicine and Science, University of Nottingham ethical committee. The clinical signs/case histories of the animals were unknown at the point of collection. In order to further provide a clear assessment between samples; samples were placed into three groups: those with 1) upright hoof wall 2) concave of the dorsal surface, or 3) convex dorsal surface. Thirty two hooves were utilized to obtain tissue samples from the dorsal coronet as well as from the quarter and heel regions – both medial and lateral (tissues were extracted from the dorsal, quarter medial and lateral for the first thirteen hooves, while the rest from the five regions that mentioned before). An additional twenty hooves were collected separately (four hooves every other month) for cell isolation and culture cell experiments (Table 2-1). All hooves were given a unique identification number.

Table 2-1: The source of hoof collection

Type of horse	N. of horse	Left forelimb	Right forelimb	Left hind limb	Right hind limb
Pony	14	4	4	3	3
Cross breed horse	40	12	12	8	8
	Total= 54	**16**	**16**	**11**	**11**

Each sample was photographed (digital camera Canon, Japan) in order to assess gross anatomical and morphological features from three different aspects: lateral, medial and frontal views. The photographs were used to illustrate the counter of

the dorsal wall and to display the angle of quarter areas for further analysis (Appendix 8.1+2). Further images from two samples were taken following dissection of the hoof capsule. These images were used to illustrate the internal surface of the hoof wall and display the interdigitation between dermal papillae and coronary groove at the coronet as well the connection between the lamellae and inner hoof wall.

Photographs were taken from the same distance and against the same background to avoid any opacity or artefacts, which might change the images. Samples were disarticulated at the fetlock joint and an incision made from the left and the right sides in order to dissect the medial and lateral digital arteries.

Paraformaldehyde (4% (w/v) PFA; pH7.2-7.3, Fisher Scientific, UK) fixative solution was injected through the main arteries (medial and lateral palmer digital arteries). Tissue samples (6-7mm thick) were extracted from area between skin and hoof capsule and from 2-15mm under this area – the perioplic segment and the coronary segment (Budras and Sack, 2012, Sherlock and Parks, 2013). Specimens were collected at the dorsal coronet, medial and lateral quarter, medial and lateral heel from the foot of each horse. A sharp knife was used to cut through the keratinized material. Duplicate samples from each area were collected, enabling fixation in 4% PFA for 24 hours at 4°C in order to allow optimisation of fixation techniques. Following fixation, samples were placed into phosphate buffered saline (PBS; Gibco® Life Technologies, UK) until processing (within 7 days). The remainder of the hooves were frozen for CT scanning measurements and applied physics analysis.

2.3 Sample processing for histology

Fixed specimens were removed from the PBS and immersed into dH_2O for 1hr. The samples were dehydrated in a series of graded ethanols at room temperature, unless otherwise stated (50% 2X 2hrs; 70% 2X 2hrs; 90%, 4ºC overnight; 95% 2hrs and 100% 2X 1.5hrs), then immersed in xylene for 3hrs, and immersed in molten paraffin wax overnight. Samples were then orientated and embedded in fresh paraffin (EG1160 embedding station, Leica, Germany).

2.3.1 Tissue sectioning

Paraffin blocks were trimmed and covered with tissue socked with 10% (v/v) ammonium solution placed on wet ice, then the blocks were serially sectioned using a microtome (Leica RM2255 Microsystems, Germany) at 8µm and mounted onto polysine coated microscope slides (Fisher Scientific, UK). A minimum of 30 slides were collected per region at the coronet to ensure that tissue could be visualised throughout the region of interest.

2.3.2 Haematoxylin and Eosin (H&E) staining

Tissue sections were dewaxed using xylene 2X 5min, and rehydrated with a series of alcohol solutions, 100%, 90% and 70% for 5min each and immersed in dH_2O for 5min. Sections were dipped in haematoxylin 2-3 times, washed with tap water for 5min, stained in eosin for 2-3min and then in tap water and dH_2O for 5min each. Sections were dehydrated in graded ethanol 70%, 90% and 100% for 5min each and cleared in xylene for 5min before coverslips mounting with DPX (Sigma, Spain).

2.3.3 PAS stain

Samples were stained using the Periodic Acid Schiff (PAS) technique (according to slightly altered manufacturers instructions; Periodic Acid Schiff, IVD, Germany). This protocol consists of two primary staining reagents. Periodic acid acts to oxidise of the 1, 2-glycols into aldehyde groups whilst the second, Schiff's reagent, reacts to form a specific red colour which as a consequence of reaction with unsubstituted polysaccharides, muco-and glycoproteins, neutral mucopolysacraides and glycol- and phospholipids). This stain was utilized for staining the basement membrane in hoof tissues.

Sections were dewaxed by incubation in xylene for 5min, followed by rehydrated via a series of descending ethanol series (100%; 90%; 70%) for 5min each, then rinsed in dH_2O for 5min. Periodic acid (200µl aqueous solution) was applied to each slide followed by immersion in running tap water for 3min then rinsed in dH_2O for 5min. Sections were incubated with Schiff's reagent (200µl) for 15min followed by washed with running tap water for 3min and then rinsed in dH_2O for 5min. Sections were stained with haematoxylin stain for 1min followed by running tap water for 3min, then sections were dehydrated in an ascending ethanol series (70%, 90% and 100%) for 5min each and cleared in xylene for 5min, they were coverslips mounted using DPX (Sigma).

2.3.4 Masson's trichrome stain

Masson trichrome with light green (Polyscience Inc, UK) staining was used to assess the presence and proportion of collagen fibres in hoof tissues. Two sets of sections from throughout the tissue (the area that is close to the basement membrane and further away from basement membrane) were stained in order to ensure coverage of the tissue.

Initially the manufacturer's protocol was followed. The slides were incubated at 60˚C until the paraffin melted (ensuring tissue adherence). Sections were deparaffinised by incubation in xylene for 2min, followed by tissue rehydration via a series of graded ethanol (100%; 90%; 70%) for 5min each, then rinsed in dH_2O for 5min. Sections were mordant in Bouin's solution in an incubator at 60˚C for 1hr then washed in tap water for 5min to eliminate the picric acid. Specimens were stained with Weigert's iron haematoxylin working solution for 10min (prepared from mixing Weigert's iron haematoxylin (A) and Weigert's iron haematoxylin (B) at a ratio 1:1) followed by a wash in running tap water for 5min and then rinsed in dH_2O. Biebrich Scarlet Acid Fuchsin solution (200µl) was added to each slide for 5min and then rinsed in dH_2O. Phosphotungstic acid/ phosphomolybdic acid was utilized at 5% (v/v) for 10min. Light green stain (200µl) was applied immediately to each slide for 1min followed by rinsing in dH_2O. The differentiation reagent of 1% (v/v) acetic acid was added for 1min. the slides were rinsed in dH_2O, dehydrated in an ascending ethanol 70%, 90% and 100% for 5min each and cleared in xylene for 5min before coverslips mounting with DPX (Sigma), however the following optimisations were made for the hoof tissue:

1) Staining was carried out in a humidity tray to prevent drying of tissue, protecting reagents from evaporating.
2) Specimens were stained with Weigert's iron hematoxylin working solution for 2min instead of 10min.
3) The concentration of Biebrich Scarlet Acid Fuchsin solution was decreased to 10% (v/v) for 30 seconds instead of 1min.
4) Phosphotungstic acid incubation was reduced from 10min to 5min.
5) The light green stain incubation was increased to 30min instead of 1min.

Sections were taken throughout the tissue and two sections photomicrographed using systematic random sampling (40X, DM 5000 B, Leica, Germany). Five photomicrographs were taken from each section. Collagen vs non collagen percentage coverage was assessed for each photomicrograph (Image Pro Plus, Version 6.3.1.542, Media Cybernetics, Inc., USA) and the percentage mean ± standard error of the mean (SEM) were recorded and calculated for each sample using Excel software (Microsoft Windows, Microsoft Corporation USA).

2.4 Immunohistochemistry

2.4.1 Spatial localisation of PCNA

PCNA staining kit (Invitrogen®, USA) was utilized to label proliferating cells. The sections were incubated at 60˚C until the paraffin melted. Thereafter the protocol provided by the manufacturer was followed:

Sections were deparaffinised in xylene for 5min, followed by tissue rehydration via a series of graded ethanol periods (100%; 90%; 70%) for 5min each, then rinsed in dH_2O for 5min.

Antigen retrieval was performed via a digital electric microwave cooker in 10mM sodium citrate, pH 6.0 for 1min at a medium high, heat which was then reduced to medium low for 4min and then left to cool at room temperature for 20min followed by rinsing in dH_2O for 5min.

Specimens were incubated with blocking solution (100µl, Reagent 1) to each slide for 10min at room temperature, then the solution was blotted off without rinsing and incubated with primary antibody (100µl Biotinylated mouse anti-PCNA primary antibody, Dako, UK (Reagent 2)) for 1hr at room temperature, Negative control slides were treated with 5% (v/v) foetal calf serum (FCS) only. Then all slides were rinsed in PBS 3X 2min. Streptavidin peroxide (100µl, Reagent 3) was applied to each specimen for 10min and then rinsed in PBS 3X 2min. DAB chromagen (100µl, Reagent 4) was added to each slide and incubated for 30min. Sections were counterstained with Mayer's haematoxylin by a brief dip in the stain, blued in tap water then rinsed in H_2O for 5min. Sections were dehydrated using graded ethanols (70% 3min; 90% 3min; 100% 3min), dipped in xylene for 3min, and mounted with coverslips using DPX mounting medium.

2.4.2 Spatial localisation of Ki-67

In order to trial a further method for assessing cell proliferation, specimens were incubated with an antibody against Ki-67 (ab66155, rabbit polyclonal, reacts with horse, Abcam, UK) and Leica kit (Leica, Novolink™ Polymer Detection System, Novocastra, Leica Biosystems, UK) in order to identify cell division in epidermal

cells of hoof tissues. The sections were incubated at 60˚C until paraffin was melted for 15min (ensuring that tissue was firmly adhered to the slide). Sections were deparaffinised by immersing in xylene for 5min, followed by tissue rehydration via a series of graded ethanol (100%; 90%; 70%) for 5min each, and then rinsed in dH_2O for 5min. Antigen retrieval was performed by heating in sodium citrate buffer solution pH 6.0. Antigen retrieval was optimised and incubated in the buffer for 5min medium/low heat and refreshed buffered and incubated for 5min medium/high heat, then reduced to and later cooled at room temperature for 20min and washed with dH_2O for 5min. Following antigen retrieval, the specimens were incubated with peroxidase block for 30min at room temperature, followed by washing in PBS 2X 5min. Protein block (Leica) were added to all sections and incubated for 30min. Sections were then incubated with primary antibody, Ki-67 (Abcam, UK) diluted in 5% (v/v) FCS (Sigma) and covered with parafilm for 1hr at room temperature; Negative control slides received FCS only. After primary antibody incubation, slides were washed in PBS (2X 5min).

Three drops of post primary solution (Leica) were applied and incubated for 30min followed by washed with PBS for 5min then after three drops of polymer (Leica) were added and incubated for 30min then washed with PBS for 5min. Sections were stained with DAB chromagen solution for 2X 5min, followed by a wash in H_2O for 5min. Sections were counterstained with Mayer's haematoxylin for 10sec to contrast the blue colour of negative nuclei, blued in tap water, then rinsed in H_2O for 5min. Sections were dehydrated with ethanol (70% 5min; 90% 5min; 100% 5min) finally dipped in xylene for 3min and mounted with glass coverslips using DPX mounting medium.

2.4.3 Spatial localisation of p63

The antibody p63 (Anti p63 antibody, rabbit polyclonal [N2C1] Gene Tex, USA) was utilised to visualise stem cells within the horse hoof tissue (Carter et al., 2011). Immunohistochemical staining was performed on the tissue collected, processed and sectioned as described above (Sections 2.2 and 2.2.1) using p63 antibody (Gene Tex). Sections were incubated first in the oven at 60˚C for 15min, then immediately dewaxed in xylene for 5min, rehydrated via a series of graded ethanol periods (100% 5min; 90% 5min; 70% 5min) then rinsed in dH_2O for 5min.

Antigen retrieval was performed by heating microwave in 10mM sodium citrate buffer solution pH6.0 was applied for 5min medium high, then reduced to medium low for 5min and later cooled at room temperature for 20min followed by rinsed in H_2O for 5min. Specimens were incubated with peroxidase block (Leica), two drops/each slide for 30min at room temperature, followed by washing in PBS 2X 5min. Protein block (Leica) were added to all sections and incubated for 30min. Sections were then incubated with primary antibody p63 (Gene Tex) diluted 1:500 in 5% (v/v) FCS and covered with parafilm for 1hr at room temperature; Negative control slides received FCS only. Following primary antibody incubation, slides were washed with PBS 2X 5min.

Three drops of post primary solution (Leica) were applied and incubated for 30min followed by washed with PBS for 5min then after three drops of polymer (Leica) were added and incubated for 30min then washed with PBS for 5min. Sections were stained with DAB chromagen solution for 2X 5min, followed by a wash in H_2O for 5min. Sections were counterstained with Mayer's haematoxylin for 10sec, blued in tap water then rinsed in H_2O for 5min.

Sections were dehydrated with ethanol graded (70% 3min; 90% 3min; 100% 3min) finally dipped in xylene for 3min and mounted with glass coverslips using the DPX mounting medium. Sections were taken throughout the tissue and two sections photomicrographed using systematic random sampling (20X. DM 5000 B, Leica, Germany). Five systematic random photomicrographs were taken from each tissue section. This immunostaining enabled visualisation of proliferating (stained brown) vs non-proliferating cells (stained purple). Every cell was counted and identified as either proliferating or non-proliferating using Fiji J software (Wikimedia Foundation Inc., USA) that identified the brown colour positive cells first, then identify blue negative cells around and further away from the dermal papillae.

Results were recorded for every photomicrograph and the mean±SEM was calculated for each sample using Excel software and graphs constructed using GraphPad software (Prism).

2.5 Statistical analysis

2.5.1 H&E

Sections were taken throughout the tissue and three sections photomicrographed in their entirety (5X, Leica). Five photomicrographs were taken of each section. This stain enabled the space between the basement membrane and the end of stained tissue at the coronary tissue to be manually measured and also the number and length of dermal papillae from dorsal quarters and heels hoof regions. Measurements were calculated using calibrated a Fiji J software. Thirty measurements were performed on each image (Figure 2-1), measuring the space between basement membrane and cell keratinization (the area where the nucleus

are just start disappeared), dermal papillae length, and the space between the basement membrane and the end of middle layer (coronary region) of hoof wall at dorsal, quarter medial and lateral and heel medial and lateral regions.

These measurements were recorded as mean±SEM and calculated for each sample using Excel software and GraphPad software (Prism).

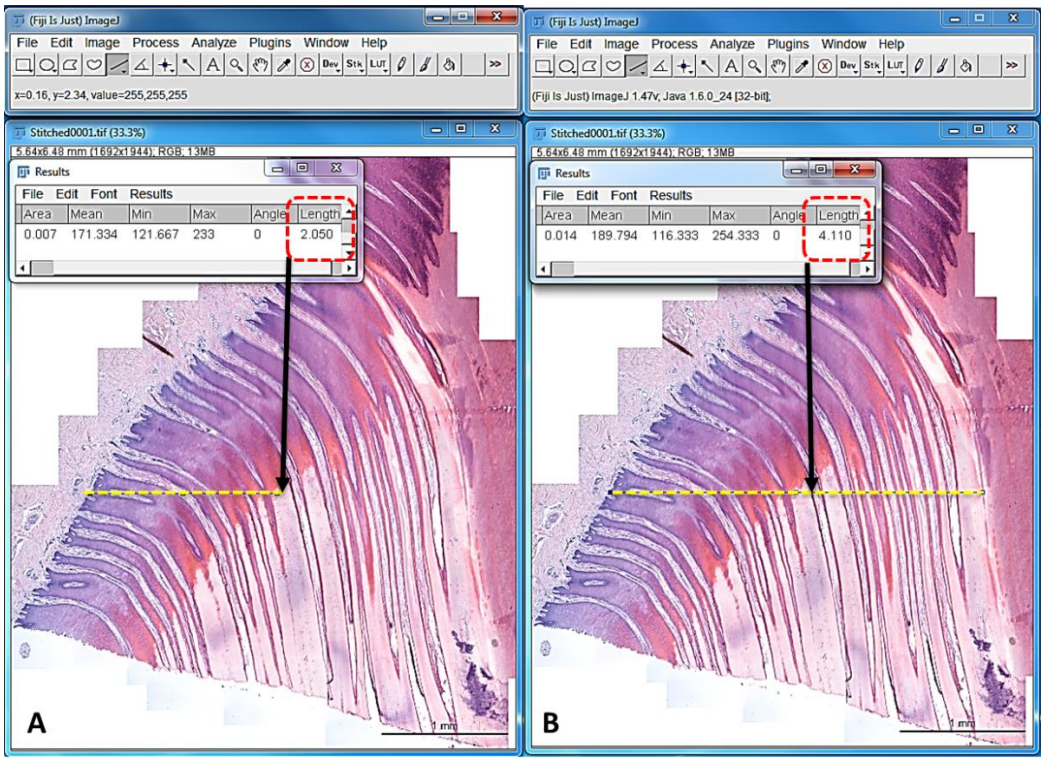


Figure 2-1: Schematic illustrating the epithelial thickness calculation

Schematic diagram illustrates how the photomicrograph images were processed through Fiji software and then were used to measure the thickness of coronary region of equine hoof. A) Shows the results of the distance measured between the basement membrane and the area where the cells start keratinization which was labelled in the yellow line. B) Displays the measurements between basement membrane and the end of middle layer (coronary region) of hoof wall marked as well in yellow line. This measurement was repeated 30 times along the whole thickness of epidermal coronary region. Scale bar represents 1mm.

2.5.2 Measuring hoof wall thickness and comparison with H&E data

Thirty two Equine hooves samples were studied via a helical computed tomography (CT scan) from the pastern joint to the ground surface of the hoof capsule (Keane et al., 2017). Prior to scanning, the hooves were thawed at room

temperature for 48hrs, then the examination was performed with a scanner (Universal Medical Systems, Sutton Bonington Campus, Bioscience building, Phoenix v| tome | xm 240, GE Sensing and Inspection Technologies, GmbH, Germany) at 125kV and 320mA with a 120µm slice thickness (resolution) on power 40 using focus standard in the transverse orientation. The segmented geometry was imported into a mesh generation software package.

The acquired CT images were then imported into a Fiji J software (Wikimedia Foundation Inc., USA) that was able to analyse 2D stack of images and enabled 3D reconstruction. The measurements of hoof wall thickness (middle layer) from the images emerged from the micro CT scan were achieved by Miss Sophie Taylor (MRes, The University of Nottingham) and the photomicrographs measured by the author of this thesis.

Measurement of the dorsal wall thickness was carried out using two-dimensional images in the YZ plane. Thereafter, CT scan images were imported using Fiji ImageJ software, corrected for the orientation of the slices by rotation or flipping the slices. Thereafter a rectangular field of view shape was selected Figure 2-2B.

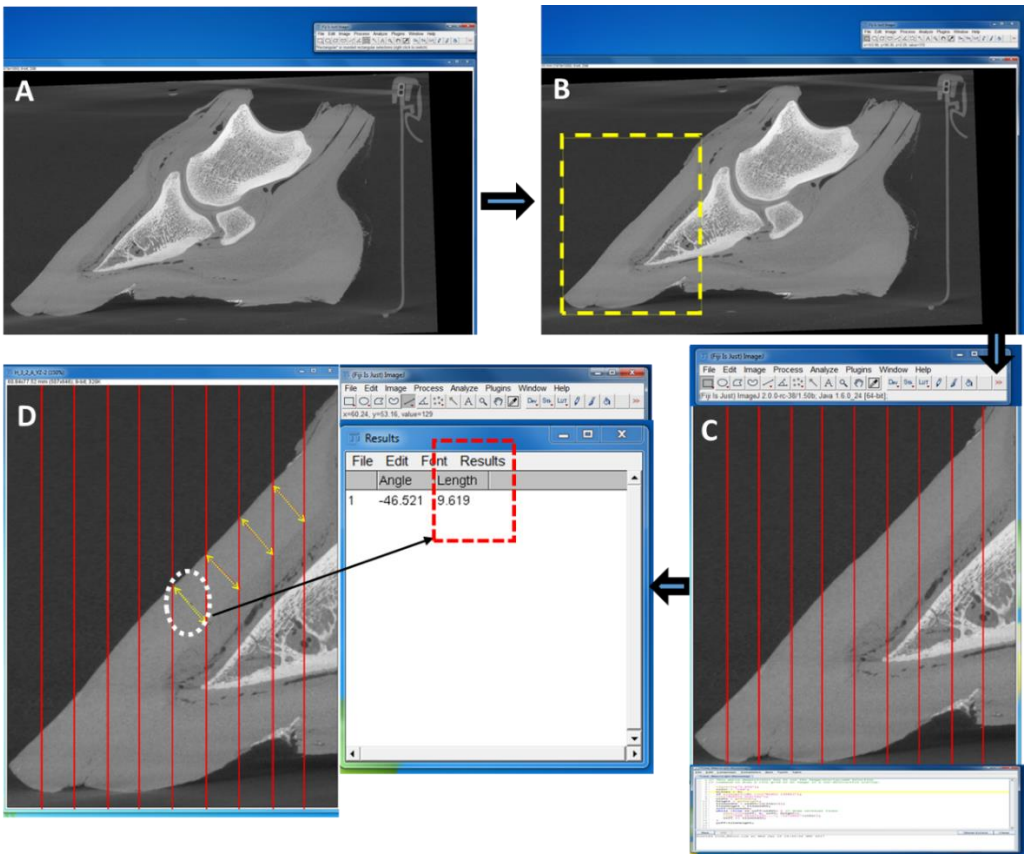


Figure 2-2: The process for hoof wall thickness calculation by CT scan

Example of dorsal hoof wall thickness measurement using Fiji software. A) Shows Fiji software and a CT scan equine hoof image. B) Determination the area of interest, which is marked with a yellow square line. C) Illustrates how vertical lines were set along the whole image. D) Represents the macro line used to draw the vertical lines, whereas yellow arrows display a perpendicular line draw on each point along the edge of the hoof capsule, representing the thickness of hoof wall which appeared in the red square.

The solar border was positioned on the bottom left angle and the coronary region in the top right angle. Nine equidistant vertical straight lines were drawn using a grid overlay macro. Thereafter, perpendicular lines were plotted from external wall surface and grid line to the dero-epidermal junction. Measurements were carried out using the same software Fiji image J and then imported to Microsoft Excel sheet, which was used to calculate the average of ten measurements, calculated. The same method was used to measure wall thickness at the quarter regions.

The wall thickness data were compared with data calculated from measuring the epithelial thickness at the coronary region for the same hooves that were used for measuring the hoof wall thickness using CT scan images (Figure 2-3A).

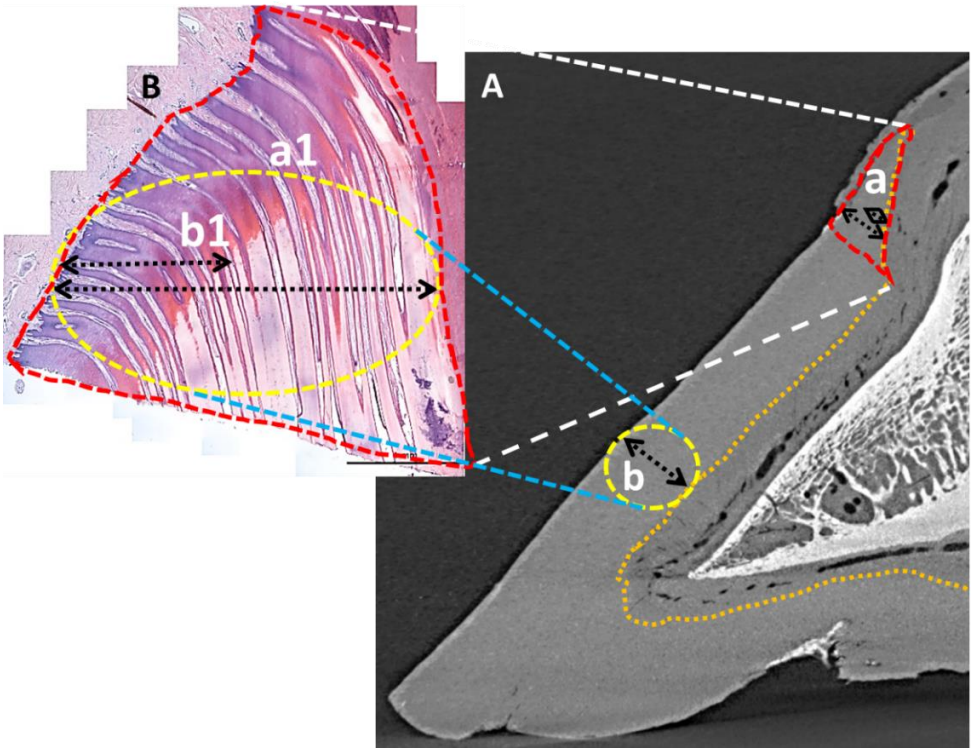


Figure 2-3: Schematic showing the link between hoof wall and coronary thickness

Illustration of how CT scan images were compared with photomicrograph images from the data that was calculated at the coronary region and hoof wall region. A) CT scan hoof image (a) represents the location of coronary region on the CT image, whereas (a1) displays the same region using a photomicrograph image; (b) CT scan hoof wall thickness encircled with yellow line and marked with black arrows, whilst (b1) shows epithelial thickness at the coronary region marked with black arrows. B) Illustrates a photomicrograph image for the coronary region. Scale bar represents 1mm.

The purpose of this comparison was to demonstrate the correlation between the thickness of active epithelial cells (keratinocytes) at the coronary region and the hoof wall thickness. This was carried out because the epithelial cells at the coronary region are the cells that form the stratum medium or the hoof wall.

Histological data shown in this thesis were compared against both of these measurements. The method was carried out using Fiji image J software

(Wikimedia Foundation Inc., USA), (Figure 2-3) illustrates the different step involved in the calculation of hoof wall thickness (stratum medium). Both the CT scanning measurements and the histological photographic measurements were assessed within this thesis.

2.5.3 Change in cell size

Sections for different horses hoof showing the entire dermal papillae were selected throughout the tissue and three sections photomicrographed in their entirety (20X, Leica). Twenty photomicrographs were taken for the entire papillae and then stitched using the Leica microscope software. Seven images were selected from seven regions along papillae. Thirty measurements for each image were carried out using Image Pro software (Image Pro Plus).

The H&E stain enabled the boundaries of cell surface area and nuclei to be measured alongside the lengths of dermal papillae from each tissue section. Measurements were performed by drawing around the surface area of entire keratinocyte and its nuclei, and the two dimensions of cell and nuclei in their long and short axis (Figure 2-4).

Measurements were carried out on the space between two papillae (middle region) and on the cells that were attached to the basement membranes of dermal papillae. These measurements were recorded as mean±SEM and calculated for each sample using Excel software and GraphPad software (Prism).

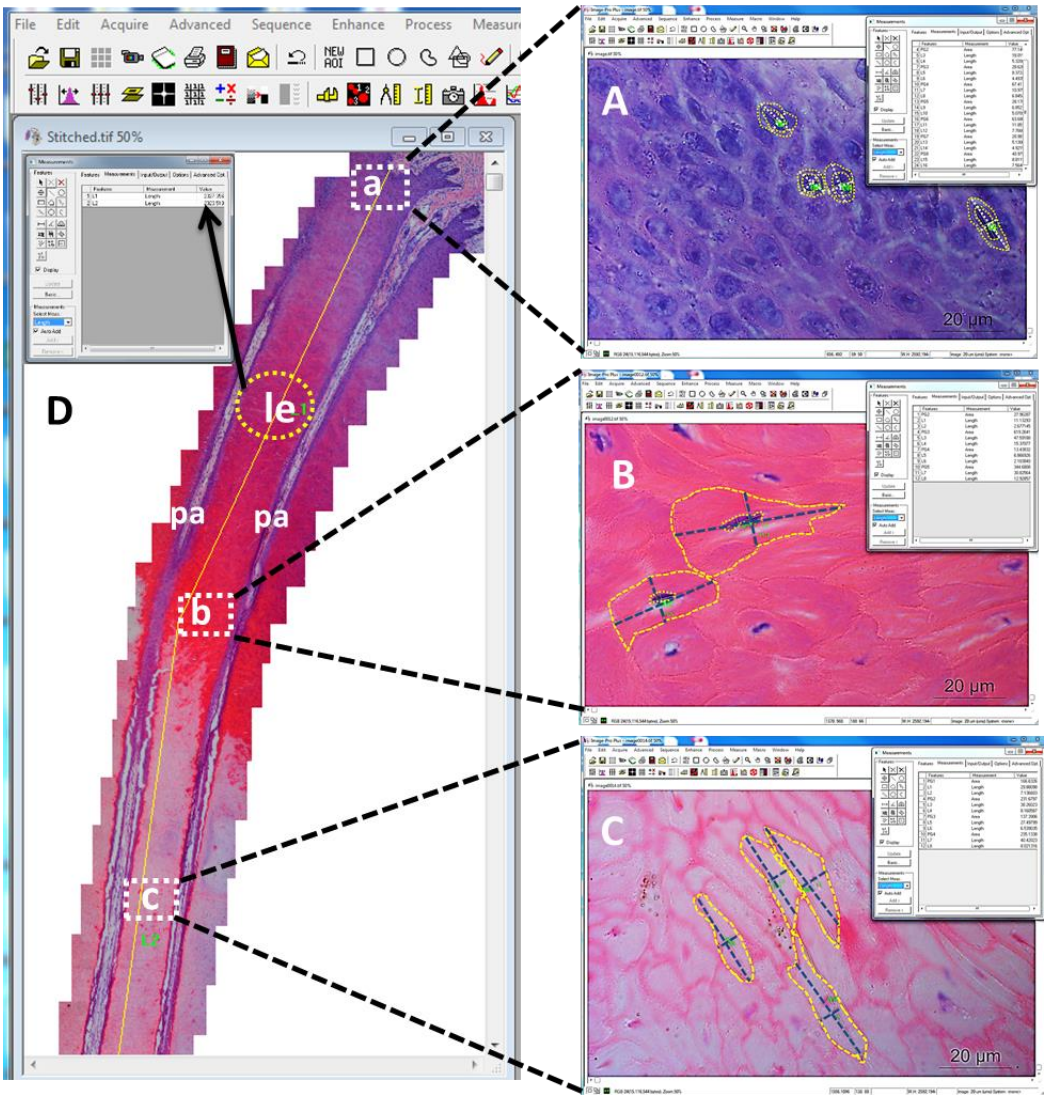


Figure 2-4: Determination of cell size calculation along the dermal papillae

Photomicrograph images were processed through Image Pro software and used to measure the changes in cell size. A) Image Pro software was used to measure the cell size for keratinocytes (nucleus surface area, long and short axis nucleus, cell surface area, long and short axis cell) at the (a) proximal part of dermal papillae close to the basement membrane. C, D) Show a similar process was also used, but at (b) middle and (c) distal region of dermal papillae. D) Represents the stitched images for the entire two papillae. le= length results shown in Excel (black arrow). pa= dermal papillae. Scale bars represent 20µm.

2.6 PAS

Sections were taken throughout the tissue and three sections photomicrographed (5X, Leica). Five photomicrographs were taken from each section. Five basement membrane thicknesses were manually measured on photomicrographs using calibrated Fiji J software. Basement membrane thickness mean±SEM were recorded and calculated for each sample using Excel software and GraphPad software (Prism).

2.7 Counting cells of proliferation PCNA, Ki-67 & stem p63

Sections were taken throughout the tissue and three sections photomicrographed in their entirety (20X, Leica). Five photomicrographs were taken for each section. This stain enabled visualisation of proliferating (stained brown) vs non-proliferating cells (stained purple). Every cell was manually counted and identified as either proliferating or non-proliferating and recorded for every sample. The mean±SEM was determined using Excel software and GraphPad software (Prism).

2.8 Immunofluorescence for coronary hoof sections

2.8.1 Keratin 14 and p63 using paraformaldehyde fixed tissue

Paraffin embedded tissue sections from the coronary region, (8µm) were used to identify expression and tissue localization of keratin K14 and anti-p63 antibody utilizing an immunofluorescence technique as described by Robertson et al. (2008).

Optimisations were carried out to ensure appropriate antigen retrieval. Slides were incubated in the oven at 60˚C for 30min and then transferred immediately for dewaxing twice in xylene for 3min (including 10sec agitation at each solution change), thereafter rehydrated using 100%, 90%, 70% ethanol, dH_2O and PBS with 10sec agitation followed by a 5min incubation for each step. Antigen retrieval was heated by electric microwave in 10mM sodium citrate buffer solution pH 6; applied for 18min at medium low and later cooled at room temperature for 20min followed by rinsed in dH_2O for 5min. All of the following incubations are at room temperature.

Sections were pre-treated with 5% (v/v) FCS (Sigma) for 30min to reduce non-specific binding of the antibody. Thereafter, the samples were incubated first with primary rabbit polyclonal antibody to p63 (GeneTex) at a dilution of 1:500 for 1hr, then washed in PBS 3X 5min. This was followed by an incubation with a secondary antibody Alexa Fluor 594 goat anti-rabbit IgG (Molecular Probes, Inc. USA) for 30min used at a dilution of 1:1000 then washed in PBS3X 5min.

Secondly, sections were further incubated for 1hr in primary mouse monoclonal anti-cytokeratin 14 antibody ([LL002] Abcam, UK; 1:50), then washed in PBS 3X 5min and followed by Alexa Fluor 488 rabbit anti-mouse IgG (Molecular Probes,

Inc. USA) used at a dilution of 1:1000 then washed in PBS for 3X5min (negative control slides were received only on both incubation with Alexa Fluor secondary antibody). Afterwards, specimens were counterstained with DAPI (Fluroshield with DAPI, Sigma, USA). Microscope coverslips were then mounted on each slide and samples were preserved short term at 4°C. Images were acquired with a digital camera on a fluorescence microscope (20X Mag. DM 5000 B, Leica, Germany).

2.8.2 Epidermal basal of keratin marker 14

Paraffin embedded tissue sections (8µm) of coronary region, were used to identify spatial localization of keratin K14. Slides were incubated in the oven at 60˚C for 30min and then transferred immediately for dewaxing in xylene twice for 3min each, following that tissue was rehydrated using 100%, 90%, 70% ethanol, dH_2O and. Antigen retrieval was performed via electric microwave, in 10mM sodium citrate buffer solution pH 6; applied for 18min medium low and later cooled at room temperature for 20min followed by rinsed in dH_2O for 5min. All following incubations are at room temperature. Sections were pre-treated with 5% (v/v) FCS (Sigma) for 30min to reduce non-specific antibody binding. Thereafter, sections were incubated first with primary mouse monoclonal anti keratin 14 antibody (Abcam) at a dilution of 1:50, for 1hr, then washed in PBS 3X 5min and followed by Alexa Fluor 488 rabbit anti-mouse IgG secondary antibody (Molecular Probes) used at a dilution of 1:500 then washed in PBS 3X 5min. Negative control slides were received only Alexa Fluor secondary antibody. Methyl green was used as a counterstain for nuclei. It was prepared by dissolving 0.5% (w/v) Methyl green (MP Biomedicals, LLC, France) in 0.1M sodium acetate (Corning, USA) and

adjusted to pH 4.0 with acetic acid. This stain was applied for 1min at room temperature, and then washed for 3X 3min in dH_2O. Thereafter, specimens were counterstained with DAPI in mounting media (Fluroshield with DAPI, Sigma, USA). Microscope coverslips were then mounted on each slide and the samples were preserved at 4ºC until imaging. Images were acquired with a digital camera on a fluorescence microscope (20X, Leica). Keratin expression was measured in a semi-automative manner using Image-Pro and the percentage mean±SEM were recorded and calculated for each sample using Excel software.

2.9 Apoptosis

Cellular proliferation and apoptosis are frequently associated with each other when regulating the mitotic cell activity through the regulatory factors and stimulating apoptosis (Alenzi, 2004), therefore apoptotic rates have an important influence on growth rates. The TUNEL test has been validated for use in epidermal tissue of equine hoof lamellae (Faleiros et al., 2004), therefore this technique was used in the hoof samples. The protocol provided by the manufacturer was followed for apoptosis assessment using peroxidase staining of paraffin-embedded tissue.

DNA fragmentation was determined using a commercial kit (Apoptag Peroxidase kits, ApopTag™, USA). Tissue sections were deparaffinised using xylene 3X 5min, and rehydrated with a series of alcohol solutions, 100% 2X 5min, 95% for 5min and 70% for 3min and washed in PBS for 5min. Specimens were pre-treated with 10mM sodium citrate buffer pH 6 for 3-5 cycles of 3min each in a microwave oven (refilled with fresh buffer between cycles), then washed in dH_2O

for 5min, and then treated with 20µg/ml (Proteinase-K) for 15min at room temperature, then washed in dH_2O for 2X 2min.

Endogenous peroxidase was quenched by applying 3.0% hydrogen peroxide (H_2O_2) for 5min at room temperature and rinsed in PBS for 2X 5min. Equilibration buffer was directly applied to the specimen (75µl for each slide) for at least 10sec at room temperature, then excess liquid was tapped off. Thereafter, 100µl working strength TdT enzyme (Terminal Deoxynucleotidyl Transferase) was added to each slide and incubated in a humidified chamber at 37˚C for 1hr.

The section of negative control, tissue was not incubated with TdT. Specimens were placed in a coplin jar containing freshly made stop wash buffer, agitated for 15sec, and then incubated for 10min at room temperature, followed by washing in PBS for 3X 1min.

After warming the aliquot of anti-digoxigenin at room temperature, 65µl was applied to each specimen surface area and incubated in a humidified chamber for 30min at room temperature, then washed in PBS for 4X 2min at room temperature. DAB-peroxidase substrate solution (3,3́-Diaminobenzidine, Sigma-Aldrich, UK) was applied for 10min at room temperature. Slides were washed three times in dH_2O for 1min each, and incubated for 5min in dH_2O. Methyl green was used to counterstain nuclei (0.5% (w/v) Methyl green (MP Biomedicals) in 0.1M sodium acetate (Corning) pH 4.0. This stain was applied for 10min at room temperature, then washed 3X in dH_2O in a coplin jar, by dipping the slide 10 times each in the first and second washes, and for 30sec without agitation in the third wash, followed by washing the specimen in 3 changes of 100% N-Butanol (1-Butanol, Sigma-Aldrich, Germany) in a coplin jar dipping the slide 10 times each in the first and second washes, and by 30sec without agitation

in the third wash. Slides were dehydrated using xylene for 3X 2min, then mounted under a glass coverslips in DPX mounting media (Sigma). Slides could then be stored indefinitely at room temperature.

2.10 Isolation of epidermal cells from equine hoof at coronary dermal papillae

Twenty equine hooves were collected in total for cell isolation (four legs were regularly collected every two months to perform cell isolation and then cell culture experiments) from the F. Drury and Sons Ltd, Swindon slaughterhouse. Ethical permission was given by The School of Veterinary Medicine and Science ethical committee. The clinical signs/case histories of the animals were examined by official vet surgery in the slaughterhouse to confirm the health of the horse.

Instantly following slaughter, hooves were disarticulated at fetlock joint and placed in a large box filled with wet ice and transported back to The University of Nottingham (3hrs). In the laboratory, hooves were cleaned thoroughly with a brush soaked in bacteriostatic soap (Persil, Unilever, UK). Then, hooves were washed in 10% bleach (Mexcel Thick Bleach, Scientific Laboratory Supplies, UK) for 3min. The hair at the coronary regions was clipped and shaved, and the skin was re-cleaned with bacteriostatic soap and washed in 10% bleach for 1min, followed by 70% ethanol for 3min. Hooves were then wrapped with cleaned cotton soaked with 70% ethanol and transferred directly to a clean and disinfected laminar flow hood class 1 (Bassaire IS Clean air, P4HBs/p, UK). A sterile blade was used to make three cuts in the dorsal region of coronary hooves at the level of the coronary band, and then carefully each small piece of hoof wall was elevated with a hoof clipper to expose the coronary tissue. Each piece of coronary tissue

was trimmed separately to expose the area of interest that contained the dermal papillae (Figure 2-5). A number of optimisations were carried out on coronary hoof tissue until successful isolation of the progenitor keratinocytes from the coronary dermal papillae was achieved as described in Figure 2-5. The dermal papillae tissues (soft tissue) were dissected from the hoof wall (hard tissue) which was discarded. The dermal papillae tissues were then rinsed with PBS with 5% (v/v) antibiotic/antimycotic (Gibco, UK) in 50ml falcon tubes for 1hr.

Thereafter, each piece of dermal tissue was cut into small pieces 0.25-0.5cm^3 and immediately transferred to a 15ml tube containing 0.25% trypsin-ethylenediamintetraaceticacid (EDTA) (Gibco, UK) solution and incubated at a room temperature for 18hrs. Subsequently, the epidermis was mechanically detached from the underlying dermal tissue using fine thumb forceps were used to grasp and hold the dermal papillae from its base and this was carried out on a heated stereomicroscope (Leica M125 connected with Leica MC190 HD, Germany) provided with heat plate 37ºC and laminar flow hood class1 (Bassaire IS Clean air, P4HBs/p, UK). Thereafter, the finger shapes projection dermal papillae were discarded and the epidermal tissues separated were transferred directly to a petri dish containing collagenase digest. Then a second enzymatic with 0.1% (w/v) collagenase type-1 (Sigma) was performed in incubator at 37˚C for 2hrs (see Appendix 8.3). The cell suspension and epidermal tissue were filtered through a cell strainer (cell strainer 40µm nylon) with 50ml tube. A piston was employed to help the tissue separation and filtered through a cell strainer. Following cell suspension, the solution was centrifuged at 300g (Heraeus Megafuge 11R Centrifuge, Germany) for 5min at room temperature. After that the supernatant was discarded, and the resulting cells were resuspended in 6ml of

stromal medium (DMEM-F12, 10% (v/v) FCS, 1% (v/v) antibiotic/ antimycotic solution) and approximately 5x 10^3 cells/cm^2 per flask seeded on collagen coated (tissue culture flasks 25cm^2 screw cap with filter, TPP, Switzerland). Cells were then incubated overnight (37˚C, 5% CO2; CO2 Incubator, MCO-18AIC (UV), Sanyo, Japan). Medium was refreshed the following day and subsequently every 2-3 days.

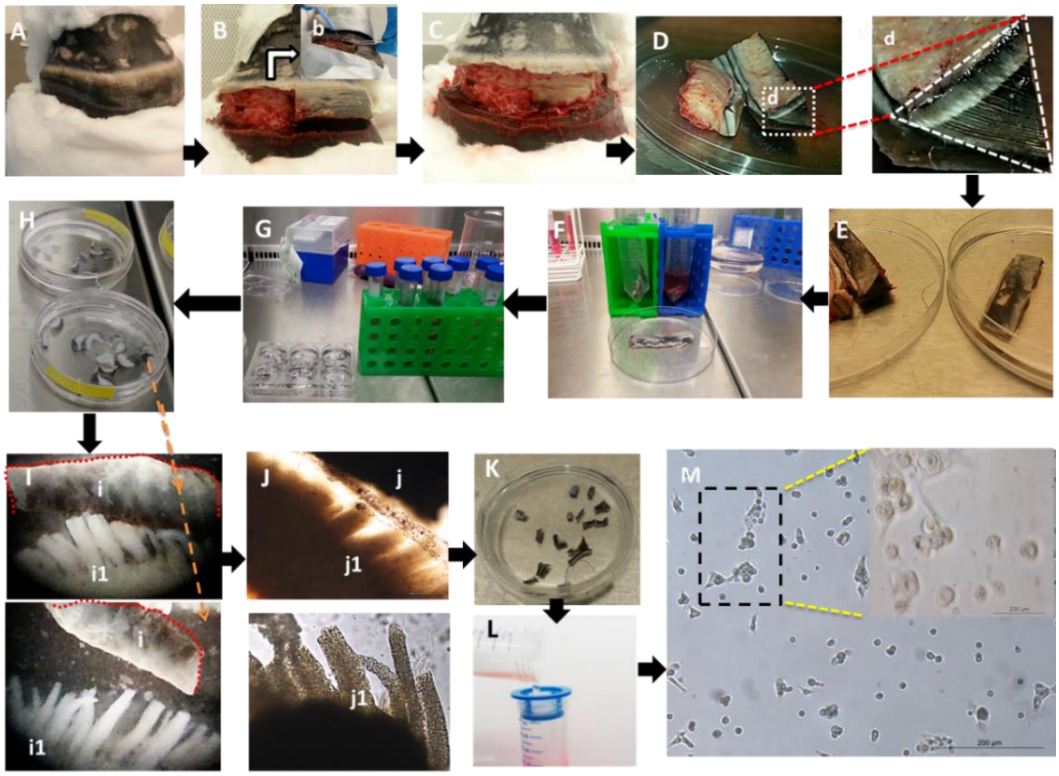


Figure 2-5: Schematic illustrating the isolation of progenitor keratinocytes

Preparation of the equine hoof and tissue extraction steps in order to isolate progenitor keratinocytes from the dermal papillae at the coronary region. A) Equine hoof cleaned, shaved and disinfected. B) Represents the area of coronary region that was extracted (b) the method that used for extracting the coronary tissue. C) Coronary region was removed. D) Coronary region trimming (d) represents the area of interest that contains the dermal papillae. E) Illustrates how the dermal papillae (soft tissue) was separated from the hoof wall (hard tissue). F) Soft tissue was then washed with 5% antibiotic antimitotic in PBS and incubated in falcon tubes for 1hr. G) Tissues were trimmed into small pieces 0.25-0.5cm^2 and incubated in 0.25% trypsin-EDTA for 18hrs. H) Shows the tissues were transferred for a new petri dish for further separation under the stereomicroscope. I) Illustrates the completely separation of (i) epidermal cells from (i1) the finger like projection dermal papillae. J) Demonstrates how (j) the epidermal cells was transferred to the next step and the rest of tissue (j1) dermal papillae was then discarded. K) Shows that the epidermal cells were incubated with 0.1% collagenase type-1 for 3hrs in an incubator. L) Cell suspension was filtered using a cell strainer to remove any tissue debris and then seeded the cells in culture flask. M) Photomicrographs illustrate after first day of culturing cells. Scale bar represents 200µm.

All cultured cells were collected on day 7-9 of culture upon reaching 80% confluence, the adherent cells were trypsinized with 0.25% trypsin-EDTA (Gibco, UK) post-seeding and cultured onto a tissue culture flask (Nunc Easy flask 75cm and 175cm, Thermo Scientific, Denmark) in DMEM-F12 to initiate second and third passages. In order to confirm the purification of keratinocytes, isolated cells were examined through three passages. These were carried out and repeated every time for each animal (N=3). This allowed identifying the maximum pluripotency on each passage. Additionally, cells were have three types of growing; first one cells were fully grown, second type cells were grown for first passage and differentiated and the third were directly differentiated after isolated and cultured. All the experiments were performed at day 8-10 from first type of culturing cells to ensure they still had maximum pluripotency.

2.11 Immunofluorescence on culture keratinocytes

Optimisations were carried out to ensure appropriate permeability of cell membrane and to obtain a high efficiency of antigen antibody reaction. The medium was first removed from the 6-well plate, and then washed with PBS. Immediately, the culture cells on coverslips were fixed with 4% (w/v) PFA for 10min at room temperature. The PFA was then discarded, and the wells washed with PBS for 3X 5min. Thereafter saponin solution (0.15 % (w/v) Saponin, MP Biomedicals, LLC, France) was added and incubated on plate shaker (Gyro-rocker, Stuart, UK) for 1hr. Afterwards, the Saponin was removed and the cells were incubated with protein blocking 2% (w/v) BSA (Fisher Scientific, USA) for 1hr at room temperature. Thereafter, the cells were incubated first with first primary antibody, which were used and are listed in Table 2-2:

Table 2-2: Primary antibodies used in immunofluorescence protocol

Antibody	Working solution	Description	Cat.No.	Company
Ki-67	1/250	Rabbit polyclonal	ab66155	Abcam
CD44	1/200	Rabbit polyclonal	ab157107	Abcam
KRT10	1/300	Rabbit polyclonal	CSB-PA012504LA01HU	CUSABIO and CusAb

All antibodies were diluted in 2% (w/v) BSA and incubated for 1hr at room temperature, and then cells were washed in PBS for 3X 5min. This was followed by incubation with an Alexa Fluor 594 goat anti-rabbit IgG diluted 1:1000 (Molecular Probes, Inc. USA) for 30min then washed in PBS for 3X 5min. different wells were incubated for 1hr in second primary antibody, which were used depending on each experiment and are listed in Table 2-3:

Table 2-3: Second primary antibodies were used in immunofluorescence protocol

Antibody	Working solution	Description	Cat.No.	Company
K14	1/200	Mouse monoclonal	ab7800	Abcam
HIF-1α	1/250	Mouse monoclonal	ab8366	Abcam

These antibodies were also diluted in 2% BSA. Afterwards, cells were washed in PBS 3X5min and then incubated in Alexa Fluor 488 rabbit anti-mouse IgG diluted 1:1000 (Molecular Probes, Inc. USA).

In some wells, F-Actin was localised and this was performed by adding 2 drops of F-Actin (Actin Green™ 488 Ready Probes™, Molecular Probes, USA) for 30min, then washed in PBS for 3X5min (in all experiments with immunofluorescence protocol, Negative control slides were incubated with only Alexa Fluor secondary antibody).

Afterwards, fine thumb forceps were used to carefully remove the coverslips from each well and cells were then immediately counterstained with one drop of DAPI (Fluroshield with DAPI, Sigma, USA).

Microscope coverslips were then mounted on each slide and boundary of the coverslips were sealed with clear nail varnish to prevent it moving and to avoid the cells dehydrating over time. The samples were wrapped with aluminium foil preventing light exposure and preserved at 4°C. Images were acquired within two days to ensure good fluorescence intensity on a fluorescence microscope (40X Mag. DM 5000 B, Leica, Germany).

The same procedure was carried out on the cells after they were cultured for 3 and 5 days. Triplicate experiments were carried out and ten photomicrographs were taken from each well. Florescent intensity was measured and assessed for each photomicrograph using Image Pro software (Figure 2-6), and the percentage mean±SEM were recorded and calculated for each sample.

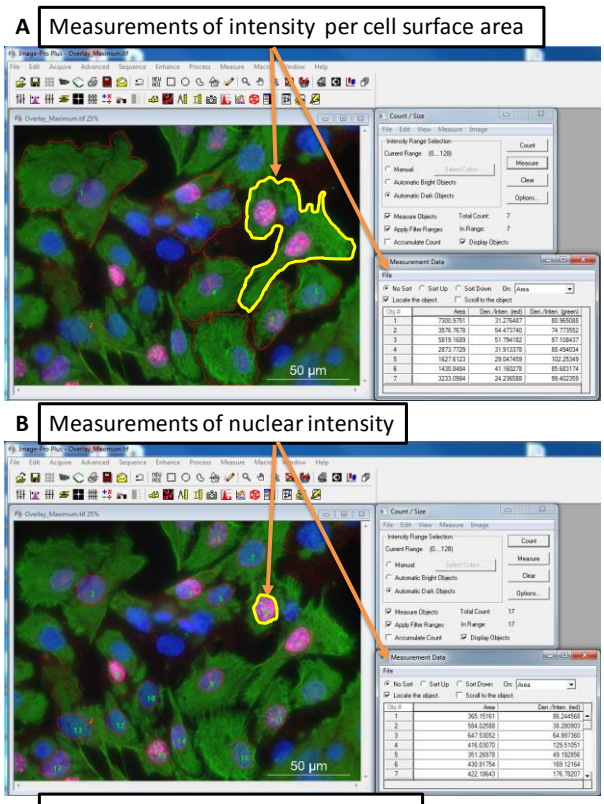


Plate	FOV	measure	Day	Oxygen	HIF-1α	Area	Den./Inten.(R)	Den./Inten.(G)	nuclei	Intensity (R)/area	Intensity (G)/area	hypertrophy index	Intensity/nuclei .(R)	Intensity/nuclei(G)
1	fov1	1	1	1%	low	1989.973	21.735	56.61825	2	0.020187	0.049945	1122.663	13.0162327	34.15352244
1	fov2	2	1	1%	low	889.8	25.62216	46.88635	2	0.030764	0.057197	600.4064	16.72663547	30.14384974
1	fov3	3	1	1%	low	1035.69	27.52022	53.07586	2	0.028691	0.057534	626.8869	16.31696337	28.88761369
2	fov4	4	1	1%	low	1063.765	24.85456	41.32585	2	0.024651	0.040983	567.5759	13.17697511	21.20898283
2	fov5	5	1	1%	low	1085.346	19.98057	39.80195	1	0.018916	0.037131	812.1059	14.95735086	28.44771795
2	fov6	6	1	1%	low	1034.481	17.6483	40.54089	2	0.021736	0.053675	794.6945	12.9144726	28.25972311
3	fov7	7	1	1%	low	1287.119	23.13255	51.57375	2	0.027906	0.070317	909.9088	14.84185651	32.90340286
3	fov8	8	1	1%	low	1087.06	27.09663	66.16913	2	0.034693	0.088184	550.0461	13.4765329	33.00922732
3	fov9	9	1	1%	low	1036.067	16.97235	43.21327	1	0.018865	0.047587	861.5385	12.75912691	33.49921485
3	fov10	10	1	1	low	1259.042	14.55299	49.57666	2	0.012489	0.042726	849.6325	10.04736106	33.3655342

Figure 2-6: Schematic showing measurement fluorescence intensity of EPKs

A) Shows measurements the intensity of cell surface area. B) Illustrates the measurements of nuclear intensity of cell nuclei. C) Shows the data categorised after averages each measurement.

2.12 Osteogenesis differentiation

Progenitor keratinocytes were isolated and cultured as described in (Chapter 2.10) and triplicated each time (N=3). The protocol provided by the manufacturer was followed for osteogenesis differentiation (StemPro® Osteogenesis Differentiation Kit, Gibco, UK). After 8 days in culture (the first passage (P1)), cells were washed with PBS and trypsinized using 0.25% trypsin-EDTA (Gibco). Afterwards, cell viability was determined and total cell density using Trypan blue

stain (Thermo Scientific, UK) and haemocytometer. Cells were seeded into 12-well culture plates at density 5×10^3 cells/cm^2. Cells were committed to the differentiating protocol to generate osteocytes using osteogenesis differentiation medium and incubated at 37°C and 5% CO_2 and medium was replaced every 2 days for 19 days. Control culture plates were seeded at the same density and time, instead of differentiating medium the cells were incubated with medium DMEM-F-12 media with L-glutamine, 15 mM HEPES, sodium bicarbonate (Sigma-Aldrichand, UK) and 1% (v/v) antibiotic/antimycotic (Gibco, UK) and 10% (v/v) FCS, Sigma, UK). After 15 and 19 days of culture, cells were fixed using 4% (w/v) PFA for 10min at room temperature and then washed carefully with dH_2O for 3X 5min. Cells were then stained with 1% (w/v) alizarin red stain pH 4.2 for both plates that were incubated with differentiating medium and growth medium for 10min at room temperature with carefully shaking. Thereafter the stain was removed and wells were washed for 3X 5min with dH_2O. Immediately images were taken for the cells directly and images were acquired within the same day using a digital camera on a fluorescence microscope (40X, Leica).

2.13 The role of insulin in culture keratinocytes

Primary equine keratinocytes were isolated from the coronary region and cultured for 8 days with medium (Dulbecco's Modified Eagle's Medium/Nutrient Mixture F-12 Ham with L-glutamine, 15 mM HEPES, sodium bicarbonate, and 1% (v/v) antibiotic/antimycotic and 10% (v/v) FCS, as described in Chapter 2.10. Keratinocytes were trypsinized and seeded into 12-well culture plates at a density of 2×10^5 cells/well containing glass coverslips for 24hr. Cells were then starved for 24hrs in medium DMEM-F-12 containing 1% (v/v) FCS. Thereafter, cells were stimulated with bovine insulin (Sigma, USA) at concentrations 0.1µg/ml or 1µg/ml for 30min, 1hr, 2hrs, 8hrs, 24hrs and 48hrs in preparation for immunostaining. In order to investigate cell proliferation, cells were labelled with anti-Ki-67 antibody and for keratin protein using K14 as described previously in Chapter 2.10. In addition to that, investigations were carried out on cell signalling pathways connected to cell proliferation. Cells were incubated for a short time and stimulated by insulin at 1µg/ml for 30min, 1hr and 2hrs. Thereafter Western blot was utilised as described in Chapter 2.18. Control cells remained untreated with insulin over the experimental times.

2.14 Mechanical cell stretching

Primary equine keratinocytes were isolated from coronary region and cultured with medium (Dulbecco's Modified Eagle's Medium/Nutrient Mixture F-12 Ham with L-glutamine, 15mM HEPES, sodium bicarbonate (Sigma-Aldrich), and 1% (v/v) antibiotic/antimycotic (Gibco) and 10% (v/v) FCS (Sigma) as described in Chapter 2.10. Keratinocytes were seeded at a density of 2×10^5 cells/well on six-well flexible silicone rubber BioFlex™ plates coated with collagen type I, (Flexcell International Corporation, Hillsborough, NC, USA).

Cells were seeded for 24hrs before mechanical stretch was applied for two phenotypes, the first one was seeded directly after cell isolation and then 24hrs was left before applying stretch whilst the second was seeded after 8 days from cell isolation. Mechanical tension at ~65% was applied using 16mm marble (Figure 2-7). The cultures plates were divided into three groups; (1) incubated with 20µM Blebbistatin (inhibitor of non-muscle myosin II, Abcam, UK) for 24hrs and then removed before mechanical stretch was applied, (2) incubated with the inhibitor whilst undergoing cell stretching, (3) incubated without Blebbistatin at all. The cell cultures were incubated in a humidifying incubator at 37°C and 5% CO_2. In addition to applying tension for shorter periods of time 30min, 1hr and 2hrs before cells were prepared for the Western blot. In addition, tension was applied for longer periods of time for 1, 3 and 5 days in preparation for both Western blot and immunofluorescence techniques. Immediately, cells were trypsinized and protein extracted as described in Chapter 2.18 for Western blot or stained with immunofluorescence as described in Chapter 2.10. Control cells were seeded on the same plates and in the same incubator without being subjected to stretch (Figure 2-7).

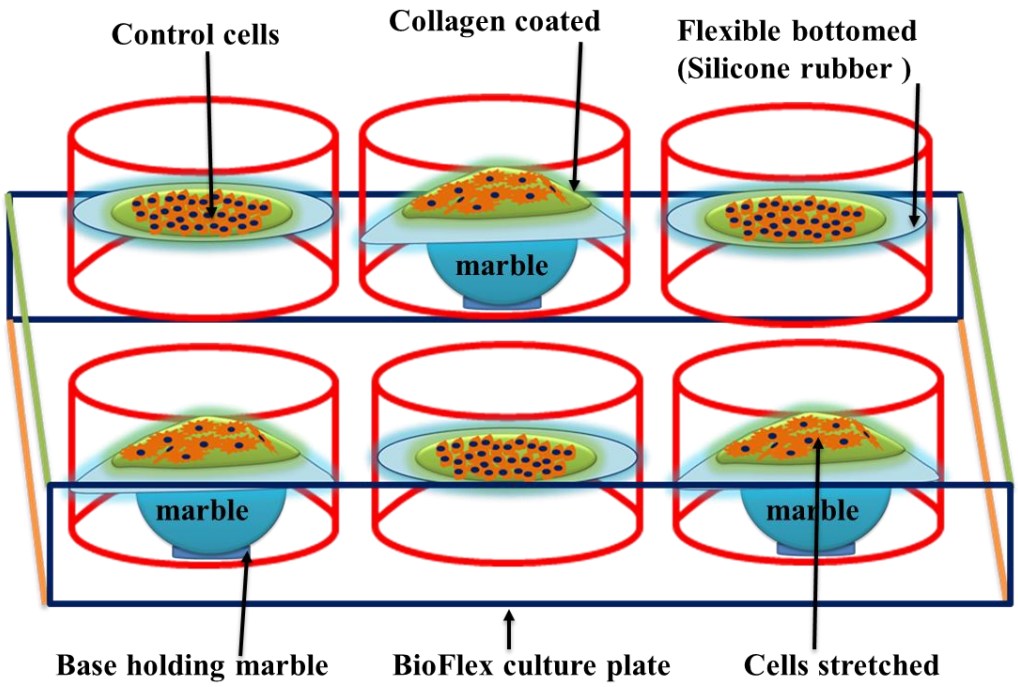


Figure 2-7: Schematic showing culturing cells in mechanically active environment

The application of mechanical tension on equine keratinocytes cultured in collagen coated BioFlex plates. Three zigzag wells show control cells without applying tension stretch while the second three zigzag wells show applying mechanical tension using a marble with a diameter of 16mm.

This experiment was performed on isolated EPKs cultured directly on deformable BioFlex culture plates pre-coated with collagen just after isolation. The aim was to investigate whether the strain on cells (i.e. proportional to the stretch) had any impact on the differentiation/proliferation of EPKs. Note that the term 'stretch' is defined as a stress (typically a force per unit of surface area) that is proportional to the strain applied via an elastic modulus. In the experiments, measuring the exact 'stretch' (i.e. the magnitude of the stress) is not possible. However knowing the typical elastic moduli of cells (100-1000Pa, see Table 2-4), it is possible to estimate the stress knowing the strain applied. In this context, we shall use the terms 'stretch' and 'strain' in an indifferent way.

Table 2-4: Elastic modulus (Y) of living cells in culture conditions measured using atomic force microscopy (AFM).

Cell origin	Y (Pa)	References
Epithelial pancreatic cancer cells (Panc-1)	100-500	(Walter et al., 2011)
Mouse embryonic carcinoma stem cells neurons (P-19)	200	(Spedden et al., 2012)
Chick dorsal root ganglion neurons	500	(Spedden et al., 2012)
Rat cortical neurons	200	(Spedden et al., 2012)
Mouse fibroblast cells (NIH3T3)	100-1000	(Cai et al., 2013)
Mouse fibroblast cells (Balb/c3T3)	700-900	(Sirghi et al., 2008)
Epithelial oral cancer cells (UM1)	600-2000	(Zhou et al., 2012)

Therefore, to create a method that mimics what happens *in vivo*, the response of these cells, which are located on the basement membrane and responsible for hoof growth, to stretch was measured. A constant strain was maintained throughout the experimental runs. Prior to strain application, EPKs were seeded and cultured for 2days in the absence of stretch to allow for cell adherence to the pre-coated collagen area.

2.14.1 Estimation of strain application at the centre of the 'flexcell' culture plate

Application of strain was applied using a marble (Figure 2-8). The calculations were performed by Dr. Cyril Rauch to determine the impact of the relative homogenous dilation, only cells labelled on the red part of the flexcell were analysed. To determine the relative dilation one starts by determining the equation of the marble in 2D, i.e. $x^2 + (y - r)^2 = r^2$, where r is the marble radius. As a result, any tangent to the circle in the half space $y \geq 0$ has a slope determined by: $dy/dx = -x/\sqrt{r^2 - x^2}$. And in particular in '$m$' the tangent is: $(dy/dx)_M = -x_1/\sqrt{r^2 - x_1^2}$. The slope in '$m$' is also equal to the slope of the straight line joining 'n'to 'm' that is: $(y_1 - e)/(x_1 + R)$. In this context, it is

possible to determine a system of two equations to find the coordinates for $M=(x_1,y_1)$ that are:

$x_1^{\,2}+(y_1-r)^2=r^2$ and $(y_1-e)/(x_1+R)=-x_1/\sqrt{r^2-x_1^{\,2}}$. To determine the surface area in red, noted S, one sees that $S=\int_{y_1}^{2r}2\pi x\,dy$ where $x^2+(y-r)^2=r^2$.

Noting $\Delta S/S_0$ the relative dilation one finds:

$$\frac{\Delta S}{S_0}=2\left(\frac{1}{\tilde{x}_1}\right)^2\int_{\tilde{y}_1}^{2}\tilde{x}\,d\tilde{y}-1$$
$$\tilde{x}_1^{\,2}+(\tilde{y}_1-1)^2=1$$
$$(\tilde{y}_1-e/r)/(\tilde{x}_1+R/r)=-\tilde{x}_1/\sqrt{1-\tilde{x}_1^{\,2}}$$

With $\tilde{x}_1=x/r$ and $\tilde{y}_1=y/r$. Given $r=16mm$, $e=6.5mm$ and $R=16mm$ one finds $\Delta S/S_0\sim 65\%$.

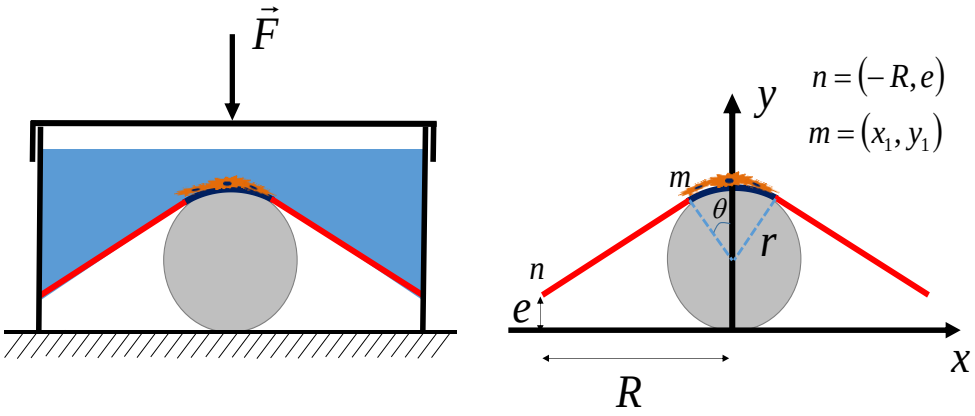


Figure 2-8: Schematic showing calculation of stretch loading on cultured EPKs

2.15 Hydrostatic pressure

Primary equine keratinocytes were isolated from the coronary region and cultured for 8 days with medium (Dulbecco's Modified Eagle's Medium/Nutrient Mixture F-12 Ham with L-glutamine, 15 mM HEPES, sodium bicarbonate, (Sigma-Aldrich) and 1% (v/v) antibiotic/antimycotic (Gibco) and 10% (v/v) FCS (Sigma) as described before in Chapter 2.10.

Keratinocytes were seeded into 12-well culture plates at the density of 2×10^5 cells/well containing glass coverslips (16mm diameter) for 24hr. Coverslips were transferred into the cap of a 50ml centrifuge tube (centrifuge tube was cut on its bottom and autoclaved to be used in this method), and then the tube was turned upside down and screwed into the cap (Figure 2-9).

The tubes were filled with medium at different levels: control cells filled up to 3ml (Pa= 99.081), while the second loading pressure up to 25ml (pa=495.405) and third up to 50ml (Pa= 990.81) for 1, 3 and 5 days and incubated in a humidified incubator at 37°C and 5% CO_2. Filter caps were then placed on the top of tubes and sealed with a para-film membrane to prevent contamination.

The loading hydrostatic pressure was calculated using the following equation and Table 2-5:

$$\boldsymbol{p = \rho g h}$$

$\boldsymbol{p}$= hydrostatic pressure

$\boldsymbol{\rho}$= density of a fluid (density of culture medium = 1010kg m^3 this was measured by weighing culture medium at 37ºC three times 1, 3 and 5days)

$\boldsymbol{g}$= gravitational acceleration ($9.81ms^{-2}$)

$\boldsymbol{h}$= height (m) Pressure (Pa)

Table 2-5: Table showing the calculation of hydrostatic pressure loading on cultured equine hoof keratinocytes

Control cells 3ml culture medium (1cm high)	Hydrostatic pressure 25ml culture medium (5cm high)	Hydrostatic pressure 50ml culture medium (10cm high)
$p = \rho g h$ =1010kg m^3*9.81ms^{-2}*(1cm/100) Pressure (Pa)= 99.081 kg/m s^2	$p = \rho g h$ =1010kg m^3*9.81ms^{-2}*(25cm/100) Pressure (Pa)= 495.405 kg/m s^2	$p = \rho g h$ =1010kg m^3*9.81ms^{-2}*(50cm/100) Pressure (Pa)= 990.81 kg/m s^2

The cells were committed to continuous hydrostatic pressure during the experimental time. Hydrostatic pressure was performed for both Western blot and immunofluorescence technique. Immediately, cells were trypsinized and extracted protein as described in Chapter 2.18 for Western blot and the coverslips were fixed and process as described in Chapter 2.11 for immunostaining. Additionally the relation between hydrostatic pressure and oxygen concentration was calculated in Appendix 8.5, which was assumed the amount of oxygen consumed per unit of cell surface area.

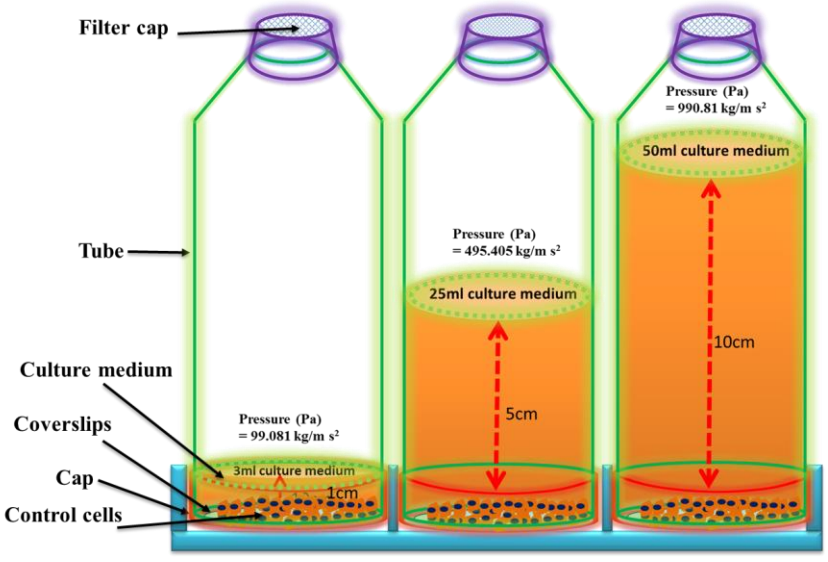


Figure 2-9: Schematic illustrating hydrostatic pressure applied on culturing cells

Diagram illustrates how the hydrostatic pressure was applied and calculated using different volumes of culture medium represented in three tubes. The first tube shows the control cells at minimum pressure which is Pa=99.081 kg/m s^2, while the second and third tubes were loaded hydrostatic pressure at Pa=495.405 kg/m s^2 and 990.81 kg/m s^2 respectively.

2.16 Culturing EPKs under low oxygen conditions

Primary equine keratinocytes were isolated from the coronary region and cultured for 8 days with medium (Dulbecco's Modified Eagle's Medium/Nutrient Mixture F-12 Ham with L-glutamine, 15 mM HEPES, sodium bicarbonate, (Sigma-Aldrich) and 1% (v/v) antibiotic/antimycotic (Gibco) and 10% (v/v) FCS (Sigma) as described before in Chapter 2.10.

Keratinocytes were seeded into 12-well culture plates at the density of 2×10^5 cells/well containing glass coverslips (16mm diameter) for 24hr. Triplicate experiments were performed using high oxygen conditions at 21% oxygen and low oxygen conditions at three different oxygen levels (5%, 3% and 1% O_2) for immunostaining as described before in Chapter 2.10. For further investigation, cells were cultured at the same time and the same level of oxygen for doing Western blot investigations as described in Chapter 2.18. In addition, cells were incubated at high oxygen condition 21% O_2 and at low oxygen condition 5% O_2 for 5hrs, 1day, 2days, 4days, and 6days for an investigation into gene expression analysis (see Chapter 2.17).

2.17 RNA extraction and quantification

2.17.1 RNA extraction

The protocol provided by the manufacturer instructions (RNeasy® Plus Mini Kit, Qiagen, Germany) was followed for RNA extraction from equine hoof epidermal papillae cell culture. The culture medium was first removed from the plates, and the cells were washed with for PBS which was then aspirated. The adherent cells (Keratinocytes) were then trypsinized and collected using 0.25% trypsin EDTA.

The cells 5 x 10^6 cells were and centrifuged at 300g for 5min, then the supernatant was removed and the cells washed with for PBS and re-centrifuged at 300g for 5min, then the supernatant was completely aspirated.

Immediately, a volume of 350µl lysis buffer RLT Plus was added to pelleted cells, followed by vortexing for 30sec. The lysed cells were then centrifuged for 3min at maximum speed. Then after, the supernatant was carefully removed by pipetting, and was placed in a new microcentrifue tube. A volume of 350µl of 70% ethanol was added to the lysed cells, and mixed by pipetting (without centrifuge).

Instantly, 700µl of the sample was then transferred including any precipitate to an RNeasy Mini spin column and placed in a 2ml collection tube, then centrifuged at 8000g for 15sec, followed by discarding the collection tube plus the solution. 350µl RW1 washing buffer was added to the RNase spin column and centrifuged at 8000g for 15sec, then the flow through was discarded. Afterwards, for further DNA removal from RNA, the spin column was treated with DNase I (RNase-free DNase set, Qiagen, Germany). This procedure was carried out to remove DNA contamination using DNase digestion following RNA.

DNase I stock solution was first prepared using the RNase-free DNase set. The RNeasy spin column membrane was directly incubated with 80µl DNase I at 24°C for 15min. Subsequently, 350µl RW1 wash buffer was added to the spin column and centrifuged at 8000g for 15sec, then the flow through was discarded.

The spin column membrane was then washed twice with 500µl buffer RPE, and centrifuged at 8000g using two different times, 15sec and 2min respectively, and on both times the flow through was discarded. After that, membrane drying was performed using an additional centrifugation at full speed for 1min. Finally, 35µl of RNAse-free water was directly added to the RNeasy spin column to elute RNA

(this method was carried out twice using the same volume of 35µl RNAse-free water in order to elute high concentration of RNA).

Following RNA extraction, the final total concentration of purified RNA was quantified using a NanoDrop8000 spectrophotometer (Thermo Scientific, UK) by UV absorption. A double blank of Nuclease free water and RNase free water was used to set the standard. The samples with A260/280 ratio reading 1.8-2.0 were used in the qPCR. Afterwards, dilution of the RNA with nuclease free water was calculated to obtain 0.1µg/µl total RNA for make reverse transcription. Then, the eluted RNA samples were stored at –80˚C.

2.17.2 Reverse transcription and first strand synthesis of RNA samples

RNA extractions from cell cultures were reverse-transcribed using SuperScript® III in a single tube. 0.1µg/µl of RNA samples were used in cDNA synthesis of all genes. Primer mix was prepared from mixing 1µl of 40µM of the primer A (GTT TCC CAG TCA CGA TCN NNN NNN NNN NNN NN) and 1µl of 10mM dNTP mix (Life Technologies, UK), and adequate nuclease free water to reach a total reaction volume of 13µl. The tubes were capped and placed in a thermal cycler (2720 Thermal Cycler, AB Applied Biosystems, Singapore), then heated to 65°C for 5min, after that transferred to ice for 1min. 7µl of a SuperScript III mix was added to each tube;

SuperScript III mix

1) 4µl Reverse Transcriptase (Invitrogen, USA).
2) 1µl of 0.1M Dithiothreitol (Invitrogen, USA).
3) 1µl of RNase Inhibitor (RNase out, 40U/µl, Invitrogen, USA).
4) 1µl of Superscript III reverse transcriptase (200U/µl, Invitrogen, USA)

Negative control was received the same conditions but without Superscript III. The mixture of the final volume was then placed on the same thermal cycler and incubated at 25°C for 5min, followed by 1hr at 50°C and the enzyme was finally deactivated by incubated at 70°C for 15min. The cDNA was then stored at -20°C to be use for PCR and real-time quantitative PCR (qPCR).

2.17.3 PCR

Polymerase chain reaction (PCR) was carried out on cDNA using a thermal cycler (2720 Thermal Cycler, AB Applied Biosystems, Singapore). Primers were used to amplify only equine-specific target genes and the housekeeping genes (Pinto, 2012, Aguiar et al., 2015). In order to amplify each gene, gene–specific primers (Table 2-6) were used for PCR amplification and for quantitative RNA using qPCR.

Table 2-6: Primers used for qPCR amplification of the ten segments equine keratinocytes gene, whereas GAPDH and β-Actin are housekeeping genes

Gene	Forward primer	Reverse primer	Amplicon sizes (bp)
GAPDH	5'–CAATGACCCCTTCATTGACC–3'	5'–GAAGATGGTGATGGCCTTTC–3'	133
β-Actin	5'–CGACATCCGTAAGGACCTGT–3'	5'–GTGGACAATGAGGCCAGAAT–3'	192
CD44	5'–CAGCACCCCTGCGGATGACG–3'	5'–TGGTCTTGGGTGGGGCGAGT–3'	114
CD29	5'–CCATTGTTCACGTTGTGGAG–3'	5'–TTGGCAAATTCCCTTCTGTC–3'	157
Keratin 14	5'–TACGAGACGGAGCTGAACCT–3'	5'–TGGCCTCTCAGGCTATTCAT–3'	179
Involucrin	5'–ACATCACAAAGCGGAAAACC–3'	5'–GAGCTTCTTCTCCTGTTCCA–3'	97
Integrin α6	5'–AGTCTGCACATCTTCTTCCTGA–3'	5'–CGCTCCAATCACTATATCTTGC–3'	122
Vimentin	5'–ACGTTCGTCAGCAGTATGAAA–3'	5'–GTTAGCAGCCTCAGAGAGGTC–3'	98
HIF-1α-1	5'–GACAAAGTTCACCAGAGCCTAA–3'	5'–CATTGACCATATCACTATCCACATC–3'	69
Keratin 10	5'–GGTTCAGTGGTGGCTCTTTTA–3'	5'–CCTAAGCTGCTGCTTCCATAG–3'	139

The volumes and final concentrations of constituents used in the PCR a presented in Table 2-7.

Table 2-7: Table showing the final concentration of constituents used in PCR reaction

Component	Volume	Final concentration
10X PCR Rxn Buffer (-MgCl2)	2.5 µl	-
dNTPs mix	0.25µl	25mM
MgCl2	1µl	50mM
Taq (DNA polymerase)	0.25µl	-
Forward primer	0.5µl	10µM
Reverse primer	0.5µl	10µM
Template cDNA	1µl (0.1µg)	_
Nuclease free water	To 25µl	_

The tubes were capped and incubated in a thermal cycler (2720 Thermal Cycler, AB Applied Biosystems, Singapore), then the following program was applied for PCR amplification:

Initial denaturation 1 cycle at 94^0C for 2min followed by 35 cycles of: denaturation at 94^0C for 30sec, annealing at 60^0C for 30sec (the annealing temperature was changed depending on the annealing temperature of each primer), extension at 72^0C for 30sec. Then, the final reaction was held at 72^0C for 7min, after that cooled down at 4^0C for 5min.

2.17.4 Agarose gel electrophoresis

The PCR amplification products were detected employing 70µg of 1% (w/v) agarose gel (Sigma) applied in the 70ml TAE buffer (TAE Buffer, Gibco, UK). The mixture was agitated and warmed microwave cooker at medium temperature

settings for 2min. The gel was then cooled to 55˚C, and 7µl Nancy (1µg/mlNancy–520, Sigma, UK) was added.

Followed cooling, the gel was transferred into a gel-casting tray, and a 10 well gel comb was placed, and then left for 45min to clot and set. The gel was placed in the electrophoresis tank. Running buffer (TAE buffer) was added into the tank up to 3mm over the gel, then after the comb was carefully pulled out.

The samples were then prepared for loading by adding 8.5µl of PCR product and 1.5µl of 6X loading dye (New England BioLabs, UK). A 1 kb bp DNA ladder (New England BioLabs, UK) was first loaded in one of the side well, then the negative control and the samples. The lid was positioned on the gel tank and the electrical current applied at 90 V for 60min, afterwards, the gel was cautiously transferred from the tray and scanned under a UV trans–illuminator (Image Quant 300, Germany).

2.17.5 Quantification of target gene mRNA levels

Quantitative reverse transcription polymerase chain reaction (qRT-PCR) was carried out on cDNA using the SYBR green PCR kit (QuantiFast SYBR Green PCR Kit, Qiagen, Germany). Primers were created that were complementary to the gene of interest in order to amplify a region >200 base pairs (200bps).

This method uses a molecule (SYBR green) which binds to double stranded DNA to produce a fluorescent signal thus allowing the quantification of gene expression. A serial dilution of a cDNA sample was created (5ng, 1ng, 0.2ng, 0.04ng, 0.008ng, and 0.0016ng) in order to create a standard curve to calculate the efficiency of the primers (Appendix 8.4). The final volumes and concentrations of constituents applied in the qPCR were demonstrated in Table 2-8.

Table 2-8: The volume and final concentrations used in running qPCR protocol

Component	Volume for light cycler 96 well	Final concentration
2X QuantiFast SYBR Green PCR Master Mix	12.5µl	for
Forward primer	0.7µl	10µM
Reverse primer	0.7µl	10µM
Template cDNA	2µl (1ng)	_
RNase-free water	To 25µl	_

The amplification real time cycler conditions were initiated by a PCR activation step at 95ºC for 5min, and then denaturation (two-step cycling) 95°C for 10sec. Followed by, 40 cycles (combined, annealing and extension) at 95°C for 10sec and at 60°C for 30sec (The same primers were used to amplify equine-specific target genes and the housekeeping genes).

Thereafter, melting curve was analysed using software of real-time cyclers (LightCycler®480 Software release 1.5.0, Roach, Germany). The Ct (cycle threshold) data was transferred to Excel sheet (Ct represents the number of cycles required for the fluorescent signal to cross the threshold). Following this gene, expression values were normalised using Pfaffl's method (Pfaffl, 2001).

$$Ratio = \frac{(E_{target})^{\Delta CP\ target\ (control\text{-}sample)}}{(E_{ref})^{\Delta CP\ ref\ (control\text{-}sample)}}$$

Mathematical equation illustrating how the method was used in calculation gene expression. In this method, expression of target gene was calculated against a control in contrast to a reference gene.

$\boldsymbol{E_{target}}$ = efficiency of target gene

$\boldsymbol{E_{ref}}$ =efficiency of reference gene

$\Delta\boldsymbol{CP_{target}}$=CP (crossing points) deviation of the control - sample of the target gene

$\Delta\boldsymbol{CP_{ref}}$=CP (crossing points) deviation of the control - sample of the reference gene

2.18 Proteins extraction, quantification, and Western blotting

2.18.1 Proteins extraction

The protocol provided by the manufacturer (NE-PER Nuclear and Cytoplasmic Extraction Reagents, Thermo Scientific, USA) was followed for nuclear and cytoplasmic proteins extraction. Cells were gently washed with for PBS buffer then incubated with 0.25 trypsin-EDTA for 3min, then trypsinized cells were collected and centrifuged using a microcentrifuge at 500g for 5min. After that, cells were washed by resuspending the cell pellet in PBS. 20µl packed cell volume (equivalent to $10x10^6$ cells, which equal to 20mg cell pellet volume) was isolated and transferred to a 1.5ml microcentrifuge tube and a pellet formed by centrifugation at 500g for 3min.

Promptly, supernatant was carefully removed and discarded using a pipette to leave the cell pellet as dry as possible (all centrifugation steps were performed at 4°C and the cell samples and extracts were preserved on ice).

100µl of ice-cold CER I (Cytoplasmic Extraction Reagent I (CER I), Thermo-scientific, USA) was added to the cell pellet and vortex the tube vigorously on the highest setting for 15sec to ensure fully resuspended the cell pellet, then the tube was chilled on ice for 10min. Then after, 5.5µl of ice-cold CER II (Cytoplasmic Extraction Reagent II (CER II), Thermo-scientific, USA) was added to the tube and vortex the tube on the highest setting for 15sec. Then the tube chilled on ice for 1min, vortex the tube was repeated for another 15sec and centrifuged at maximum speed in a microcentrifuge (16000g) for 5min (the first two reagents cause disruption to cell membrane and release of cytoplasmic contents). The supernatant (cytoplasmic extract) was instantly transferred to a clean pre-chilled

tube and placed on ice until completion of the nuclear protein extraction, in order to carry out for both protein quantification.

Immediately, the insoluble pellet fraction, which contains nuclei, was resuspended in 50µl of ice-cold NER (Nuclear Extraction Reagent (NER), Thermo-scientific, USA) and continues vortexing the tube on the highest setting for 15sec every 10min chilling on ice for a total 40min. The tube was then centrifuged at 16000g for 10min, and then the supernatant (nuclear extract fraction) was immediately transferred to a clean pre-chilled labelled tube and placed on ice. The supernatant volume of both cytoplasmic and nuclear extraction was quantified and calculated their total protein in the next step.

2.18.2 Protein Quantification

The procedure of standard microplate protocol for protein quantification was followed by the instructions of the manufacturer (Coomassie Plus (Bradford) Assay Kit, Thermo-Scientific, USA). Preparation of diluted albumin standard (Thermo Scientific, USA) was first performed by diluting the contents of one albumin standard ampule into eight 1.5ml micro-centrifuge tubes. Each 1mL ampule of albumin standard was sufficient to prepare a set of diluted standards.

Coomassie plus reagent solution (Thermo Scientific, USA) was immediately mixed before use by gently inverting the bottle ten times to mix the solution without shaking it, and then the amount of reagent needed was removed and equilibrate it to room temperature before use. 5µl of each standard or blinded sample were added into the appropriate microplate wells (Thermo Scientific 96-Well Plates, USA), each diluted standard and sample were triplicated. Then, 150µl of the coomassie plus reagent was added to each well and incubated at

23°C for 10min at 250 rpm (rotation/minute) in a thermomixer (BioShake iQ - Quantifoil Instruments GmbH, Germany). Thereafter, each plate was removed from the thermomixer and the absorbance measured at 595nm wavelength with a plate reader (FLUOstar OPTIMA, BMG-LABTECH, Germany). Protein concentration of each sample was determined from the standard curve by plotting the average absorbance for each albumin standard versus its concentration in using Microsoft Excel synchronised with OPTIMA software (OPTIMA, Germany).

2.18.3 Polyacrylamide gel preparation for protein electrophoresis

Polyacrylamide gel electrophoresis protocols were followed using the instructions of the manufacturer (TGX™ FastCast™ Acrylamide Kit 10%, Bio-Rad, USA).

0.75 mm glass plates (Glass plates, Bio-Rad, USA) were first cleaned with dH_2O and ethanol. Glass plates were vertically assembled, aligned, and held in the casting stand with spacer plate on top of it, then placed in casting frame, and tested with dH_2O to ensure no leaks during the gel casting process.

Acrylamide kit 10% (w/v) SDS contains four solutions (A-Resolver and B-Resolver; A-Stacker and B-Stacker). Therefore, to prepare one gel, 2ml of resolver (A) solution was added to 2ml of resolver (B) solution, then, 2µl N,N,N´,N´-tetramethylethane-1,2-diamine (UltraPure™ TEMED, Thermo Fisher, USA) and 20µl of freshly made 10% (w/v) ammonium persulphate (Fisher Scientific, Belgium) were added and mixed.

The final solution was then pipetted thoroughly and carefully, and added into the cassette (filled to 1cm below bottom of comb teeth) the space left by the comb was refilled with isopropane to prevent gel drying and left for 30min until fully polymerised. Once set, stacking gel acrylamide solution was prepared by

combining 1ml stacker A and 1ml stacker B solutions which was added to 2µl TEMED and 10µl 10% (w/v) APS and then mixed. Then, the solution was filled to the top of the short glass plates. Thereafter, the comb was carefully aligned and inserted into the cassette to prevent air from being trapped beneath the comb teeth. The gel was then left to polymerise for 30min. After that, the cast gel was either used directly or covered with a paper towel wetted with dH_2O and stored in a sealed plastic bag at 4°C for less than 2 weeks. Protein samples (20µg) were prepared by adding 7µl protein sample buffer (10% (v/v) β-mercaptoethanol, (Sigma, UK), in Laemmli Sample Buffer, BIO-RAD, UK), then made up with water, afterwards were boiled at 100˚C for 7min.

In order to determine the optimum concentration of protein sample, an optimisation trial was first carried out with different concentrations including 15, 20,25,30,35 and 40µg respectively (Figure 2-10).

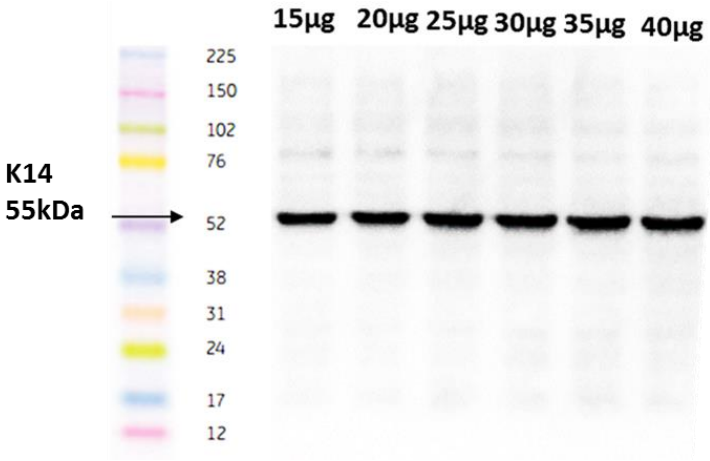


Figure 2-10: An example on optimisation the concentration of K14 protein loading

Serial keratin protein K concentration was used with different concentrations ranging from 15µg to 40µg. This method enabled the use of the optimum concentration loading protein.

The gel cassette sandwich was then first placed into electrode assembly and closed clamping frame cams, after that the electrode assembly was positioned into electrophoresis chamber assembly (Western gel tank). Afterwards, 200-250ml of

running buffer (Tris-Glycine SDS Running Buffer, Novex, USA) was added to the mini tank, and loading guide (Bio-Rad's patented sample loading guide) was then placed over the mini tank between the two gels in the electrode assembly.

The samples were loaded using pipette tips into the spaces of the loading guide to fill the corresponding wells. The first well was always loaded with 5µl molecular weight marker ((molecular weight marker 12000-225000Da) Amersham™ ECL™ Rainbow™ Marker, UK) and subsequent wells were loaded with samples. Following sample loading, the chamber assembly was filled with maximum for running buffer, and then the led was placed and inserted the electrical leads into power supply (Power Pac™, Bio-Rad, USA). Power was then applied on the gel and electrophoresed at constant 200V for 40-50min.

2.18.4 Protein transfer

PVDF membrane (PVDF Transfer Membrane, 0.45µm, Thermo Scientific, USA) was instantaneously activated by incubation in methanol for 15min prior to transfer and after that washed with transfer buffer (Tris-Glycine Buffer, Bio-Rad, Germany) for 3min. Blotting papers were wetted in transfer buffer. Once the electrophoresis was completed, gel cassette was removed from the gel tank and washed with dH_2O. The gel was then removed from cassette sandwich by slightly splitting the two plates of the gel cassette. Thereafter, gel was equilibrated with transfer buffer and prepared in a blotting paper.

The sandwich was then transferred to electroblotter for protein transfer (Semi-Dry Transfer Cell, Bio-Rad, USA). Membrane blotting was carried out at 25V for 50min. The membrane was carefully removed and tested with Ponceau stain (BDH Chemicals Ltd Poole, England) for 1min using gyro-rocker (Stuart, UK),

after that the membrane was first washed with dH2O, then in TBST (Tris-buffered saline, 0.1% (v/v) Tween (Tween 20®, France) 3X 5min.

2.18.5 Western blot

Once protein transfer had been achieved the membrane was incubated with blocking solution 5% (w/v) BSA in TBST solution (Tris-buffered saline tween-20) for 1hr at room temperature using the gyro-rocker. After blocking, the membrane was directly incubated with primary antibody ((Table 2-9) see also Appendix 8-6 for specificity of antibody) overnight at 4ºC using roller mixer.

Table 2-9: Primary antibodies used for Western blot

Antibody	Size (kDa)	Working solution	Cat.No.	Company
B-actin	42	1/100000	GTX110564	GeneTex
K14	55	1/3000	ab7800	Abcam
K10	60	1/2000	CSB-PA012504LA01HU	CUSABIO
Akt (pan)	60	1/3000	C67E7	Cell Signalling Technology
Phospho-Akt	60	1/1000	Ser473	Cell Signalling Technology
CD44	82	1/2000	ab157107	Abcam
B-catenin	92	1/3000	D10A8	Cell Signalling Technology
HIF-1α	92	1/3000	ab8366	Abcam

The next day, the membrane was washed for 3X 5min in TBST, followed by incubation in a secondary antibody (Table 2-9) for 1hr. The secondary antibody was diluted with 5% (w/v) skimmed dried milk (Marvel, UK) in TBST. Thereafter, the membrane was washed with for TBST 3X 5min each.

Table 2-10: Secondary antibodies used for Western blot

Antibody	Working solution	Cat.No.	Company
Anti-mouse IgG, HRP-linked Antibody	1/10000	7076	Cell Signalling Technology
Anti-rabbit IgG, HRP-linked Antibody	1/10000	7074S	Cell Signalling Technology

2.18.6 ECL detection

Luminol-based enhanced chemiluminescent substrate (SuperSignal™ West Femto Maximum Sensitivity Substrate, Thermo Scientific™, USA) was used to detect horseradish peroxidase (HRP) on immunoblots.

This procedure was carried out by first preparing working solution from mixing equal volume of the stable peroxide solution and the luminol/enhancer solution in new pre-child tube (100µl was used from working solution per cm^2 of membrane). Western blot membrane was covered with working solution for 5min. The blot membrane was then removed from the working solution and the excess reagent drained. The blot membrane was then placed in clear plastic film and wrapped and expose to imaging system as described in Chapter 2.18.7.

2.18.7 Image acquisition with imager

Western blotmembrane was placed on the black chemiluminescence exposure box and close the imager door. The exposure box was connected with a camera (Photex Camera, Photek HRPCS-3PSU, Germany) and computer. Photic software was turned on and the ‘imager acquires’ function was selected. The imager calculates was then displayed with the exposure time with maximum dynamic range and minimum pixel saturation. The acquired image was captured and saved in named file. The acquired images were then imported into a Fiji J software (Wikimedia Foundation Inc., USA), which then enabled quantification of each protein band in all samples again using this software. After that, the data were transferred to Excel spreadsheets and then the ratio of each protein in sample was calculated in relation to the housekeeping protein β-Actin.

2.19 Measuring hoof angle

All the hooves were given an identification number and photographed (using a digital camera Canon, Japan) from three aspects; the lateral, medial and frontal view. The photographs were used to illustrate the counter of the dorsal wall and to display the angle of quarter areas for analysis. Photographs were taken from the same distance and against the same background to avoid any opacity or artefacts which might change the images. The images were then imported into a Fiji J software (Wikimedia Foundation Inc., USA) that is able to measure the dorsal hoof angle (Figure 2-11).

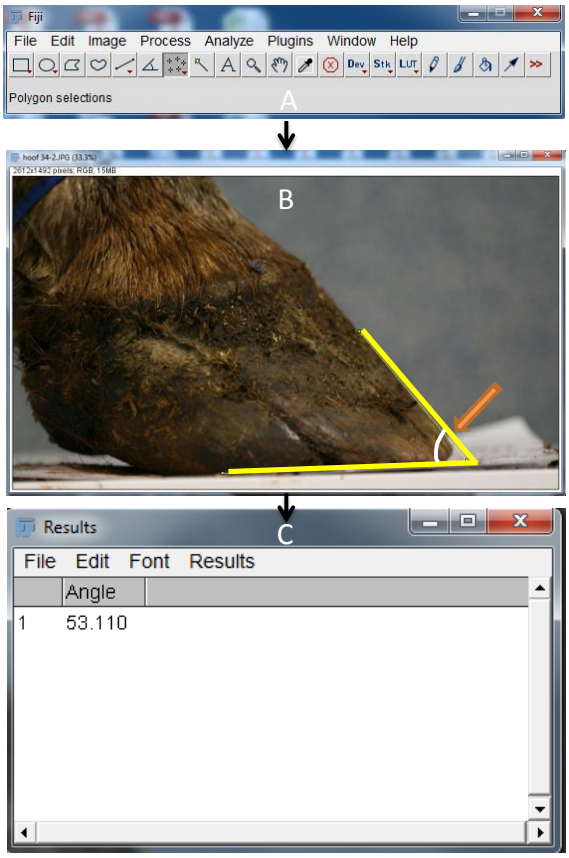


Figure 2-11: The process for hoof angle calculation

Schematic diagram illustrates how the images were processed through Fiji software and then were used to measure the dorsal hoof angle. A) Shows Fiji software. B) Illustration hoof image (orange arrow indicates the yellow line was drawn for measuring hoof angle. C) Shows the result of hoof angle.

2.20 Measuring hoof curvature

The measurements of hoof curvature from the images emerged from the micro CT scan were performed by Miss Emily Paul (MRes, The University of Nottingham) and the gross anatomical measurements by the author of this thesis (Keane et al., 2017). Histological data shown in this thesis were compared against both of these measurements. The procedure was performed using Fiji J software (Wikimedia Foundation Inc., USA), Figure 2-12 shows the different step involved in the calculation of hoof curvature. In addition, the same method was applied in this study using photos obtained from the lateral side of equine hooves using a calibration of 1cm. Both the CT scanning measurements and the gross anatomical photographic measurements were assessed within this thesis.

Physical assessments for the hoof curvature were conducted through using micro CT scan images. This method was performed by a sequence of about 20 marks situated on a sagittal axis alongside the outer dorsal edge of the hoof capsule (Figure 2-12). Using the imaging software Fiji J, each mark was performed a set of coordinates to locate it on the hoof capsule in 2D. The coordinates were then imported into Excel and used to determine the curve of the hoof capsule using a non-linear polynomial regression. Then, the polynomial equation was a dimensioned using a dimension factor as the total length of the outer dorsal edge of the hoof capsule. It was then possible to calculate the average curvature of the hoof capsule using the following derivative formula:

$$C = \frac{[y].\frac{\hat{y}''}{[x]^2}}{\left(1+\left([y].\frac{\hat{y}'}{[x]}\right)^2\right)^{3/2}} \ .$$

[*C*, represents each point measured at the dorsal hoof wall surface, [y], [x] are the averages of y and x variables; $\hat{y}'$, $\hat{y}''$ are the primary and secondary derivatives of y variables, $[x]^2$ is mean square of x variables]

To re-dimension the curvature, the dimensioned curvature was multiplied by the dimensioned factor determined above.

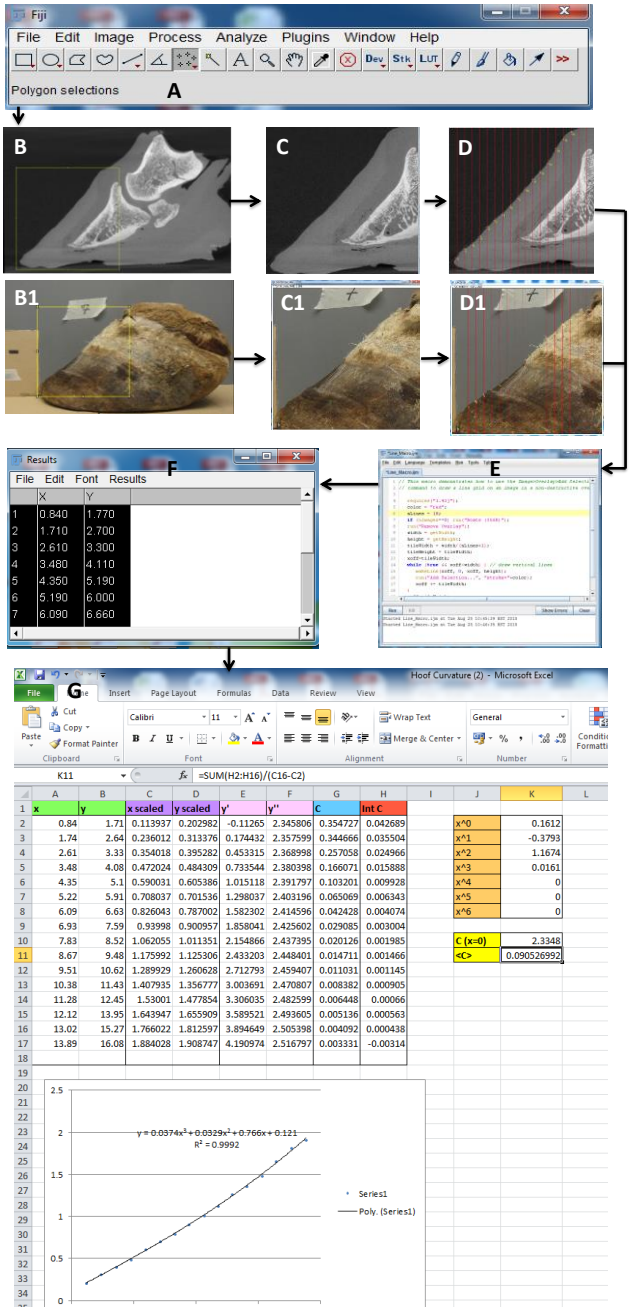


Figure 2-12: Schematic illustrating the process hoof curvature calculation

Schematic shows how the images were processed through Fiji software and then were used to measure the dorsal curvature of the hoof. A) Shows Fiji software. B) Illustration CT scan image. C, D) Represent duplicate image at first, then vertical lines was set along the whole image. B1, C1, D1) Show a similar method was also used, but with hoof photos. E) Represents the macro line was used to draw the vertical lines, whereas (F) display the measurements of each point along the edge of the hoof capsule. G) Shows the imported data to Excel software and the (X, Y) coordinates of the dorsal part of the hoof capsule were determined using Fiji from which was determined the curvature using the second derivative of the nonlinear regression of (X, Y) coordinates obtained using Excel.

The same method as described above was applied to measure the curvature of distal phalanx were each image imported to Fiji image J. Then, the image was cropped down to the extensor process on the right top of distal phalanx to solar margin on the bottom of distal phalanx. Followed by the grid and overlay macro were employed, and the points where line intersected bone measured. Both calculation of hoof and bone curvature were compared with histological data and assessed in this thesis.

2.21 Statistical analysis

Results are presented as mean±SEM using Excel software and all graphs were created using GraphPad software (Prism 6). Data obtained from counting PCNA, p63 and Ki-67 proliferating cells using immunohistochemistry and the data calculated from measuring the florescent intensity using immunofluorescence staining were analysed by ANOVA methods using statistical analysis software (IBM® SPSS® Version 22, USA) and the same software was used for examined the normality and homogeneity. In the One Way ANOVA test, the effects of dorsal hoof angle (hoof angle was measured using a Fiji J) and its interaction on the mean percentage of PCNA, p63 or Ki-67 positive proliferating cells in each region of the equine foot (dorsal, quarter medial, quarter lateral, heel medial and heel lateral) were calculated. Hoof curvature (hoof curvature was measured from acquired CT images using a Fiji J software, and its relation to the percentage of PCNA, p63 or Ki-67 positive proliferating cells in each region were evaluated using non-linear regression GraphPad software. For all experiments significant difference analysis was employed for comparisons, and significance was set at $P<0.05$.

Chapter 3

Histo-morphological structure of equine hoof growth

3.1 Introduction

The mammalian distal limb integumentary appendages for instance claws, nails, and hooves display enormous morphological variation, not specifically between distantly related mammalian, but as well among intimately related species at the same family (Hamrick, 2001, van Asperen, 2010), which is consequence of the adaptive development of the mammalian limb accompanying with the modification of foraging behaviours (Hamrick, 2001, van Asperen, 2012). The equine hoof was reported as the most complicated mammalian integumentary structure that can be considered an intemperate exposition of claw or nail morphogenesis (Wu et al., 2004). This complexity is specified entirely by the epithelial tissue of the dermal papillae that is located between soft tissue attaching weight bearing animal and hard tissue attaching hoof capsule (Thomason et al., 1992, Bragulla and Hirschberg, 2003). The dermal papillae constitute the middle hoof layer that is one of the biological materials recognised as being the most resistant to fractures (Kasapi and Gosline, 1997, Wang, 2016). The developing equine hoof dermal papillae exhibit some particular individualities which are relatively different from even-toed cattle or pigs and mostly different from those in the other homologous in digital end organs for example the nail and claw (Bragulla, 2003). Above all these animals, both canine and feline claw (Homberger et al., 2009, Bowden et al., 2009), and the avian claw (Van Hemert et al., 2012) have poorly developed dermal papillae in comparison to the most adaptive digital end organs in bovine, and, particular, the equine hoof (Bragulla and Hirschberg, 2003). This corresponds to the theory of homology in view of evolutionary history (Hamrick, 2001). The hoof compartments in terms of the stratum externum, medium and internum, in addition to sole region are similar to

those in hooves for example pigs or cows, or claw of the feline and canine, (Dellmann and Eurell, 1998, Eurell and Frappier, 2013), and also to those in the primate nail (Maiolino et al., 2016). These particular digital end structures can be outlined to certain structures that is enable to adapt to withstand different mechanical forces. As a consequent, this leads to generate a cornified layer which provides mechanical resistance, for instance the distal compartments of the common mammals (Bragulla and Hirschberg, 2003). As an example, equine capsular wall has a high rate of keratinization, which produces horn tubules (Reilly et al., 1998a, Eurell and Frappier, 2013). The function of these tubules, therefore, has a great influence on the mechanical features of corneous structures by having long dermal papillae, which increase the surface area of keratin production (Bragulla, 2003). This supports the idea of the primary function of a papillary body to enhance the supply of nutrients in the epidermis (Hirschberg et al., 2001, Bragulla, 2003). The ultimate forms of the hoof wall are mainly defined by the conformation of the interface between dermal and epidermal tissue, which is represented in hoof wall by dermal papillae (Hamrick, 2001, Davies et al., 2007). The presence of a constant amount of collagen fibres in the dermal lawyer is essential in protecting the architecture of hoof shape (Kuwano et al., 2005). These fibres are organised and extended over the reticular lawyer to formative primary dermal laminae, which attach with the secondary laminae that interface with the epidermal laminae (Bragulla et al., 2007). Consequently, any defect of these fibres can cause a detachment between the dermal and epidermal connection and then separation of the distal phalanx. It is now well recognised from a variety of studies, that the bulk of the keratinised hoof wall (stratum medium) is generated by the stratum basale which covers and lining the dermal papillae

(Bragulla and Hirschberg, 2003, Daradka and Pollitt, 2004, Eurell and Frappier, 2013). The inter tubular horn is generated by interpapillary stratum basale and the tubular horn is generated by the stratum basal lining the dermal papillae (Leach, 1980, Dellmann and Eurell, 1998, Eurell and Frappier, 2013). This combination of tubular and intertubular horn growth proximodistally forms the bulk of hoof wall which is either being worn off or trimmed at the sole surface border (Eurell and Frappier, 2013, O'Connor et al., 2015).

Studies over the past three decades have provided information on labelling mitotic cells on the stratum basale of the epidermal coronary region which was stated previously by Leach (1980), and then by Daradka and Pollitt (2004) who studied the cell division and hoof growth in ponies via injection of 5-bromo-2'-deoxyuridine (BRdU). The latter study showed that the highest percentage of proliferating cells (12.04%±1.59) was observed in the coronary region in comparison to the lamellae average (0.11%±0.04 to 0.97%±0.29). Similarly, some researchers used p63 markers to investigate stem cells (Senoo et al., 2007) whilst also labelling proliferating cells in the coronary hoof region (Carter et al., 2011, Linardi et al., 2015). However, research on the question has been frequently been restricted to limited comparisons between cell division and specific diseases for example laminitis (De Laat et al., 2013b, Carter et al., 2011). As such it is still not known about how hoof growth or in relation to determining where in the capsular wall, epidermal cell proliferation happens. In addition, there are no investigations on the mitotic cell number present along the length of the papillae, this study aimed to provide more knowledge on the dermal papillae in hoof growth. It is also not clear what predisposing factors act directly/indirectly on the coronary region via cell proliferation thus producing new cells that mature and keratinize, adding

consistently to the length of capsular wall, which might in turn have further impacts upon the integrity of the equine foot. Because knowledge of the hoof wall growth rate is a requirement to understanding its structure and function, the investigation of the coronet, in particular the region-specific dermal papillae, will deliver new evidence on the basic mechanism by which hoof walls grow and will also provide principles showing correlation with hoof wall thickness. It is well known that the hoof grows from the coronet not from the lamellae (Bragulla, 2003, Daradka and Pollitt, 2004, Linardi et al., 2015), consequently, what is not yet clear is the how the hoof grows and what signals drive the progenitor cells at the stratum basale to increase/decrease mitotic cell division.

Therefore, this chapter determines the link between the numbers of mitotic cells per length unit along the papillae to the number of apoptotic cells along the papillae, as well to looking at the locations of apoptotic and mitotic cells. In addition, the chapter explores the relationship between the thickness of the epidermal tissue in general and the thickness of hoof wall. As an example on the importance for studying the coronary region in particularly dermal papillae, it appears the most promising method to this demand for understanding the method by which hoof grows.

3.2 Hypothesis

The overarching hypothesis for this chapter was that the physical forces acting at the basal epidermal papillae have an impact on the progenitor keratinocytes via increased cell proliferation. This was defined and subdivided into mini hypotheses for the different experiments:

1. An increased number of dermal papillae/mm^2 will increase the surface area available for the potential production of equine hoof material.
2. Physical forces borne from changing cell size/cell volume which in turn apply tension on the dermal papillae will increase proliferation of proximal basal progenitor keratinocytes.
3. As cell size increases, the physical forces they generate will increase. As cell size increases, increased proliferation of basal cells will be observed in the proximal dermal papillae and within the interpapillary space. Cell size and proliferation rates will differ in relation to the distance from the proximal part of the basement membrane.
4. A critical transition zone of cell cornification represented by epithelial thickness at the coronary region will increase the proportion of proliferative cells at the proximal papillae thus enabling the hoof to grow.
5. The integrity of the basement membrane zone will decrease cell proliferation by decreasing the basal cell attachment and its nutrition.
6. The amount of collagen fibres at the dermal epidermal junction will determine the integrity of dermal epidermal attachment.
7. Mitotic cells/apoptotic cells per unit of length along the papillae will increase cell division by controlling the counter balancing of the development of hoof growth at the proximal part of papillae.

3.3 Aims and objectives

The overall objective was to determine what key factors would hypothetically develop during hoof growth allowing basal keratinocytes to adapt their function. In order to achieve these objectives, concentrating on the coronary dermal papillae of the equine foot, the following techniques were used:

Histology and staining with different histochemical and immunohistochemical staining including:

1. H&E for identifying the epithelial region and to count the number of papillae, measuring cell size and the epithelial thickness.
2. PAS stain for measurement of the basement zone and to evaluate the integrity of the basement membrane.
3. Masson's stain for measuring the amount of collagen fibers at the dermo-epidermal junction.
4. Immunostaining techniques to measure the proportion of proliferating cells using Ki-67 and p63 antibodies and apoptosis using TUNEL assay.

3.4 Results

3.4.1 Analysis hoof shape

Analysis of the external hoof shape showed a wide range of conformational features in the shape of capsular wall and the outline of the front surface (dorsal wall Figure 3-1 also full results are shown in Chapter 5 with full analysis). The hoof capsule had a distinctly concave shape to the dorsal wall. The case histories of the animals were unknown; consequently, all of those hooves taken from horses had suspected foot lameness and underwent analysis to detect the biological and physical effects on the hoof capsule. In the majority of the results, the techniques have been optimised for the appropriate tissues and work was carried on the samples.

As there were no any information on the case history of collected samples. The results revealed that the hoof conformation might be developed as a cause and a consequence associated with hoof growth, and therefore capsular wall shape variation contrasting from the optimal conformation as either very low or too upright which consequently leads to foot lameness. The full data obtained from the analysis of hoof shape, which involved measuring hoof angle, and hoof curvature and comparing to the distal phalanxmeasurements are presented together with the data analysing the coronary hoof tissue in Chapter 5.



Figure 3-1: Equine foot show a distinct curvature in the dorsal hoof wall

3.4.2 Haematoxylin and Eosin (H&E) staining

A number of optimisations were carried out until the hoof tissue showed clear histological features using H&E. Examination of tissue samples stained with H&E revealed the occurrence of the periople (stratum externum) a white band mass of tissue which was located between the junction of the capsular wall and skin. The cells of this layer attached to underline stratum medium (Figure 3-2pe+pe1), and it was appeared clearly diminished and disappeared from the underling hoof wall. Therefore, and since this layer has no functional role in hoof growth it will not be considered in this study. The next layer was coronary tissue (stratum medium) (Figure 3-2co+co1), this stratum formed the bulk of the hoof wall and consisted of tubules arranged parallel and vertically oriented and originated from dermo-epidermal junction at the coronary region (Figure 3-2tu+tu1). Finally, some parts of proximal lamellae (stratum internum) were observed in most sectioned tissues (Figure 3-2la+la1).

In this study, stratum medium is important, as it constitutes the main hoof wall and the cell population of this part of stratum medium controls hoof growth. This study revealed that normal interdigitation between dermal and epidermal tissues were clearly observed in area attached the epidermal tissue to underling dermal tissue (Figure 3-2i). Additionally, at the coronary region numerous perioplic and coronary dermis were invaginated and papillated under the epidermis in a precise orderly way, which seemed to have a finger like projection extended and protruded deeply in epidermal tissue (termed dermal papillae) and were visible in longitudinal tissue sections (Figure 3-2pa+pa1).

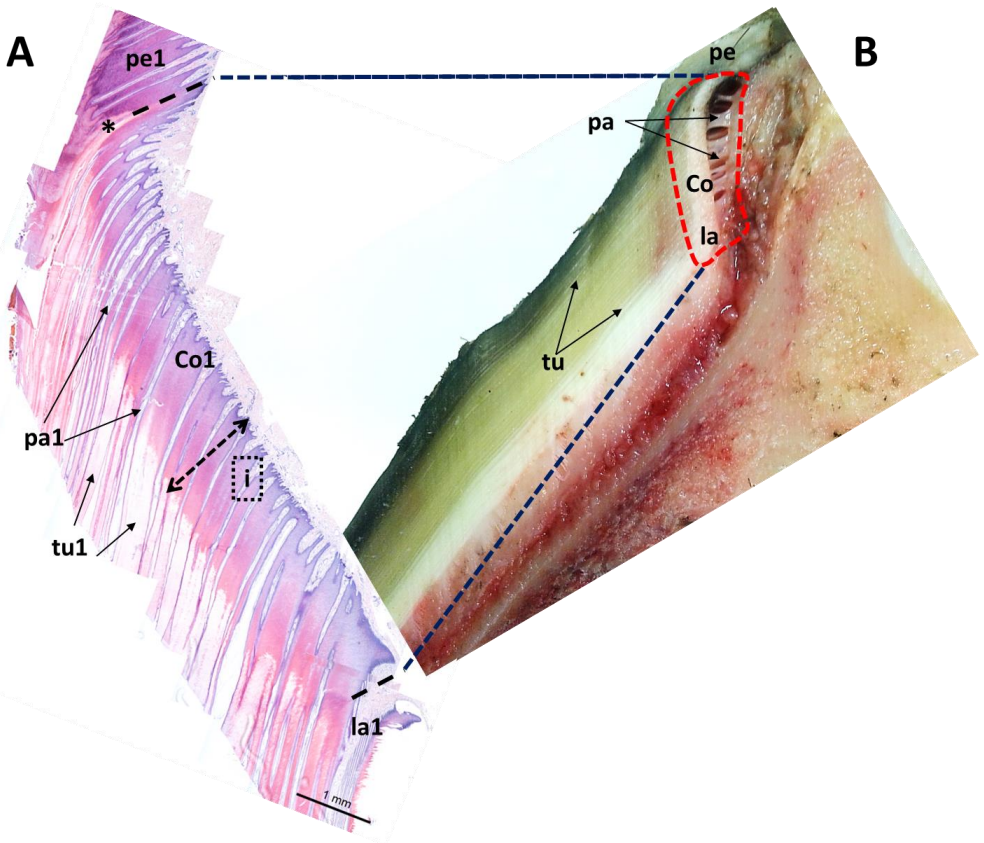


Figure 3-2: H&E stained coronary hoof tissue

Diagram illustrates hoof sagittal section and photomicrographs stitched together to show different areas throughout sections represented in; A) Shows coronary region which is appeared clearly in stitched photomicrographs, while (B) represents the hoof sagittal section marked with red line showing the site of coronary region, whereas (*) the asterisk mark illustrates the area which is situated between (pe, pe1) perioplе (stratum externum) and (co, co1) the coronary region (stratum medium), while (la, la1) represents the proximal part of lamellae (stratum internum), in addition (i) signifies the interdigitation between dermal and epidermal tissue, the black arrows referred to the thickness of epithelium, furthermore (pa, pa1) shows the long finger shape dermal papillae, likened to finger like projections in keratinous materials and (tu, tu1) represents the tubular horn that originated from papillae. Scale bar represents 1mm.

The numbers of dermal papillae were counted on each stitched image for 15 equine feet at quarter and heel regions, while 7 feet for the dorsal, as it was unable to obtained the same stitched images at the dorsal region only 7 section images were counted and uncounted the one that was not the same in Figure 3-3B. This results revealed that there were no significant difference between the numbers of papillae in each hoof region (dorsal; n=7, 19.93±0.86/(mm^2)), (quarter; n=15, 22.15±0.69/(mm^2)) and (heel; n=15, 20.38±1.11/(mm^2)) (Figure 3-3).

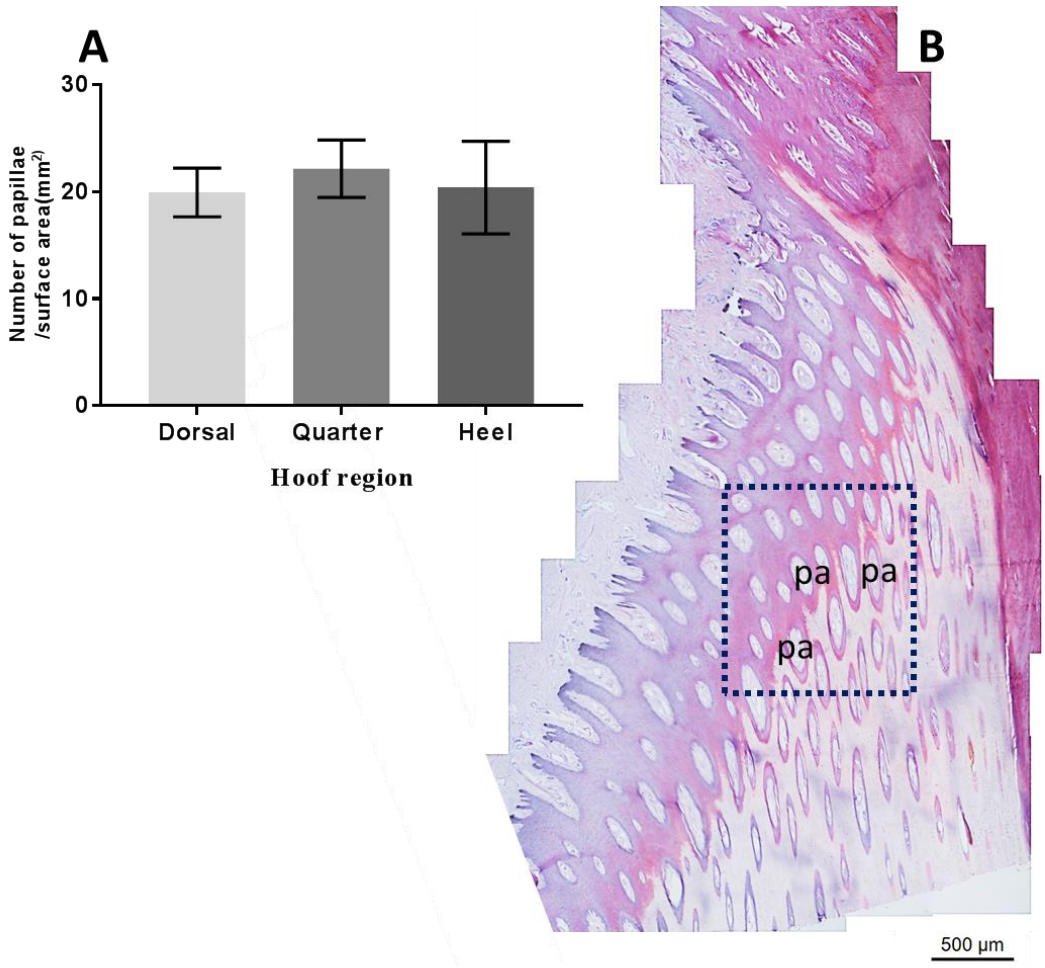


Figure 3-3: Graph and photomicrograph stitched showing the number of papillae

Dermal papillae in each cross section of stitched images were counted per surface area (mm^2) showing in graph (A) no significant difference were found between different hoof regions (dorsal quarter and heel), and this data was obtained from counting the stitched images appeared clearly in image (B) which showed black square represents sites of accounting papillae (pa) were counted in each stitches for different horse feet. Statistical comparisons between groups were analysed using One Way ANOVA with Post Hoc testing SPSS. Scale bar represents 500µm. N= 15 for quarter and heel and 7 for dorsal.

Analysis for measuring entire length of dermal papillae revealed that the average length of each papilla was 3.96±1.49 mm; two of these papillae are shown in sagittal section in Figure 3-4. The core of each papilla revealed that it contained connective tissue and blood vessels; in addition, there were clear divergences between the acidophilic stained nuclei of the keratinocytes and the basophilic connective tissue staining. The diameter of central core of each papilla was similar to that of the distance between the core and the surrounding dermal tissue

and in the most distal region of dermal papilla it became gradually constricted until the end of papilla (Figure 3-4c2). As the dermal tissue become further away from the coronary border, the amount of vasculature also diminished (Figure 3-4, yellow arrows).

In longitudinal sections of the proximal portions of the dermal papillae, many of the basal cells populations were more apparently columnar in shape and, in some areas; these cells seemed to have a pseudostratified columnar organization. They were characterized by a basophilic nucleus and a pale eosinophilic cytoplasm, and their longitudinal axis was oriented perpendicularly to the interdigitating junction between dermis and epidermis (Figure 3-4a2). In addition, some of these cells were obscured by the occurrence of a black pigment related to melanocytes (Figure 3-4a2 white asterisk marks).

Cells within two third of papillae manifested with a rounded shape of both their nucleus and general cell morphology. Most of the keratinocytes in the proximal two thirds of dermal papillae stained intensely with H&E (3-4b2+c2). The distal two thirds of the dermal papillae showed an increased eosinophilia and their nuclei were paralleled with the orientation of dermal papilla which later formed the tubular horns extended with vertical orientation of papillae. This manifestation of cell increase was related to the cells being fully cells keratinized and in some areas, it was noted that no nuclei were present (Figure 3-4c2).

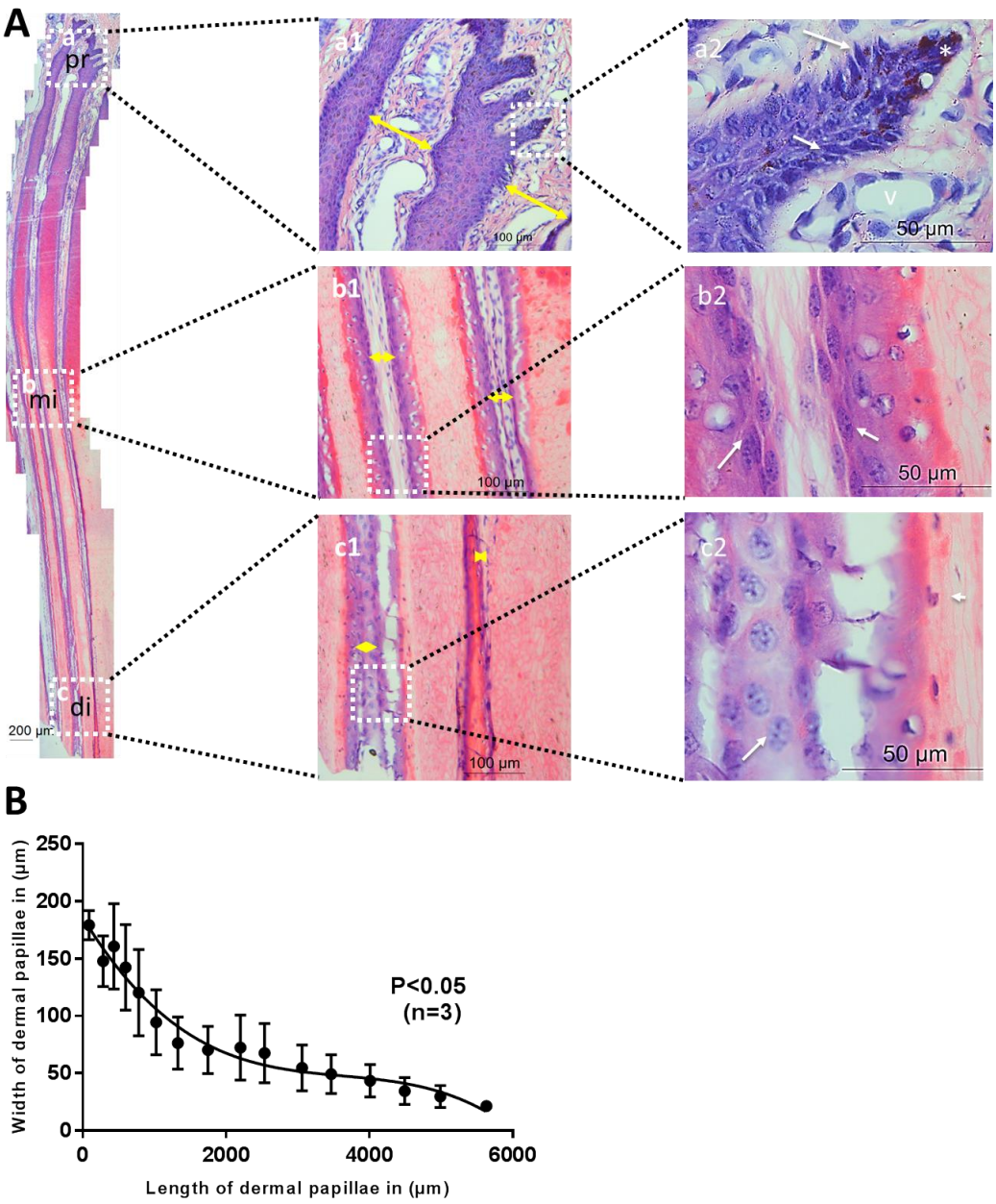


Figure 3-4: Photomicrograph stitched images and graph show dermal papillae diameter

Dermal papillae stitched images were used to measure diameter of papillae. A) Represents stitched images of dermal papillae showing three portions, (a) the first part represents (pr) the proximal region of papilla shows yellow arrows a wide diameter of the papilla in high magnification (a1) and columnar shape nuclei (a2) (white arrows), whereas (*) white asterisk marks refers to melanin pigment and furthermore (v) indicates the blood vessels. While, (b) the second part of papilla (mi) represents the middle region shows the diameter was become narrowed in (b1) yellow arrows and the keratinocytes in (b2) (white arrows) was parallel with orientation of dermal papilla, and then finally (c) the third part illustrates the diameter appeared clearly constricted at the distal end of papilla (di) which is showed in (c1) yellow arrows, additionally the keratinocytes was become more rounded in (c2) (white arrows). B) Shows a nonlinear regression was plotted on the papillae diameter against papillae length. Image (A) scale bar represents 200µm and images (a1), (b1) and (c1) 100µm, and (a2), (b2) and (c2) 50µm.

Furthermore, analysis using the H&E stain exhibited the dermal and epidermal tissues in contrasting colours in pink and purple respectively, and highlighted the basement membrane border in a purple colour. The results indicated that the coronary and periople corium appeared to be formulated from a mesh dense matrix of connective tissue encompassing arteries, veins, capillaries, and nerves (Figure 3-5A). In contrast, the epidermal layers, constituted from stratified squamous keratinised epithelium were continuous with skin from the leg and seemed divided clearly into the three expected layers: The thin deepest layer of basal cells (stratum basal) was arranged along the basement membrane. It appeared as a double layer of cuboidal to columnar cells characterized by a large oval to elongated oval basophilic nucleus, generally each cell had 2-3 nucleoli, and their cytoplasm had a pale eosinophilic staining, and their long axis of the nucleus were oriented at an acute angle to the basement membrane (Figure 3-5a1). After that the staining affinity in this layer revealed a gradation effect from a pale eosinophilic cytoplasm staining at the stratum basale to gradually medium to dark eosinophilic staining at the end of the next layer, (Figure 3-5b1+c1). This alteration observed as very close variation, which appeared in the beginning of second layer. The second layer (stratum spinosium) (Figure 3.5b1+c1) was comprised of numbers of polyhedral cells tightly adhered to each, and their large oval nucleus encompassing 2-3 nuclei (Figure 3-5b1). Further distally, as the cells become more flattened toward the external layer (stratum corneum), the nucleus became smaller comparative to cell size and the staining affinity of the cytoplasm become more intensely eosinophilic. More distally and at the level where intersection was apparent between the end of stratum spinosium and the beginning of stratum corneum, cells were observed as partially stained and incomplete

cytoplasm staining intensity was observed (Figure 3-5d1). The outermost layer (stratum corneum) was comprised from dead keratinocytes, which have lost their nuclei, while the granulosum and lucidum layers were not present (Figure 3-5A). The results revealed (Figure 3-5e1), that the cytoplasm of completely keratinized cells did not exhibit any staining with H&E stains. The keratin layer was oriented consistently at an angle from the surface of dermal papillae towards the ground which constituents the intertubular horn (Figure 3-5A+a-e).

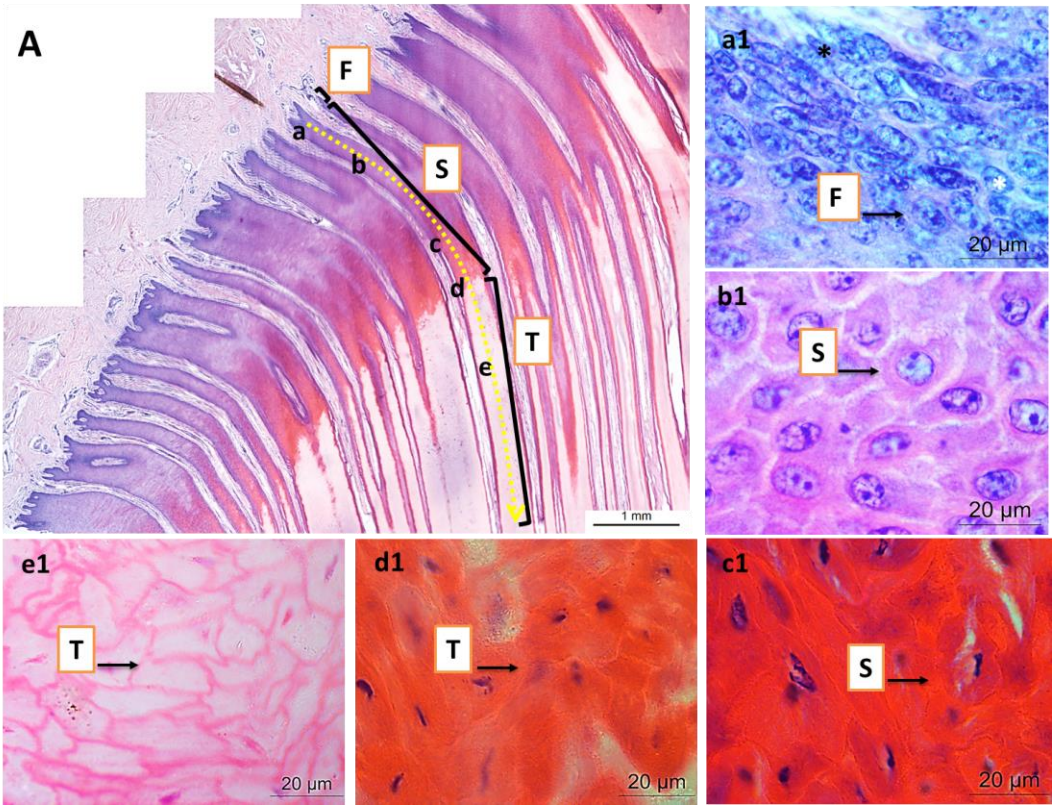


Figure 3-5: H&E stained photomicrographs illustrate intertubular epidermal layers

H&E stained tissue photomicrographs show the three layers of intertubular epidermal tissue appeared in A) first layer (stratum basale) (F), second layer (stratum spinosium) (S), and third layer (stratum corneum) (T), while(a, a1) shows the basal and supra basal layers appear contained two types of cell shape, cuboidal (white asterisk marks) and the black asterisk marks shows columnar cells set on the basement membrane with longitudinal axis at right angles to the derma-epidermal junction while in (b, b1) the second layer (S) formed from polyhedral cells move as it is appeared in (c, c1) to convert to the keratinised cells (d, d1) in third layers (T) with a fully keratinized appeared clearly in (e, e1). Image (A), scale bar represents 1mm and images (a1) (b1) (c1) (d1) and (e1) 20µm.

In some other fields, at the ends of papillae appeared to have a greater diameter leading to the cells overlying one another, which disorganized the layers of epidermal cells (Figure 3-6).

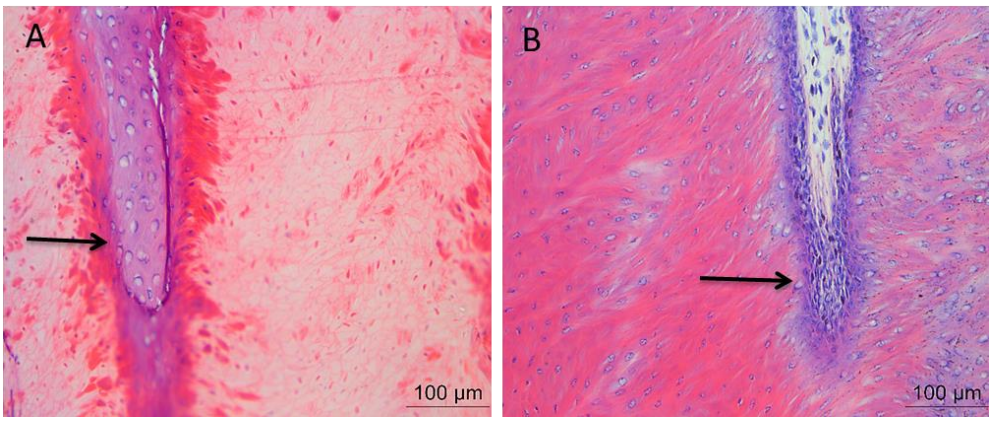


Figure 3-6: Photomicrographs represent appearance different papillae

H&E stained tissue photomicrographs illustrate in some fields, dermal papillae (black arrows) appeared in A) thicker at the ends of papillae leading to the cells overlying one another, while in B) the dermal papilla (black arrow) appears to contain it's clear layers. Scale bar represents 100µm.

3.4.2.1 Changes in cell size of tubular and intertubular horn

The results of H&E stained sections of coronary hoof region revealed that during keratinocytes differentiation, cells forming tubular and intertubular horn are subjected to an orderly sequence of morphostructural changes. In order to ass such changes, further analysis was carried out to calculate the cell volume for each group of cells at a distance from the basement membrane. The results and analysis for each cell population started from cells visibly positioned between dermal papillae that forms later the tubular horn. Basal cells were observed as a population of basal progenitor keratinocyte cells (Figure 3-7a1). The cytoplasm of these cells was stained clearly with purple stain, and as the cells move distally, their cytoplasm becomes pink-red coloured (Figure 3-7b1). Finally, cells show a

transition displaying no particular colour and that can be referred as horn formation (Figure 3-7c1). The cell surface area (Figure 3-7) and the data presented in Table 3-1 demonstrate that the cell surface area of basal layer was 83.01±1.343µm^2 at a distance 17.4±1.26µm and reach its maximum value around the transition area to 981.1±5.3µm^2 at a distance 1859±151µm, then dropped down to 498.2±16µm^2 at a distance 2142±152µm. The results revealed that the transition appeared as a critical part probably linked to cornification. It can be hypothesized that the change in cell size measured may counterbalance the gravity and the adhesion together and that the transition correspond to the balance of stresses whereby cells cannot grow further and have to die at that point. The results indicated that there was a significant nonlinear regression between cell surface areas against papillae length (Figure 3-7B). Similar correlation was found between the nucleus surface area against papillae length and the same found with the ratio of whole nucleus (Figure 3-7C+D).

Table 3-1: Characteristics of data analysis for cell volumes at a distance from basement membrane (n=3).

Epidermal layers	Cell surface area in µm²	Distance in µm
Stratum basal	83.01±1.343	17.4±1.26
suprabasal	224±7.87	69.43±10
	331.3±10.35	154.7±12
Stratum spinosium	378.6±9.25	223.2±10
	436.3±4.93	339±15
	477.1±12.1	400.8±8
	627.1±19.84	744.8±33
	732.9±9.67	1056±24
	831.8±8.88	1315±57
	912.4±10.97	1604±130
	966.7±16.26	1851±146
	981.1±5.3	1859±151
Transition area between stratum spinosium and stratum corneum	965±11.84	1923±154
	913.3±16.59	2014±155
	865.2±20.79	2069±151
Stratum corneum	498.2±15.88	2142±152
	459.9±9.17	2202±154
	441.8±11.68	2255±144
	398.7±19.12	2316±129
	332.6±20.65	2362±123
	288.2±14.38	2409±136
	262.3±5	2483±131
	239.5±1.93	2546±124
	227.9±6.55	2606±121
	231.7±1.17	3194±139
	287.1±1	4398±371

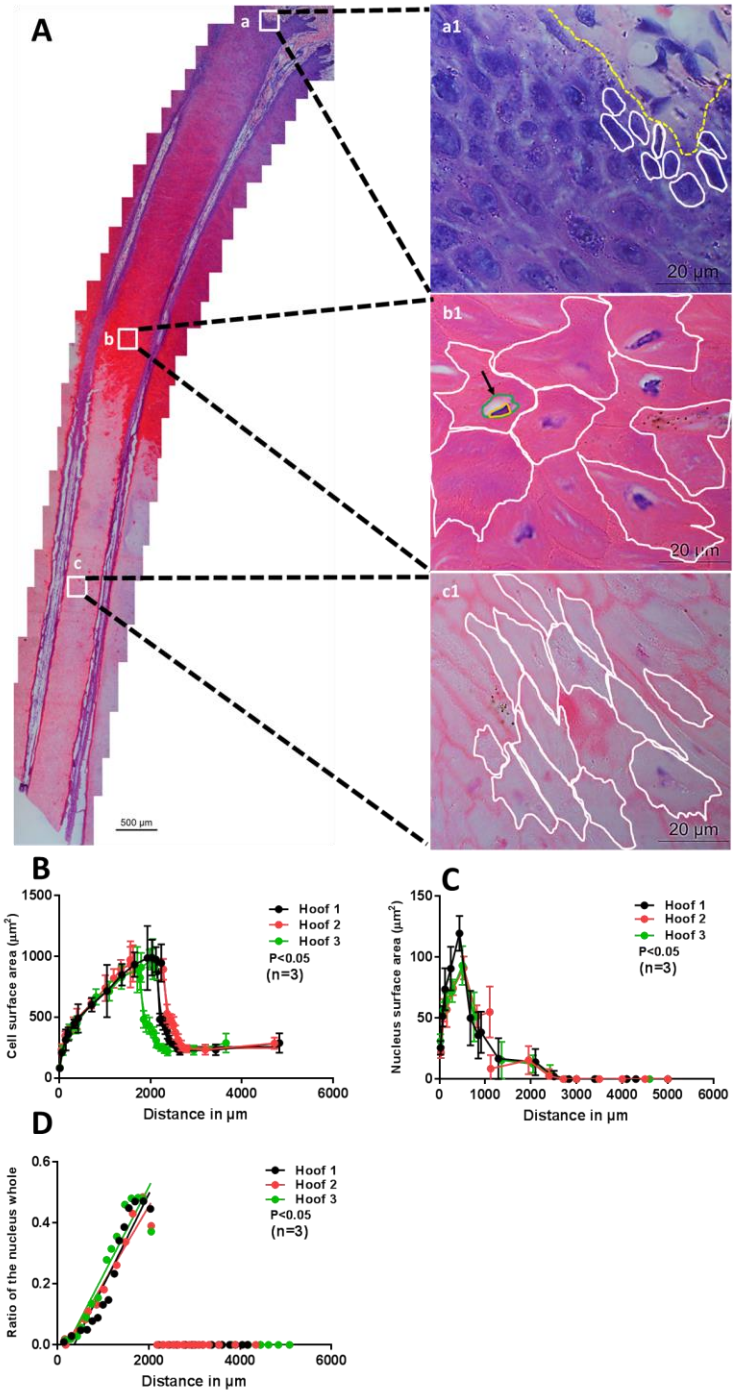


Figure 3-7: The cell size changes in the interpapillary epidermal cells

A) Represents stitched images of dermal papillae showing three portions, (a) the first part represents (a1) the proximal interpapillary region where the dashed yellow line represents the BM and the white line encircle basal cells next to the BM. (b) the second part of interpapillary region where (b1) the cell surface area increases. The yellow line represents a collapsed nucleolus, whereas the green line surrounds the whole of nucleus also pointed with a black arrow. Finally, (c) the third part illustrates the distal end of interpapillary region which shows (c1) how the cell surface area has changed pointed with white line encircle. B) A nonlinear regression shows a significant correlation when plotted between the cell surface area against papillae length. C) Similar correlation was found between the nucleus surface area against papillae length and the same found, (D) with the ratio of whole nucleus (* indicates P<0.05 vs papillae length). Image (A) scale bar represents 500µm and images (a1), (b1) and (c1) 20µm.

Further analysis was performed measuring the cell surface area of cells lining and alignment the dermal papillae. The population of basal and supra basal cells constituting the tubular horn at the proximal portion of dermal papillae were similar to those adjacent cells forming the intertubular horn (Figure 3-8a1). Most of these cells had their long axis positioned at a right angle to the basement membrane. However, distally the orientation of these cells was visibly changed becoming orientated along the papillae (Figure 3-8b1). The results showed that the alterations in the long axis of nucleus and the cell orientation from perpendicular on BM to along the papillae was a function of the distance from the basal layer to suprabasal layer of the coronary epidermis. Analysis for cell surface area or short to long axis did not show many differences between different papillary regions (Figure 3-8). However, the cell surface area and surface area of nuclei decreased further away from the maximum proximal portion 56±2μm^2 toward the minimum at distal portion 29±1μm^2 (Figure 3-8). This drop was visible at the level of the transition area between the stratum spinosium and stratum corneum (Figure 3-8b1). Results indicated the tubular structure appeared distinct from interpapillary (intertubular horn). The results indicated that there was a significant correlation regression between cell surface area against papillae length (Figure 3-8B), while was not shown the same correlation with nucleus surface area against papillae length (Figure 3-8C).

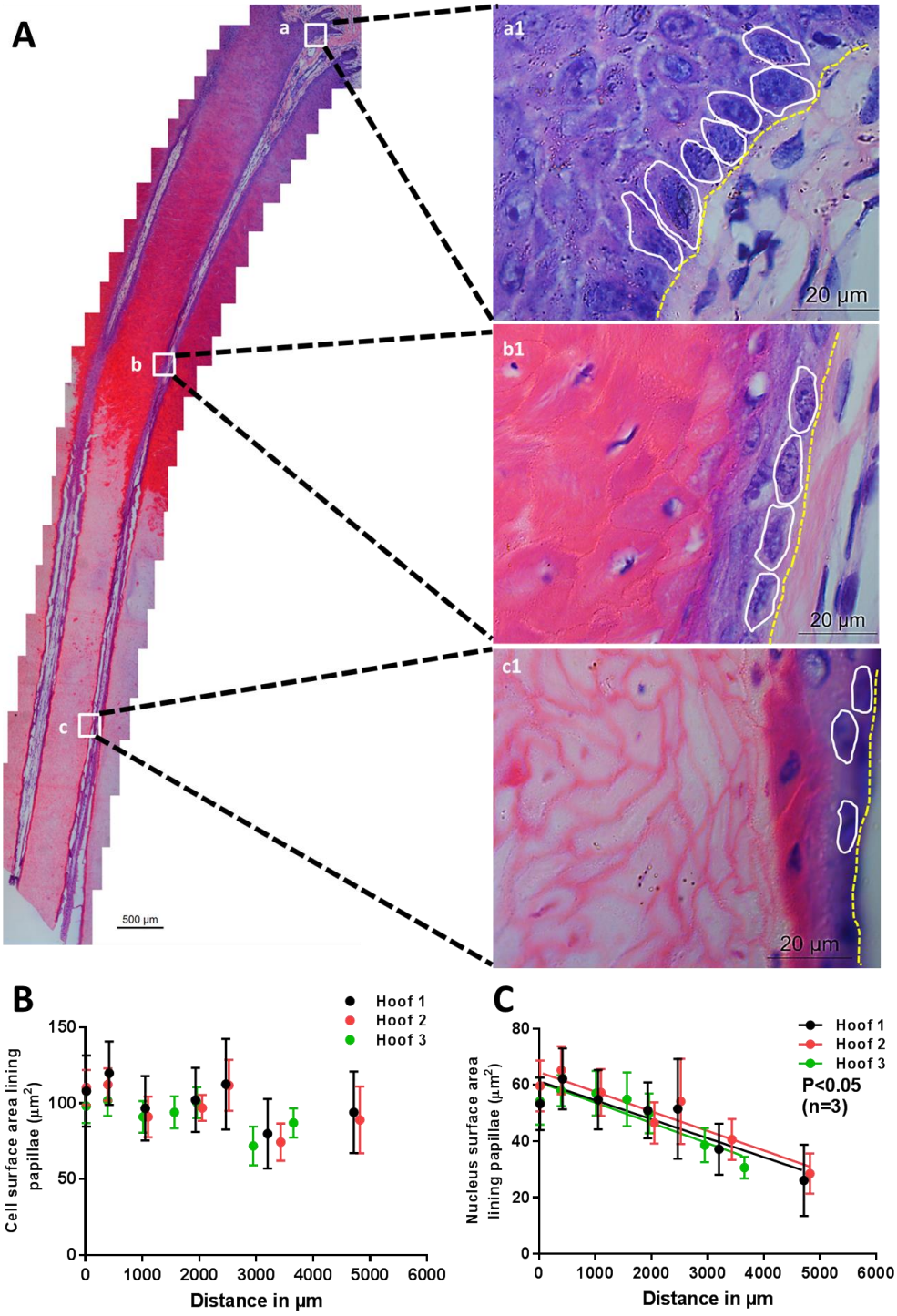


Figure 3-8: The cell size changes lining dermal papillae

A) Represents stitched images of dermal papillae showing three portions, (a) the first part represents (a1) the proximal papillary region where the dashed yellow line represents the BM and the white line encircle basal cells next to the BM. (b) the second part of papillary region where (b1) the cell surface area decreases. Finally, (c) the third part illustrates the distal end of papillary region which shows (c1) how the cell surface area has changed pointed with white line encircle. B) No correlation was found when plotted the cell surface area against papillae length, whereas (C) show a correlation regression between the nucleus surface area against papillae length (* indicates $P<0.05$ vs papillae length). Image (A) scale bar represents 500µm and images (a1), (b1) and (c1) 20µm.

3.4.2.2 Epithelial thickness of coronary region

Another investigation was carried out comparing the epithelial thickness of the coronary region at different regions (dorsal, quarters and heels regions). The results obtained from the analysis of epithelial thickness between the basement membrane and the junction between stratum spinosium and stratum corneum were presented as mean±SEM (Figure 3-9A-D). The results revealed there was a significant difference between hoof regions at the heels region ($p<0.05$; n=16, 1.34±0.14mm) in comparison with both the dorsal region (n=16, 0.97±0.05mm) and quarters region (n=16, 0.81±0.05mm). The average epidermal thickness at the heel was increased by 41% in the heels region in comparison to the dorsal region and 65% in comparison to the quarter region. A similar observation was indicated (Figure 3-9A-C+E), as the epidermal thickness for the stratum corneum was marked between the junction of stratum spinosium and stratum corneum to the external surface of hoof wall. This analysis also indicated a significant difference between hoof regions at the heels region ($p<0.05$; n=16, 0.9±0.13mm) in comparison with dorsal (n=16, 0.54±0.06mm) and quarters regions (n=16, 0.7±0.06mm). The average stratum corneum thickness was increased by 67% in the heels region in comparison to the dorsal region and by 28% in comparison to the quarter region.

However, the results from calculating the ratios of thickness of both stratum basal and spinosium to the space between the basement membrane and the external wall surface (Figure 3-9 both red and black arrows) was not shown significant differences between hoof regions (3-9F).

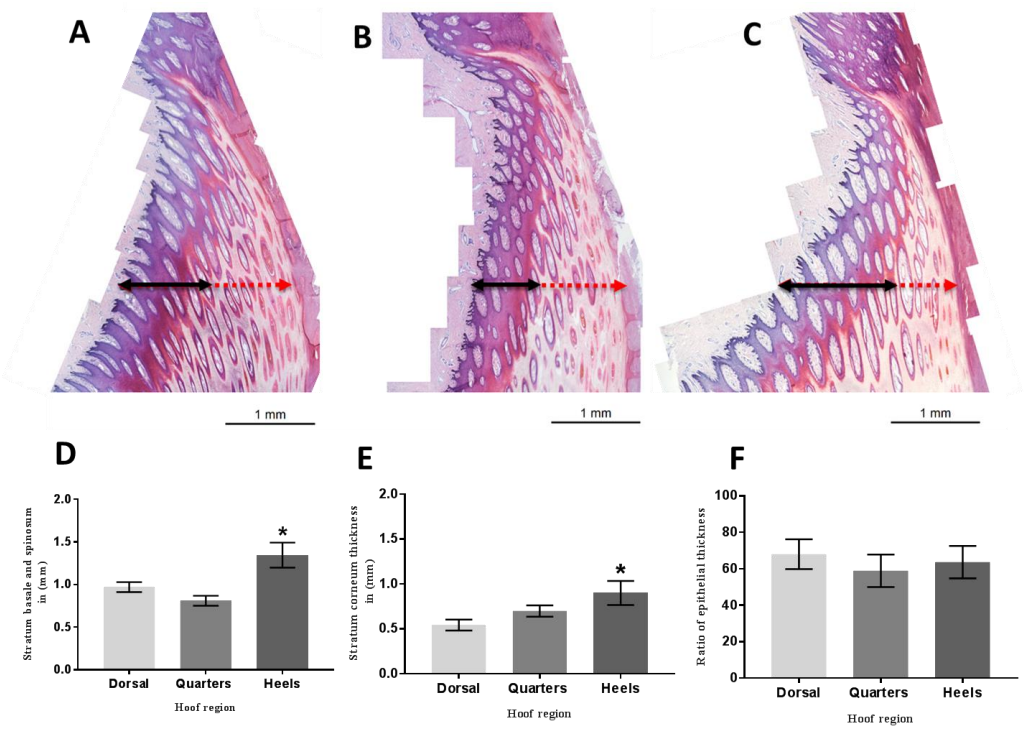


Figure 3-9: Epithelial coronary thickness

Photomicrograph stitched images and graphs showing epithelial thickness measured in mm, epidermal tissue thickness were compared at three different hoof regions; A) dorsal, B) quarters, and C) heels, whereas black arrows represent the stratum basale and corneum, while red arrows show the stratum corneum. Statistical comparison between epidermal layers showing a significant difference in graph (D) and (E) for stratum basale and spinosum, and corneum respectively at heels region, while in graph (F) shows a significant difference for the ratio of epithelial thickness at dorsal region in comparison to quarters region. Scale bar represents 1mm. (* indicates $P<0.05$, heel vs dorsal and quarter regions). Statistical comparisons between groups were analysed using One Way ANOVA SPSS. N= 16 per group.

Another investigation was carried out comparing the epithelial thickness of the coronary region at different regions (dorsal and quarters regions) and capsular wall thickness at dorsal and quarters regions (Figure 3-10A+B). The ratio of the epidermal layer thickness was measured using Fiji J software whilst the thickness of the hoof wall was measured using CT scan images for the same hoof.

The results of the correlational analysis were presented in Figure 3-10C+D, it can be seen that in the dorsal region, there was no correlation between epithelial and hoof wall thickness. However, there was a strong correlation between the ratio of epithelial thickness and the hoof wall thickness at the quarter regions (Figure 3-

10D). From the linear regression analyses in Figure 3-10D, it is apparent that there was a clear regression in the ratio of epithelial thickness against the hoof wall thickness, as when the epithelial thickness was small the hoof wall was smaller, and when the epithelial thickness ratio was high, the hoof wall was thicker. This proposes that thinner hoof wall had thinner epithelial thickness than thicker hoof wall. In addition to this correlation, their relative ratios were calculated and analysed (Figure 3-10E) and this showed no correlation between epithelial thickness and hoof wall thickness relative ratios.

Further analysis was carried out on hoof wall thickness between two different regions (dorsal and quarters regions). There was a significant difference between the hoof wall thickness at the quarters region ($p<0.05$; n=19, 13.9±0.4mm) in comparison with dorsal (n=19, 9.7±0.3mm). The average hoof wall thickness was increased by 43% in quarter regions in comparison to dorsal regions.

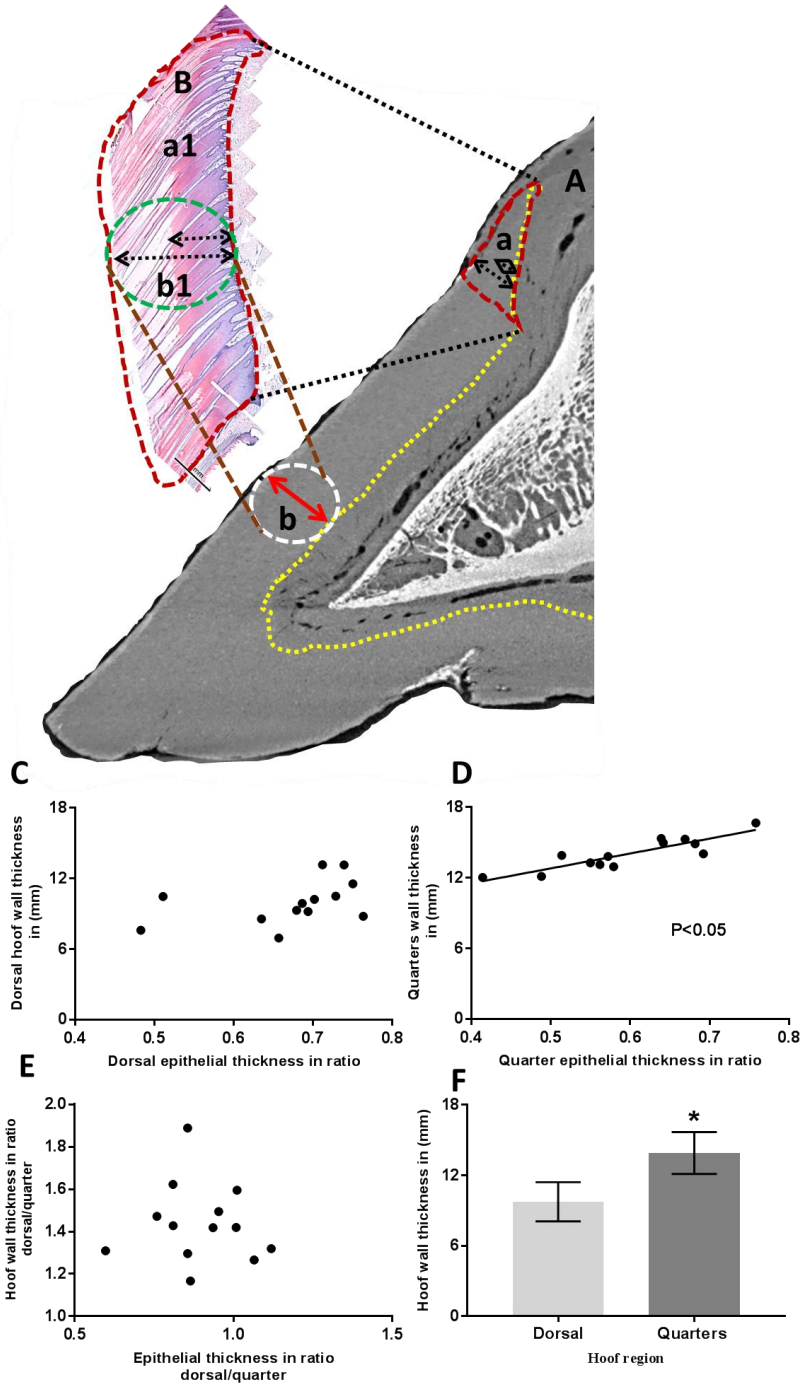


Figure 3-10: Schematic diagram showing wall and coronary tissue thickness

A) CT scan hoof image (a) represents the location of coronary region on the CT image, whereas (a1) displays the same region using a photomicrograph image; (b) CT scan hoof wall thickness encircled with white line and marked with red arrows, whilst (b1) shows epithelial thickness at the coronary region marked with black arrows. B) Illustrates a photomicrograph for the coronary region. Linear regression was plotted between epithelial coronary thickness and hoof wall thickness showing no correlation at dorsal region (C), while at quarters represents in graph (D) shows a significant regression coefficient between wall and epithelial thickness, furthermore no significant difference were plotted between the ratio of both thickness (E), whereas comparison between wall thickness showing a significant difference at quarters region. Scale bar represents 1mm. (* indicates P<0.05 vs dorsal region). Statistical analysis was carried out using T-test. N= 13 per group.

3.4.3 PAS

Following extensive optimisation, PAS stained sections obviously exhibited the basement membrane (BM) at the dermo-epidermal interface of the equine feet. The PAS stained sections distinctly demarcated glycoprotein constituents of the BM, which appeared as a fine pink line (Figure 3-11 A+B). The BM was intimately surrounded by the epidermal tissue and epidermal papillae and the basal germinal epidermal cells were directly in contact with the BM. However, in some areas there were epidermal variations encompassing a variable degree of pyknosis, vacuoles, and disintegration in germinal basal cells and some separation was observed between the basal cells and BM, as well as in the cross section of some dermal papillae where clear separations occurred (Figure 3-11A+B).

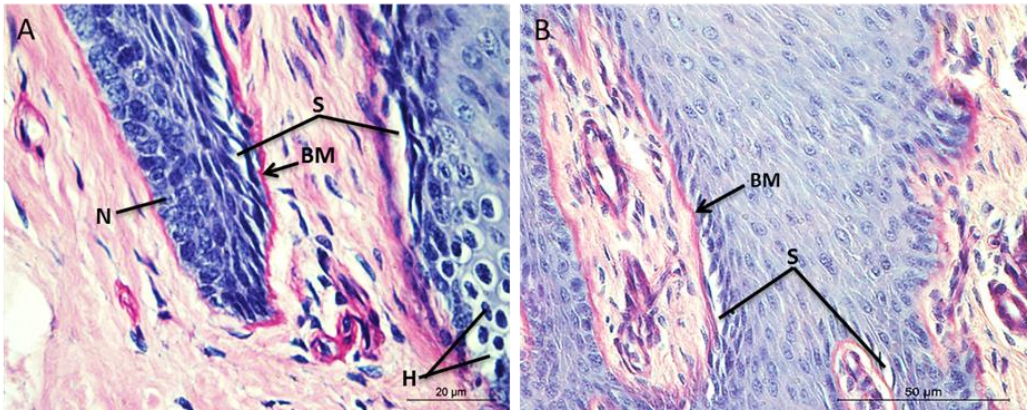


Figure 3-11: Photomicrograph of PAS stained hoof tissue.

Black arrows on the images (A+B) indicate the basement membrane (BM) showing there were spaces between the BM and basal germinal cells which could potentially result from tissue sectioning in these areas. In addition, changes in the shape of basal cells transforming from a normal cuboidal (N) shape into a hydrocele (H) shape a distended shape (S). B) Shows the separation around the cross section of dermal papillae which can be observed. Image (A) scale bar represents 20µm and image (B) 50µm.

The PAS stain displayed the BM as an isolated dark pink to purple line, whereas it was twisted into multiple longitudinal folds at the dermal papillae and was mostly seen along the epidermal edge (Figure 3-12A+B). The thicknesses of BMs in each

sample were measured in order to evaluate the integrity of the basal epidermal cells (Figure 3-13).

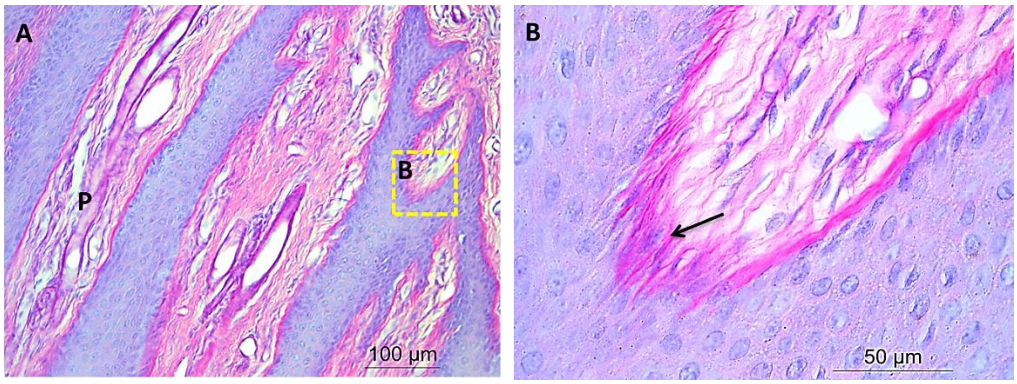


Figure 3-12: PAS stained photomicrograph of dermal papillae

A) Shows dermal papillae (p), as yellow box representing in high magnification (B) Showing twisting of the BM into multiple longitudinal folds at the tapered tip of dermal papillae (black arrow). Image (A) scale bar represents 100µm and image (B) 50µm.

The results indicate that there was no significant difference in the thickness of basement membrane between dorsal (n=11, 2.32±0.12µm) and quarters regions (n=11, 2.29±0.18µm) (Figure 3-13A&B).

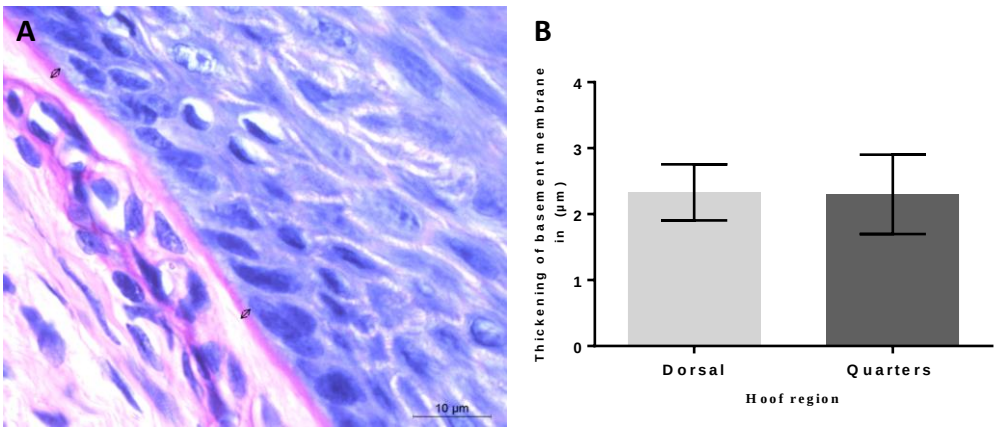


Figure 3-13: PAS stained photomicrograph and graph showing BM thickness.

PAS stained tissues were identified with the basement membrane showing as a dark pink colour, rounded the epidermal tissue, which is marked by black arrows (A). The integrity of the specimen sample and the configuration of epidermal cells were observed. B) Graph showing the comparison between BM thicknesses at dorsal and quarter regions, there was no significant difference between these two regions. Scale bar represents 10µm. Statistical analysis was carried out using T-test. N= 11 per group.

3.4.4 Masson's trichrome stain

The initial stages of these experiments concentrated on optimising the Masson's Trichrome for the equine hoof tissue. Following optimisation of the Masson's trichrome stain, collagen fibres became apparent through their green colouration. Microscopic investigation revealed how the labelled collagen was distributed in the tissue, especially underlying the BM and throughout the dermal tissue, especially as an interdigitation of the epidermal and dermal tissues along the BM. The collagen filaments appeared to be attached to the BM, in both cross and longitudinal sections of the coronary tissue (dermal papillae of coronet; Figure 3-14A+B). The histological consistency of collagen fibres revealed that, the bundles of collagen fibres seemed to be thicker in deeper tissue than in underlying BM (Figure 3-14B).

Sstatistical analysis for quantification the amount of collagen fibres inside the dermal papillae revealed there was no significant difference between the amount of collagen fibres (Figure 3-14C) at the dorsal (n=12, 45±3.3%) and quarters regions (n=12, 43±3%).

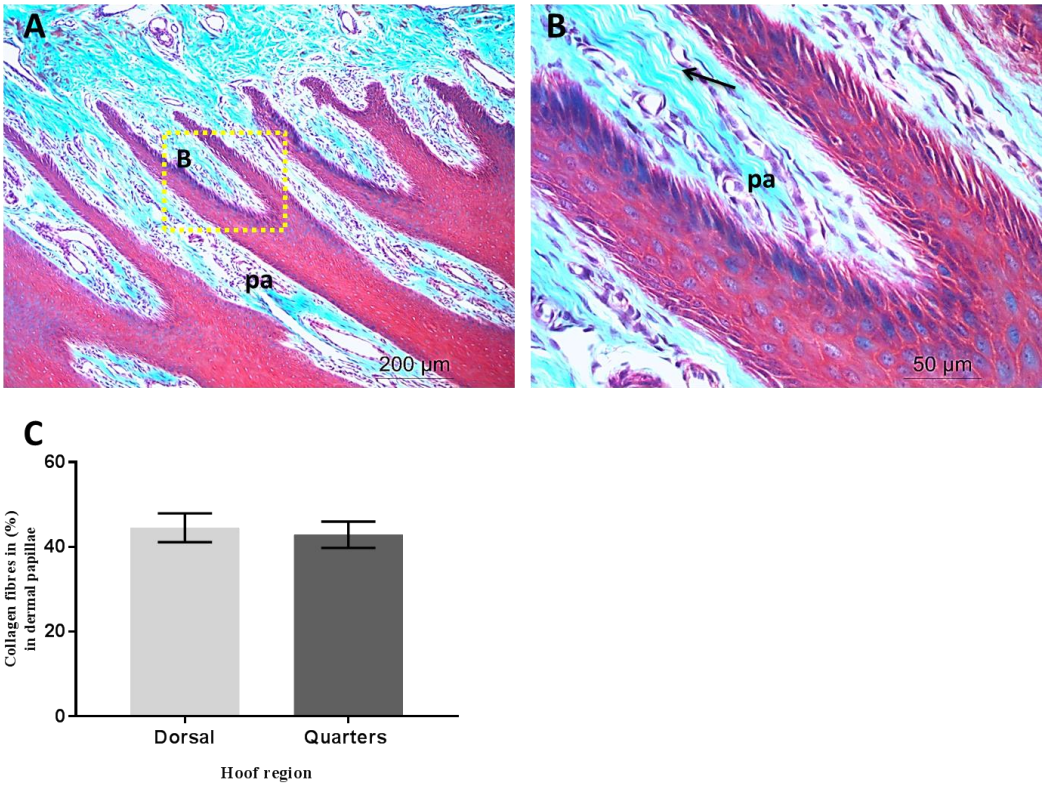


Figure 3-14: Masson's Trichrome stained photomicrographs at dermal papillae

Masson's Trichrome stained the green collagen fibres apparent in A and B. The collagen fibres arrangement appeared as parallel lines near the connection between the dermis and epidermis in dermal papillae (pa). C) Graph shows no statistical differences between the amount of collagen fibres in dermal papillae at dorsal and quarter regions. Image (A) scale bar represents 200µm and (B) 50µm. Statistical analysis was carried out using T-test. N= 12 per group.

In addition, the results of Masson's stained sections indicated that the collagen fibres of dermal tissue were arranged in long organised bundles with green and some of them had red colour, no abnormalities in collagen fibre arrangement were observed in the samples investigated (Figure 3-15A+B). There was no significant different between the amount of collagen fibres at dorsal (n=12, 35±3.68%) and quarters regions (n=12, 33±1.64%). However, there was a strong correlation between the ratio of collagen fibres in dermal papillae and the ratio of collagen fibres inside dermal tissue (Figure 3-15D).

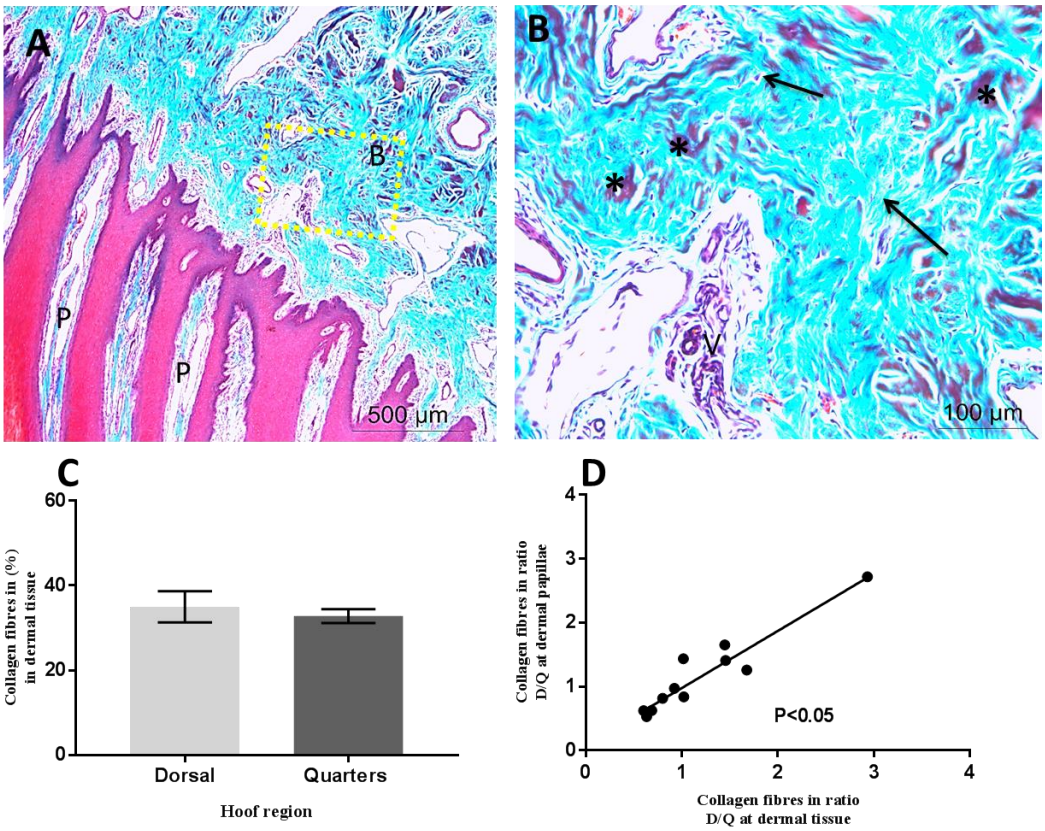


Figure 3-15: Photomicroscope images illustrating the collagen bundles at dermal tissues

A) Collagen fibres were diffused and extended inside the papillae (p) collagen bundles lay close to the epidermal tissue at varying levels of thickness contained blood vessels represented by the black arrow, whereas rectangle yellow (B) showing a deeper tissue where collagen appeared in longitudinal sections, which was more condensed, the asterisks show mixing green and red colour without observing any abnormalities. C) Graph shows no statistical difference between the amount of collagen fibres in deeper dermal tissue at dorsal and quarter regions. However, a clear correlation coefficient was observed (D) between the ratio of both papillae and deeper collagen fibres. Statistical analysis was carried out using T-test. Image (A) scale bar represents 500µm and (B) 100µm. N= 12 per group.

Overall, the current data measured and assessed collagen fibres which did not show any abnormalities in collagen fibres either when they were attached inside dermal papillae or when they were in the deep dermis at the coronary region.

3.4.5 Immunohistochemistry

3.4.5.1 Assessment p63 +ve cells along the dermal papillae

At the coronary region, investigation on the epidermal stem cell marker at the stratum medium (dermal papillae; Figure 3-16A) revealed that most of the stem cells were labelled with p63 immunostaining brown colour (+ve cells). The p63 +ve cells were appeared clearly in the nuclei of stratum basale and supra basal cells and few figures were observed at the beginning of the stratum spinosium (Figure 3-16a1).

The proximal part of interpapillary region showed that the stratum basale and suprabasal were responsible for creating the intertubular horn, and had the highest density of p63 +ve cells (Figure 3-16a1). The frequency of +ve cells was clearly seen in the basal cells and was not shown in supra basal cells located beyond the level of the stratum spinosium of the intertubular horn. In addition, at the level of distal end of papilla, p63 +ve cells were exhibited in fewer numbers at the stratum basale cells (Figure 3-16c1).

These basal cells were lining the whole length of dermal papilla. Therefore, in order to determine whether p63 +ve cells varied along the dermal papillae, microscopic images were stitched together electronically and p63 +ve and -ve cells counts were undertaken along the length of the papillae. The result, indicated there was a significant correlation between the percentage of p63 +ve cells ($p<0.05$; $n=7$) and the length of dermal papillae (Figure 3-16B). When the distance from the proximal part of the dermal papillae increased, a decrease in the percentage of p63 +ve cells was counted (Figure 3-16a1-c1).

The current results revealed that p63 +ve cells were in their highest density at the base of the dermal papilla and decreased in number progressively towards the tip of the papilla (Figure 3-16A). In addition to the percentage of p63 positive cells per length unit being analysed, their surface area ratios were calculated and analysed. There negative correlation within the ratio of p63 +ve cells per surface area and length of papillae ($p<0.05$; $n=7$). This ratio demonstrated the correlation between the frequency of p63 +ve cells and the surface area as defined in Figure 3-16C.

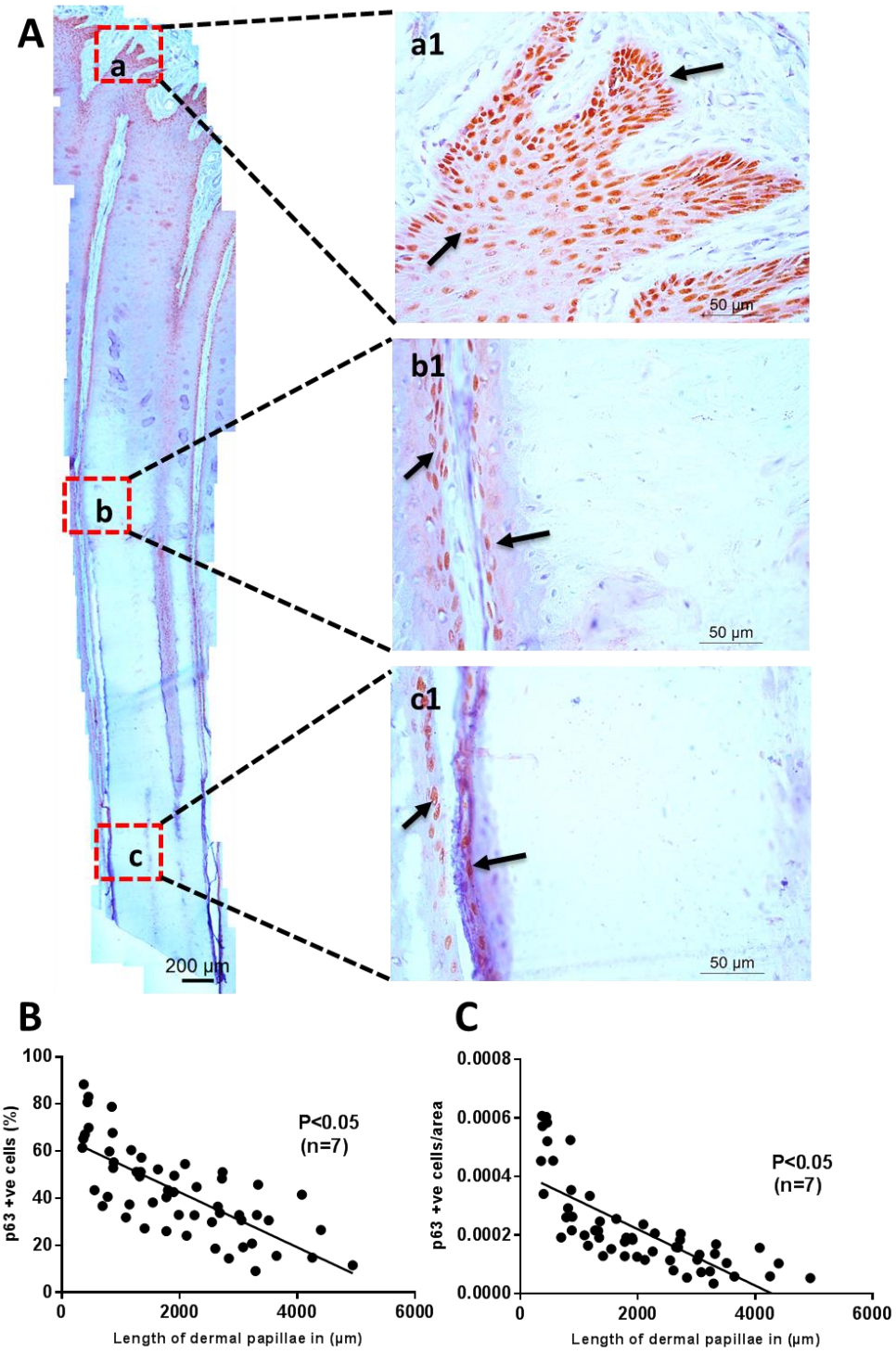


Figure 3-16: The frequency of p63 +ve cells plotted against papillae length

A) Photomicrograph stitched images illustrating p63 +ve cells scattered along the papilla, which appeared clearly at the basal and suprabasal layers of proximal papilla (a, a1; black arrows) and very few cells at the middle (b, b1) and/or at the end of papilla (c, c1). B) There was a clear variation in the percentage of p63 +ve cells as a function of the distance from the proximal dermal papilla. C) A significant correlation was recorded between the surface area and the ratio of p63 expression using GraphPad software (* indicates P<0.05 vs papillae length). Image (A) scale bar represents 200µm and (a-c) 50µm. N= 7 per hoof animal, 20 images per animal.

3.4.5.2 Assessment Ki-67 +ve cells along the dermal papillae

In order to trial a further method for assessing cell proliferation, specimens were incubated with the proliferation marker antibody against Ki-67 (Figure 3-17A). It is apparent from Figure 3 that epidermal cells labelled with Ki-67 were mostly localised in the nuclei of cells in the basal germinal layer of dermal papillae and was observed in very few cells in the supra basal layer at the intertubular portion. However, entire length of papillae, almost non-existent Ki-67 staining was present at the suprabasal layer of the dermal papillae. Additionally, a large numbers of these +ve cells were visibly observed close to the basal layer lining the proximal part of papillae as well as in basal layer of inter papillary area. These +ve cells indicated their responsibility for the constituent intertubular horn. Ki-67 +ve cells were not shown beyond the suprabasal layer and visibly diminished further away from the basal layers (Figure 3-17a1). In addition, in the second half of dermal papillae (Figure 3-17b1), very few Ki-67 +ve cells were observed clearly in the basal cells and had no cells away from the basal and supra basal cells labelled the antibody. Moreover, at the level of distal end of papilla, Ki-67 +ve cells was not shown within the basal and supra basal cells (3-17c1).

The result, as presented in Figure 3-17B, indicated there was a significant correlation between the percentage of Ki-67 +ve cells of dermal papillae, and the length of dermal papillae from the proximal part of the dermal papillae increased, a decrease in the Ki-67 +ve cells was counted (Figure 3-17a1-c1).

Additionally, the percentage of Ki-67 positive cells of dermal papillae, their surface area ratios were calculated and analysed. The statistical analysis using nonlinear regression indicated that there was a significant correlation between the percentage of proliferating cells Ki-67 per surface area and length of papillae

($p<0.05$; n=7). This ratio demonstrated the correlation between the frequency of Ki-67 positive cells and the surface area as defined in Figure 3-17C.

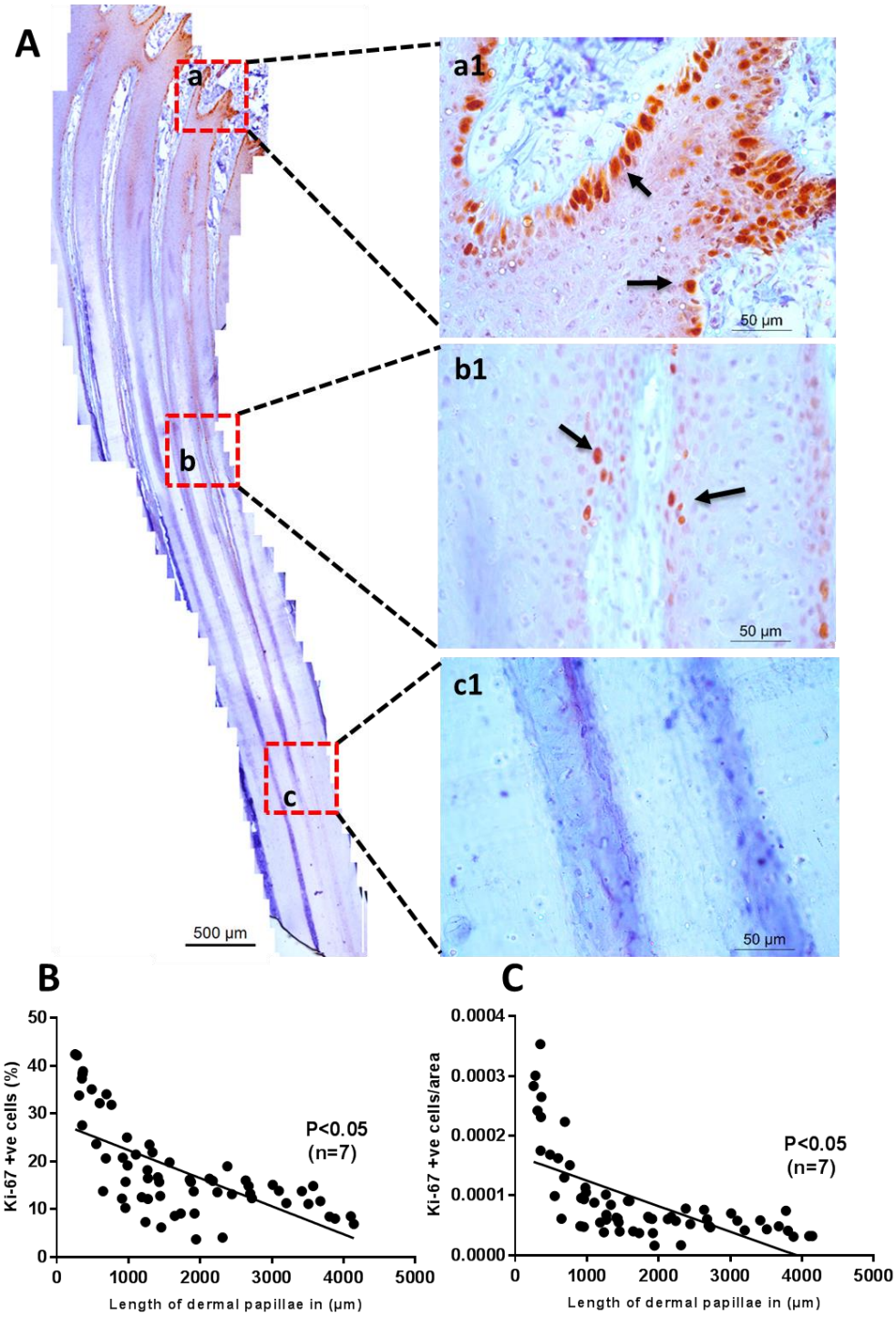


Figure 3-17: The Ki-67 +ve cells plotted against papillae length

A) Photomicrograph stitched images illustrating Ki-67 +ve cells scattered along the papilla, which appeared clearly at the proximal papilla (a, a1; black arrows) and very few cells at the middle (b, b1) and/or at the end of papillae (c, c1). B) There was a clear variation in the percentage of Ki-67 +ve cells as a function of the distance from the proximal dermal papilla. C) A significant correlation was recorded between the surface area and the ratio of Ki-67 expression using GraphPad software (* indicates $P<0.05$ vs papillae length). Image (A) scale bar represents 500µm and (a-c) 50µm. N= 7 per hoof animal, 20 images per animal.

3.4.5.3 Assessment apoptotic TUNEL positive cells along the papillae

In order to determine and compare the site, and dissemination of apoptotic epidermal cells in the coronary hoof dermal papillae. A TUNEL assay was employed and the number of apoptotic cells per length of papila were counted and measured along the distance of the papillae.

The results obtained from the analysis presented in Figure 3-18A revealed that apoptotic cells were not shown in the first quarter part of the papilla length (Figure 3-18a1). The first part which was located on the middle between two papillae showed that the stratum basale and suprabasal, in addition to the proximal most cells of the stratum spinosium did not exhibit apoptotic cells. However, as the keratinocytes were located further distally into the second layer stratum spinosum (Figure 3-18b1). The localisation of apoptotic figures was indicated visibly at the level of the fully keratinized cells in distal most stratum spinosium and the proximal most cells of stratum corneum. At the same level, apoptotic cells were seen in the suprabasal cells of the dermal papillae. Whereas, more distally almost no cells were stained positively for TUNEL (Figure 3-18c1).

The result indicated there was a significant correlation between the percentage of apoptotic +ve cells of dermal papillae and the length of dermal papillae ($p<0.05$; $n=7$) (Figure 3-18B).

The statistical analysis using nonlinear regression in Figure 3-18C indicated that there was a significant correlation between the percentage of apoptotic cells per surface area and length of dermal papillae ($p<0.05$; $n=7$). This ratio demonstrated the correlation between the frequency of TUNEL positive cells and the surface area as defined in Figure 3-18C.

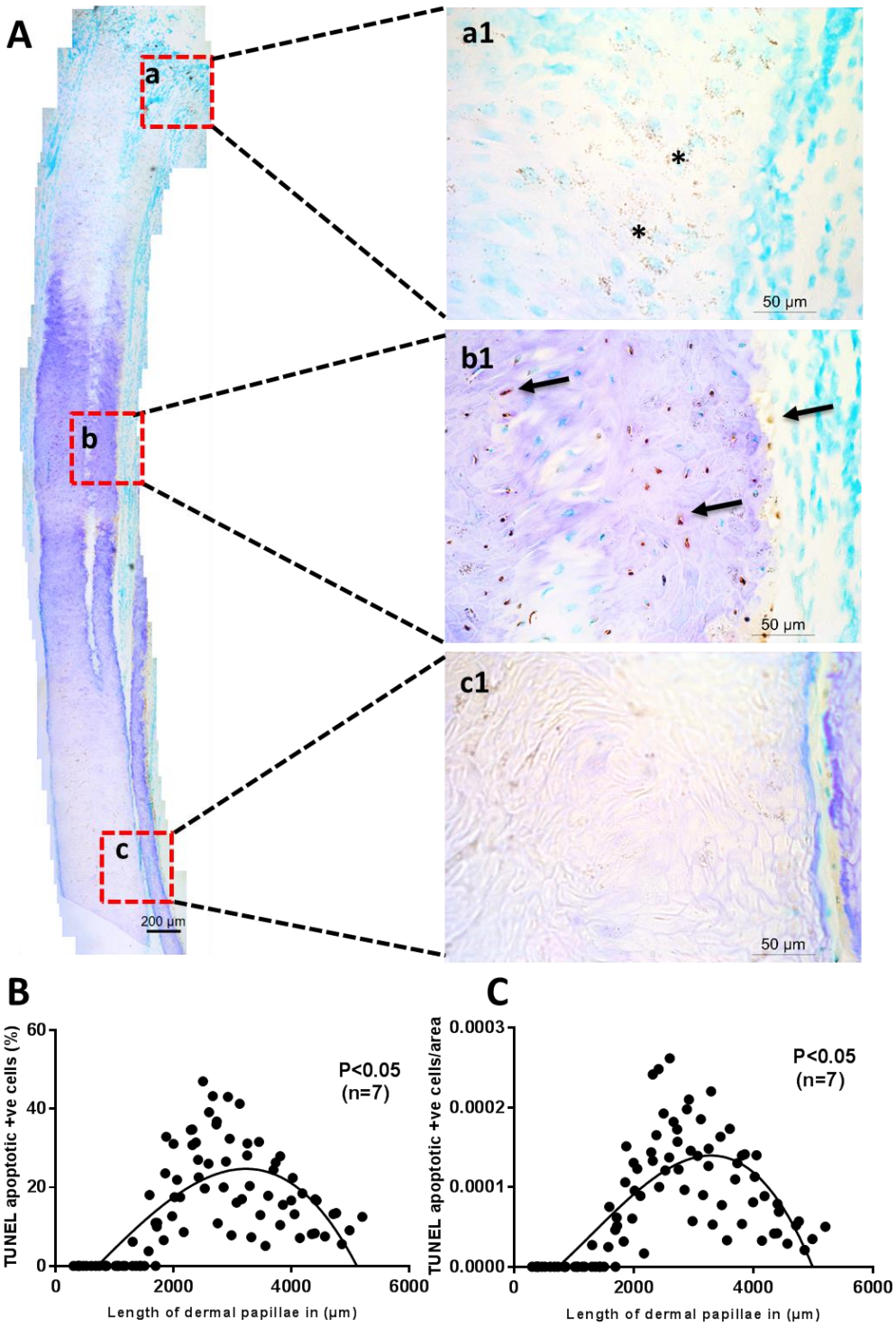


Figure 3-18: The TUNEL +ve cells plotted against papillae length

(A) Photomicrograph stitched images illustrating positive TUNEL +ve cells scattered only along the middle and very few at the end of papillae, which appeared clearly (a, a1), and labelling the basal and supra basal layer at the middle (b, b1; black arrows) and very few at the end of papillae (c, c1), whereas (*) asterisk marks represent the melanin pigment. B) The nonlinear regression coefficient revealed that there was a clear variation in the density of apoptotic cells along the distance of the dermal papillae. C) Significant correlation was recorded between the surface area and the ratio of apoptotic cell expression using GraphPad software (* indicates P<0.05 vs papillae length). Image (A) scale bar represents 500µm and (a-c) 50µm. N= 7 per hoof animal, 20 images per animal.

3.5 Discussion

This study set out with the aim of assessing the importance of how the hoof grows and responds to the physical environment. Some pathological factors, for example hoof lameness/laminitis seem to involve augmented and stimulation of normally hoof growth (Cripps and Eustace, 1999, Daradka and Pollitt, 2004). It is essential to know accurately which processes and mechanisms control the growth rate of hoof wall. This chapter assessed the hoof growth rate by detecting and counting mitotic cell indices in the coronary hoof dermal papillae.

The results of this study indicate that the significant difference of epithelial thickness at the heel region in comparison to dorsal and quarter (Figure 3-9), suggested that these difference may be have an influence on the production and reduction of horny material. It seems possible that these results are due to influenced by nutrition (Ott and Johnson, 2001) environment (Hampson, 2011), genetics (Ducro et al., 2009); age (Frackowiak and Komosa, 2006) and season (Florence and McDonnell, 2006, Lewis et al., 2014). It is therefore probable that such differences have an impact on hoof wall growth, along with foot lameness (Dyson et al., 2011b).

Another important finding was the correlation between the epithelial thickness at the coronary region and the hoof wall thickness at the quarter regions, whereas there was no relation at the dorsal region (Figure 3-10). These results are potentially related to what has been suggested by Lancaster et al. (2013) who attributed to the difference in the density of tubular horns between different hoof regions. It can thus be suggested that the area of the toe and medial side of hoof wall contains high tubular density, conversely these area have thicker hoof wall which may become more likely to be subject to greater forces loading (Lancaster

et al. 2013). This current finding on the correlation at the quarter region may provide further insights into the dermal papillae structure and function and potential adaptive variations in relation to growth forces on the coronary region. The adaptation of dermal papillae has strongly been thought to be the site of growing the hoof wall (Leach, 1980, Daradka and Pollitt, 2004, Eurell and Frappier, 2013).

Another finding was that H&E stained coronary tissue sections indicated the presence of finger-like projections called papillae, clearly visible at low microscopic magnifications (Figure 3-2A+B). These papillae appeared in two areas: the periople and the coronet, and were oriented towards the keratinous layer as expected from previous investigations (Dellmann and Eurell, 1998, Stewart, 2013). These findings are consistent with other studies, which highlighted that the dermal papillae are found in different areas: the periople, the coronet, the sole, the frog, and the bulbs of the heel (Bragulla, 2003, Konig et al., 2007). Local differences in the length, diameter, and number of papillae and orientation of the dermal papillae of the wall were also found. In terms of the number of papillae at the coronary region, no one reported the number of papillae at the coronary region; most of the research reported showed the density of tubular horn at the middle hoof region (Reilly et al., 1996, Reilly et al., 1998a, Pollitt, 2004a, Lancaster et al., 2013). One of these studies reported, counts of tubules on four zones at the stratum medium of 22, 16-22, 11-16, and 11 tubules/mm^2 respectively, with average 16 tubules/mm^2 (Reilly et al., 1998a). However, these previous studies have not counted the number of papillae at the coronary region. The average number of dermal papillae in the current study was found to be 21±0.67/mm^2 across 15 horses is more than reported in cattle, which showed

13.4±0.927/mm^2 (Singh et al., 1992). These findings are likely to be related to the nature and mechanism of hoof growth and raise the possibility that the dermal papillae and dermal lamellae adaptations of the dermis, which are understood as an endeavour to increase the surface attachment with inner, hoof (Davies et al., 2007). A possible explanation has been stated by Budras et al. (1996) that the papillary region at the coronet is highly vascularised and has a high rate of horny production when comparing to the poorly vascularised lamellae. This could be a similar rationale behind the differing amounts of horny material produced in the horse and cattle. Another possible explanation for this is that most of the hoof wall growth is from cell division at the dermal papillae are supplied entirely by the underline dermal vessels. There is evidence that any disturbance or minor changes in the microvasculature will potentially lead to responses and changes in the overlying epidermal tissue. As a consequence of this reaction, there is an impact on the hoof growth resulting in changes in shape and thickness of the hoof capsule (Budras et al., 1996, Hirschberg et al., 2001, Davies et al., 2007). There are, however, other possible explanations on the differences in number of papillae in the horse and cow. The biomechanical method of horse feet to absorb or to reduce the ground force applied on the coronary region during racing or trotting (Kasapi and Gosline, 1997, Salo et al., 2010) could alter these papillae number. Overall, it has been suggested that it is the dermal papillae of the coronet, which control hoof wall growth (Bragulla, 2003, Bragulla et al., 2007, Budras and Sack, 2012). In the current study, the results of histo-morphological compartments of specific region dermal papillae of the equine hoof wall has provided further evidence in support of early researchers Leach (1980), Dellmann, and Eurell (1998) on the concept of the cell migration and keratinization at the coronary

equine hoof wall. Progenitor keratinocytes resting on the basement membrane were shown to be columnar to cuboidal at the proximal papillary region and then distally become permeable and keratinized, as they were moved proximodistally from the basal layer constituent at the end of papillae their tubular and inter tubular horns. This sequential development of cell division and cornification are analogous to that of most structural hard keratin, for example hairs, nails, wool, quills, hooves, horns and claws (Lynch et al., 1986, Marshall et al., 1991, Rouse and Van Dyke, 2010),

The results of Periodic Acid-Schiff (PAS) staining attested for the visualization of the basement membrane (BM), as it provides the junction between the germinal epidermal cells on one side, and the fine collagen dermal tissue on the other. The results of this chapter indicate that the BM at the end of dermal papillae was folded into several ridges corresponding with the long alliance of the papilla. These results corroborate the ideas of Davies et al. (2007), who stated that these folds act as guides for the orientation of tubular horns in a properly oriented proximodistal direction. In addition, there are equivalents to the secondary epidermal lamellae, which might play a significant role in increasing the attachment between the dermal and epidermal tissue to the periosteal surface of the distal phalanx. The integrity and borderline nature of the BM is important in indicating lesions of the epidermal tissue (Pollitt, 1996, Pollitt, 2004b). The PAS staining technique revealed some changes in the BM, including interruptions, and the separation of the BM from the germinal cells of the epidermal papillae, which permitted the visualization of the unfilled space between the BM and epidermal cells, of which some appeared more spherical and expanded (Figure 3-11). This finding supports the evidence found that laminitis could be initiated by changes in

the BM which have been suggested to indicate the beginning of laminar failure (Pollitt, 1996, Kyaw-Tanner and Pollitt, 2004, Visser and Pollitt, 2011).

Masson's trichrome stain was used to assess the proportions of collagen versus other connective tissues, particularly muscle. This method has been shown to be appropriate in investigating abnormal lesions of collagen fibres (White et al., 2004). The preliminary results showed the normal distribution of the green-coloured collagen fibres in the dermal tissue of equine foot (Figure 3-14), and red-coloured collagen bundles were also observed in some of the stained sections (Figure 3-15B). Previous studies have found that the red colour is due to a normal tension in collagen fibres before fixation, and suggested that the collagen held the Acid Fusichn (red colour) for a long period of time, which consequently mixed with the green colour of the collagen fibres (Flint et al., 1975, Flint and Merrilees, 1977). However, the current study was in agreement with a later study conducted by Pollitt and Collins (2015) that showed the importance of collagen fibres in the structure of the suspensory apparatus of distal phalanx of equine hoof. They used Masson's trichrome to demonstrate the connection of the parietal surface of the distal phalanx to the lamellar hoof wall. As is it, the chronic condition of this apparatus will consequently leads to disorders in capsular growth rate (Collins et al., 2010, Pollitt, 2010). This proposes that the amount of collagen fibres inside the dermal papillae was originated and extended from the under attachment deep dermal tissue and this might be explain if any abnormalities or degeneration appeared in deep dermis, consequently it will affect severely on both collagen fibres inside dermal papillae and the attachment with epidermal tissue.

This study has demonstrated that it is achievable to utilize a p63 antibody to identify epidermal stem and proliferating cell lines, as the antibody recognized

antigenically different forms of the p63 of the nucleus (Koster et al., 2007). This study confirms the work of p63 as a valid marker of epidermal stem cells in equine coronary hoof tissues (Carter et al., 2011, Linardi et al., 2015). In addition, Ki-67 was used as availed cell division marker (Scholzen and Gerdes, 2000, Liu et al., 2003). The p63 and Ki-67 proliferation marker of mitotic cells were shown in the nuclei of basale layer of the proximal interpapillary part of the epidermal and lining the dermal papillae (Figure 3-16A+3-17A). This evidence suggests that it is distinctly possible that the proliferating cells in basal cell layer are adding to the cell population and potentially into the intertubular horn in a mechanism that pushes the cells to move for further differentiation (Figure 3-16+3-17). As a result of this and because of these cells generated from the same part of basale layer, this could suggest that the adjacent cells would be moved distally at varying periods of differentiation (Eurell and Frappier, 2013). It is likely that those keratinocytes located close to the basal layer are in the early stages of differentiation, whereas those further away or a distance located beyond the basal layer are almost in the late stage of differentiation. This configuration of differentiation and cell migration are in agreement with Dellmann and Eurell (1998), and Eurell and Frappier (2013) findings, which stated that the epidermal basal cells as they move distally are subjected to different differentiation and pass through a widespread of stratum spinosium. Thereafter being completely keratinized the cells start losing their nucleus and form the stratum corneum of the intertubular horn of the stratum medium (Banks, 1993). It is possible to hypothesise that these cyto-differentiation of keratinocytes along the dermal papillae are likely to disrupt causing differences in the differentiation along the length axis of dermal papillae. These cells might also be predisposed by biomechanical modifications that happen in the

catastrophe of the suspensory apparatus of the distal phalanx during laminitis, as observed by Carter et al. (2011). In addition to another causes such as glucose metabolism (Pass et al., 1998, French and Pollitt, 2004b), endocrinopathic causes (McGowan, 2010, Karikoski et al., 2011, Johnson, 2017), all these causes and more may play a significant role in dysregulation in the basal epithelial attachment which consequently have an impact on the cytoskeletal and cell junction, and eventually on cell differentiation (Pollitt, 2016). Another important finding was that the TUNEL positive apoptotic cells were found in the junction between the stratum spinosium and corneum of the keratinized axes of the dermal papillae and was absent beyond the stratum spinosium (Figure 3-18). This may be a significant and applicable finding that no one has considered the importance of the apoptotic cells along the dermal papillae and what has been reported so far was related to lamellae in particular equine laminitis. However, Faleiros et al. (2004) who assessed the apoptotic cells in laminitic horse concluded that increasing cell death at the interjection between the secondary and primary lamellae may perhaps help to accelerate in the structural failure of hoof wall attachment and distortion of the hoof wall that develops later.

The observation of positive proliferating cells in the epidermal cells of the dermal papillae confirmed the findings of previous studies of the equine hoof, which found these to be the main areas of hoof growth (Bragulla, 2003, Daradka and Pollitt, 2004, Pollitt, 2010, Carter et al., 2011, Linardi et al., 2015). This study has highlighted that the counting of these proliferating cells provided several important facts, as these cell indices, create an original method for comparing the growth rate between hooves (Figures 3-16+3-17). The current results also showed a high number of Ki-67 positive proliferating cells scattered only in the basal

layer of the proximal part of papillae and interpapillary space (Figure 3-17). Similarly, results indicated p63+ve stem cells were labelled in both the basal and supra-basal layer of the same proximal papillary part (Figure 3-16), as expected by Daradka and Pollitt (2004), whereas +ve cells for both Ki-67/p63 were absent in the subrabasal layer along the axis of dermal papillae. This finding supports previous research in terms of the way that hoof capsule distorted. These studies stated that the forces applied to the large area of the dorsal hoof wall were likely to act in the direction of the coronet at the toe, causing compression dorsally and rotation at the quarters. This could be understood when the known forces applied to the foot, then the consequent distortion of its capsular wall (Thomason et al., 1992, Thomason, 1998, Thomason et al., 2004). Furthermore, external aspects, such as training, trimming and feeding, have been suggested to have an impact on the hoof growth, which consequently may influence the conformation of hoof wall (Moleman et al., 2006, Moorman et al., 2013). The interpretation of these findings suggests the need for further investigation into the physical factors of hoof growth using CT scan images for example. More analyses of the biological factors involved in determining the shape of the hoof capsule are also needed and, in particular, the changes, which occur in lame horses, which might be consistent with the anatomy and have significant consequences for hoof, function. The present study confirms previous findings and contributes additional evidence that proposes an important question. This question is why was there a high proliferation index at the proximal part of interpapillary and papillary region which was not shown the same at the middle and distal end of the papillae, whereas stem cell p63 marker labelled cells at basal layer of papillae was almost absent at distal end of papillae. Taken together, the possible explanation could be

attributed to forces acting at the basal epidermal papillae that as a result may have an impact on the progenitor keratinocytes via cell proliferation and induced cell division. Indeed, this force might arise from either hydrostatic pressure or stretch, or may be due to the level of oxygen in this area, or hormonal disturbance such insulin. One suggestion is that once these cell are fully keratinized this results in decreasing or diminished forces being applied on the middle and distal end of papillae and that is why decreasing proliferation rates were observed at the middle and distal end of papillae. However, this study has also raised important questions about the mechanisms by which hoof grows on the coronary region. This concept is further explored in the next chapter, which provides evidence on the method of responding cultured progenitor keratinocytes, which are subjected to different environments, for example low oxygen level, hydrostatic pressure, mechanical stretch and insulin.

3.5.1 Conclusions

This study considered the localization and expression of stem cell and proliferation markers in addition to apoptotic cells along the dermal papillae of equine coronary epithelial tissues. Explanations of histological morphology of epithelial cells along the dermal papillae and markers for proliferating cells, apoptotic cells, and epithelial thickness together with analysis of the hoof wall thickness were provided. Taken together, these findings suggest a role for these methods in aiding further investigation of problematic issues in the histopathology of epithelial tissues of horse feet and provide insights for increasing the field of regenerative medicine in treatments of laminitic horses in particularly equine laminitis.

Chapter 4

Isolation and characterization of equine hoof keratinocytes and physical applications

4.1 Introduction

Epidermal stem cells possess an extraordinary potency for self-renewal during the lifespan of the tissue, although they produce daughter progeny cells that can differentiate into one or several lineages (Alonso and Fuchs, 2003). Two distinct populations of epidermal progenitor cells in epidermal tissue are self-renewing stem cells and transit amplifying cells (Blanpain et al., 2004, Clayton et al., 2007). These progenitor basal cells are multipotent progeny cells that divide into new keratinocytes with continuous differentiation (Blanpain et al., 2004). These cells interact and manage the signals from several growth factors, adhesion molecules and cytokines, and control the renewal of the epidermal tissue (Tomic-Canic et al., 1998, Rangarajan et al., 2001). A previous study by Barrandon and Green (1987) found that human keratinocytes are varied in their ability for self-renewal, and can generate three types of cell colony: holoclones, meroclones and paraclones which have the greatest, intermediate or non-proliferative potential respectively. The authors concluded that holoclones *in vitro* might be stem progenitor cells *in vivo* (Barrandon and Green, 1987).

The characteristics of stem cells isolated from adult tissue are defined by high plasticity and that they are amenable to differentiation to different cell types (Blau et al., 2001). These cells also express specific stem cell surface markers, including CD44, CD24 (Mani et al., 2008), CD29, CD166, CD106, CD105,CD34, α6-integrin, β1- integrin and CD34 (Tumbar et al., 2004). It has been previously reported by Kaya et al. (1997) that the transmembrane glycoprotein CD44 is one of the main stem cell-surface receptors for hyaluronic acid in skin, serving as a regulator of keratinocyte proliferation (Blacking et al., 2011).

In addition, CD44 is involved in self-renewal and differentiation as well in signal transduction in cell migration and cancer progression (Williams et al., 2013). Furthermore, CD44 participates in establishing regular signals by binding ligands associated with actin microfilaments or receptor tyrosine kinases and also acts as a co-receptor with tyrosine kinases (Ponta et al., 2003).

Recently, researchers have shown that purification of equine skin epidermis provides the benefit of being able to purify cells with these characteristics – that it is a potential source of stem cells which shows the ability to express stem cell markers such as CD44, CD29, CD90, CD49f, p63, Casein kinase 2β, and Ki-67, as well as a low expression for K14 and negative expression for CD105, K18, Pan CK and Wide CK (Broeckx et al., 2013, Borena et al., 2014). Other studies on equine skin and lamellae confirmed that keratinocytes generate Ln-332 and integrin α-6 as well as Hemidesmosome proteins, bullous pemphigoid antigen 1/2 and plectin (Visser and Pollitt, 2010).

Keratinoblasts are the stem progenitor cells in the epidermal basal layer of the stratified epithelium (Bragulla and Homberger, 2009). Keratin proteins are the main constitute of keratinocytes, comprised of intermediate filament (Bragulla and Homberger, 2009). Keratins expressed in epidermal tissues are closely associated with the differentiated state (Porter et al., 2000). They are encoded through a multigene family of more than 50 genes that form part of distinct developing pathways (Bragulla and Homberger, 2009, Ramms et al., 2013). Several studies on equine epidermis have indicated that cytokeratin 14 (K14) and (K5) are the major dominant keratin pair (Romano et al., 2009, Bragulla and Homberger, 2009, Sharma et al., 2016). It has also been reported that additional cytokeratins K15 and K19 may be expressed (Porter et al., 2000, Pinto, 2012).

These are the essential keratins of all keratinocytes, particularly in the basal stratified epithelium (Porter et al., 2000, Lloyd et al., 1995). These keratins are synthesized in the basal layer of hair follicle, skin and nail in human (Waseem et al., 1999), and in the coronary and lamellae of the equine hoof (Carter et al., 2011). K14 is vital for the structure and function of the proliferation cells (Romano et al., 2009). For example, the lack of K14 filaments in basal epidermal cells causes epidermolysis bullosa simplex in humans (Chan et al., 1994). Keratins 14, 5 and 15 as well 19 are expressed in basal epidermal tissues, indicating that they are expressed in self-renewing progenitor stem cells. As these cells start differentiate and move outward the levels of keratin expression changes. For example, keratins 1 and 10 are expressed in the suprabasal cells of the epidermal tissue and are hence considered as essential for post-mitotic differentiation in stratification and cornification of the epithelium (Poumay and Pittelkow, 1995, Bragulla and Homberger, 2009, Park et al., 2016). In contrast, equine skin keratinocytes in terminal differentiation exhibit a distinct polyhedral and flattened cornified morphology which expresses Involucrin, a marker of final cell differentiation (Carter et al., 2011, Sharma et al., 2016) (Figure 4-1). Therefore, the type and nature of specific keratin markers expressed by epidermal cells determines a precise state of cell differentiation (Candi et al., 2005). This heterogeneity of the cell population within the epidermis enables cell characterization and helped to understand the dynamic process of growing tissue (Taylor et al., 2000). Hence, the pattern of keratin protein expression offers a useful tool for studying the progression of epithelial cell differentiation and cycles of epithelial self-renewal (Candi et al., 2005, Eckhart et al., 2013).

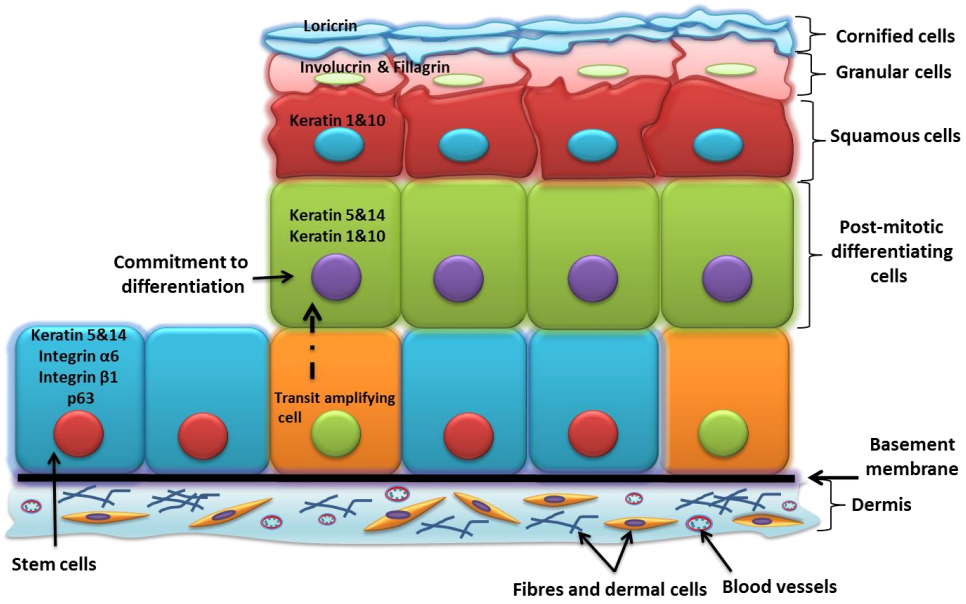


Figure 4-1: Schematic diagram illustrating the stages of epidermal skin epithelization

Basal keratinoblasts attach to an underlying basement membrane. Once they move from the basement membrane, they start to cease cell division and strengthen their cytoskeletal structures by +ve different keratins. As the cells move toward the terminal stages of differentiation, cell death results in flattened squamous at the skin surface. This figure is adapted from (Fuchs and Cleveland, 1998, Porter and Lane, 2003).

Oxygen could be one of the predisposing factor that accelerate cell differentiation (Bath et al., 2013, Park et al., 2016), as responding and reacting to low oxygen is vital for many physiological processes (Studer et al., 2000, Hubbi and Semenza, 2015). For example cell cycle and differentiation are essential such as wound healing via activation of low oxygen-inducible factor 1α (HIF-1α) and generation reepithelialisation (Rodriguez et al., 2008). HIF-1α induced to expression of transcription factors that control stem cell renewal such as OCT4 as well as changing cellular metabolism and inducing angiogenesis (Keith and Simon, 2007). In response to low oxygen, smooth muscle cells of the pulmonary artery and myocytes of cardiac muscle are shown continuity to proliferate (Hubbi and Semenza, 2015). In addition, low oxygen may lead to abnormal differentiation of cell keratinocyte through inhibition of K1 and K10 production via HIF-independent pathways (Park et al., 2016).

The importance of low oxygen on hoof material synthesis, and therefore the underlying cell differentiation of the keratinocytes have been indicated in the pathology of laminitis (Pawlak et al., 2013). In equine cultured keratinocytes, some evidence has been indicated on a possible connection between the damage in basement membrane and low oxygen via up-regulation of matrix metalloproteinase-2 and -9 (MMPs) (Medina-Torres et al., 2011). Recently, a significant elevation of HIF-1α expression in laminitis feet was shown (Gardner, 2015). However, to date it is unclear how progenitor keratinocyte cells respond to low levels of oxygen and whether these are involved in laminitis.

The cytoskeleton of mammalian cells is composed of three types of filamentous networks (Fuchs and Cleveland, 1998, DePianto and Coulombe, 2004). (1) The 6 nm actin filaments (F-actin) located directly beneath the plasma membrane is the major constituent of filopodia and lamellipodia, and participates in the mechanical resistance of cell stretching (Lulevich et al., 2010). (2) The 10nm intermediate filaments (IF) are keratin filaments in most epithelial cells and participate in cell integrity during mechanical strain (DePianto and Coulombe, 2004). (3) The 23nm microtubules exist as composites in numerous cellular structures (Fuchs and Cleveland, 1998). Many studies have confirmed that IF provide a malleable intracellular scaffolding that enables the resistance to mechanical strain exogenously applied to the cell (DePianto and Coulombe, 2004, Clayton et al., 2007). Thus, such changes or modifications in the molecular structure of IF, for instance mutation could be one of the coexisting factors that change this structural framework and help to increase the potentiality of cell damage, as well as causing a diversity of human disorders (Fuchs and Cleveland, 1998). Keratinocytes are stiffer by 6–70 times than other cell types including fibroblasts, breast epithelial

cells, neuronal cells or white blood cells, and this high strength and flexibility is attributed to keratin IF networks within keratinocytes (Lulevich et al., 2010). Other studies have shown that IF induce cell growth and morphology by regulating protein production (Kim et al., 2006, Ramms et al., 2013). Additionally, it has been demonstrated that mechanical stretching of human keratinocytes induced cell proliferation via calcium influx and phosphorylation of EGF receptor (EGFR) in addition to induction of K6 expression and reduction of K10 expression (Yano et al., 2004). Furthermore, the compressions strain of keratinocytes altered expression of keratin mutant i.e. (K125b) that is different from normal keratin K14 (Lulevich et al., 2010).

Little however is known about the consequences and biophysics of stretch stimuli on equine keratinocytes, especially those are epidermal coronary hoof region. Mechanical stretching/hydrostatic pressure or compression forces can influence hoof keratinocytes. Similarly, physiological hoof capsule renewal is achieved through continued progenitor keratinocyte differentiation within the basal layer of epidermal-specific tissue dermal papillae (Daradka and Pollitt, 2004, Eurell and Frappier, 2013). However, in chronic pathological cases such as chronic foot lameness/laminitis (Carter et al., 2011) and chronic coronary wounds, the endogenous healing mechanisms might be inadequate. Therefore, isolation and purification of EPKs might be valuable in the treatment of these hoof diseases. However, very few studies are available on the isolation and purification of EPKs (Broeckx et al., 2013, Borena et al., 2014) or from equine hoof lamellae (Pinto, 2012, Visser and Pollitt, 2010) using cell culture. In addition, very few methods are established to optimize the processes to enable prolonged growing of keratinocytes from equine epidermis for instance lamellae (Visser and Pollitt,

2010). Keratinocytes within the epidermal tissue are constantly under physical strains such as hydrostatic/shear pressures, and compression/tension strains (Lulevich et al., 2010). Cells can adapt to this dynamic force through changing their behaviour and modifying their microenvironment. They also respond to these strains through mechanoreceptors and counter strains by using reverse actomyosin and cytoskeletal-dependent cell-generated force (Butcher et al., 2009). The cellular response during biophysical stimulation is described recently by Barnes et al. (2017) (Figure 4-2).

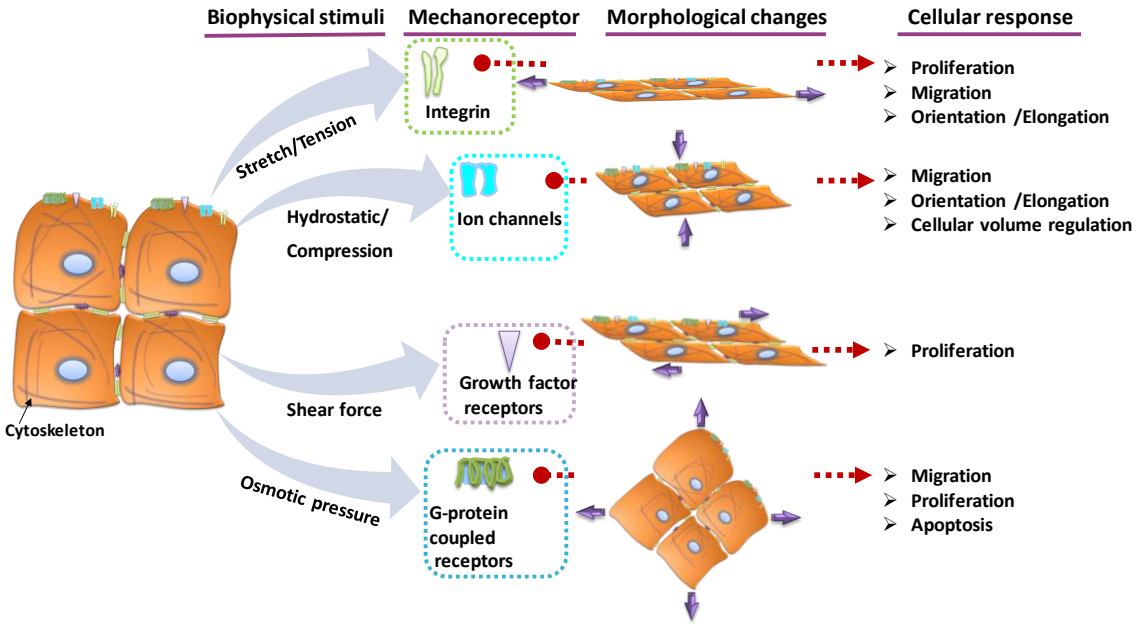


Figure 4-2 : Schematic diagram illustrates cells response for biomechanical stimuli

This diagram adapted from Barnes et al. (2017).

Outlining the role of mechanical signalling on progenitor keratinocytes lining the dermal papillae and their behaviour depends on exploring what participates in generating force in the cell. This includes the mechanism in which keratinocytes respond and integrate to external force signals within their cultured microenvironment, and subsequently the mechanism that these cells utilize for protein production in response to external force. Therefore, this chapter sought to

expand on the current understanding of tensional strength in cell development and differentiation in order to determine important areas for investigation. Additionally, responding and reacting to different levels of oxygen is vital for numerous physiological activities, of which cell cycle and differentiation are essential. The pattern of keratin protein expression offers a useful tool for studying the progression of epithelial cell differentiation and cycles of epithelial self-renewal. The importance of how hoof grows, and understanding how the coexisting factors might be involved in accelerate keratinocytes differentiation being part of the pathology of laminitis.

To date it is unclear how progenitor keratinocyte cells respond to low levels of oxygen and how these factors could be involved in laminitis, therefore they are investigated. This study also proposed a novel method of epidermal progenitor keratinocyte production for hoof diseases and tissue engineering. The aim of this study was to establish progenitor stem keratinocytes in epithelial cell cultures and to understand the biophysical mechanism of cell signalling. An additional aim was to investigate cell type characterisation in these cell cultures and to assess the regulation of HIF-1α and the transcription and expression of different keratin proteins in equine progenitor keratinocytes incubated in high oxygen or low oxygen conditions. Understanding equine hoof diseases is typically a big economic problem for breeders; therefore this work aims to help generate methodologies and comprehension of the systems involved. These diseases are also highly complicated due to limited information about the disease prognoses, and the lack of understanding of hoof growth. Therefore, progenitor keratinocytes could be used for physio-pathological research and understanding of such diseases is a valuable starting point in tissue engineering applications.

4.2 Hypothesis

The overarching hypothesis for this chapter was that equine progenitor keratinocytes at the basement membrane may initiate or adapt their behaviour via increased cell proliferation/differentiation following a change in biophysical forces. This was defined and subdivided into mini hypothese for the different experiments:

1. Blocking actomycin contractility (F-actin microfilaments) via blebbistatin decreases cell proliferation and commitment of cells to differentiation.
2. Progenitor keratinocytes isolated from the dermal papillae are pluripotent.
3. A model of cultured keratinocytes under different stresses such as stretch, hydrostatic pressure and/or low oxygen levels increases proliferation/differentiation, and upregulates keratin levels, leading to changes in morphology and cell surface area.
4. Stretching cultured keratinocytes imitates the stress borne from cells changing their size thus applying a tension on the papillae resulting in decreased cell differentiation.
5. Hoof growth is involved in laminitis via increased hyper-proliferative responses which is induced by insulin via Akt pathways

4.3 Aim and objectives

The introduction has shown many factors *in vivo/in vitro* that may affect cell behaviour. The aim was to determine the behaviour of EPKs (proliferation/differentiation) *in vitro* and provide a distinctive method to examine hoof pathologies related to keratinocytes function under biophysical stimuli such as stretch/hydrostatic pressure. In addition, the low level of oxygen in equine

cultured keratinocytes may provide a tool for better understanding the pathophysiology of equine laminitis (insulin mediated vasoconstriction).

For these objectives, concentrating on the behaviour of equine progenitor keratinocytes isolate from the coronary dermal papillae of the equine foot, different parameters were tested using the following techniques:

1. Cell pluripotency was assessed using immunofluorescence stem cell marker CD44 and keratin marker K14.
2. Alizarin red stain was utilised for detecting the cell differentiation into osteoblasts.
3. Cell contractile system was assessed via blocking with blebbistatin and measuring cell proliferation using Ki-67 labelling and cell differentiation with keratin marker K14 and K10.
4. Under hydrostatic pressure, stretch and/or low oxygen levels, cell proliferation was measured by labelling with Ki-67 and cell differentiation with keratin marker K14 and K10. Both immunofluorescence and Western blot were used. For low oxygen levels (5%), RNA levels were quantitated with real time PCR.
5. To measure cell proliferation under insulin incubation at a concentration of 0.1µg/ml (=2400µU/ml) similar to that needed to induce acute laminitis in live horse (>1036µU/ml) (Reeves et al., 2001, Asplin et al., 2007, De Laat et al., 2010), immunofluorescence and Western blot were used to examine the pathways of cell proliferation.

4.4 Results

4.4.1 Phenotypic characterisation of cultured progenitor keratinocytes

A number of optimisations were carried out until coronary equine progenitor keratinocytes (EPKs) were successfully isolated from the coronary epidermal tissue using a double enzymatic digestion method (trypsin and collagenase). The optimised method enabled the separation and extraction of the cells that attached to the dermal papillae, as described previously in detail in Chapter 2.10. Epidermal keratinocytes were completely separated and detached from the underlining dermal tissue. Figure 4-3, the dermal papillae were easy to observe and were dissected away clearly without any attachment (Figure 4-3D). As a consequence, mechanical methods including the use of fine forceps were applied to remove the epidermis without the inclusion of other dermal debris.

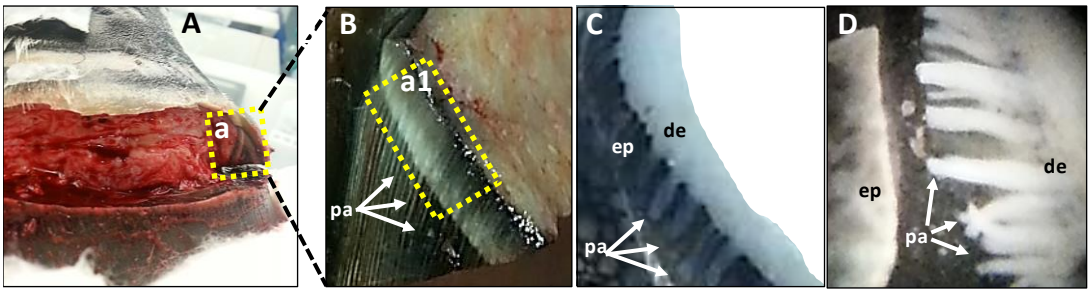


Figure 4-3: Schematic diagram showing the area of interest for isolation EPKs

A) Equine hoof showing (a) the area of coronary region that was extracted. B) Illustrates the coronary region that was removed (a1) and the dermal papillae (pa). C) Shows the location of the dermo-epidermal junction (de) including the epidermal tissue (ep) and the dermal papillae (pa). D) Represents the complete separation of the epidermal tissue (ep) from the dermal tissue (de) which contains the finger like projections of the dermal papillae (pa) following incubation in 0.25% trypsin-EDTA for 18hrs.

Following the second enzymatic digestion with collagenase, homogeneous mixtures of cells were yielded, mostly containing keratinocytes from basal and suprabasal cells in addition to melanocytes (containing black pigmentation). The

isolated EPKs were seeded at a density of $5x10^3$ cells/cm^2 onto the collagen coated plate surface and attached within 10min (Figure 4-4A). A number of cells were observed to be unattached with a spherical shape which persisted in their detachment post seeding for at least 24hrs. Those cells were removed during the first change of culture medium.

24hrs after seeding, the cultured EPKs were observed as they divided and formed small colonies of closely packed keratinocytes. Some observed EPKs grew as small epidermospheres (Figure 4-4A&B). The early stage of the cell growing and increasing in number was visible by the presence of cobblestone cells which could be detected in all cultures as early as 24hrs (Figure 4-4B). The present study indicated that the attached cells continued to grow relatively constantly during the first 1-10 days. These results indicated that most of the sphere of EPKs formed sustained their phenotype and were efficient in generating further generations of EPK cell lines.

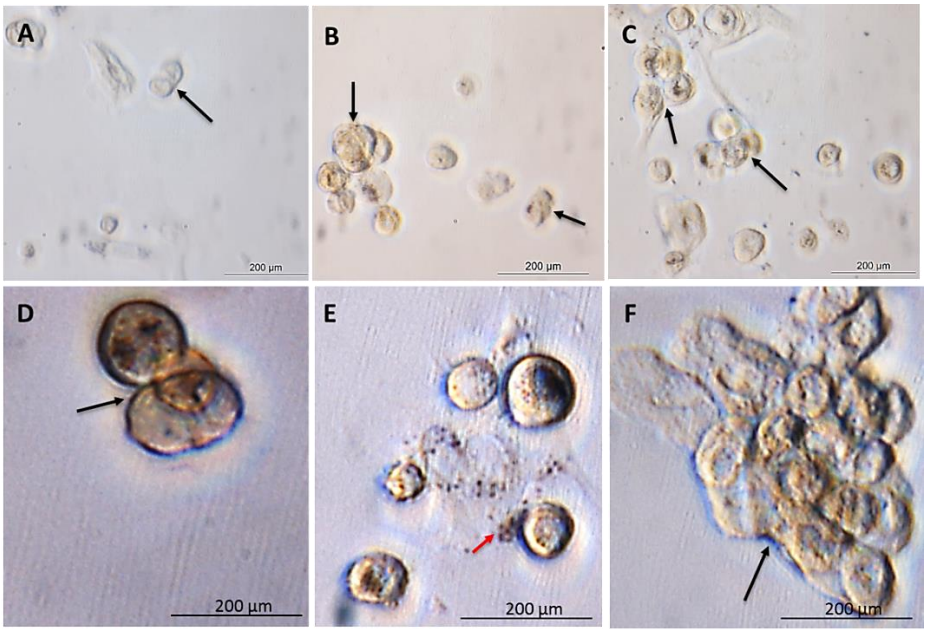


Figure 4-4: Sphere development in equine progenitor keratinocytes (EPKs)

EPKs from the coronary region were seeded and cultured in growth medium to illustrate the early stage of cell cycle. A) Shows the early stage of cell cycle after 12hrs. B) Indicates an increase in the number of cells after 24hrs and this augmentation becomes more obvious in image (C). D) EPKs appeared as cobblestone-shaped cells, the black arrow shows a division between cells. (E) Melanin pigmentation (red arrow) in melanocytes was visible. F) Sphere formation and the appearance of keratinocytes as islets of cobblestone-shaped cells. Scale bar represents 200µm.

The current study revealed that EPKs developed small colonies on day 2, shown by the small spheres characteristic of the cobblestone morphology (Figure 4-5). Additionally, it can be seen from (Figure 4-4) that cell division was taking place between day 1 and day 10. Indeed, epidermosphere development started within the first 24hrs and was clearly visible, encompassing 3–10 small cobblestone shaped cells (Figure 4-4). The size of these initial colonies and spheres expanded with time and exhibited the morphology of cobblestones (Figure 4-5). On day 2, EPKs colonies appeared as small patches of cells that increased in size by day 6 (Figure 4-5F). Colonies expanded outward such that by day 10, they were fused to create large, sporadically shaped colonies (Figure 4-5). Isolated spheres of cells could be seen on day 7-11. Cell confluence reached 90% at approximately 11 days post-seeding.

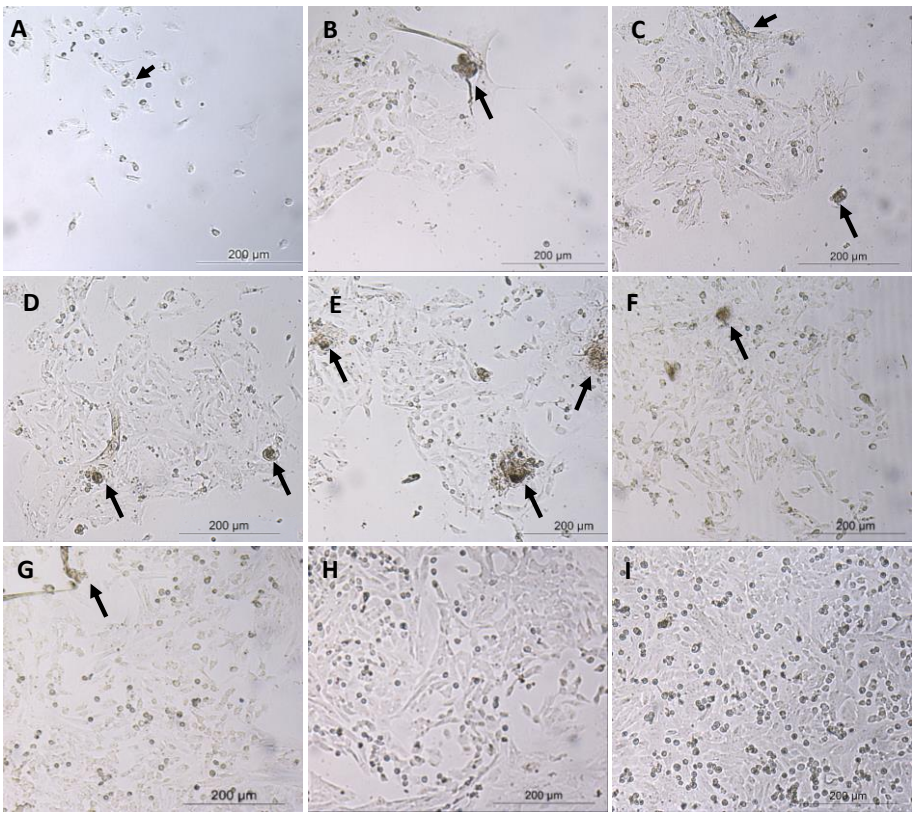


Figure 4-5: Growing and expansion of equine progenitor keratinocytes (EPKs)

Photomicrographs were taken every day over a period of 10 days to monitor cell expansion and growth. A) After 24hrs cells were attached to collagen-coated culture flask. B) After 48hrs epidermosphere development (black arrow), was observed. This expansion appeared clearly over time (C) 3 days, (D) 4 days, (E) 5 days, (F) 6 days, (G) 7 days and (H) 8 days, whereas (I) at 10 days. Scale bar represent 200µm.

Figure 4-6A shows the first phenotype that determines how cultured keratinocytes packed densely into dark spheres were relatively small in size. These structures represent the epidermosphere, and cells surrounding these spheres had the characteristic features of cobblestone and flattened shaped cells. These were further seeded, cultured with serially passages undertaken (Figure 4-6A), while the second cell phenotypes were grown for 3-6 days then differentiated. Third phenotypes were small and flattened and quickly terminated growth and could not be subcultured, thus both the second and third phenotypes were excluded from the experimental study and only cells with the first phenotype that had the ability to be pluripotent were retained.

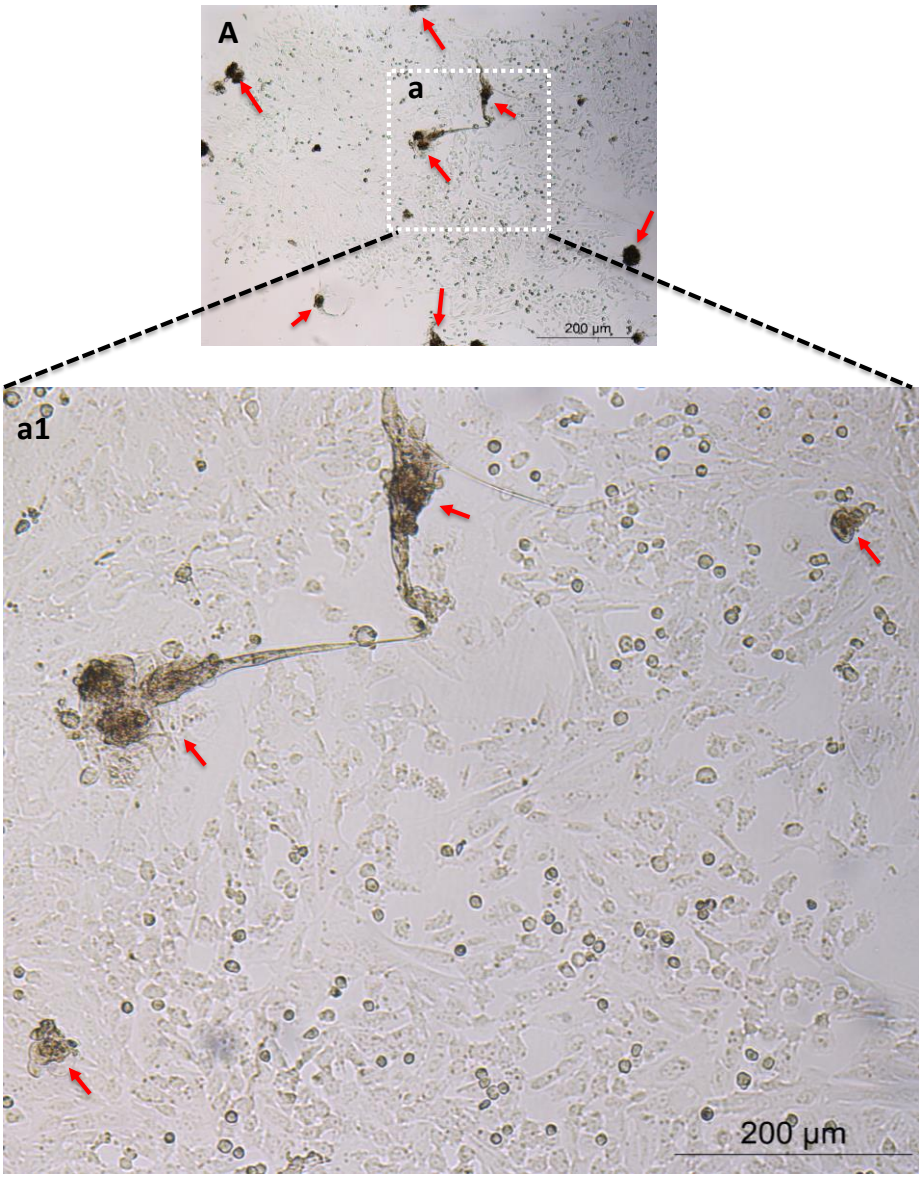


Figure 4-6: Epidermosphere showing the source of EPKs increase growth

A) Epidermospheres were spread on cultured keratinocytes (red arrows). Scale bar represents 200µm.

4.4.2 Immunostaining of cultured EPKs spheres

Further investigation confirmed that the spheres observed were EPKs. Primary cells cultured were categorised based on morphological appearance by immunofluorescence staining. Cultured EPKs were labelled using cytoskeletal protein K14 distinctive for epithelial cells in order to identify primary keratinocytes, CD44 a stem cell marker and Ki-67 a proliferation marker. EPKs were also stained with F-Actin against microfilaments to label the overall structural morphology of cells. Almost all EPKs were positively labelled for the stem cell surface marker CD44, K14 and Ki-67. All the antibodies were assessed for cross-reactivity in the negative control via immunofluorescence. The EPKs were characterized by immunostaining with antibodies against CD44 and F-Actin (Figure 4-7). EPKs appeared as three dimensional, exhibiting the phenotypical sphere form and providing a representation of the distinct borders of the cobblestone shaped cells. Additionally, the expression of K14 in cultured cells confirmed that the established culture system were EPKs (Figure 4-7).

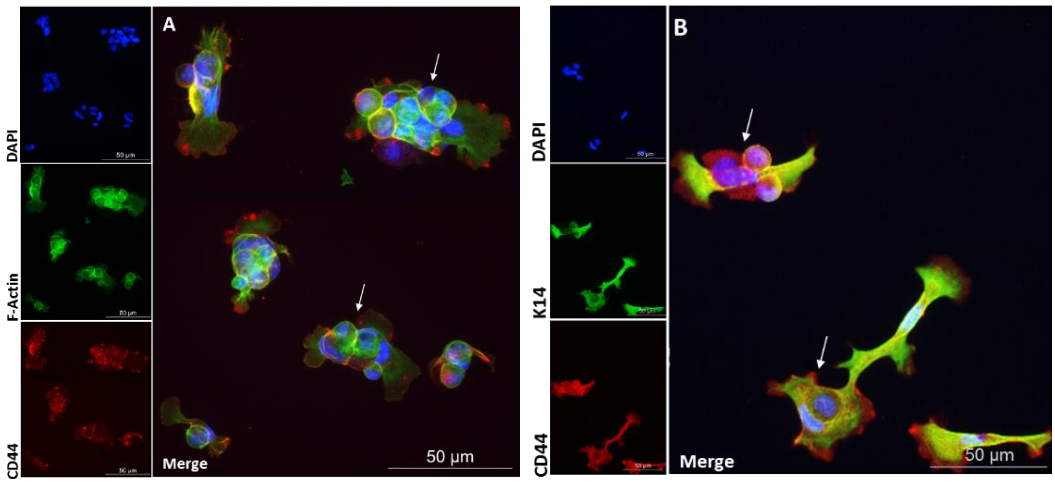


Figure 4-7: Epidermosphere identification with immunofluorescence staining

A,B) Fluorescent images of EPKs identified with F-Actin and K14 (green colour) and CD44 (red colour). White arrows point islets of cobblestone-shaped cells/ grapes-shaped cells. Scale bar represents 50µm.

4.4.3 The role of blebbistatin on the spreading of EPKs

The previous figure demonstrates that cells did not spread readily on their substrate once the culture started, which may be related to the presence of tension stress across the EPKs. In order to investigate the precise role of F-actin (or non-muscle myosin II filaments (NNMII)) a well-known component of cell tension in cell spreading, blebbistatin was used to promote tension-free EPKs. EPKs were cultured on a coated collagen plate surface and treated with 20μM blebbistatin for various times (1day, 3days, 5days), while controls were untreated. Non-treated EPKs did not show a strong cytoplasmic expansion, while the blebbistatin-treated EPKs exhibited variations in EPKs morphology after 12hrs of treatment and were observed to spread out (Figure 4-8A). These morphological changes demonstrated the presence of branches with distinctive leading and irregular edges connecting other neighbouring cells by day 3 (Figure 4-8B). Untreated cells were rounded with minimal extension (Figure 4-4). After 3-5days treated EPKs were less branched and did not present with cytoplasmic extensions between spheres. These observations highlight the role of F-actin and cellular tension of EPKs which is naturally present.

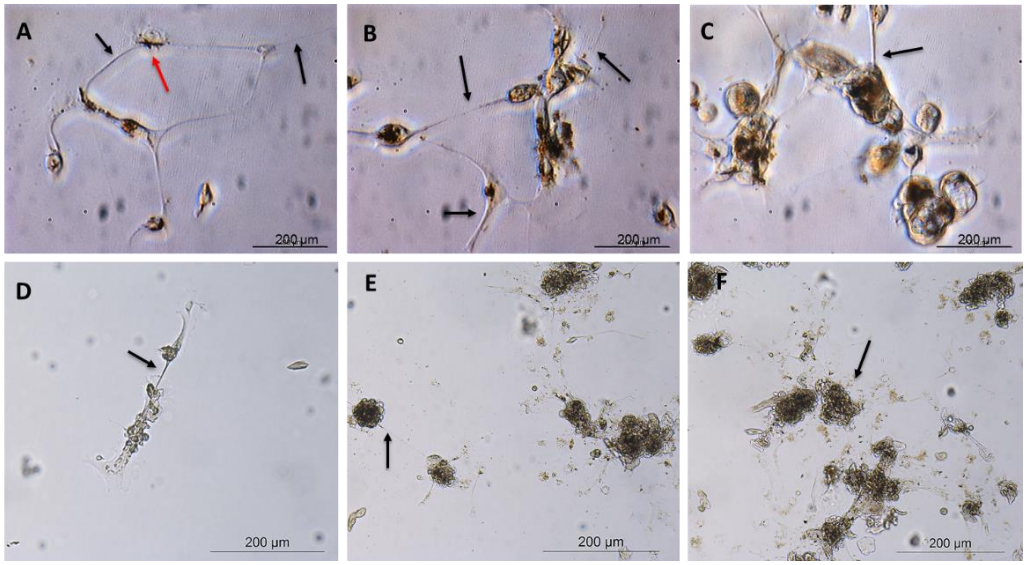


Figure 4-8: Cytoskeletal organization of the contractile system in EPKs treated with bleb.

EPKs incubated with 20µM blebbistatin show the early stage of inhibition of non-muscle myosin II (NMII). (A) Indicates that the EPKs have very long extensions (red arrow) after 12hrs. (B) Illustrates an increase in the number of cells after 24hrs, further illustrated after 48hrs (C). D) EPKs showing long extensions between spheres (black arrow) at day 3. (E) Shows enlarged epidermospheres connected to each other after 4days. (F) After 5days similar observation as in (E) (black arrow). Scale bar represents 200µm.

4.4.4 Assessment of the influence of blebbistatin on cytoskeletal EPKs

To determine the impact of blebbistatin on cytoskeletal K14 and stem cell CD44 protein expression EPKs were treated with 20µM blebbistatin, an inhibitor of NMMII, for a period of time. The results obtained revealed that on day 1 blebbistatin induced alterations in cyto-morphological features of cell growth, represented by the long extensions of cytoplasmic protrusions (Figure 4-9A+B). Similarly, at day 3 these changes became observable, with cells appearing as a mesh of flat membranous networks (Figure 4-9C+D). Incubation for 5 days with blebbistatin however revealed that there were fewer cell extensions and that cells exhibited morphological changes characteristic of cell differentiation (Figure 4-9E+F). In comparison, non-blebbistatin treated cells did not show any extension and these EPKs grew as cobblestone-shaped spheres. There were a significant

differences between K14 and CD44 markers in the EPKs when blebbistatin was used with regard to the control on day 1, 3 and day 5 (Figure 4-10A+B). Analysis indicated that approximately 60% of relative expression levels of K14 and CD44 after 3 days in blebbistatin treated cells, an overall decrease ($P<0.05$). These results revealed that CD44, K14/surface area were visibly decreased on day 3 and 5 ($P<0.05$) (Figure 4-10A+C), while results for the intensity of CD44, K14/number of nuclei did not show any significant differences at day 3 and 5 (Figure 4-10B+D). However, cell surface areas of the treated cells was significantly increased at day 3, and 5 in comparison to untreated control cells ($P<0.05$) (Figure 4-10E+F).

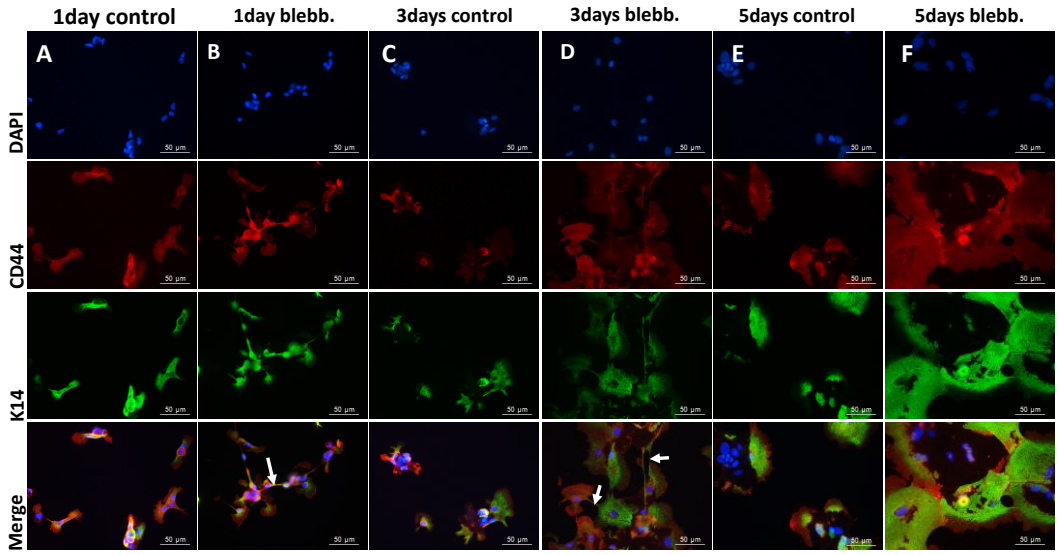


Figure 4-9: Cell marker expression in EPKs in control and treated with bleb.

Immunofluorescence staining images presenting the expression of CD44 and K14 in control conditions or following blebbistatin treatment. A) Shows control at 1 day with normal epidermospheres without cytoplasmic extensions. B) Indicates the presence of cytoplasmic extensions marked with white arrows. Cytoplasmic extensions become more evident in day three (D) in comparison to control (C). A similar observation was concluded at day five (E) and (F). Scale bar represents 50µm.

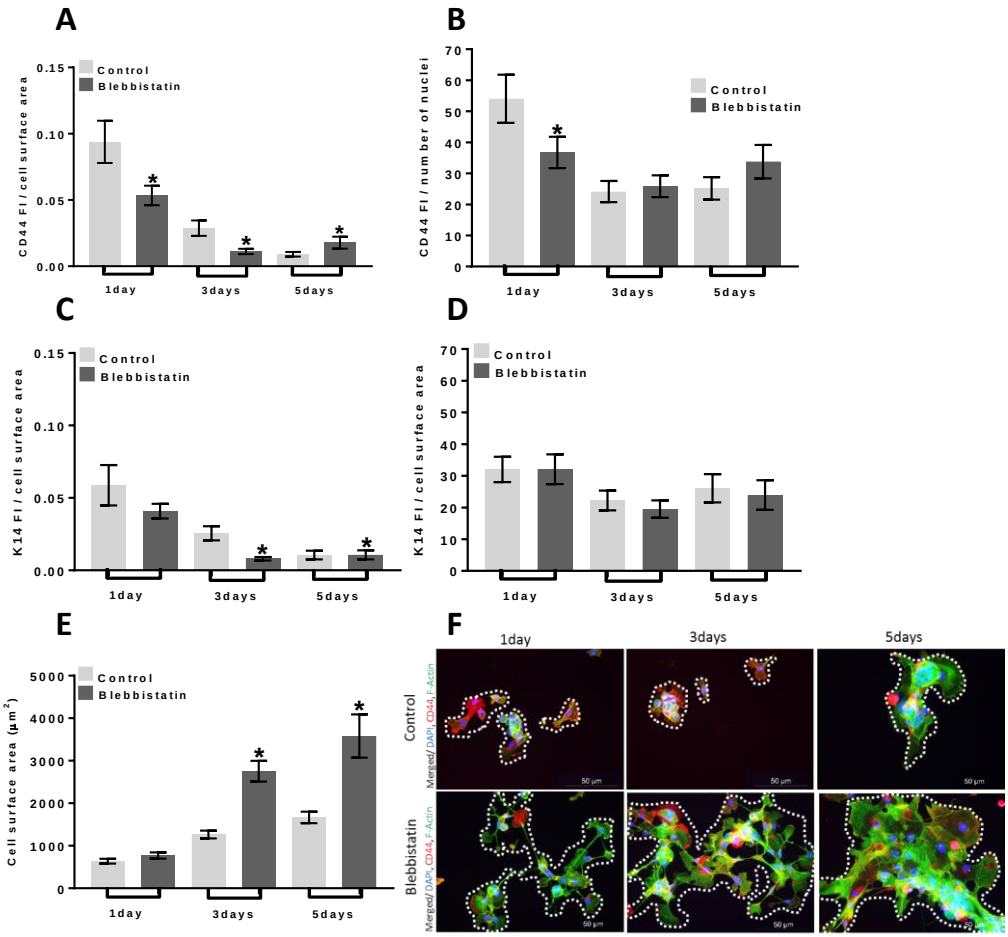


Figure 4-10: Graphs showing statistical analysis of EPKs treated or not with bleb.

(A, B) Significant variations were found between the intensity per surface area between control and blebbistatin treated cells at day 1 and 3. (C, D) Show no significant difference between the intensity per nuclei. (E) Displays a clear significant difference between the surface areas of the control and treated cells at day 1, 3, and 5. This is also shown in (F). Statistical comparisons between groups were analysed using One Way ANOVA, (* indicates P<0.05 vs control). N=3 animals, each in triplicate-10 micrographs, averaging 15 measurements/micrograph.

4.4.5 Expression and localization of inhibition myosin isoforms in EPKs

When compared to the control (Figure 4-11A) immunofluorescence staining of EPKs at day 1 treated with blebbistatin demonstrated that blebbistatin treatment resulted in modifications in actin filament organization (filaments were not visible compared to control) and cell attachments, and as a result exhibited changes in cell morphology generating large dishevelled boundaries and elongated extensions (Figure 4-11B). Similarly, at 3 days those changes were more obvious and were

observed as a mesh of networks. However, incubation with blebbistatin for 5 days resulted in fewer cell extensions. CD44 did not seem to be affected by blebbistatin and was present at some localization at the cell boundaries. An example of actin filaments organization and expression of CD44 at day 1 is given below. Addition of blebbistatin for 24 hrs resulted in concentrating F-actin at the edge of cells that was also strongly present in the membrane extensions joining cells, i.e. lamellipodia and in finger-like protrusions, i.e. filopodia (Figure 4-11).

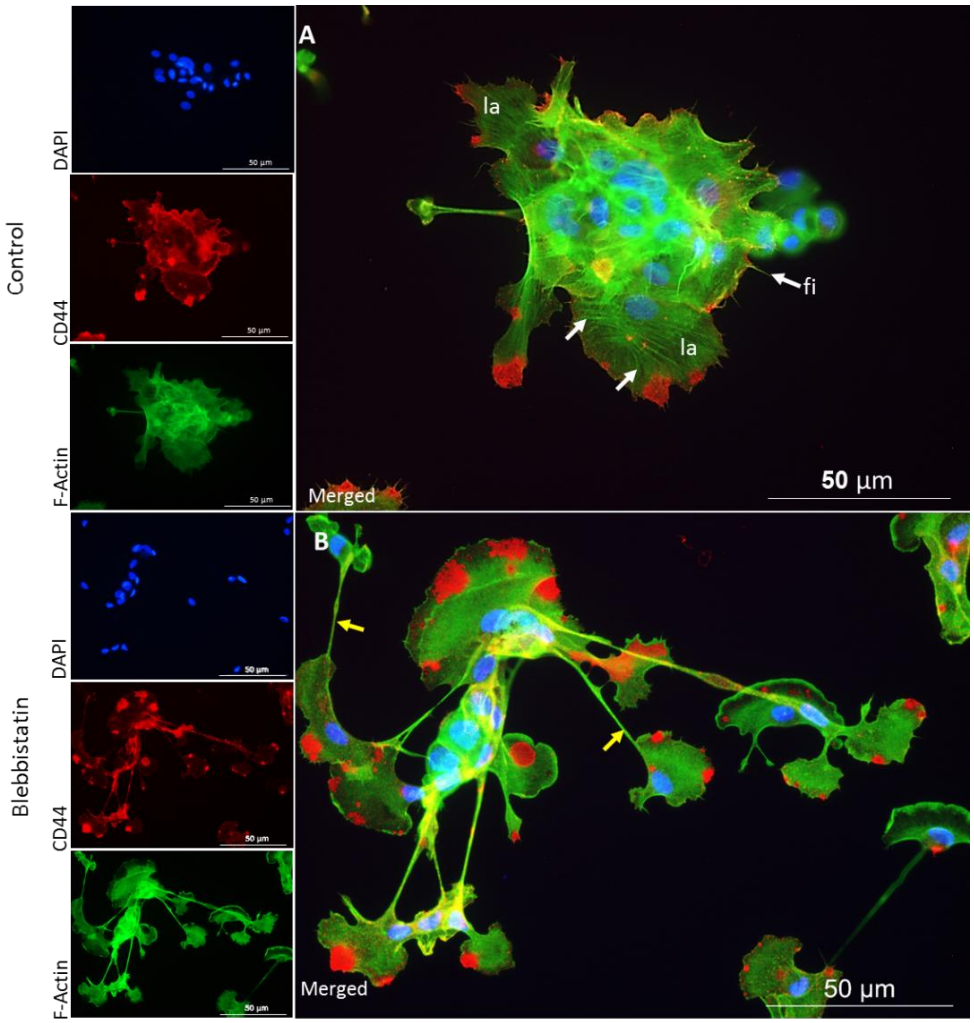


Figure 4-11: Structural organization of the microfilaments in cells treated with bleb.

(A,B) Fluorescence photomicrographs of EPKs stained with F-actin and CD44 in untreated (A) and 20µM blebbistatin treated (B) cells. F-Actin marked with white arrows was expressed and formed filaments in control cells; in particular, wide distribution of F-Actin was detectable in (A) but not filamentous detected in (B). Treated cells with blebbistatin did not show the formation of filaments but the strong presence of F-actin at the edge of cells as well as within the membrane bridge between cells (yellow arrow). (la) refers to lamellipodia and (fi) to filopodia. Scale bar represents 50 µm.

4.4.6 Assessment of EPKs pluripotency during cell passages

Seeding on collagen coated culture flasks during the 1st and 2nd passages (both 7-9 days) revealed that the cells initially in the spheres became dispersed and EPKs reached 80% confluence at approximately 7-9 days. However, trypsinization and re-plating after the second passage resulted in the subsequent differentiation of EPKs (Figure 4-12+4-13).

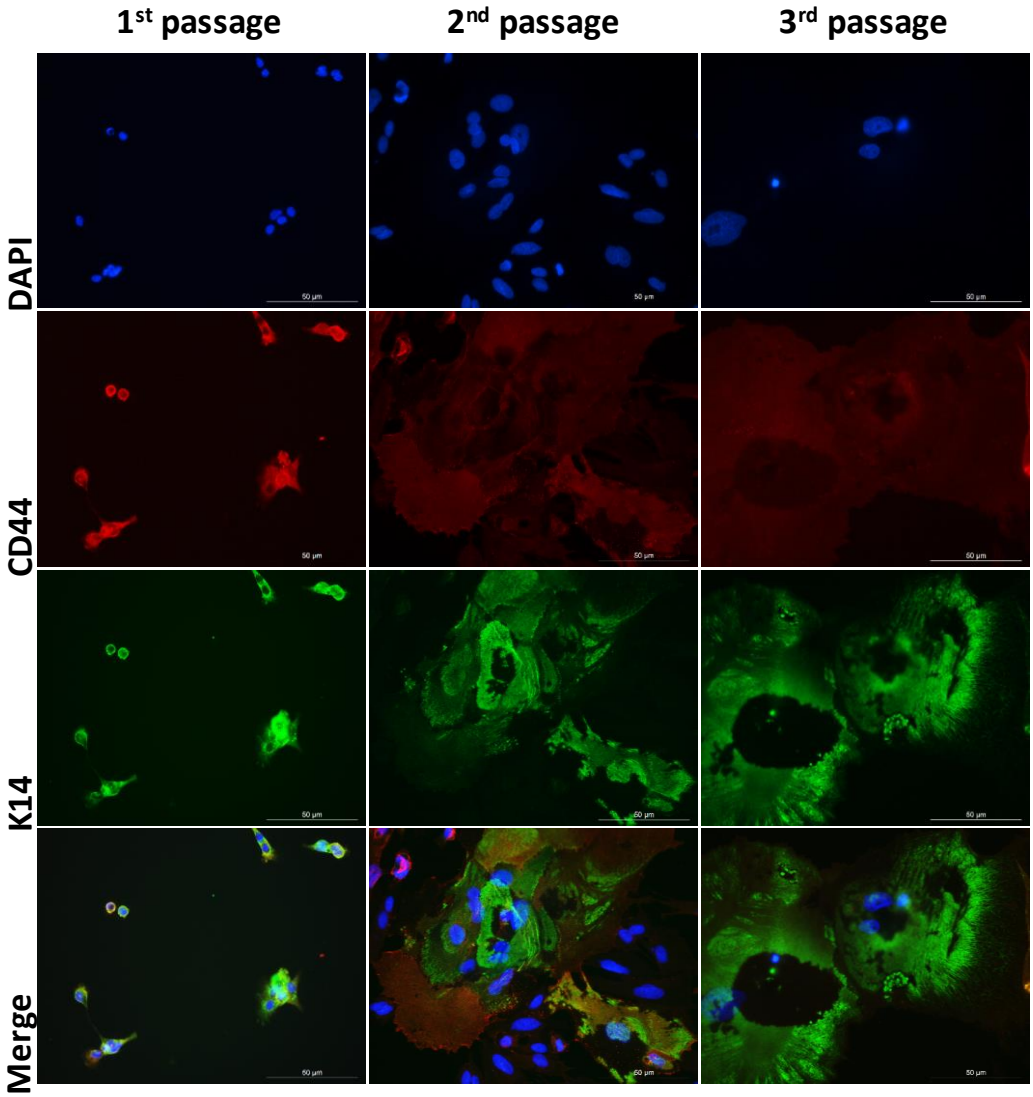


Figure 4-12: CD44 and K14 expression in EPKs during cell passages

Immunofluorescence staining showing the expression of CD44 and K14 during cell passages. Spreading of cells on the culture plate was clearly visible after the second passage including a drop in CD44 intensity. Scale bar represents 50µm.

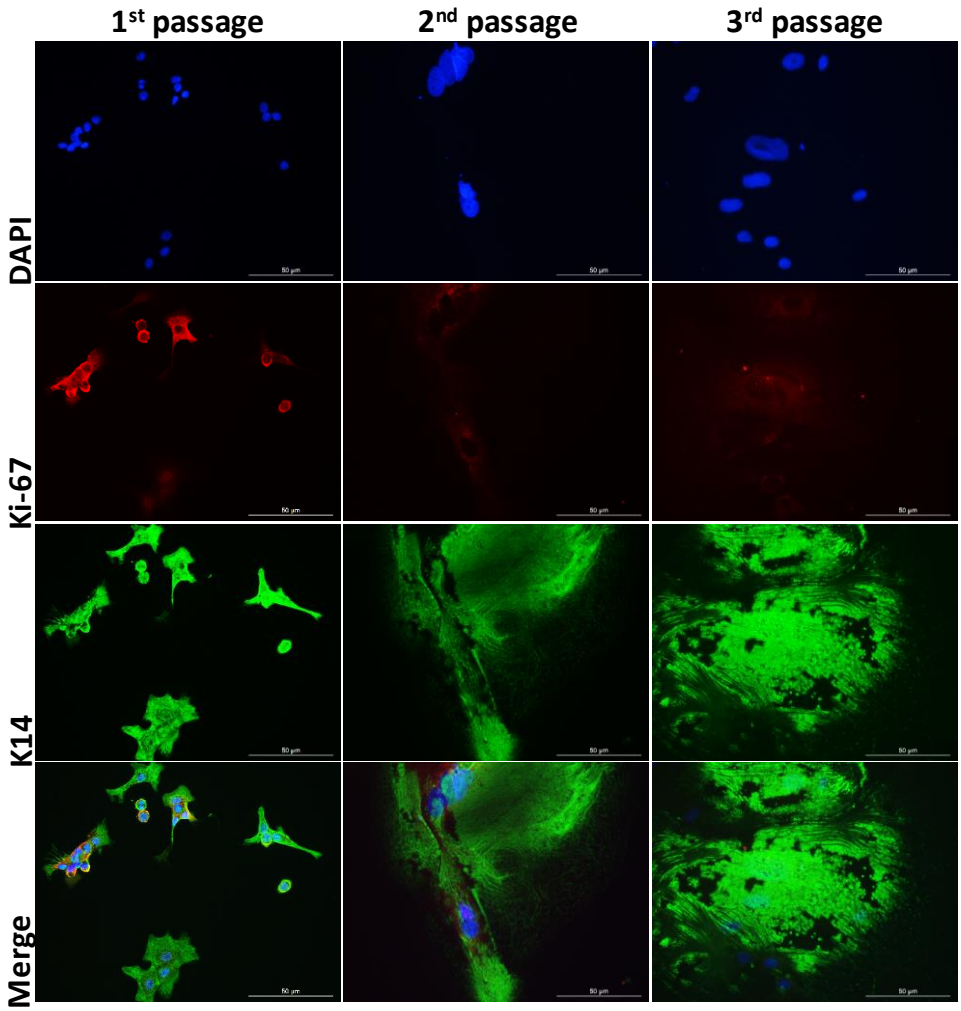


Figure 4-13: Ki-67 and K14 expression in EPKs during cell passages

Immunofluorescence staining illustrating the expression levels of Ki-67 and K14 during cell passages. The level of Ki-67 was visibly decreased with time after the passages. Scale bar represents 50µm.

The statistical analysis for assessing the expression of CD44 indicated (Figure 4-14A), that CD44/cell surface area decreased in the 2nd and 3rd passages in comparison to the 1st ($P<0.05$). However, the CD44/number of nuclei were similar in the 1st and 2nd passages but decreased in the 3rd passage ($P<0.05$) (Figure 4-14B). Similarly, the same results were found for the intensity of K14 and Ki-67 /surface area or /number of nuclei ($p<0.05$) (Figure 4-14C-F). Finally, there was a clear significant difference found between the cell surface areas in the 2nd and 3rd passages in comparison to the 1st ($P<0.05$) (Figure 4-14G).

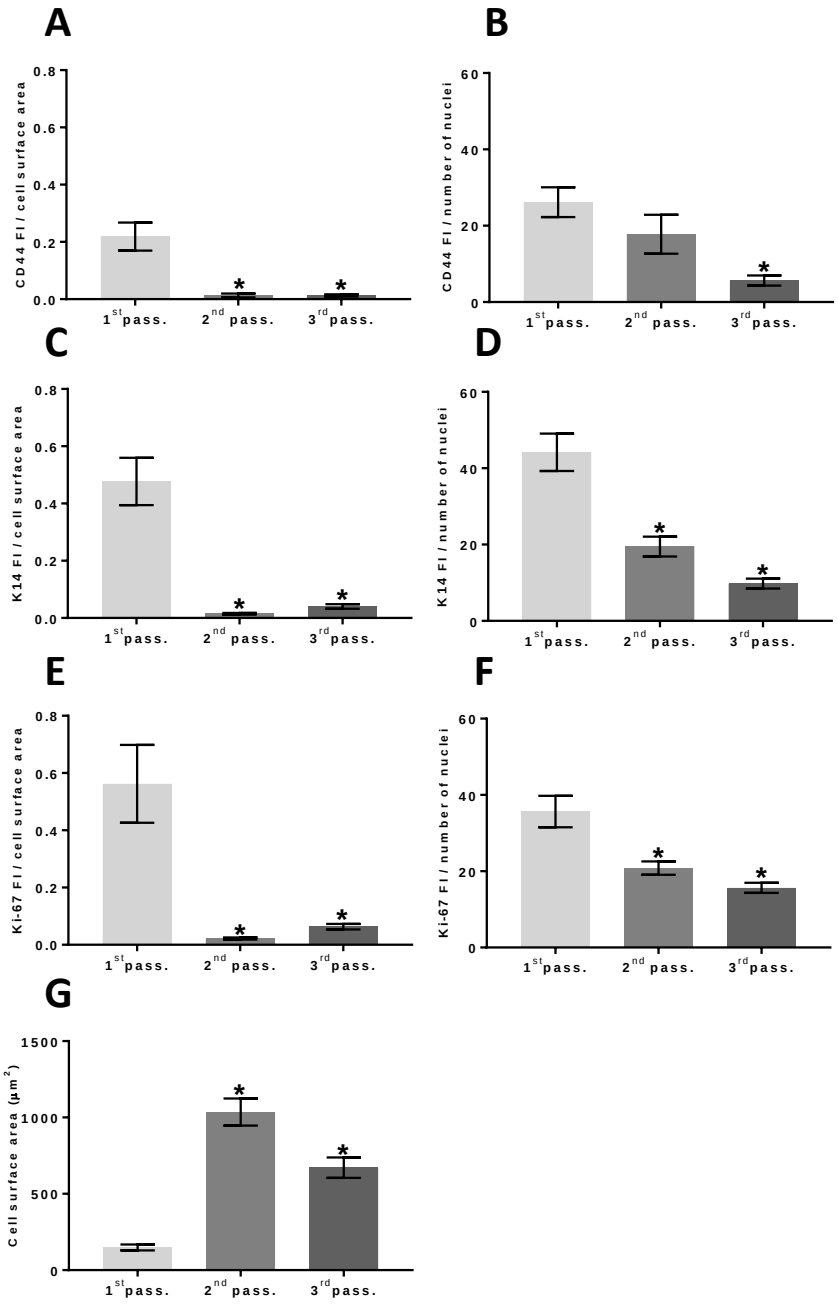


Figure 4-14: Quantification of CD44, K14 and Ki-67 after EPKs passages

K14, CD44 and Ki-67 expression levels through cell passages. (A, B) represent the variations of CD44 intensity per surface area and per nuclei between the first and subsequent passages. (C, D) represent the variations of K14 intensity per surface area and per nuclei between the first and subsequent passages. (E, F) represent the variations of Ki-67 intensity per surface area and per nuclei between the first and subsequent passages. (G) A clear significant difference between the surface areas of cell between passages was found. Statistical comparisons between groups were analysed using One Way ANOVA, (* indicates $P<0.05$ vs 1st passage). N=3 animals, each in triplicate-10 micrographs, averaging 15 measurements/micrograph.

Further analysis were carried out using F-Actin labelling revealing that the actin filaments where initially at the centre of cells after the first passage and at the periphery of cells at the last (Figure 4-15A+B). Those results suggest that actin organization and its dynamic are probably essential for full differentiation.

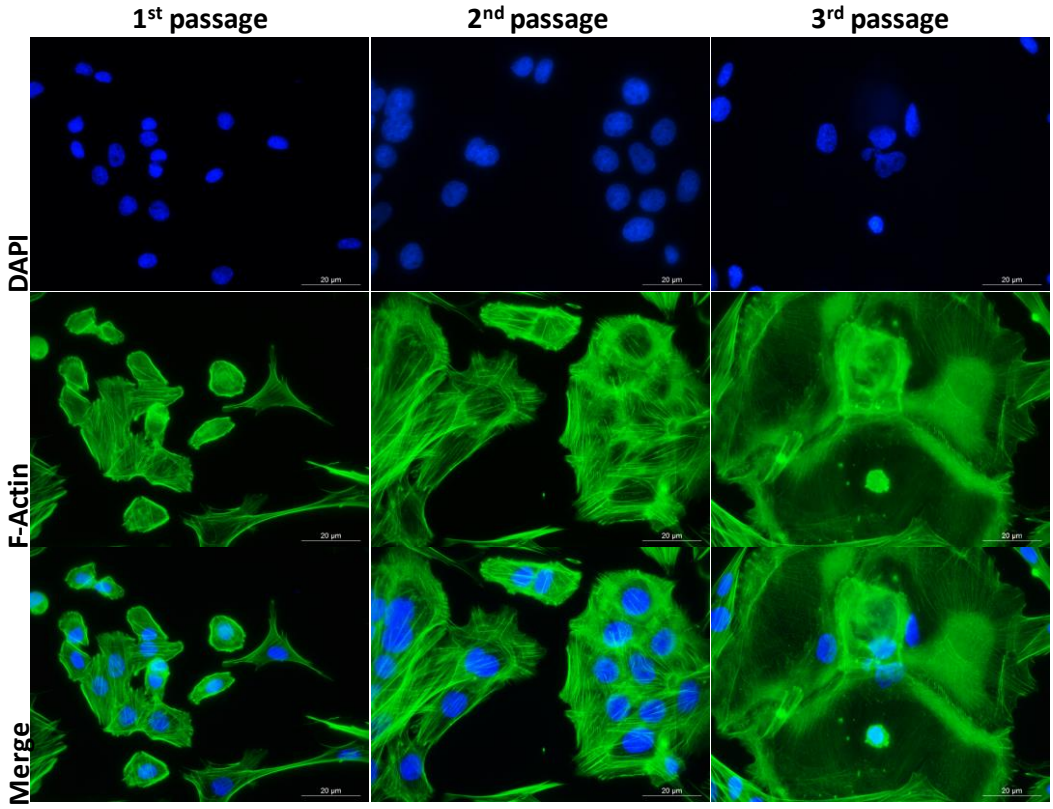


Figure 4-15: Immunofluorescence staining of F-Actin in EPKs during cell passages

Immunofluorescence images showing the localization of F-Actin filaments during cell passages. F-actin is located toward the edge of the cells at passage 3 and the cytosols of those cells appear devoid of F-actin. This was not observed for the 1st and 2nd passages. Scale bar represents 50µm.

4.4.7 Osteogenesis of EPKs

Osteogenesis of isolated EPKs confirmed their pluripotency for differentiation into osteoblasts. The results revealed that committed EPKs to differentiation to osteoblasts showed that the control and differentiation of cells were examined by staining with Alizarin red stain (Figure 4-16A+B). It was found that osteogenic cells had calcium deposition, which was stained with Alizarin red in the osteogenic culture plate**.** The positive osteogenic cells appeared as clustered rounded cells stained in red indicating calcium deposition. The results indicated more than 89% of keratinocytes passed through osteogenesis at day 19, while a lower percentage of 66% was shown at day 15 (Figure 4-16; $P<0.05$). The control samples showed no staining indicating no calcium deposition.

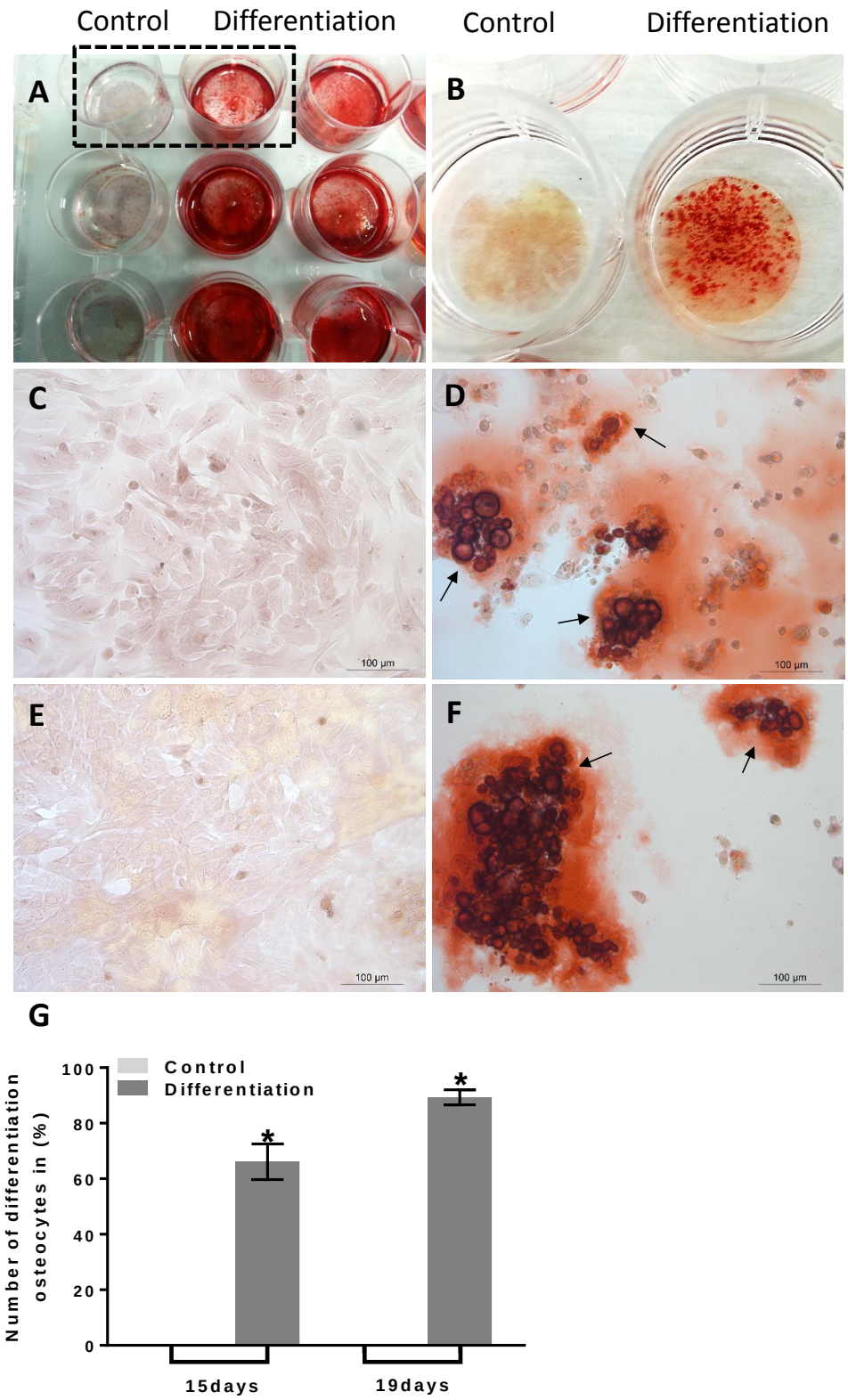


Figure 4-16: Photos and photomicrographs show osteogenesis of EPKs

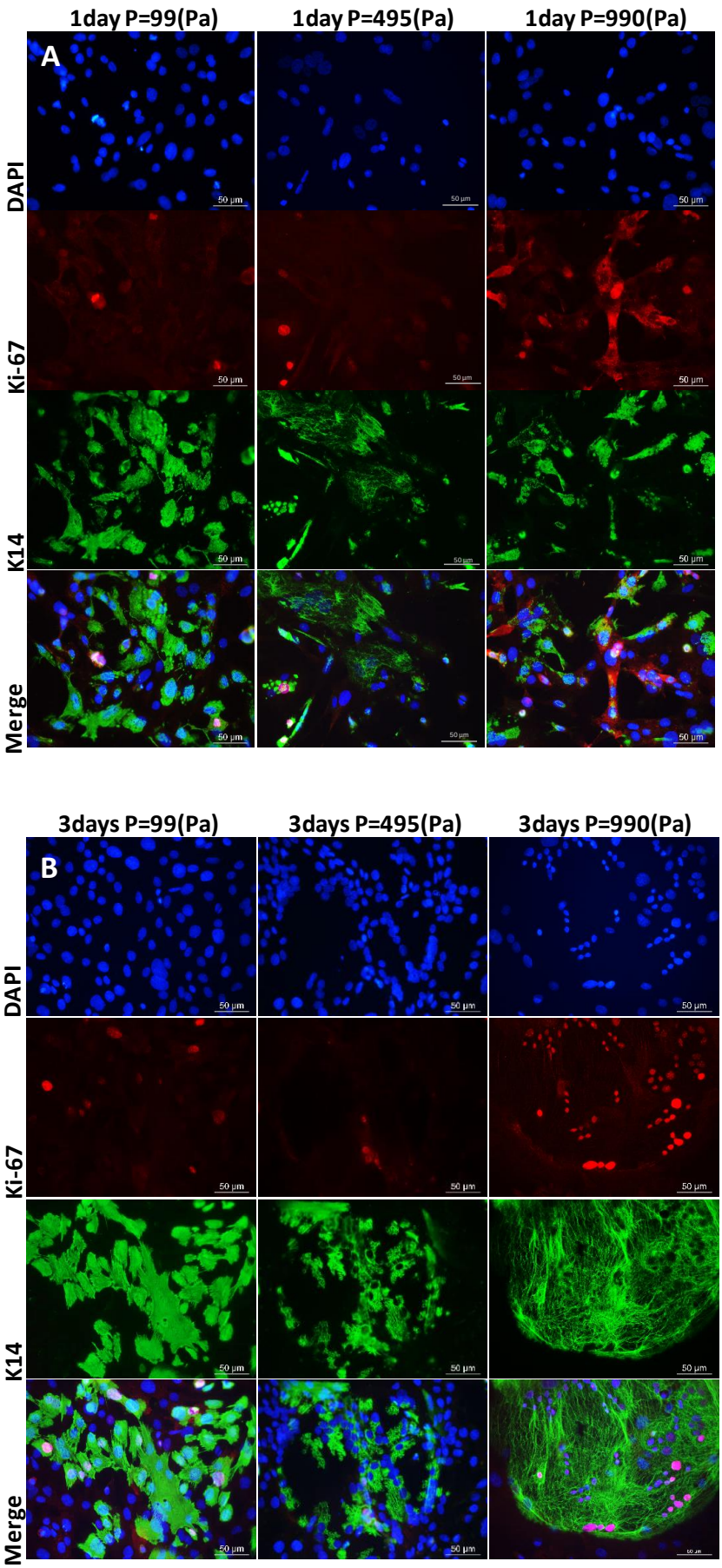
(A, B, C, D, E, F) EPKs differentiation into osteoblasts showing Alizarin stained cells (Last two right rows in (A), right well in (B) magnified in (F) compared to control (E) 19days, the same at 15days in (D) compared to control (C). (G) More than 89% of cells are differentiated in the osteogenic medium at day 19 while 66% at day 15. Scale bar represents 100µm. Statistical comparisons between groups were analysed using One Way ANOVA, (* indicates $P<0.05$ vs control). N=3 animals, each in triplicate-15 micrographs, averaging 15 measurements/micrograph.

4.4.8 The influence of hydrostatic pressure on EPKs

The next stage was to investigate whether alterations in cell morphology, cell proliferation and cell differentiation were affected with continually applied hydrostatic pressure (HP). Three pressure regimes were employed. The atmospheric pressure set as the control one was at 99 Pa, the second at 495 Pa while the third at 990 Pa, each for 1, 3 and 5 days.

The present study demonstrated that HP treatment altered in Ki-67 expression; and K14 and K10 expressions; compare to normal cellular balance of force was changed. Equine keratinocytes pressurized for 1, 3 and 5 days using pressure values of 495 Pa and 990 Pa induced noticeable nuclear rounding and the appearance of aggregation of cells similar to the presence of multinucleated cells, as well as changing in overall cell size. The degree of multinucleation and the repetitive increase cell surface area increased with increasing pressure and time. Some cells separated from the coverslip under a pressure of 990 Pa for 5 days.

For adherent cells there was a clear and visible upregulation in the expression of Ki-67 at 990 Pa on both day 3 and 5. At a pressure of 990 Pa, accumulation of rounding nuclei labelled with Ki-67 was accompanied by a pronounced increase in the expression of K14 and K10 compared to control values (Figure 4-17; $P<0.05$). Pressurized cells at 990 Pa exhibited smaller nuclei and a filamentous organisation of keratins (Figure 4-17C). This resulted in the creation of a dense network of K14 surrounding each group of retracted nuclei.


1day P=99(Pa)
1day P=495(Pa)
1day P=990(Pa)
A
DAPI
Ki-67
K14
Merge
3days P=99(Pa)
3days P=495(Pa)
3days P=990(Pa)
B
DAPI
Ki-67
K14
Merge

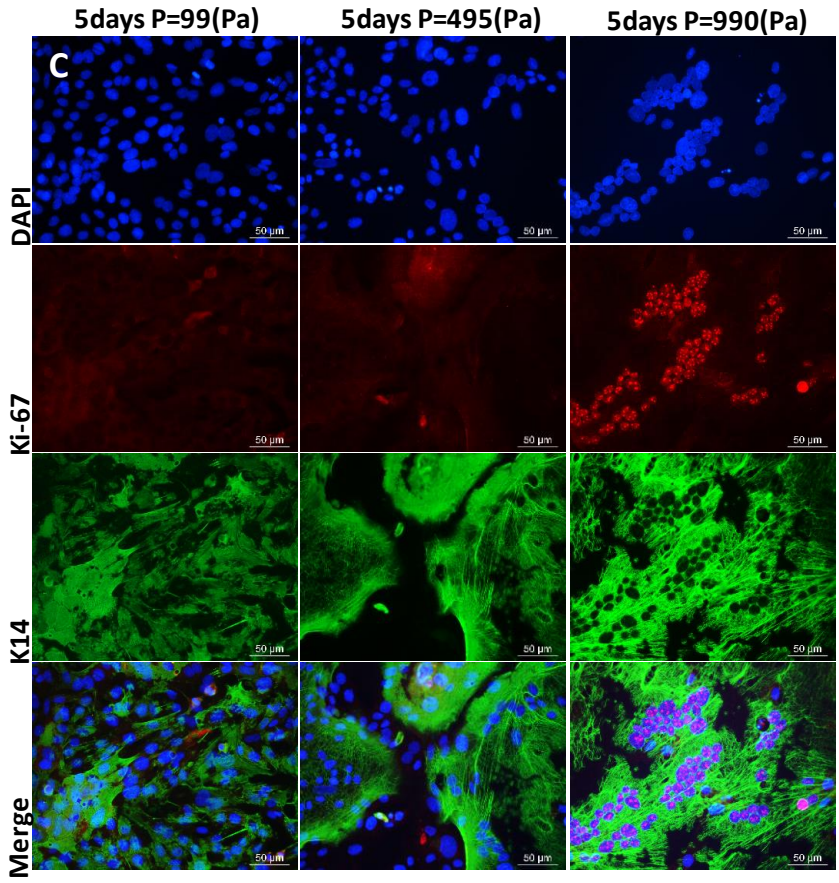


Figure 4-17: The impact of HP on Ki-67 and K14 expression levels

Immunofluorescence images of cell keratinocytes reveal a distinct distribution of Ki-67 and K14 under hydrostatic pressure. (A) Shows a clear expression of Ki-67 at the hydrostatic pressure 990pa at day 1 that is sustains and localized in the nuclei at day 3 (B) and day 5 (C). Similarly, (B) and (C) indicated an increase in K14 at day 5 at the pressure of 990pa. Scale bar represents 50µm.

Additional analysis was carried out in order to examine the cytoskeletal structure and to assess the changes in the location and organization of F-actin filaments caused by HP. The organization of actin filaments in cells at pressure of 495 Pa and 990 Pa appeared to be similar to controls (Figure 4-18). However, it was possible at day 5 under 990 Pa to distinguish a preferential localisation of F-actin toward the edge of cells similar to what was seen using blebbistatin but to a much lesser extent.

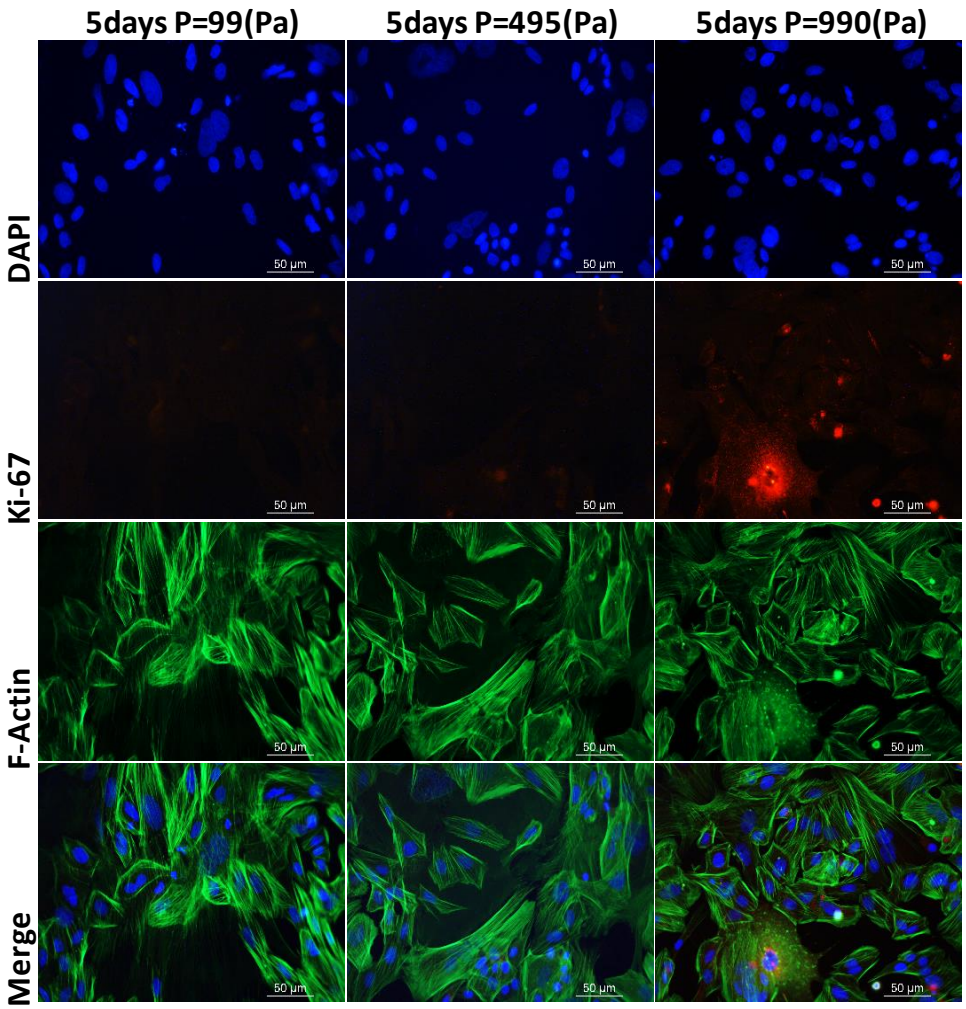


Figure 4-18: Immunofluorescence showing HP effect on actin filaments

EPKs labelled with Ki-67 and F-actin markers. A visible, albeit modest, relocalisation of F-actin toward the edges of the cells was observed at day 5 under high pressure. Scale bar represents 50µm.

The statistical analysis assessing the localization and expression of Ki-67 and cytokeratin markers K14 and K10 in pressurized keratinocytes indicated in that there was no statistically significant differences between the fluorescence intensity of the treated cells and control cells at day 1 and 3 (Figure 4-19A-D; $P<0.05$). However, there was a statistically significant difference found in the upregulation of Ki-67 nuclear intensity at day 3 and 5 at 990 Pa ($P<0.05$) (Figure 4-19E). Similarly, a number of statistically significant differences were found of the increase intensity per surface area and per nuclei for K14 and K10 (Figure 4-

20; P<0.05) at day 5 under 495 Pa and 990 Pa. In addition, the same significant results increase in the cell surface area were indicated between the cell surface area under HP and control cells at day 1 under 495 Pa and 990 Pa, the same at day 3 and 5 under both pressures 495 Pa and 990 Pa (Figure 4-19F; P<0.05).

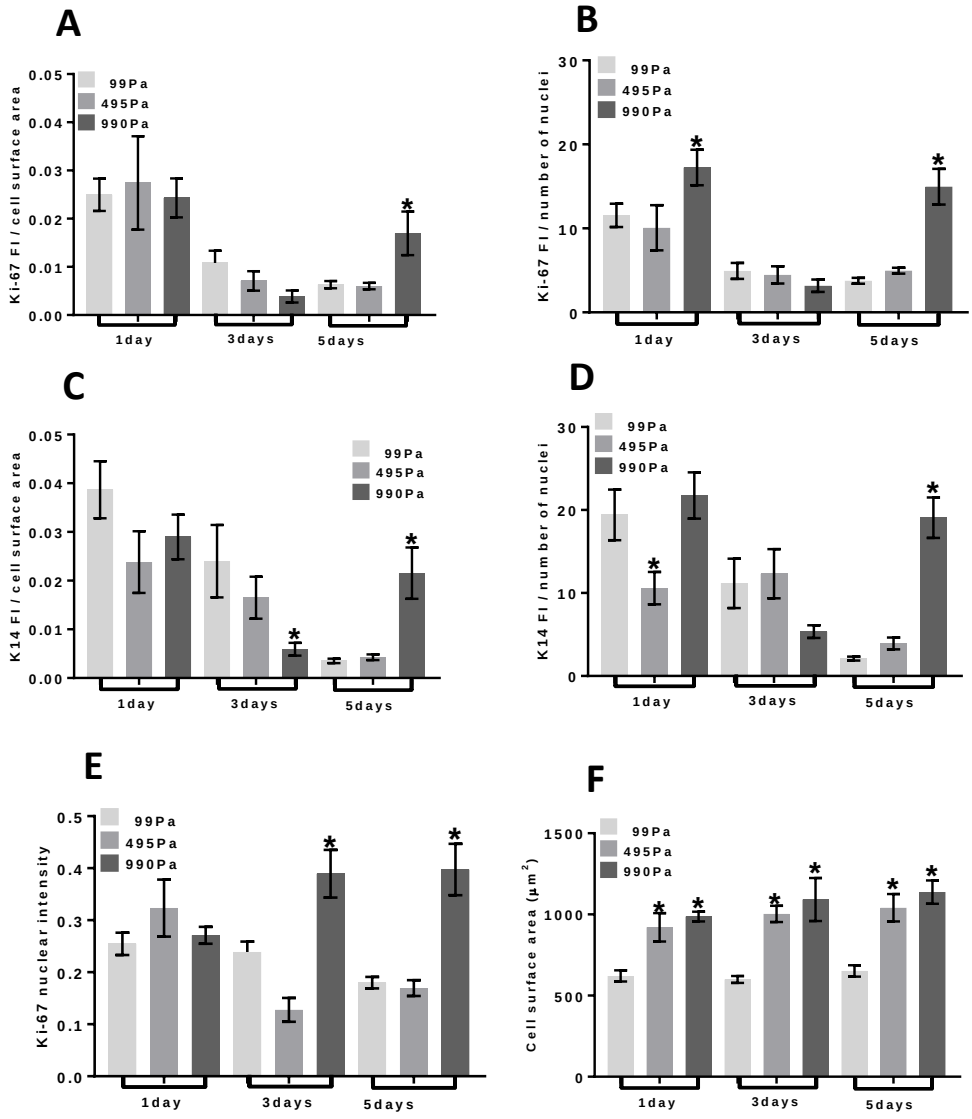


Figure 4-19: Quantification the impact of HP on the expression of Ki-67, K14

A, B) Significant variations were found between the intensity of Ki-67 measured per surface area and per nuclei of cells at day five as a function of the HP applied. (C, D) Significant variations were found between the intensity of K14 measured per surface area and per nuclei of cells at day five as a function of the HP applied. (E) Ki-67 was also measured per nucleus and it was found a strong nuclear accumulation of Ki-67 at high HP overtime. (F) Identified a clear and significant difference found between the surface area of control and pressurized cells at day 1, 3 and 5. Statistical comparisons between groups were analysed using One Way ANOVA, (* indicates P<0.05 vs 99 Pa within that day). N=3 animals, each in triplicate-10 micrographs, averaging 15 measurements/micrograph.

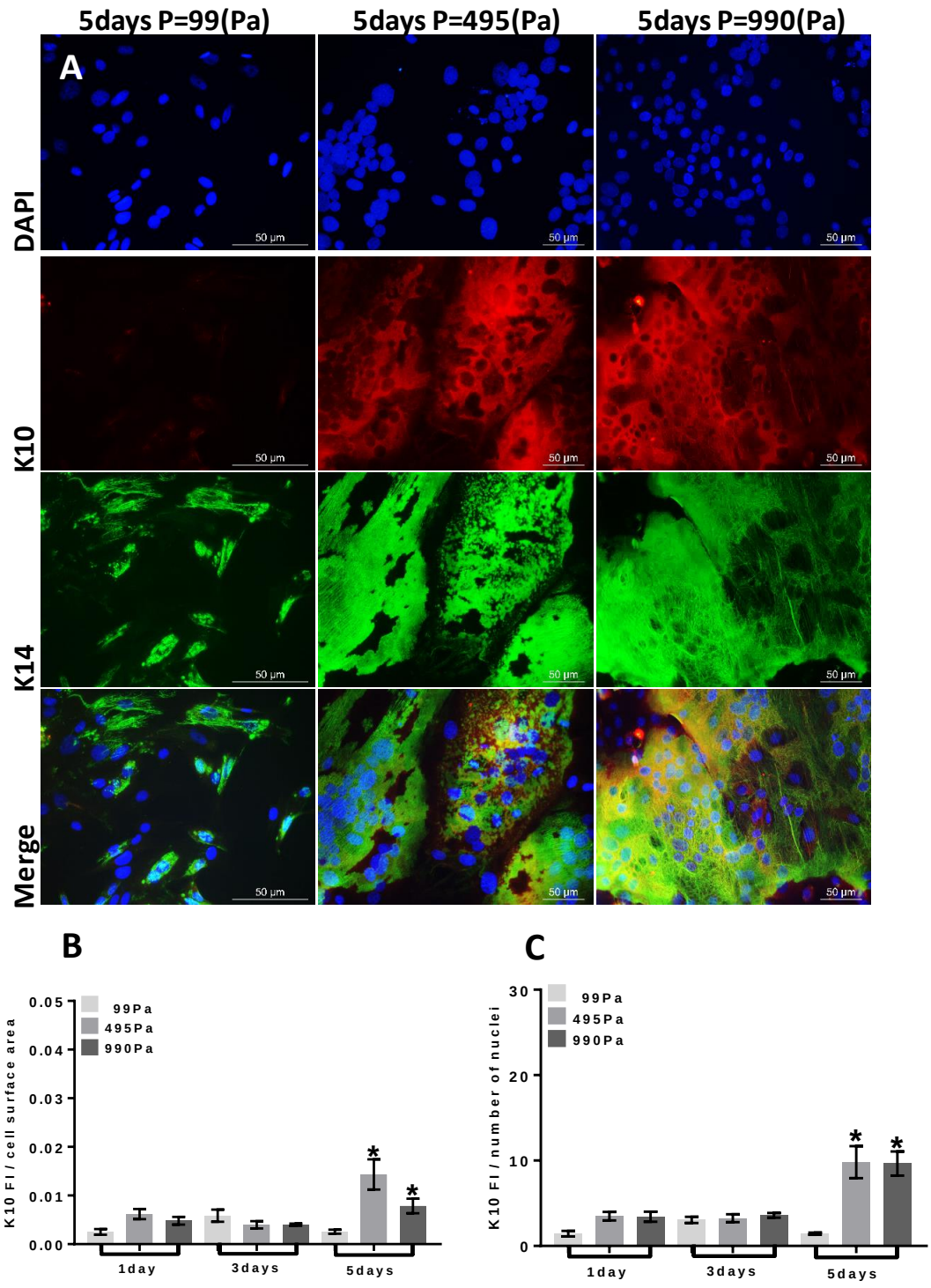


Figure 4-20: The impact of HP on K14 and K10 expression levels

Immunofluorescence images of keratinocytes revealed a distinct distribution of K10 and K14 at day 5 when HP was applied. A) A clear expression of K10 and K14 under hydrostatic pressure (990Pa) was found at day 5. (B, C) Significant variations were found between the intensity of K10 measured per surface area and per nuclei of cells at day five as a function of the HP applied. Statistical comparisons between groups were analysed using One Way ANOVA, (* indicates $P<0.05$ vs control). N=3 animals, each in triplicate-10 micrographs, averaging 15 measurements/micrograph. Scale bar represents 50µm.

4.4.9 Stretch cultured EPKs

Three types of experiments were performed. First, stretched EPKs were incubated for 24hrs with blebbistatin, followed by a media change to remove blebbistatin. The second study was performed to investigate whether incubation of EPKs for long period with blebbistatin had an influence on cell activity. Thirdly, stretch was applied on EPKs without incubation with blebbistatin.

4.4.9.1 Stretch of EPKs after incubation for 24hrs with blebbistatin

This study was carried out to determine the effect of mechanical force on isolated EPKs using collagen coated BioFlex plates and preincubation with blebbistatin for 24hrs prior to strain application. Knowing the strain and given the elestic modulus of the cells it was possible to estimate a stretch ~50-70 kPa. In the present study the influence of blebbistatin was clearly noticeable in stretched cells. It was found that stretch force induces EPKs differentiation. Blocking of NMMII by 20µM blebbistatin causes further cytoplasmic extension resulting in cells becoming sparser. Immunostaining revealed obvious expressions of K14 and of the differentiation marker K10 especially at day 3 (Figure 4-21). As expected, the cytoskeleton networks were also disrupted (Figure 4-21). In contrast, non-stretched cells appeared to have lower expression for both K14 and K10.

Statistical analysis were found a significant increases in the expression of K10 and K14/number of nuclei at day 1 and 3 in stretched cells vs non stretched cells (Figure 4-22B+D; $P<0.05$), however, the expression of K14 and K10/surface area under stretch conditions were not significantly different from control group on either day 1 or 3 (Figure 4-22A+C). Furthermore, a significant increase of the cell

surface area was observed between stretch and control cells at day 1 and 3 (Figure 4-22E; $P<0.05$).

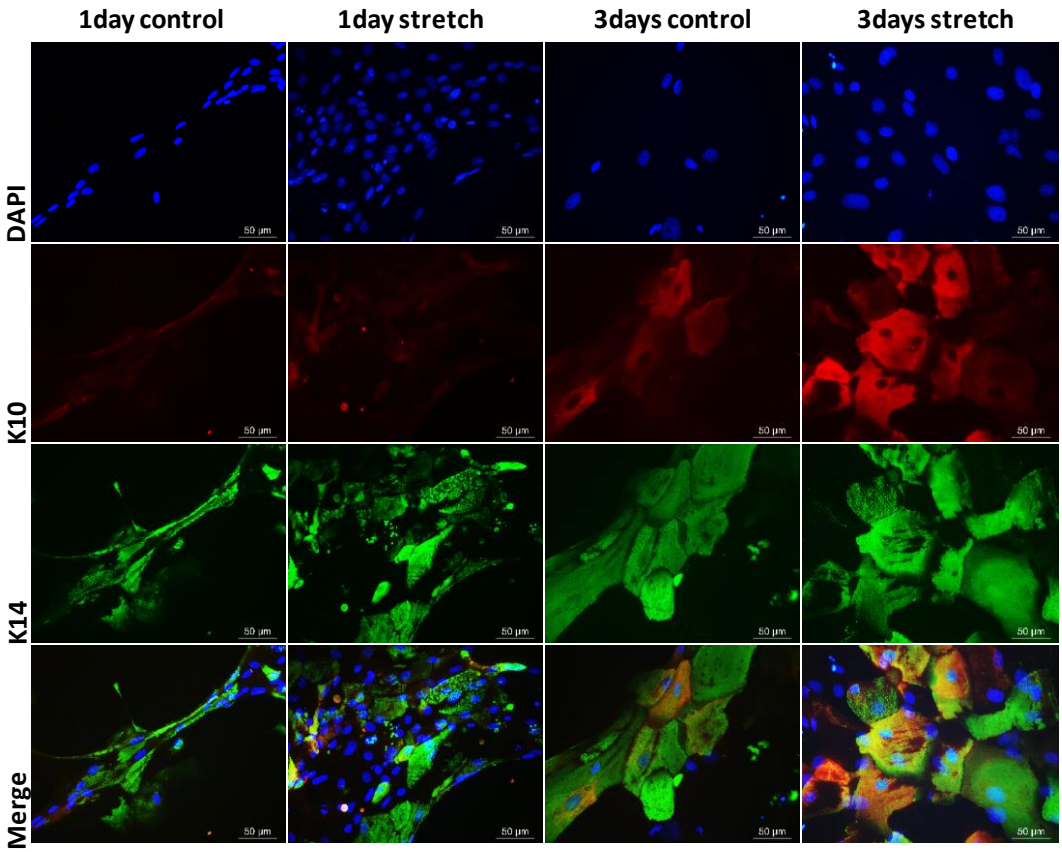


Figure 4-21: The impact of stretch force after incubated 24hrs with blebbistatin

Immunofluorescence images of cell keratinocytes revealed a distinct distribution of K10 and K14 throughout cell stretching. EPKs under stretch at day 1 shows little expression of K10 and K14, whereas at day 3 obvious upregulation in the expression of both markers K10 and K14 between control and stretch. Scale bar represents 50µm.

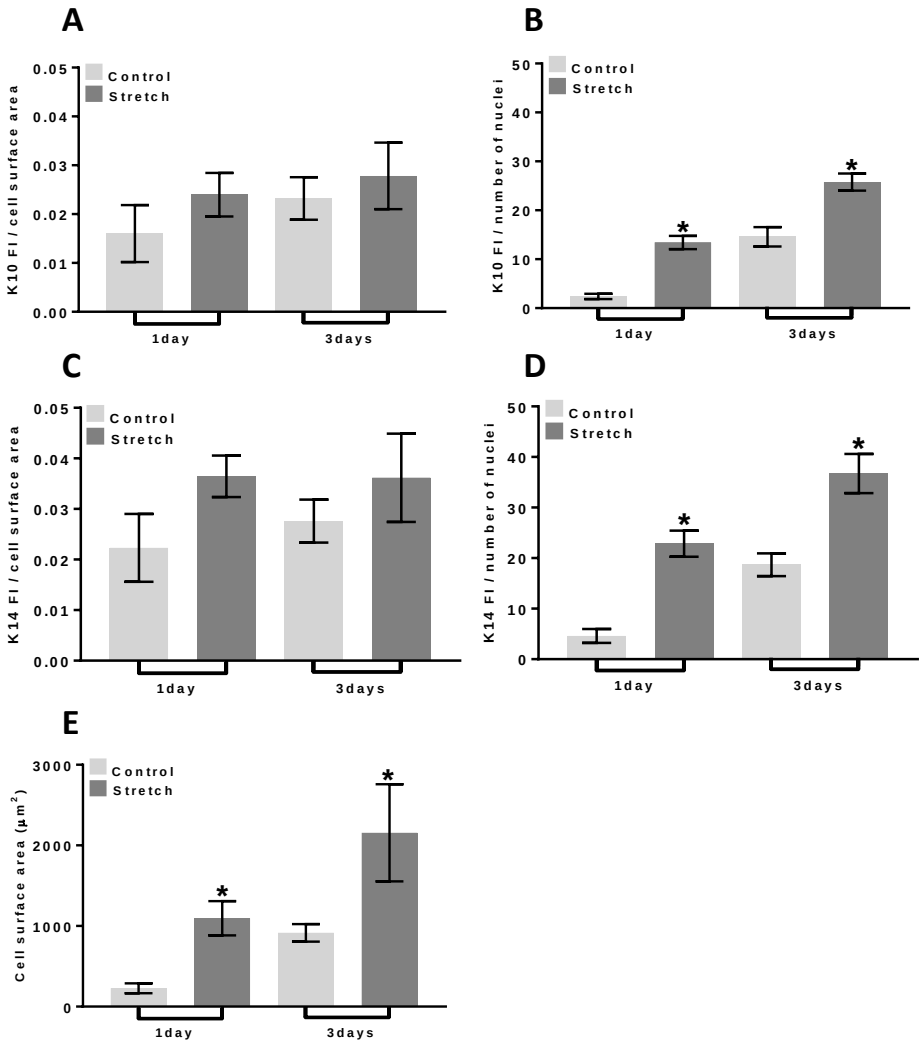


Figure 4-22: Quantification the expression of K14 and K10 under mechanical stretch

Fluorescent intensity per surface area or per number of nuclei for the differentiation markers K14 and K10 under mechanical stretch, after incubated 24hrs with blebbistatin. (A, B) Significant variations were found between the intensity of K10 measured per nuclei at day one and three as a function of the stretch applied. Similarly, (C, D) significant variations were found between the intensity of K10 measured per nuclei at day one and three as a function of the stretch applied. F) Identifies a clear and significant difference found between the surface area of control and stretched cells at day 1 and 3. Statistical comparisons between groups were analysed using One Way ANOVA with Post Hoc testing SPSS, (* indicates $P<0.05$ vs control). N=3 animals, each in triplicate-10 micrographs, averaging 15 measurements/micrograph.

Additionally, the results of Ki-67 was detected in stretched and control cells at day 1, while at day 3 there appeared to be little to no expression of Ki-67 (Figure 4-23). These results indicated that mechanical stretching induces keratinocytes differentiation via increased expression of keratin proteins. Consequently, cells appeared to form monolayer of differentiated cells under stretch in comparison to

control. In addition, it was found that most cells expressed keratin at day 3, and that they displayed a squamous-like appearance. Interestingly, cells were detaching from the flexcell membrane at day 5 (not shown) suggesting a full process of differentiation had been undertaken. However, a number of statistically significant differences were found for the intensity of Ki-67/cell surface area revealed a clear decreased in the expression of Ki-67 at day 3 in comparison to day 1 ($P<0.05$) similarly, for the intensity of Ki-67/number of nuclei decreased at day 3 in comparison to day 1 ($P<0.05$) (Figure 4-23B+C).

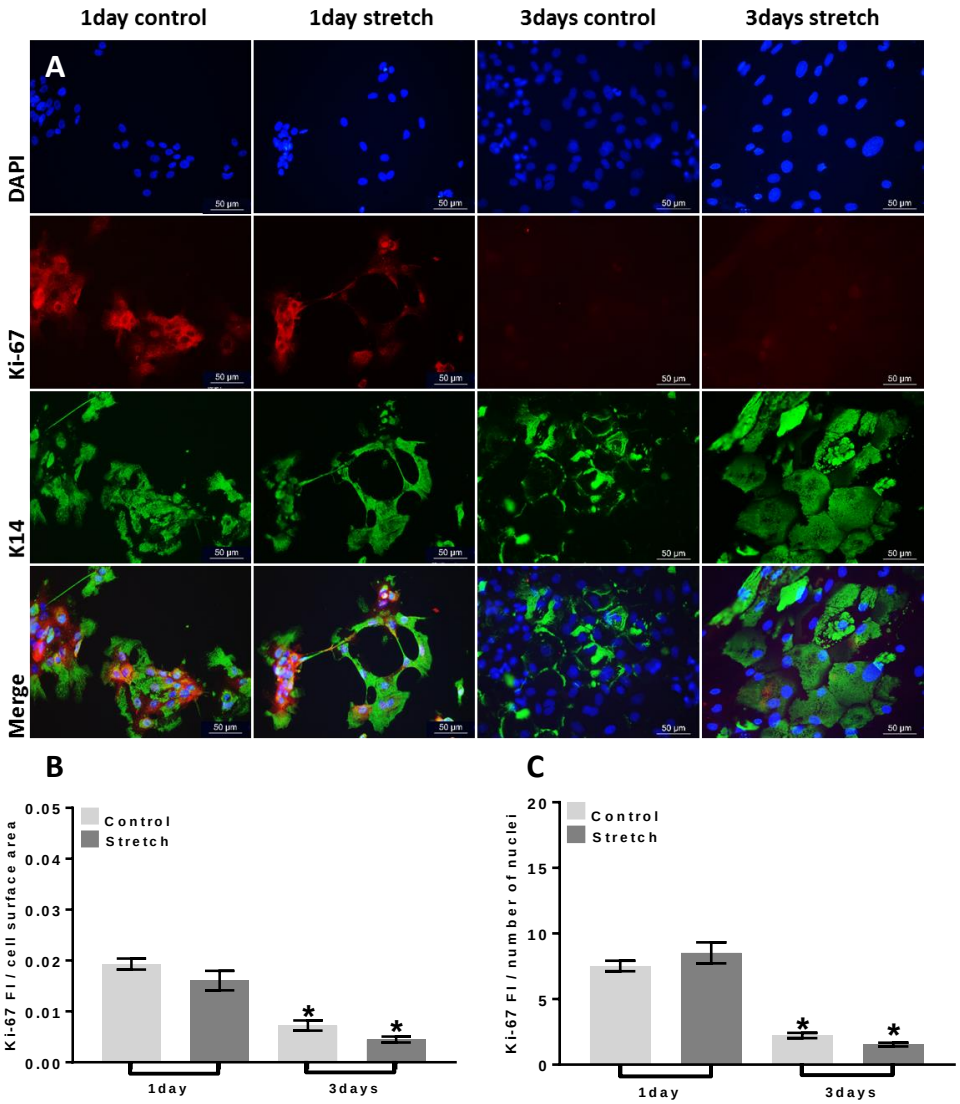


Figure 4-23: The impact of stretch force on the Ki-67/K14, after being treated for 24hrs with bleb.

Immunofluorescence staining and graphs illustrating the impact of mechanical force on the Ki-67 and K14 expression levels after incubated 24hrs with blebbistatin. A) A clear expression of Ki-67 and K14 under stretch was found at day 1. (B, C) Significant variations were found between the intensity of Ki-67 and K14 measured per surface area and per nuclei of cells at day three under stretch compared to control levels. Statistical comparisons between groups were analysed using One Way ANOVA, (* indicates $P<0.05$ vs day 1). N=3 animals, each in triplicate-10 micrographs, averaging 15 measurements/micrograph. Scale bar represents 50µm.

Furthermore**,** to assess the expression levels of CD44 a Western blot assay was performed. The results from quantification of CD44 indicated significant differences ($p<0.05$) were found under stretched conditions at days 3 and 5 for the expression levels of CD44. Two-fold increases in stretched cells were indicated in

comparison to non-stretched cells. Stretch cells exhibited a strong band for CD44 (Figure 4-24).

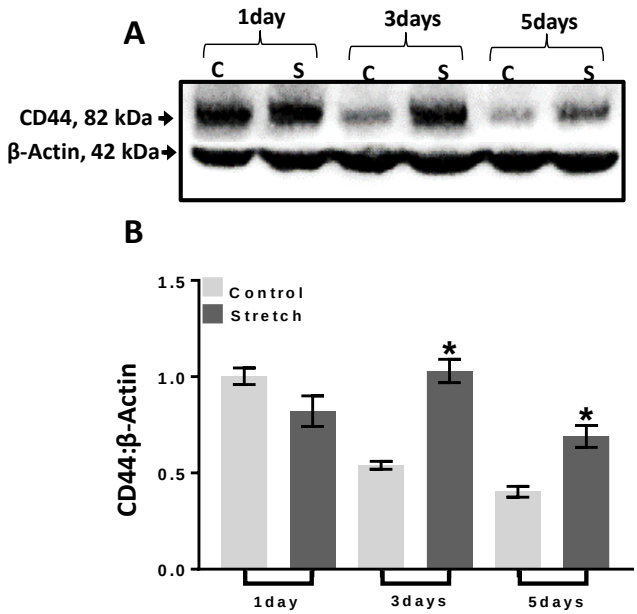


Figure 4-24: Quantification of the impact of stretch force on CD44 protein expression

Graphs show statistical analysis of Western blot protein expression levels after incubated 24hrs with blebbistatin when normalized to dominant β-Actin protein. A) a clear band of protein expression of CD44 at 82 kDa. B) Significant variations were found between the protein expression levels of CD44 measured at day three and five as a function of the stretch applied. Statistical comparisons between groups were analysed using One Way ANOVA, (* indicates $P<0.05$ vs control). N= 3 animals, each in triplicate.

4.4.9.2 Stretch of EPKs incubated with blebbistatin

To investigate whether applying mechanical stretch while blocking F-actin have an impact on cell proliferation/differentiation, cells were incubated with blebbistatin and a stretch was continuously applied for 1, 3 and 5 days. These results revealed that the cells were indeed affected by the addition of blebbistatin in comparison to non-stretched cells. Blebbistatin incubation triggered differentiation (Figure 4-25), whereby keratin 14 expressions increased in stretched cells, in contrast to the control cells. Cells detached from the silicon substrate around day 5 making it impossible to collect cells and acquire results. It is apparent from Figure 4-25 that the influence of blebbistatin becomes more

obvious when incubated for longer than 3 days. Cells under stretch were forming monolayer of differentiated cells when compared to control cells. In addition, most cells expressed keratin at day 3, structure appearance, similar to keratinization. As cells also detached from the silicon membrane at day 5 it was not possible to carry out analyses. A number of statistically significant differences were found nonetheless regarding K14 per surface area or per number of nuclei at day 1 and 3 (Figure 4-26C+D; $P<0.05$). Similarly, the same significant results was found regarding the cell surface area that increases under stretch compared to control cells at day 1 and 3 (Figure 4-26G; $p<0.05$). However, there was no significant differences for the levels of Ki-67 and K10 per surface area or per nuclei under stretch conditions (Figure 4-26A+B &E+F) except decreases was found in the expression of Ki-67 per surface area at day 3 (Figure 4-26A; $p<0.05$).

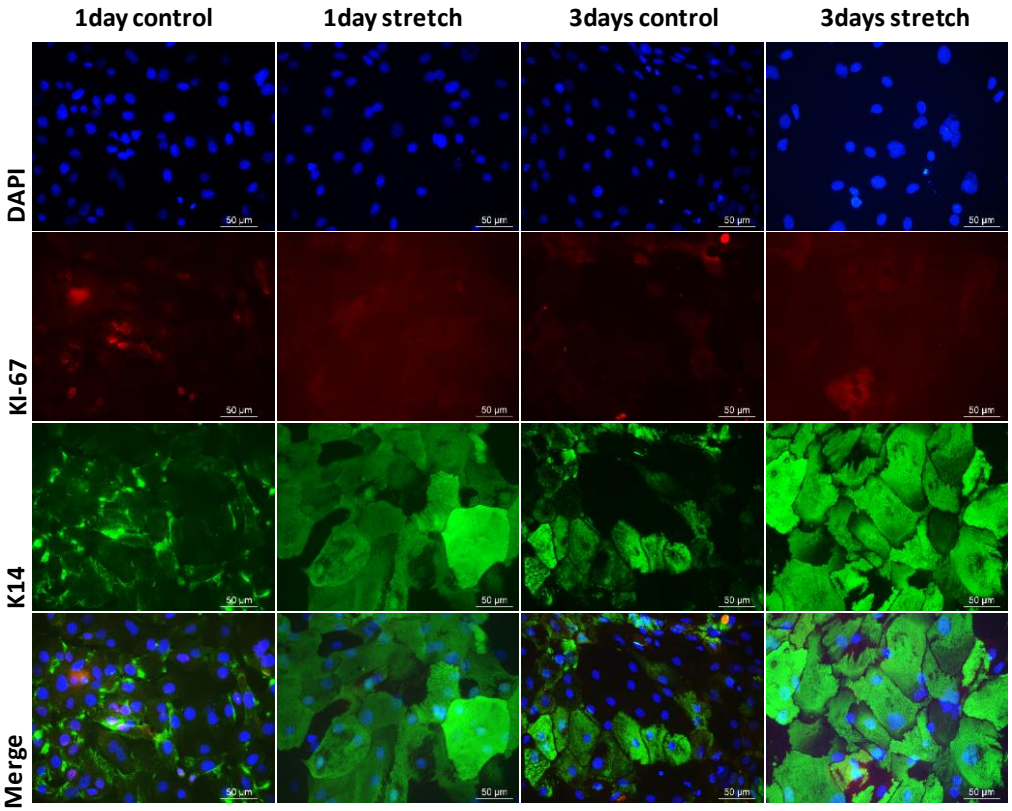


Figure 4-25: The impact of stretch force on Ki-67 and K14 expression levels

Immunofluorescence images of cell keratinocytes reveal a distinct distribution of K14 and little expression of Ki-67 after incubated all time with blebbistatin. Scale bar represents 50µm.

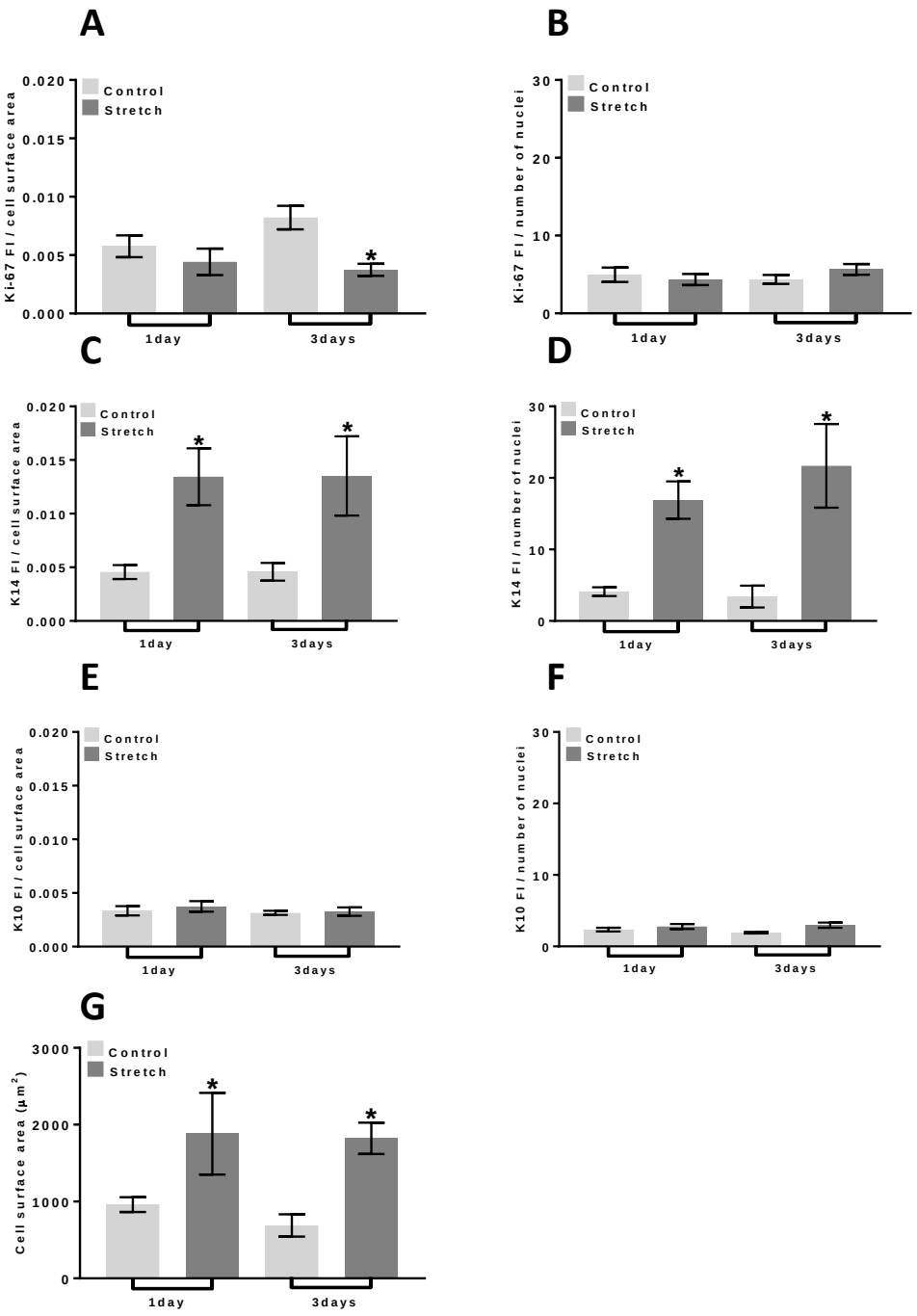


Figure 4-26: Quantification of Ki-67, K14 and K10 expression under stretch force

Fluorescent intensity per cell surface area or per number of nuclei for the proliferation marker Ki-67 and cytokeratin K14 and K10 under mechanical stretch after incubated all time with blebbistatin. (A, B) A significant variations were found between the intensity of Ki-67 measured per nuclei and per surface area of the cells except at day three when the intensity per surface area was considered significantly different. However, (C, D) significant variations were found between the intensity of K14 measured per nuclei and per surface area of the cells at day one and three as a function of the stretch applied, while (E, F) no significant variations were found for the expression of K10 per surface area of cells and per nuclei. G) Identifies a significant difference between the surface area of control and stretched cells at day 3. Statistical comparisons between groups were analysed using One Way ANOVA, (* indicates $P<0.05$ vs control). N=3 animals, each in triplicate-10 micrographs, averaging 15 measurements/micrograph.

Further analysis was carried out labelling F-Actin to reveal actin filaments organisation. Initially at the centre of cells at day 1 for both the control and stretch experiments, F-actin is found more predominantly at the periphery after 3 days under stretch conditions, and to a lesser extent, under control conditions (Figure 4-27). Those results suggest that actin organizations and its dynamics are probably essential for full differentiation.

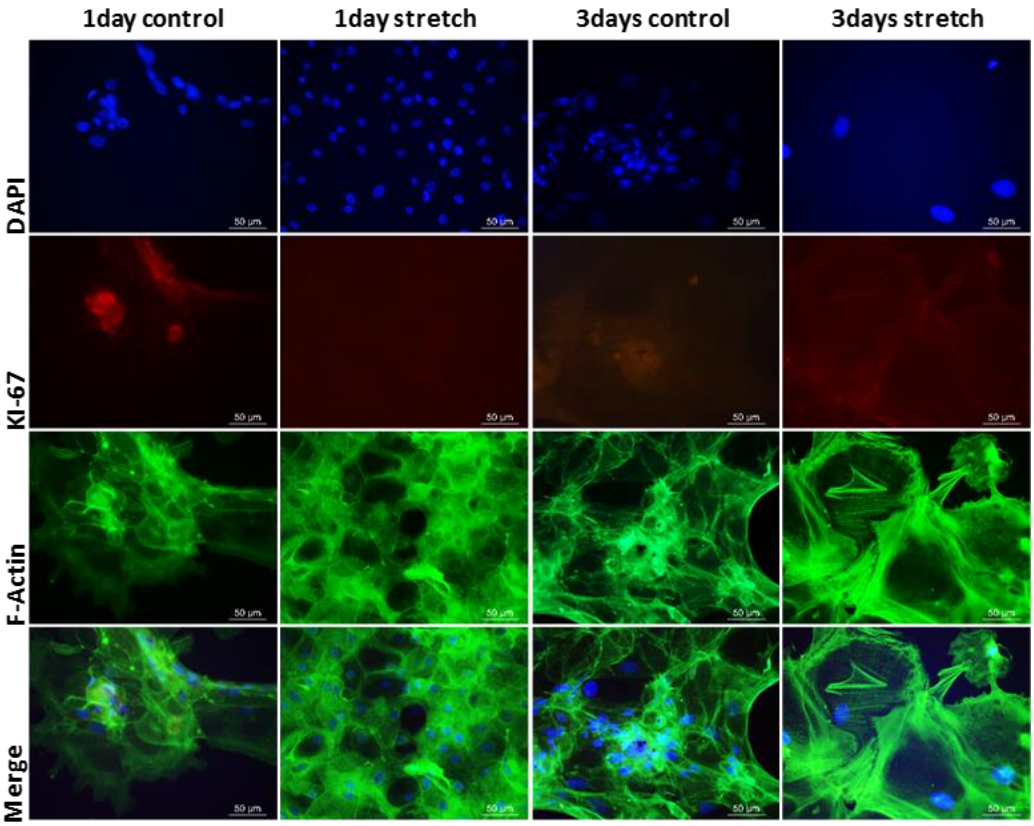


Figure 4-27: The impact of stretch force on F-actin in EPKs incubated with blebbistatin

Immunofluorescence images showing the localization of F-Actin filaments at days 1 and 3. F-actin was located towards the edge of the cells at day 3. Scale bars represent 50µm.

4.4.9.3 Stretch of EPKs without blebbistatin

This study was carried out without incubation with blebbistatin for 1-3 days. The results revealed that there were no difference in the expression of K14 between stretched and control cells on any day (Figure 4-28). However, Ki-67 expression decreased significantly under stretch when compared to control levels in both cell surface area on day 3 and the number of nuclei on days 1 and 3 (Figure 4-29A+B; $P<0.05$).

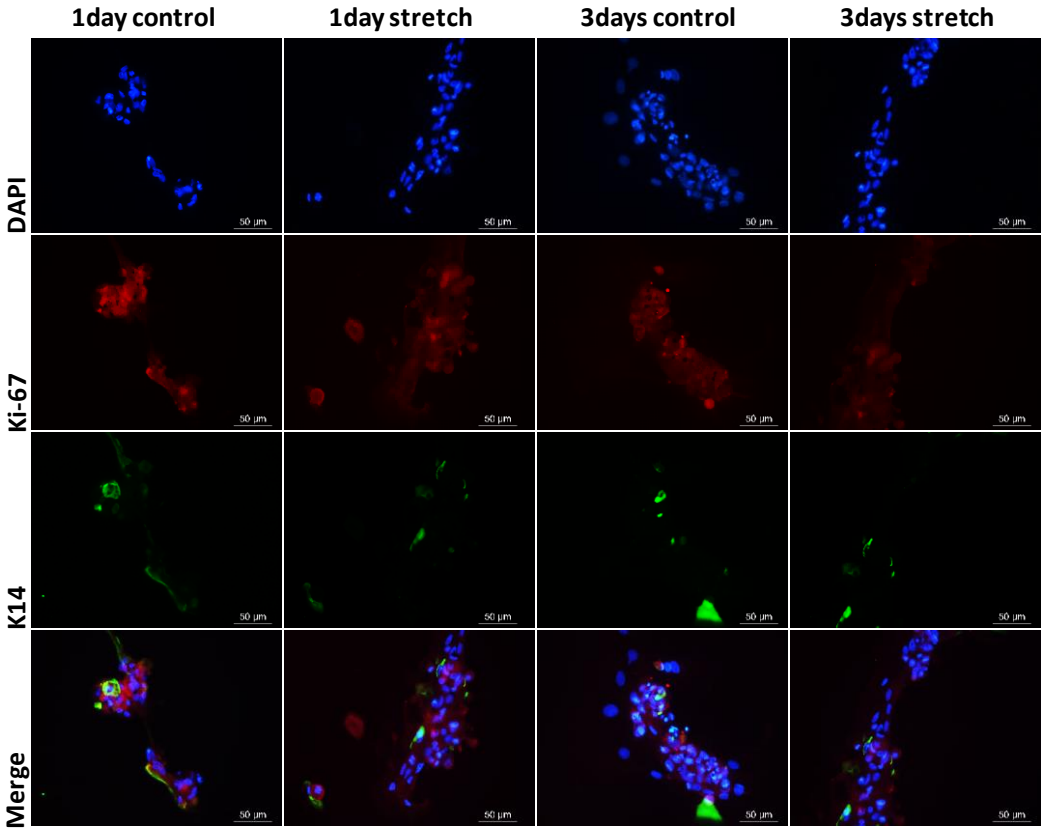


Figure 4-28: The impact of stretch force in the absence of blebbistatin

Immunofluorescence images of cell keratinocytes revealed little Ki-67 and K14 expression levels following stretch application. Scale bars represent 50µm.

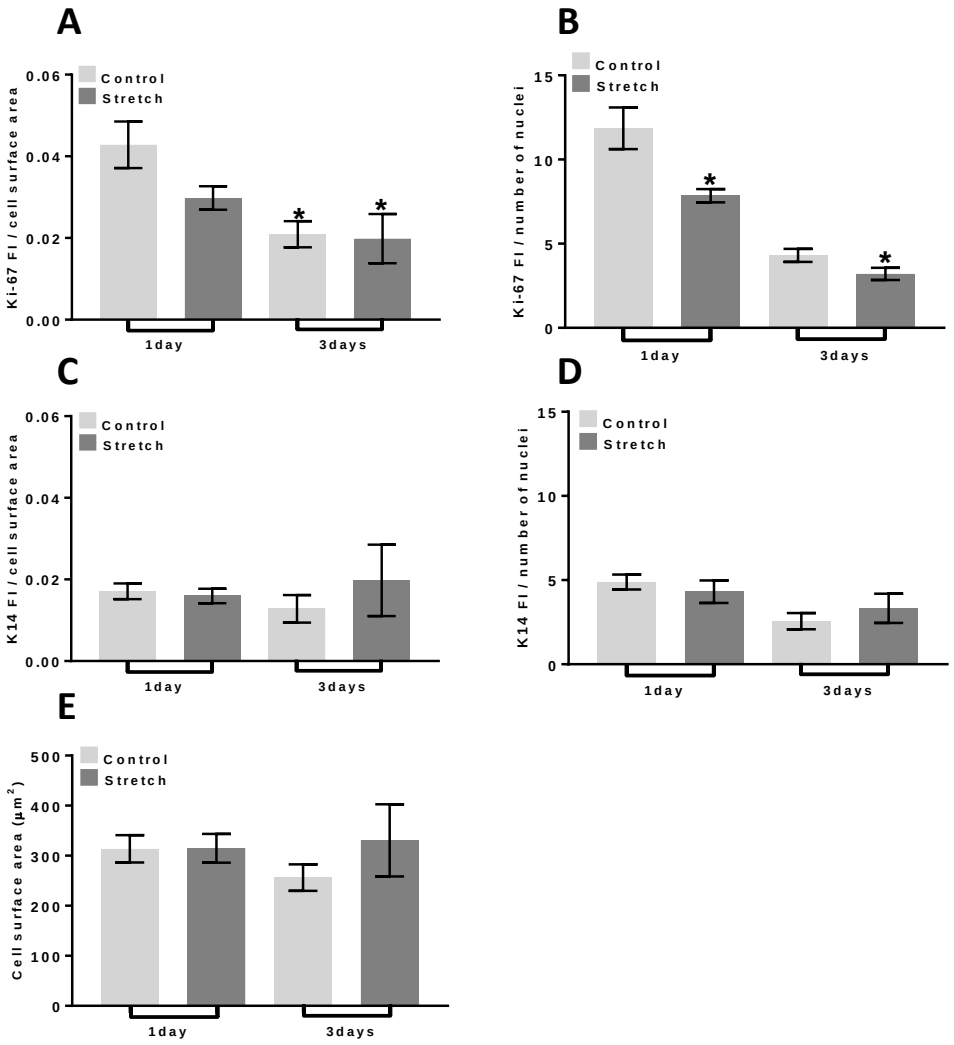


Figure 4-29: Quantification of Ki-67 and K14 expression under mechanical stretch

Fluorescent intensity per surface area or per number of nuclei for the proliferation marker Ki-67 and cytokeratin K14 under mechanical stretch. (A, B) Significant variations were found between the control and stretch regarding the intensity of Ki-67 measured per nuclei and per surface area of the cells at day three. (C, D) No significant variations were found in K14 measured, similar (E) no changes in the cell surface area. Statistical comparisons between groups were analysed using One Way ANOVA, (* indicates $P<0.05$ vs control). N=3 animals, each in triplicate-10 micrographs, averaging 15 measurements/micrograph.

4.4.10 Stretch of EPKs after 10 days of culture

Keratinocytes were subjected to 50-70k Pa stretch for 1, 3 and 5days. Immunofluorescence staining indicated noticeable expressions of K14 (Figure 4-30) and differentiation marker K10 (Figure 4-31) in stretched cells evolving with time. In contrast, non-stretched cells had low expression levels for both K14 and K10. The proliferation marker Ki-67 was detected in stretched and control cells at day 1, while at days 3 and 5 they showed little to no expression of Ki-67 (Figure 4-30). These results suggested that stretch promotes keratinocytes differentiation. Consequently, cells under stretch appeared to form a better monolayer of differentiated cells in comparison to control cells. In addition, it was found that most cells expressing keratin at day 1, 3 and 5 did not display the squamous-like appearance.

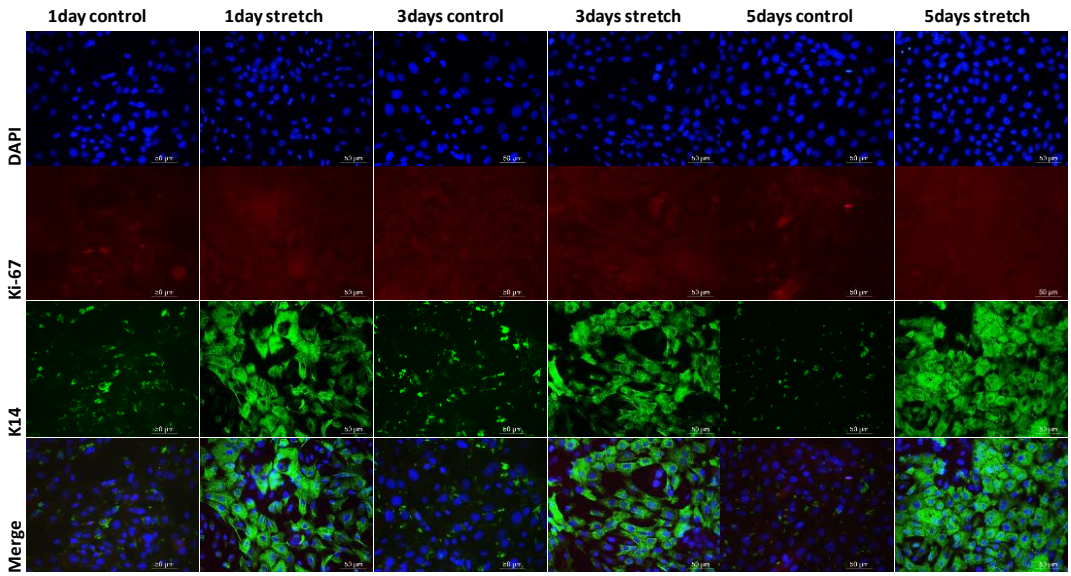


Figure 4-30: The impact of stretch force on Ki-67 and K14 expressions after 10 days culture

Immunofluorescence images of keratinocytes reveal a distinct distribution of K14 and little to no expression of Ki-67. Scale bar represents 50µm.

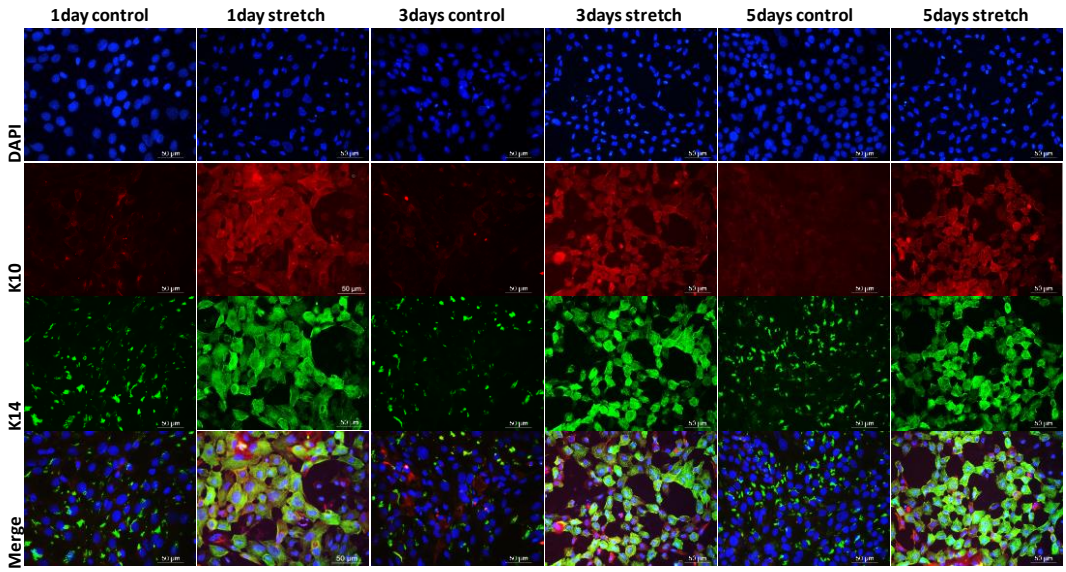


Figure 4-31: The impact of stretch force on K10 and K14 expressions after 10 days culture

Immunofluorescence images of cell keratinocytes reveal a distinct distribution of K10 and K14 when cells are stretched. Scale bar represents 50µm.

Staining with F-actin indicated the appearance of stress actin filaments after continuous stretch for 5 days. However their organization differed being located toward the edge of cells for the control and with a less smooth and punctuated appearance for the stretched cells (Figure 4-32).

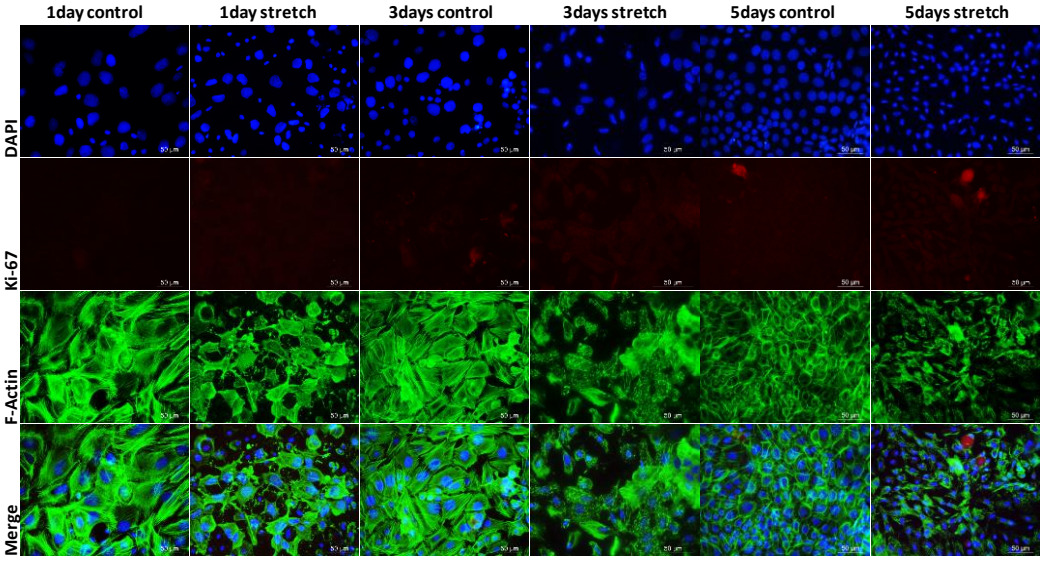


Figure 4-32: The impact of stretch force on F-Actin filaments after 10 days culture

Immunofluorescence images showing the localization of F-Actin filaments at day 1, 3 and 5. F-actin was redistributed under stretch. Scale bars represent 50µm.

A number of statistically significant differences were observed regarding upregulation of the intensity per cell surface area and per nuclei for Ki-67, K14 and K10 at days 1, 3 and 5 under stretch (Figure 4-33A-F; $P<0.05$). However, no significant results were indicated between the cell surface area under stretch and control cells at day 1, 3 and 5 (Figure 4-33G).

The results indicated in this experiment were different from the previous one that were performed on isolated cells and stretched immediately. These differences included that cells were quick to differentiate/ increase in cell surface area when treated with blebbistatin after being incubated for 24hrs/all the time. While changes were not shown when treated with blebbistatin. However, the impact of mechanical stretch on 10 days cultured cells indicated by increasing in keratin expression in stretch vs control and was not shown increases in cell surface area.

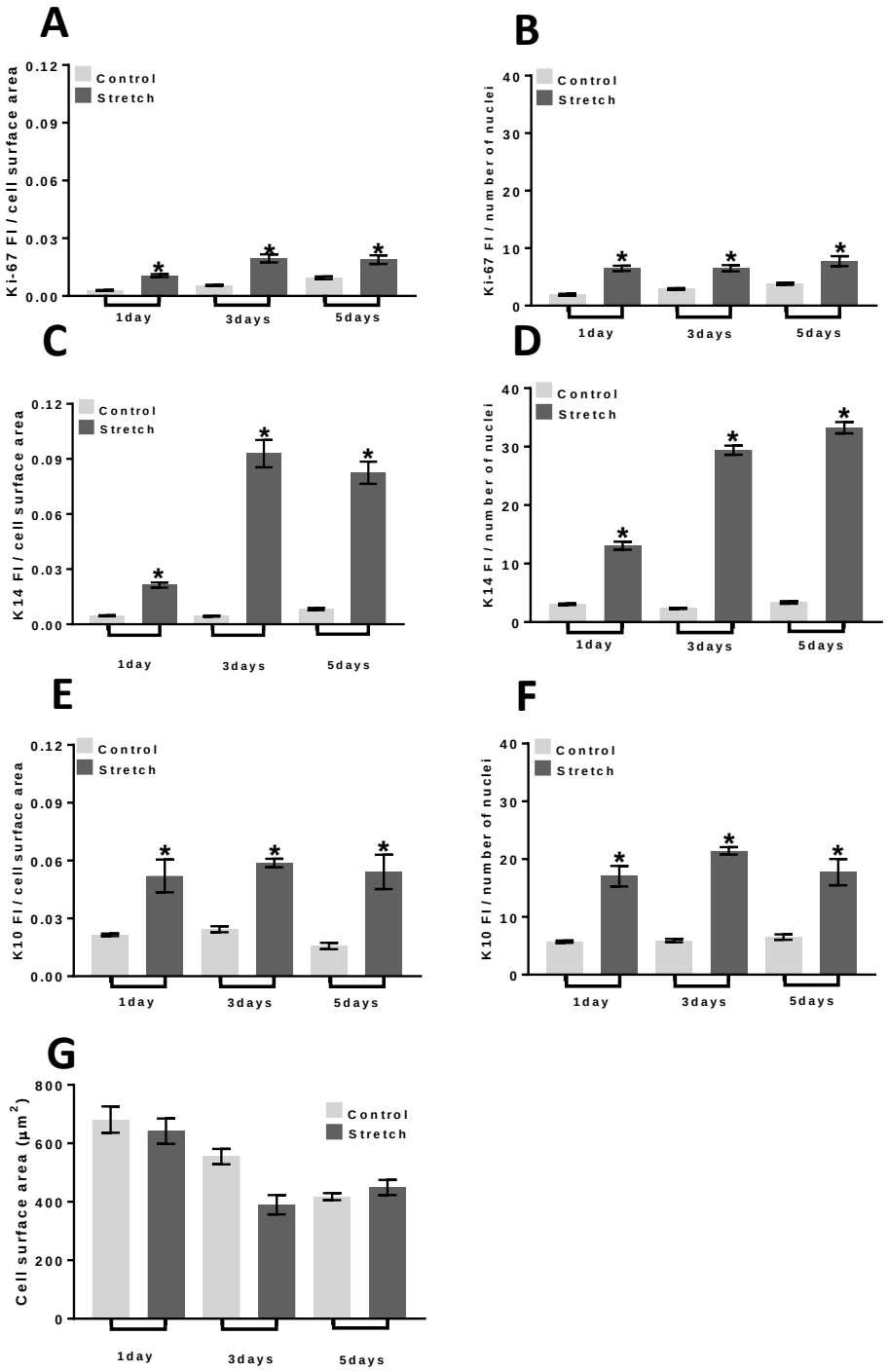


Figure 4-33: Quantification of Ki-67, K14 and K10 expression under stretch, after 10 days culture

Fluorescent intensity per cell surface area or per number of nuclei for the proliferation marker Ki-67 and cytokeratin K14 and K10 under stretch. (A, B), (C, D) and (E, F) Significant variations were found between the intensity of Ki-67, K14 and K10 measured per cell surface area and per nuclei of cells at day 1, 3 and 5 as a function of the stretch applied. However, (G) identified no significant differences between the surface area of control and stretched cells at days 1, 3 and 5. Statistical comparisons between groups were analysed using One Way ANOVA, (* indicates $P<0.05$ vs control). N=3 animals, each in triplicate-10 micrographs, averaging 15 measurements/micrograph.

To assess the expression levels of K14 and CD44 when stretch was applied, a Western blot assay was performed at days 1, 3 and 5. Stretch cells exhibited a strong band for K14 at 55 kDa and significant increases were found under stretched at day 1, 3 and 5 and the expression level of K14 was three times higher in stretched cells in comparison to non-stretched cell with a significant difference ($p<0.05$) at those days (Figure 4-34). However, no significant differences were found for protein expression level for CD44 between the days or stretched and control cells.

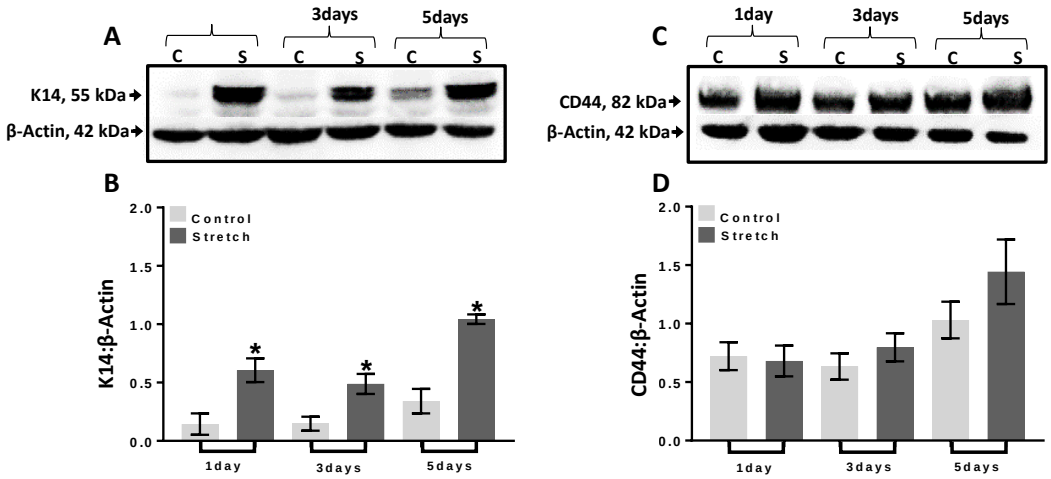


Figure 4-34: Quantification of K14 and CD44 protein under stretch after 10 days culture

Graphs show statistical analysis of Western blots when normalized to β-Actin. A) A clear band of protein expression of K14 at 55 kDa. B) Significant variations were found between the protein expression levels of K14 measured at day 1, 3 and 5 as a function of the stretch applied, while (C, D) no significant variations were found between control and stretch groups for CD44. Statistical comparisons between groups were analysed using One Way ANOVA, (* indicates $P<0.05$ vs control). N= 3 animals, each in triplicate.

4.4.11 EKPs assessment under different oxygen levels

The immunostaining results from incubated keratinocytes under low oxygen conditions revealed clear expression of hypoxia inducible factor-1α (HIF-1α) and differentiation marker K10 under the low oxygen condition of 1% O_2. The fluorescent intensity of both HIF-1α and K10 increased with time, indicating cell differentiation on day 3 and 5 (Figure 4-35). In contrast, in high oxygen condition cells appeared to have lower expressions for both HIF-1α and K10. Additionally, a double labelling of HIF-1α and Ki-67 (Figure 4-36) demonstrated an increase in the expression of Ki-67 at day 5 under the low oxygen condition of 1% O_2 (Figure 4-37). Finally, double labelling of K14 and K10 showed that both cytokeratin markers increase under low level of O_2 over time (Figure 4-38).

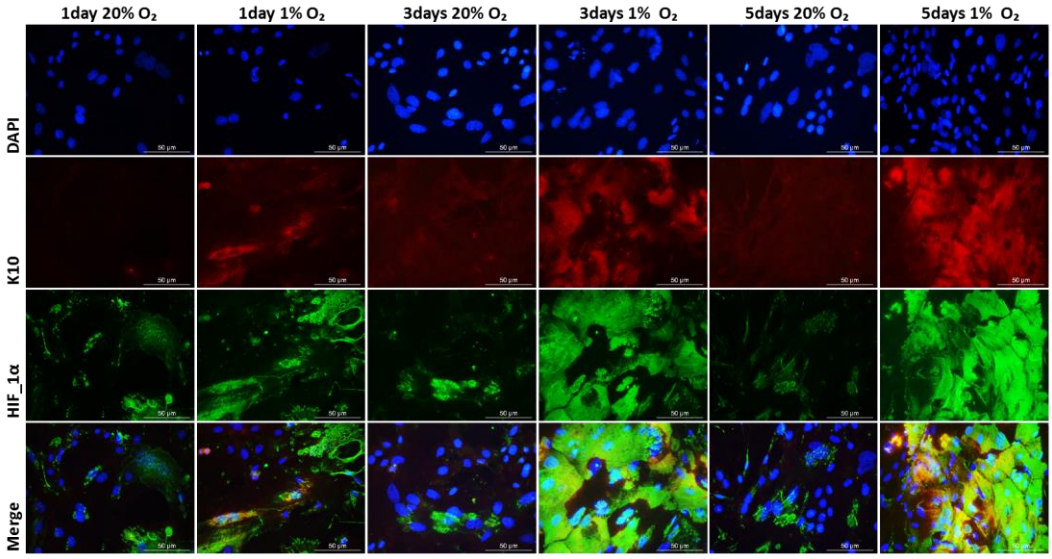


Figure 4-35: The impact of low oxygen levels on HIF-1α and K10 expression

Immunofluorescence images of cell keratinocytes reveal a distinct distribution of HIF-1α and K10 under low oxygen condition 1% O_2 from day 3. Scale bar represents 50µm.

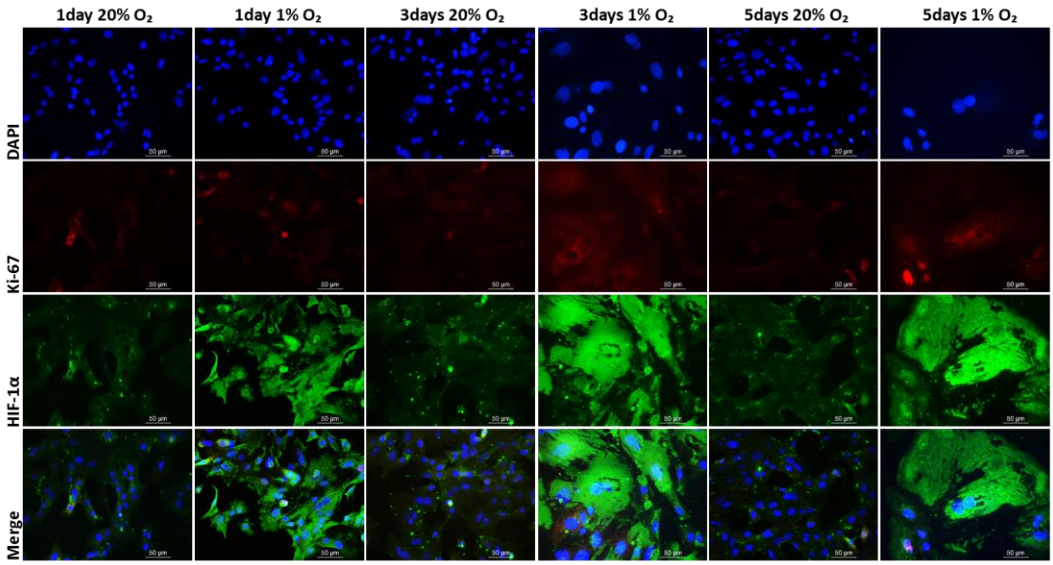


Figure 4-36: The impact of low oxygen levels on HIF-1α and Ki-67 expression

Immunofluorescence images of cell keratinocytes reveal a distinct distribution of HIF-1α from day 1 and little expression of Ki-67 under the low oxygen condition 1% O_2. Scale bar represents 50µm.

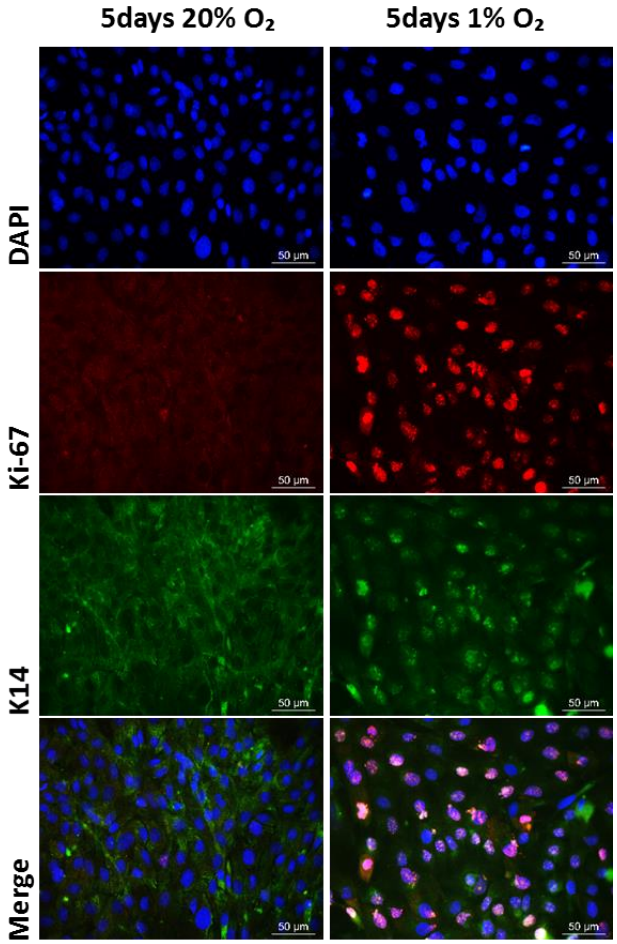


Figure 4-37: The impact of low oxygen levels on K14 and Ki-67 expression

Immunofluorescence images of cell keratinocytes revealing the nuclear localisation of Ki-67 under low oxygen condition 1% O_2 at day 5. Scale bar represents 50µm.

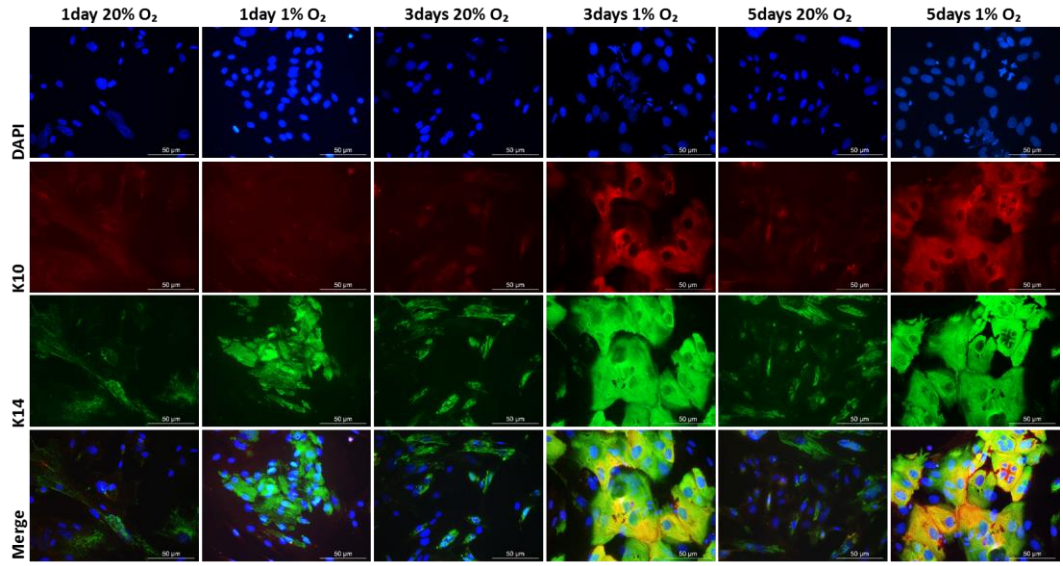


Figure 4-38: The impact of low oxygen levels on K14 and K10 expression

Immunofluorescence images of cell keratinocytes revealed a distinct distribution of K14 and K10 under low oxygen condition 1% O_2 from day 3. Scale bar represents 50µm.

Further investigation on the role of stem cell marker CD44 under low oxygen revealed that the expression of CD44 under 1% O_2 level is decreased but that the expression level of K14 increases (Figure 4-39). Additionally, most cells expressed keratin at day 5 and showed a squamous-like structure.

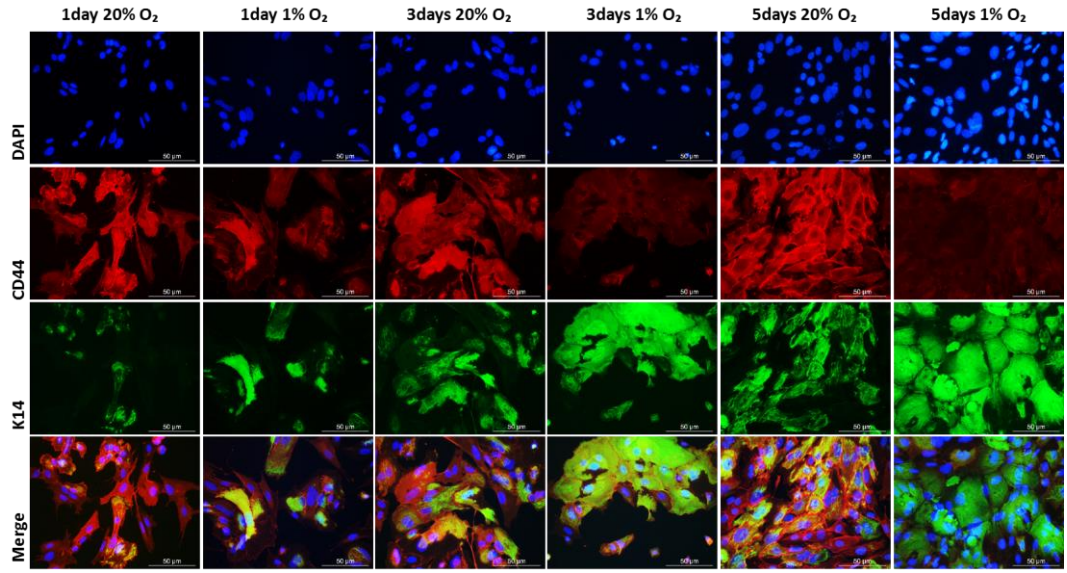


Figure 4-39: The impact of low oxygen levels on CD44 and K14 expression

Immunofluorescence images of cell keratinocytes revealed a distinct distribution of CD44 and K14 under low oxygen condition 1% O_2. The expression level of CD44 dropped under low oxygen whereas the level of K14 expression increased under similar low oxygen conditions (both compared to control levels). Scale bar represents 50µm.

A number of statistically differences were found regarding the fluorescence intensity per cell surface area and per number of nuclei. The results in the intensity of HIF-1α/surface area were increased at day 1, 3 and 5 under 1% O_2 levels, the same at day 1 and 3 under 3% O_2 levels, while at 5% O_2 shown only at day 1 (Figure 4-40A $P<0.05$). HIF-1α/number of nuclei were increased at 1%, 3% and 5% O_2 levels at day 1,3 and 5 (Figure 4-40B; $P<0.05$). Additionally, Ki-67/surface area was increased at day 1 and 3 under 3% and at day 5 under 1% O_2 levels under low oxygen conditions vs high oxygen conditions (Figure 4-40C; $P<0.05$). Similar results were found regarding the fluorescence intensity per nuclei for Ki-67 under low oxygen conditions 1% and 3% O_2 levels at day 1, 3 and 5 (Figure 4-40D; $P<0.05$).

Furthermore, K10/surface area was increased at day 3 and 5 only under 1% O_2 levels (Figure 4-40E; $P<0.05$) and decreased at day 1, 3 and 5 under 5% O_2. Similar results were found regarding the fluorescence intensity per nuclei for K10 under low oxygen conditions 1% at day 1, 3, 5 and, under 3% O_2 levels at day 3 and 5 ($P<0.05$), while no difference were measured under 5% O_2 levels (Figure 4-40). Finally, K14/surface area was increased at day 3 and 5 under 1% and 3% O_2 levels (Figure 4-40G; $P<0.05$). Similar results were found regarding the fluorescence intensity per nuclei for K14 under low oxygen conditions 1% and 3% O_2 at day 1, 3, 5 ($P<0.05$), while no differences were measured under 5% O_2 levels (Figure 4-40H). However, increased cell surface area over time were measured under 1% and 3% O_2 low oxygen conditions at day 1, 3, 5, while were measured only at day 3 and 5 under 5% O_2 level (Figure 4-40I; $P<0.05$).

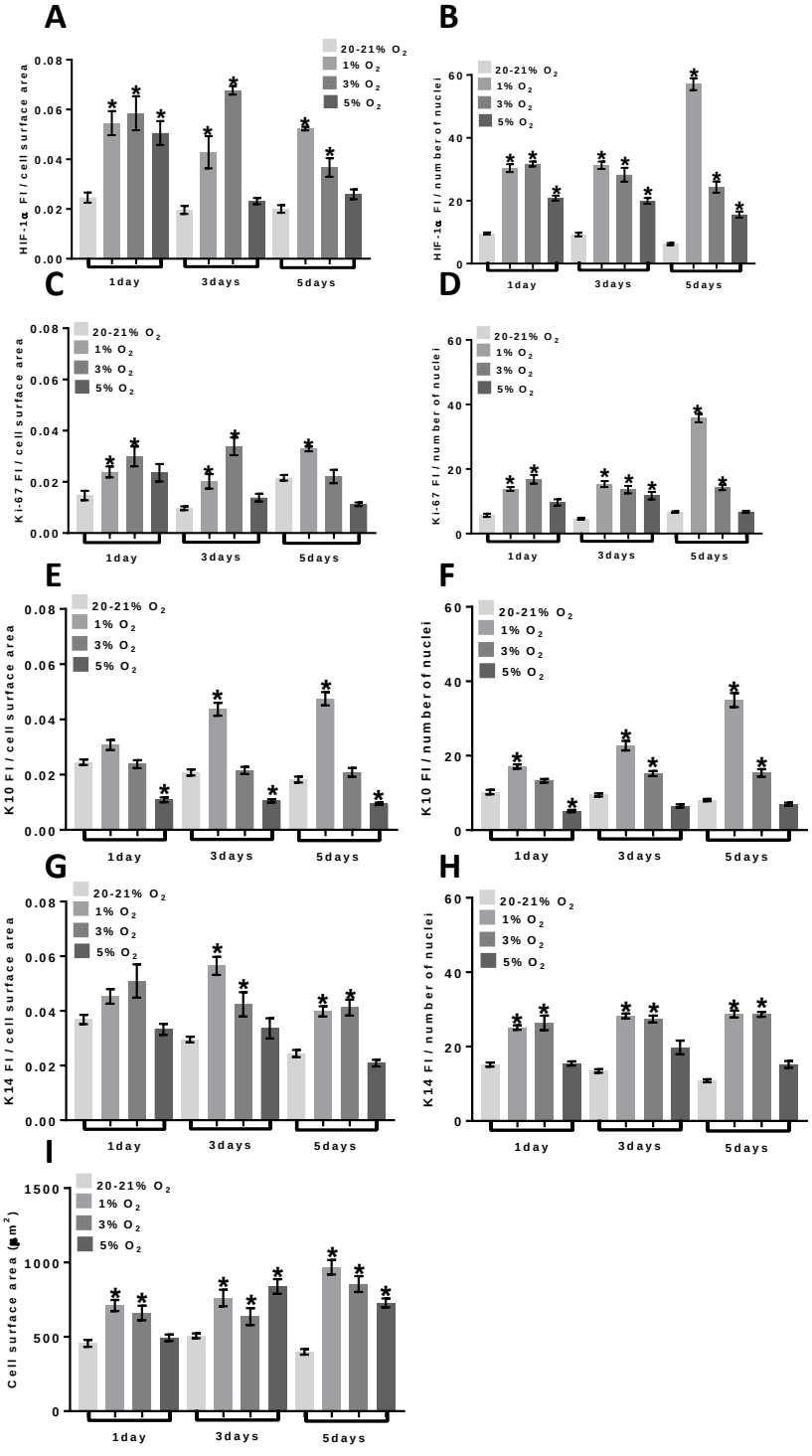


Figure 4-40: Quantification of HIF-1α, Ki-67, K10 and K14 expression levels under low O_2

A, B & C, D) Significant variations were found between the intensity of HIF-1α and Ki-67 measured per nuclei at day 1, 3 and 5 with 1 and 3% O_2, while day 5 did not reveal any significant differences for Ki-67. Similarly, (E, F & G, H) showed significant variations between the fluorescence intensities of K10 and K14 measured per nuclei at day one and three as a function of the stretch applied, while no significant variations were found under 5% O_2. G) Identified clear and significant differences between the surface area of cells between high 20-21%O_2 and low oxygen 1% O_2 at day 1, 3 and 5. Statistical comparisons between groups were analysed using Two Way ANOVA (* indicates $P<0.05$ vs control 20-21% O_2). N=3 animals, each in triplicate-10 micrographs, averaging 15 measurements/micrograph.

Additionally**,** CD44 levels were decreased at day 1, 3 and 5 under 1% O_2 in comparison to high oxygen condition (Figure 4-41A+B P<0.05).

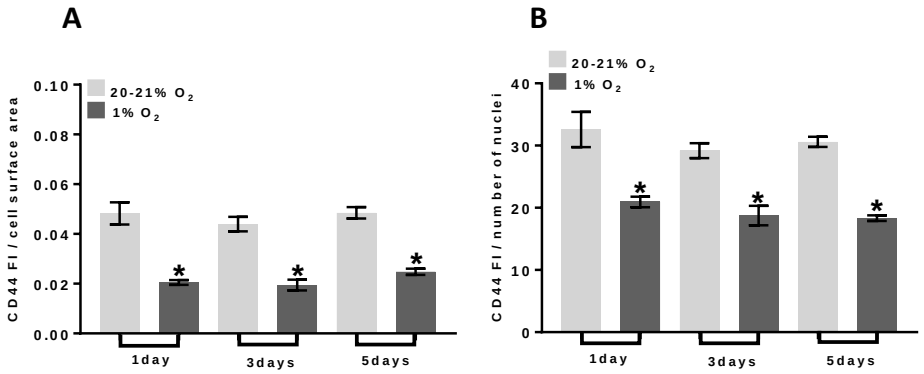


Figure 4-41: Quantification CD44 expression under 1% O_2

Fluorescent intensity per surface area or per number of nuclei for the CD44 under low oxygen condition 1% O_2. (A, B) Significant variations were found between the intensity of CD44 measured per surface area and per nuclei at day 1, 3 and 5 on 1% O_2. Statistical comparisons between groups were analysed using One Way ANOVA, (* indicates P<0.05 vs control 20-21% O_2). N=3 animals, each in triplicate-10 micrographs, averaging 15 measurements/micrograph.

The results of Western blot indicated that cells incubated under low oxygen exhibited a strong band for K14 at 55 kDa and significant differences under 1% O_2 level at day 3 and 5 as the expression level of K14 was three times higher in comparison to high oxygen cells (at 20-21% O_2 level) (Figure 4-42; P<0.05). However, no significant differences were found for protein expression levels of K14 at 3% and 5% O_2 levels.

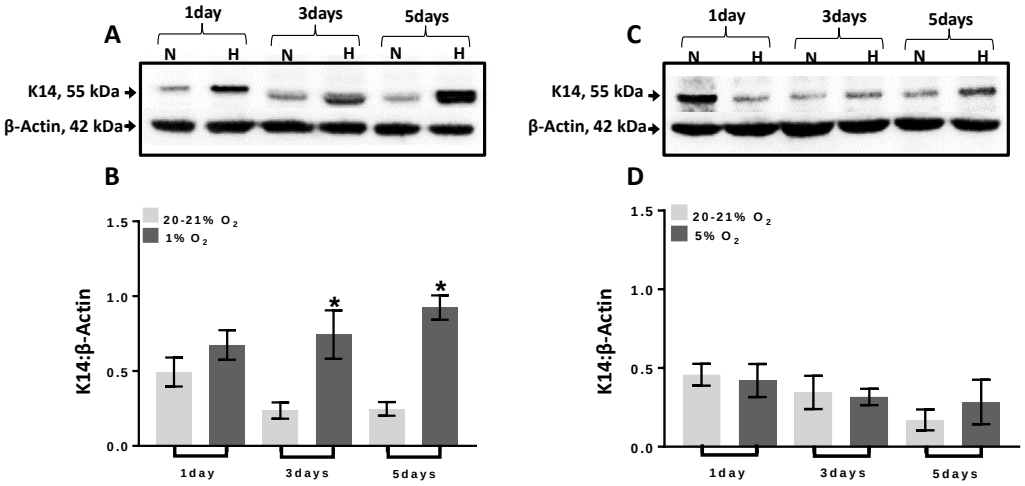


Figure 4-42: Quantification K14 protein expression under 1% and 5% O_2

Graphs and Western blot representing the impact of low oxygen on the K14 protein expression levels. H: low oxygen condition; N: high oxygen condition. A) K14 expression levels increase under low oxygen condition and as time goes on. B) As expected significant variations were found between the protein expression levels of K14 measured at day 1, 3 and 5 under 1% O_2, while (C, D) show no significant was found under 5% O_2. Statistical comparisons between groups were analysed using One Way ANOVA, (* indicates $P<0.05$ vs control 20-21% O_2). N=3 animals, each in triplicate.

4.4.11.1 Assessment the level of gene expression under 5% O_2

While no detectable changes were observed under 5% oxygen levels as far as protein expression was involved, there were noticeable changes in cell size that may suggest that cells sense this low oxygen condition while not fully expressing the protein over time. If this is the case, this means that the 5% oxygen levels may represent a threshold level of low oxygen. In order to investigate this further, additional experiments were performed to determine the mRNA levels of HIF-1α, K14, K10, CD44, CD29**,** Integrin-α6, Involucrin and Vimentin-related genes, under the low oxygen condition of 5% O_2 levels. The gel result for K14 is given as an example (Figure 4-43). The band sizes of gene K14 were detected by comparing with a 1 kb ladder.

The results of mRNA quantifications are represented as fold-changes in HIF-1α, K14, K10, Involucrin, CD44, CD29**,** Integrin-α6 and Vimentin with reference to β-Actin and GAPDH as housekeeping genes. The data calculated with reference to β-actin indicated that there were not significant differences in HIF-1α, K14, K10, CD44, CD29**,** Integrin-α6, Involucrin and Vimentin-related genes overtime between high oxygen and low oxygen conditions (Figure 4-44).

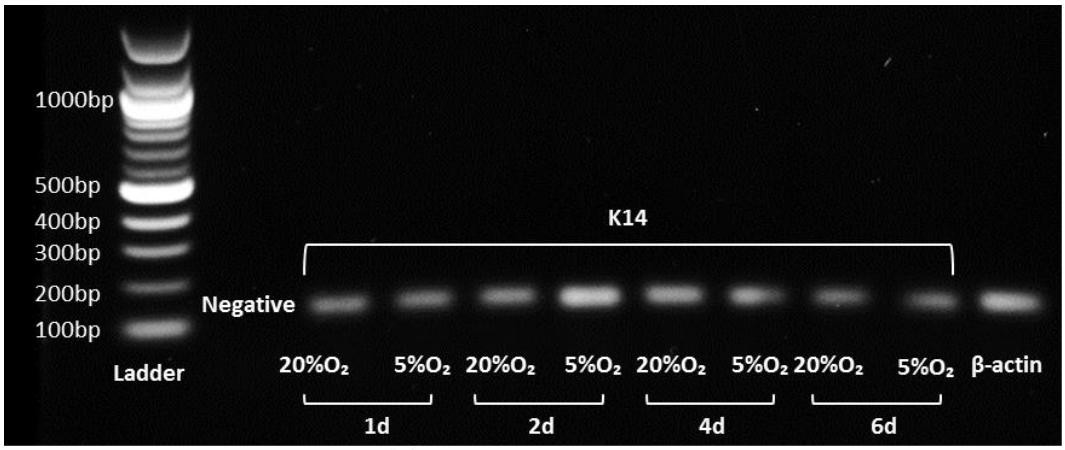


Figure 4-43: PCR products of amplification K14 gene from EPKs

PCR image shows a clear band of K14 gene expression size 179bp.

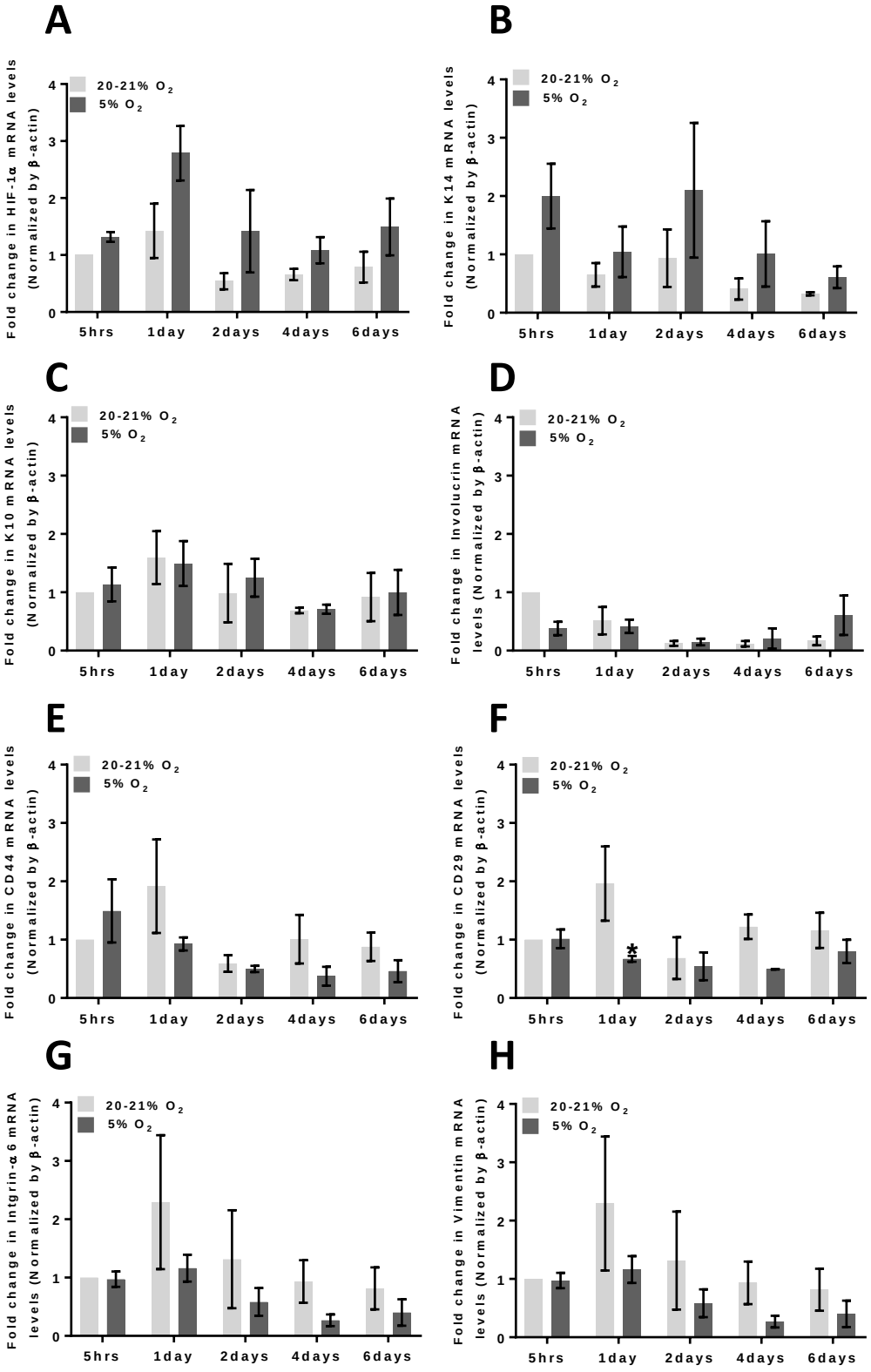


Figure 4-44: Quantification of gene expression levels under 5% O_2 conditions

Graphs are presented as fold-changes in mRNA levels of HIF-1α, K14, K10, Involucrin, CD44, CD29**,** Integrin-α6 and Vimentin, which are calculated as the relative copy number (copy number of gene of interest/normalisation factor). Statistical comparisons between groups were analysed using Two Way ANOVA, (* indicates $P<0.05$ vs control 20-21% O_2). N= 3 animals, each in triplicate technically and practically.

4.4.12 Assessment the impact of insulin on culture EPKs

The results obtained from measuring the fluorescence intensity of proliferation marker Ki-67 and cytokeratin protein K14 revealed clear response with an increase of Ki-67 and an increase expression of K14 as a function of time and insulin concentrations (Figure 4-45). A number of statistically significant increases were found for the fluorescence intensity per surface area and per nuclei for Ki-67 and K14 at 2hrs, 8hrs, 24hrs and 48hrs in comparison to untreated cells (Figure 4-46A-D; $P<0.05$). Furthermore, a significant increases in the cell surface area was observed between the insulin-treated and untreated cells at 2hrs, 8hrs and 48hrs (Figure 4-46E; $P<0.05$).

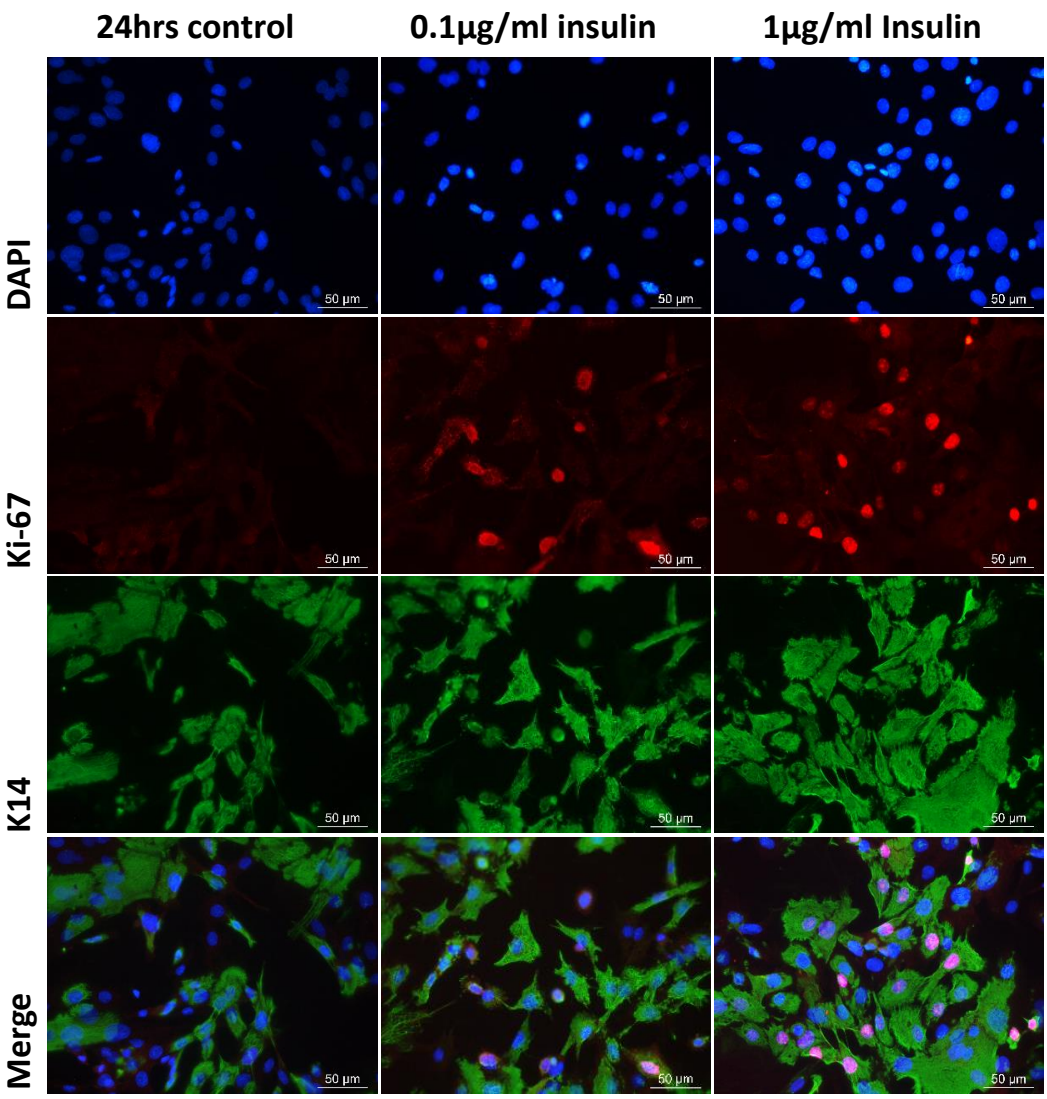


Figure 4-45: The impact of Insulin on Ki-67 and K14 expression levels

Immunofluorescence images of cell keratinocytes revealed a distinct distribution of Ki-67 and K14 incubated with 0.1µg and 1µg insulin/ml. At 24hrs expression of Ki-67 localized inside nuclei were detectable with 0.1µg/ml and became more obvious with cells incubated with 1µg/ml. Scale bars represent 50µm.

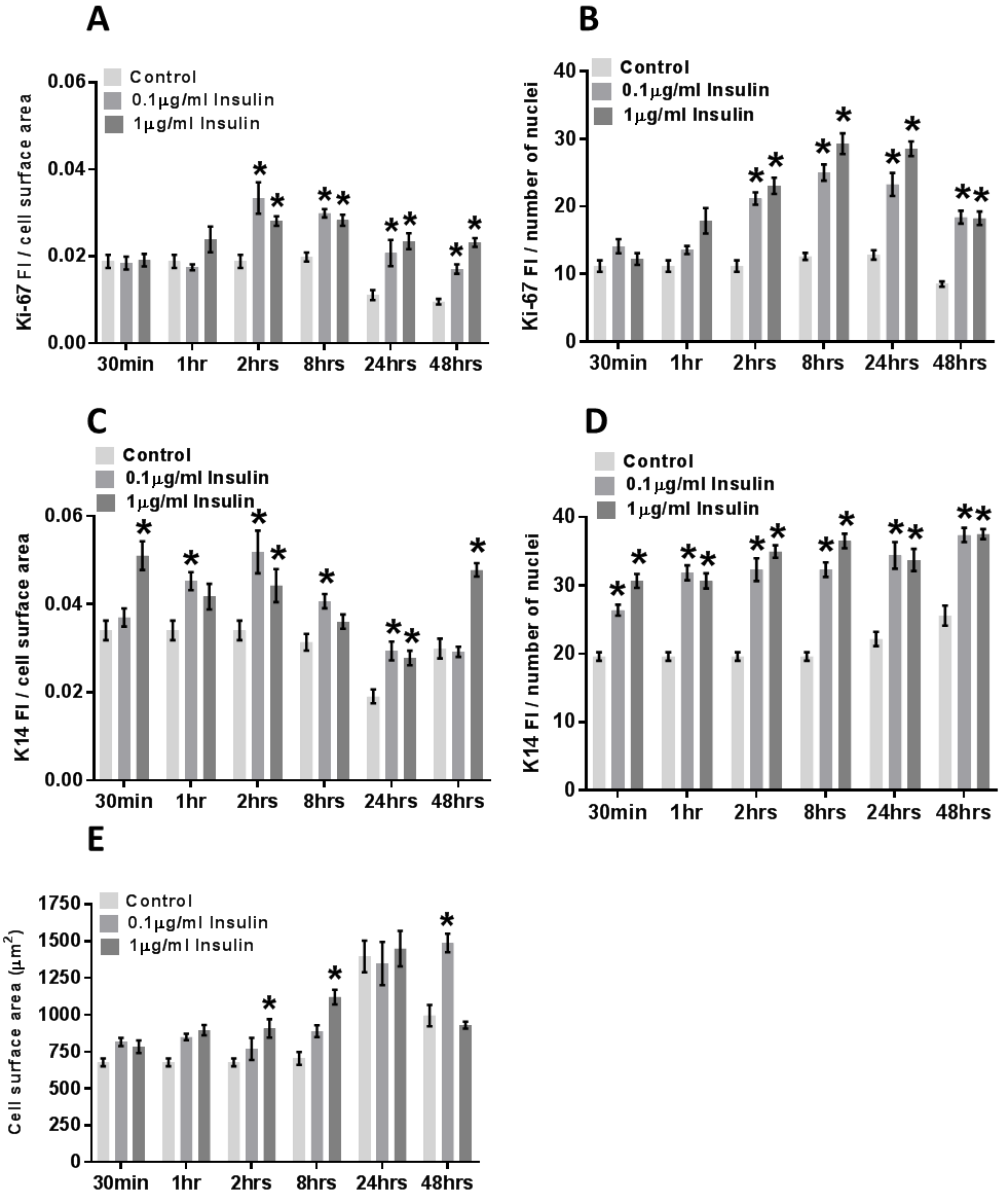


Figure 4-46: The impact of different insulin doses on the expression of Ki-67 and K14

A, B) Significant variations were found between the intensity of Ki-67 measured per the cell surface area or per nuclei at 2, 8, 24 and 48hrs while 30min and 1hr did not reveal significant differences in Ki-67 expression levels. Similarly, (C, D) shows significant variations between the intensity of K14 measured per cell surface area and per nuclei over time. E) Clear and significant differences were found between the surface area of untreated and treated cells over time. Statistical comparisons between groups were analysed using Two Way ANOVA GraphPad Prism 7, (* indicates $P<0.05$ vs control within that time point). N=3 animals, each in triplicate-10 micrographs, averaging 15 measurements/micrograph.

4.4.12.1 Assessment the PI3k/Akt pathway in cultured keratinocytes treated with Insulin

The results of the Western blot showed a strong and a clear band at 60 kDa of the phosphorylation status of PI3k/Akt proteins at 30min, 1hr and 2hrs in treated cells vs untreated cells. This was found as an indicator for the pathway activation of PI3K drives to phosphorylation of Akt pathway when compared with the band observed in control cells with a significant difference at 30min, 1hr and 2hrs (Figure 4-47; $P<0.05$).

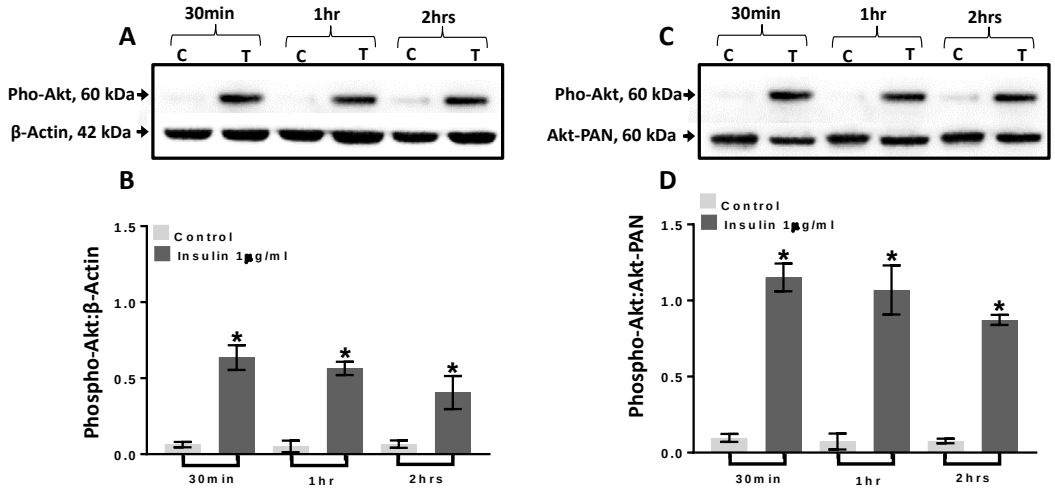


Figure 4-47: Quantification Akt protein pathway when treated with 1µg/ml insulin

Graphs show statistical analysis of Western blot when normalized to dominant β-Actin protein. A) A clear band of protein expression of Phospho-Akt at 60 kDa. B) Significant variations were found between the protein expression levels of Phospho-Akt measured at 30min, 1hr and 2hrs, similarly (C, D) significant variations were found between control and treatment groups for Phospho-Akt when normalized to Akt-PAN. Statistical comparisons between groups were analysed using One Way ANOVA with Post Hoc testing SPSS, (* indicates $P<0.05$ vs control). N=3 animals, each in triplicate.

4.5 Discussion

Equine hoof disease is a multifactorial disease (Pollitt, 2004b, Heymering, 2010, Katz and Bailey, 2012) that is a challenging to totally imitate with experimental models. Therefore, understanding the behaviour of epidermal hoof wall keratinocytes *in vitro* provides a promising model to examine this problematic disease. The current findings of this study revealed that cultured keratinocytes that were efficient at generating actively growing spheres and colonies can be purified with the aid of high cell surface expression of stem cell markers CD44 and cytoskeletal K14, as well as their quick adhesion to collagen type IV. However, although a number of studies investigated the isolation and characterization of equine keratinocytes from skin (Dahm et al., 2002, Broeckx et al., 2013, Sharma et al., 2016). This were others conducted on hoof (Visser and Pollitt, 2010, Pinto, 2012), none investigated whether the isolation of EPKs from coronary specific region basal dermal papillae may result in biophysical or biomechanical responses that might affect the growth rate of the hoof wall. Additionally, although keratinocytes are the first cell line to encounter chemical, physical and biological stresses, their role in responding to these stresses has not been entirely characterised. The current study was designed to investigate the molecular mechanisms triggered in keratinocytes in response to mechanical physical/chemical stresses. This chapter in particular examined the cell behaviour involved in proliferation and differentiation, which might have an impact on cell morphology. This chapter is essential in the understanding of how EPKs at the basement membrane initiate adaptive biophysical responses.

It should be noted that the isolation and cultured equine hoof keratinocytes was not as straightforward as other cell types in this thesis. Isolation was successfully achieved by avoiding cell contamination, as the hoof is the biggest source of microorganisms. The results of this study illustrated purification and establishment of primary epidermal keratinocyte cell culture from epidermal tissue (Figure 4-4), seeded on collagen coated plates. This result is supported by earlier studies (Dahm et al., 2002, Broeckx et al., 2013), who utilised mechanical and enzymatic methods to yield a great number of viable cells while avoiding contamination. However, their study was conducted on equine skin with which it is more able to control contamination (Broeckx et al., 2013). Other similar studies have been conducted on the equine hoof, but these investigations investigated keratinocytes isolated from lamellae and not form the coronary region (Visser and Pollitt, 2010, Pinto, 2012). One finding to emerge from the cultured EPKs in this study is that the adherent spheres and colonies were vary in size, growth and morphology. Consequently, most of these primary cultured cells may contain both the meroclones and holoclones found by Barrandon and Green (1987). An alternative hypothesis is that these cells are paraclones, which displayed a short replicative lifespan, and were therefore excluded from cell culture experiment. This result could be explained by the fact that differences in growth heterogeneity beside clonal expansion and self-renewal of the isolated keratinocytes become main features of stem cells spheres, as described by Borena et al. (2014). The findings presented in this chapter indicates that primary coronary keratinocytes were cultured either directly or after first passages (9-11 days), as long as appropriate medium and substrate environments were provided (Visser and Pollitt, 2010).

The results of this study showed that equine hoof keratinocytes have a distinctive cellular morphology and express intermediate filament keratin analogous to keratin produced from human skin (Porter et al., 2000, Lloyd et al., 1995) or human nail (De Berker et al., 2000). This morphology is also analogous to other species, for instance bovine claw (Kvedar et al., 1986, Hendry et al., 2001, Mills et al., 2009), ovine (Zhang et al., 2015) or murine (Tani et al., 2000). The purity of cultured keratinocytes was confirmed and determined by K14 immunostaining the primary cytoskeletal marker of the basal epidermal cell type, as performed in similar studies on equine progenitor keratinocytes (Broeckx et al., 2013, Linardi et al., 2015) as well as in human keratinocytes (Li et al., 1998, Webb et al., 2004).

The results of this study indicated a specific role for blebbistatin in the organization of actin microfilaments, cell morphology and cell adhesions via blocking non-muscle myosin II. It has been reported that blebbistatin is one of the important pharmacological methods in which to examine the role of myosin II in cells and tissues (Zhang and Rao, 2005, Limouze et al., 2004). EPKs treated with 20µM blebbistatin for 1, 3 and 5 days showed visible changes in cell morphology and completely blocked actin filaments in comparison with untreated cells, without noticeable cytotoxicity (Figure 4-8). The dose used in this experiment has been stated to inhibit mostly skeletal muscle myosin II and non-muscle myosin filaments *in vitro* (Straight et al., 2003, Limouze et al., 2004, Zhang and Rao, 2005). The consequences of blebbistatin on EPKs in this study was the modification of F-actin microfilaments and commitment to final differentiation (Figure 4-11). However, little is known on how the inhibition of actin filaments influences EPKs behaviour. The current findings demonstrated that continuous incubation of EPK culture with blebbistatin decreased the growth rate and

increased the commitment of cells to further differentiation, elongated cytoplasmic extension and cell movements (Figure 4-9). These observations corroborate with observations by Sarkar et al. (2009) who found that inhibition of actin microfilaments with blebbistatin significantly increased keratinocyte migration after 6 hrs, and that this effect was controlled by both MLCK and Rho-kinase pathways. Additionally, the current findings were consistent observations that Rac1 and Y27632 inhibition in stem human keratinocytes by reduces clonal growth, and stimulates clonal conversion and terminal differentiation (Nanba et al., 2013). Although cells treated with blebbistatin are stimulated and change in cell movement, shape, diminished stress fibres, and prompted detachment in primary cell cultures, their changes in shape in drug-perfused eyes were not visible (Zhang and Rao, 2005). On the other hand, it has been reported that blebbistatin could block differentiation without any effect on the cell cycle (Straight et al., 2003, Engler et al., 2006). However, this effect could be due to the individual epithelial migration detected in keratinocytes (Sarkar et al., 2009). Inhibition of actin filaments by 20µM blebbistatin resulted in post immunostaining with F-actin (Figure 4-11) in control cells. F-actin filaments were labelled clearly at lamellipodia and stress fibres, whilst no staining was observed in treated cells. These results are consistent with other study, which found that actin filaments staining disappeared after treatment with 100µM blebbistatin (Shutova et al., 2012). It can thus be suggested that blebbistatin induced EPKs are demarcated by microfilament organization, which is involved in cell growth and differentiation. There are, however, other possible explanations are based on the fact that non muscle myosin II able to attach to stressed conformation F-actin microfilaments, comparative to non-stressed filaments (Uyeda et al., 2011).

The results obtained from applied hydrostatic pressure (HP) on cultured keratinocytes revealed that the cells pressurized under 495 and 990 Pa at day 3 and 5 had an influence on the morphological and biomechanical changes of cell size. For instance, the organization of intermediate filaments, increased expression of K14 and K10 at day 5 and multinuclei that observed in immunofluorescence staining (Figure 4-17). These results match those detected in earlier studies that the hydrostatic forces are responsible for the modification of endothelial and nuclear shape, via actin and myosin filaments translocation in myofibrils (Sims et al., 1992). Additionally, in this study HP promoted proliferation at day 3 and 5 under impact of 495/990 Pa via significant ($P<0.05$) expression of Ki-67 (Figure 4-19)/differentiation, and promoted expression of differentiation marker K10 at day 5 (Figure 4-20). These results are in accord with current studies indicating that mechanical stimuli via HP induces osteogenesis/chondrogenesis differentiation and/proliferation of bone marrow stem cells by stimulating the cell cycle (Liu et al., 2009, Zhao et al., 2015). The value of HP application suggests that it could be used as an effective method for encouraging the biological activity of keratinocytes, and that Ki-67 and cytoskeletal keratin could be utilized to dynamically control the stress response of keratinocytes. Some studies also revealed that intermediate filaments could undergo modification in reply to mechanical force such as tensile stress/fluid flow (Knight et al., 2006). Additionally, new evidence has suggests that osmotic-mechanical sensitive ion channels have a potential role in the organization of stem cell differentiation that transfer biophysical signals such as osmolality/temperature and intracellular Ca^{2+} (Pedersen and Nilius, 2007, Christensen and Corey, 2007, Guilak et al., 2009).

The application of 50-70% tensile stretch on cultured keratinocytes treated with 20 μM blebbistatin indicated significantly ($P<0.05$) increased the expression of keratins K14 and K10. Tensile tension over one and three days resulted in numerous changes in keratin expression (Figure 4-21) and suppressed the expression of cell proliferation marker Ki-67 (Figure 4-23). These observations might be due to distinctive cell migration reported in human keratinocytes treated with 30μM blebbistatin as it is reported by Sarkar et al. (2009). Based on the current study, it may also be hypothesised that cell stretching is involved in directing cell spreading in EPKs, and its activity is controlled by the amount of keratins expressed in cell stretching. In contrast to these findings, studies working on cancer cells have reported that low expression of keratins detected through epithelial/mesenchymal alteration contributes to the migration and invasion of cancer cells (Seltmann et al., 2013). This could explain the unique role/behaviour of keratin filaments in cell stiffness, as the disruption of cytoskeletal keratin filaments could decrease cell stiffness and cause cell deformity (Beriault et al., 2012). Normally interconnections between cytokeratin filaments and cell junctions such as desmosomes and hemidesmosomes participate in the integrity of epithelial tissue, and mediate cell-stretching essential for cell maintenance with the aid of keratin (Russell et al., 2004). It seems important then to study the role of non-muscle myosin and their contractile features in cell stretching. It should noticed that the role of the contractile function in EPKs treated with blebbistatin has not been previously investigated. This may provide additional insight into knowledge of how cell response to contractile function.

Additional experiments revealed a significant ($P<0.05$) difference in the expression of keratin via immunostaining and Western blotting. These current

findings indicated a clear elevation in the expression of K14 and K10 and proliferation marker Ki-67 in cultured stretched cells vs non stretched cells (Figure 4-30&31). It should be remarked that previous and current research focus on the impact of stretch on cultured human or mouse cells rather than equine keratinocytes extracted from coronary epidermal papillae (Yano et al., 2004, Reichelt, 2007, Tokuyama et al., 2015, Bonakdar et al., 2015).

It is interesting to note that the behaviour of equine hoof cultured keratinocytes in response to mechanical stretch *in vitro* seems to be analogous to the response of the basal epidermal cells *in vivo*. It could be hypothesised that basal progenitor keratinocytes at the dermal papillae are subjected to tensile stretch as a consequence movement. These physical forces may have an effect on cell roles from transit amplifying cells to differentiation. In the equine skin epidermal tissue, lamellae and coronet, keratin K14 were revealed to be expressed at basal and suprabasal layers for both the skin and coronet, while at the basal layer for the lamellae, K10 expressed only in skin spinosium and granulosum layers (Carter et al., 2011, Linardi et al., 2015). However, it should be noticed that in this study polyclonal antibodies against K10 were used as a differentiation marker, and revealing the expression of K10 in stretching cells in comparison to non-stretched cells. K10 was used as the differentiation marker in this study because it was difficult to find antibodies specific to equine specific-cell keratinocytes.

These results are consistent with a previous study by Yano et al. (2004) on the stretching of human keratinocytes via increasing the proliferation index, who reported the suppression of expression K10 and induction of expression K6. However, this was conducted on human skin keratinocytes which are completely different from equine hoof keratinocytes in terms of the forces they experience *in*

vivo. Additionally, these results are in line with what have been reported on the role of mechanical stretching in the stimulation of proliferation/differentiation in numerous cell types (Pavlin et al., 2000, Otis et al., 2005). Sanchez-Esteban et al. (2001) stated that the forces applied via a flexor-cell stress unit triggered differentiation/maturation of foetal alveolar epithelial cells, Di Palma et al. (2003) and Wang et al. (2017) have indicated stimulate differentiation in osteoblasts planted on metallic biomaterials, and induce cardiomyogenic differentiation. On the other hand, some studies have reported that mechanical forces promote proliferation and inhibit differentiation (Saha et al., 2006, Zhou et al., 2015). Although a number of studies have lately been reported in human cell culture, the biophysical mechanisms in equine hoof keratinocytes are unknown. However, the findings of the current study reveal that biomechanical force plays an essential role in inducing keratinocyte differentiation.

Investigation under low oxygen conditions 1%, 3% and 5% O_2 showed that the findings from the data analysis of keratinocytes under low oxygen conditions was significant ($p < 0.05$) in relation to the expression of HIF-1α, K14, K10 and Ki-67, in particularly under 1% O_2 conditions (Figure 4-35-39). These findings revealed increased cell proliferation and enhanced cell differentiation under very low levels of oxygen, suggesting that this may also occur in *vivo*. These results are in accordance with previous studies, where lowered oxygen (2% O_2) induced proliferation and dopaminergic differentiation, and decreased apoptosis in cultured mesencephalic stem cells (Studer et al., 2000). Other studies conducted on neonatal skin keratinocytes reported the suppression of differentiation via the downregulation of differentiation markers K1 and K10, with no effect on HIF-1α expression under 1% O_2 (Park et al., 2016). However, the studies performed on

equine skin found that HIF-1α increased significantly in stress tissue such as injured skin (Deschene et al., 2011). Additionally, according to Pawlak et al. (2013) *in vivo* equine lamellar tissue contains a higher concentration of HIF-1α compared to skin and visceral tissues, and that this increases in laminitic horses in comparison to non laminitic. HIF-1α is also expressed in cultured lamellar keratinocytes under 3% O_2, suggested that hoof keratinocytes may be present in extremely lowered levels of O_2 (Gardner, 2015, Gardner et al., 2017). Therefore, this current investigation on the role of HIF-1α in equine cultured keratinocytes provided a tool for better understanding the role of HIF-1α in horse feet. Interest in the pathophysiology of equine laminitis has recently gained attention due to the roles that both infection and ischaemia/vasoconstriction and/or low oxygen are supposed to be involved in the hoof disease process (Pawlak et al., 2013, Gardner, 2015). Overall, the combination of current findings in this study provides some support for further understudying the mean by which cell responds to lower oxygen level.

4.5.1 Conclusions

This chapter described a novel method for cell isolation and purification in order to understand the mechanism of equine hoof growth. This chapter demonstrated provisionally how the cultured keratinocytes responded to different environment stresses including hydrostatic/mechanical forces. These stresses together with low oxygen conditions stimulated cell differentiation, demonstrated by the upregulation of their cytoskeletal protein levels, leading to changes in their morphology and cell surface area based on their normal environmental tissue. This investigation also determined that certain parameters for isolation or cell

culture such as the pattern of cell growing, cell passages, influence cell contractile system, biomechanical responses, particularly stretch and/or hydrostatic forces and low oxygen conditions. Together this provides some novel elements to improve our knowledge of natural cell stimulation and aids our understanding of how equine hoof keratinocytes would hypothetically respond to external stimuli. Finally, this could aid our understanding of how normal epidermal papillary tissues are developed from a basal progenitor keratinocytes, and how these cells can accommodate to an unexpected imbalance in tissue environment as can happen in equine hoof diseases.

Chapter 5
Physical biology of hoof growth

5.1 Introduction

This introduction adds to the information provided in the literature review. In brief this comprises of hoof shape, microstructure and histology, disorders which cause hoof shape abnormalities, hoof growth (including proliferation and apoptosis), and physical forces which act upon hoof growth.

5.1.1 Hoof growth

5.1.1.1 Growth rate of hoof wall

Hoof growth rate is generally measured by marking the external surface of the hoof wall and by measuring the distance between the coronet and the mark (Pollitt, 1990, Ryan, 2013, Lewis et al., 2014). The growing cells from the papillae play a pivotal role in replacing the wearing of hoof wall upon contact with the ground (Pollitt, 1998), as the horse's feet require to balance the wear with new keratinized material (Ramsey, 2011). In general, 9-12 months is required for the hoof to grow from the coronary region to the ground (Dellmann and Eurell, 1998).

A number of authors have reported results on equine hoof growth rate. Faramarzi et al. (2009) indicated that, the average growth of the hoof wall range is 6.08-6.5 mm/month (mm/mo) which is similar to the rate of 6.4 mm/mo reported by Dellmann and Eurell (1998) and somewhat less than the rate of 10.2 mm/mo reported in other studies (Pollitt, 1990, Florence and McDonnell, 2006). Variances between the rates in these studies are thought to be attributed to season/temperature differences during the year or the breed of horses used. Florence and McDonnell (2006) showed that hoof growth rate in ponies is significantly greater between June and August (Summer time) than between

August and September. In addition, the growth rates between the front (10.2 mm/mo) and hind (9.6 mm/mo) hooves differ.

A considerable number of the studies published on the variability of the growth rate of equine hooves have pointed out that nutrition (Reilly et al., 1998b, Ott and Johnson, 2001, Jančíková et al., 2012), environment (Hampson, 2011), genetics (Ducro et al., 2009); age (Frackowiak and Komosa, 2006) and season (Florence and McDonnell, 2006, Lewis et al., 2014) can all impact on hoof wall growth. Other influences, such as exercise and stress, (Faramarzi et al., 2009, Bowker, 2003) and genus (Lewis et al., 2014) have been considered with regard to hoof growth but no significant differences were observed between different conditions on the rate of hoof growth.

Only a limited number of studies have uncovered a relationship between capsular deformities and hoof wall growth. For example, it was revealed that there was a decreased proliferation rate of epidermal cells at the coronary hoof capsule in lame horses in comparison with the non laminitic horses (Carter et al., 2011) and others have investigated the proliferation rate at the lamellae (Daradka and Pollitt, 2004), but to date no studies have considered the effect of hoof curvature on growth rate.

To date, the epidermal cell renewal in hoof wall remains poorly explored, particularly with regards to how the basal cells in the dermal papillae proliferate and differentiate to form the cornified tissue of the hoof.

It is known that the germinal cells that rest on the basement membrane of epidermal tissue proliferate to produce daughter cells over the length of the dermal papillae (Dellmann and Eurell, 1998, Eurell and Frappier, 2013). In the coronary region, the length and width of dermal papillae are variable, whereas in

the sole and frog segments, the width and length of the papillae are constant with dimensions similar to the ones measured most distally at the tip of the toe (Bragulla, 2003). As the nutritional supply of these cells relies entirely on the underlying dermal region, the capillary blood vessels near the basement membrane work as a direct line for germinal basal cells to increase proliferation rates (Bragulla and Hirschberg, 2003); each new generation adds to the length of the hoof wall (Pollitt, 1998). In the same way, mitotic cells in the basal layer of the proximal portion of the capsule wall lamellae multiply simultaneously, which might produce a distal movement of primary epidermal lamellae (Bragulla, 2003, Daradka and Pollitt, 2004). The remainder of epidermal lamellae do not show the same proliferation rate, but divide at a rate to sustain the downward growth of the coronary region (Daradka and Pollitt, 2004, Eurell and Frappier, 2013). This is demonstrated by Daradka and Pollitt (2004) who stated that there was a large variance in the rates of proliferating cells between the proximal (7.13%) and middle lamellar areas (0.24%). This might be due to inadequate mitotic germinal cells capability to flow with the capsule (Bragulla, 2003). The rate of proliferation in the coronary region (12.4%) was reportedly much higher (Daradka and Pollitt, 2004).

Recently, investigators have studied the effects of insulin on proliferating cells at the epidermal lamella. Karikoski et al. (2014) showed an increase in numbers of apoptotic and proliferating cells at the middle and abaxial epidermal lamellae with insulin-induced laminitis (Asplin et al., 2010, De Laat et al., 2011b, De Laat et al., 2013a). Others have suggested that excessive stimulation of basal cells of the secondary epidermal lamellae could probably debilitate the interdigitation of the

lamellar suspensory apparatus and as a consequence prompt the onset of laminitis (De Laat et al., 2013a).

A full understanding of how hoof curvature represented by a physical force borne form misshaped hoof which contributes to the growth rate of hooves is therefore lacking. Even if some studies have started to examine the correlation between hoof angle and hoof shape (Dyson et al., 2011a) and the growth rate between laminitic and non-laminitic horses as shown by Carter et al. (2011).

Recent efforts have tried to determine whether the hoof shape is a disposing factor in foot lameness-causing lesions. The comprehension of the pathophysiology and progression of hoof distortions is incomplete, and this limits the efforts to prevent and treat devastating diseases, such as foot lameness and laminitis, successfully. Scientific investigation is proceeding at a phenomenal pace, shedding light on the pathophysiologic events involved in laminitis. Although extensive studies have been carried out on laminitis and biomechanical variations of the equine hoof, no study has been reported on the relationship between hoof shape and growth rate. It is possible that the interconnection between the hoof capsule and the growth rate, with regard to the orientation of the distal phalanx, is key.

This study aims to uncover how histological, gross morphological and physical forces act within and upon the equine hoof to influence hoof shape. These aims will be investigated using a number of methods, including immunostaining (cell proliferation, keratin expression and apoptosis), tissue composition (epithelial thickness), gross morphological differences in whole foot, hoof and/or bone curvatures measurements and angles (micro-CT imaging) and elements of physics techniques to incorporate information gathered from biological techniques. The

figure below suggests a mechanism by which cellular responses can be elicited through biophysical stimulation as investigated in this chapter.

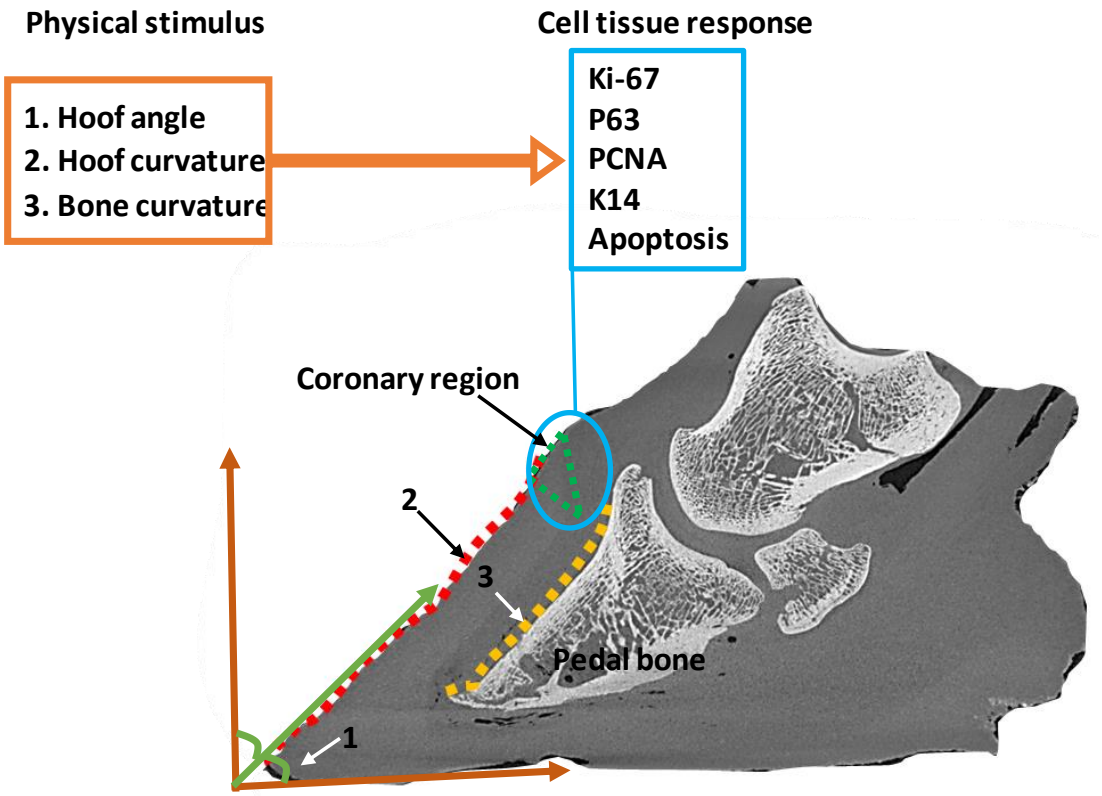


Figure 5-1: Schematic diagram illustrating the physical stimulus on the coronary region

Schematic illustration suggesting a correlation between the degree of the dorsal hoof angle, dorsal hoof curvature and/or dorsal bone curvature with regard to the level of biological response at the level of the coronary hoof region and in particular in dermal papillae.

5.2 Hypothesis

The overarching hypothesis for this chapter was that the physical forces borne from the hoof's contact with the ground increases hoof growth rate via altered proliferation rates and patterns. This was defined and subdivided into mini hypotheses for the different experiments:

1. Hoof deformities are related to increase in cell proliferation from the coronet region, which is dependent on changes in the ground reaction stress or physical forces.
2. Changing the hoof curvature increases hoof synthesis by increasing the percentage of cell proliferation via physical forces.
3. Increased ability of cells to proliferate from the quarters results in distorted hoof shapes with resulting increases in hoof curvature.
4. The distortion patterns of the curvature of distal phalanx that are developed from the interplay between physics and biology, result in changing hoof curvature will increase in hoof synthesis via an increase in the number of proliferative cells.
5. The proportion of keratin production/apoptotic cells at the coronary region will increase by increasing the proliferation cells from the coronet region.
6. Changing the hoof curvature results in increases/decreases in the epithelial thickness in the coronary region affecting the hoof synthesis.

5.3 Aim and objectives

The aim was to determine the specific response that EPK cells increase when faced with a change in physical forces borne from hoof angle, hoof curvature or distal bone curvature, and the ground reaction stress explaining the chronic aspect of hoof deformities. For these objectives, concentrating on the impact of physical forces on the coronary papillae of the equine foot was achieved using different techniques including:

1. Measuring and comparing cell proliferation (Ki-67), stem progenatoir keratinocytes (p63), basal keratin production (K14) and cell apoptosis (TUNEL assay) of the coronary epidermal cells using immunohistochemical and immunofluorescence methods in differing hoof types.
2. Measuring hoof contact angles and hoof and distal phalanx bone curvatures using micro CT-scanning.
3. Measuring and comparing the epithelial thickness on the coronary region and comparing with hoof curvature measurements.

5.4 Results

5.4.1 Evaluation of staining patterns of PCNA proliferating cells

The results from PCNA protein localisation experiments using immunohistochemical staining indicated a markedly higher number of brown positive cells in the epidermal cells of the coronary tissues. The cells that were not in the proliferation stage were observed to have their nuclei stained blue to purple in colour, and considered as non-proliferative cells. The positive cells appeared to be disseminated throughout the basal, suprabasal, and deeper tissue layers of the cross and longitudinal sections of epidermal papillae. A large number of these mitotic indexes were visibly observed close to the basal layer, but diminished in number further away from the basal layers (Figure 5-2A+B). However, a number of cross and longitudinal sections appeared to contain positive cells only in the basal layer and had no positive cells further away from the basal cells (Figure 5-2C). In some areas of tissue, the staining was obscured by melanin pigment, and these areas were therefore not counted (Figure 5-2D). Cells were counted as described in Chapter 2.7.

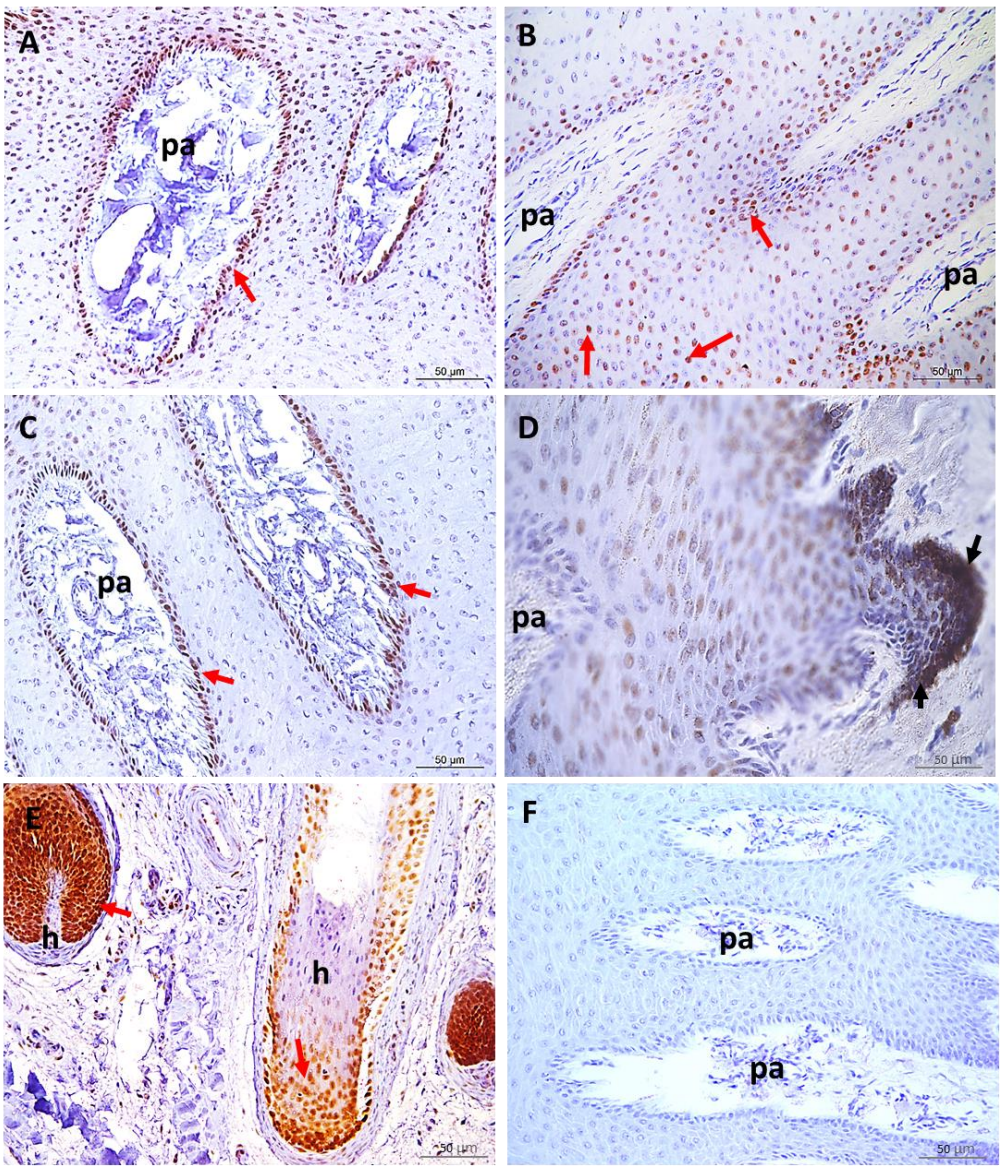


Figure 5-2: Photomicrographs of PCNA stained sections

These images show A) PCNA +ve cells scattered along the germinal layer and in deeper layers in the coronary epithelium (red arrows); B) PCNA positive cells scattered between the tubular horn, while image C) shows that there were no positive cells around the tubular horn, an area that is further away from the dermoepidermal junction. D) Shows melanin pigments obscuring the PCNA positive cells (red arrows). E) Shows in equine skin epithelium (black arrow indicates the proliferating cells at hair follicles). F) Negative control of the coronary region Scale bar represents 50µm.

The results of the average percentage of mitotic cells for each of the hoof sectiosn presented a significant variation in the percentage of mitotic indexes observed between different hoof shapes (Figure 5-3A+B). A variation in the localisation of PCNA was revealed that a normal dorsal hoof curvature had less PCNA positive

cells at the dorsal/quarter regions (Figure 5-3C+E), while a dished (or positively curved) hoof wall had a high percentage of PCNA positive cells on dorsal/quarter region (Figure 5-3D+F). However, the results revealed that there were no significant differences between the hoof angle and percentage of PCNA in the different hoof regions (Figure 5-4).

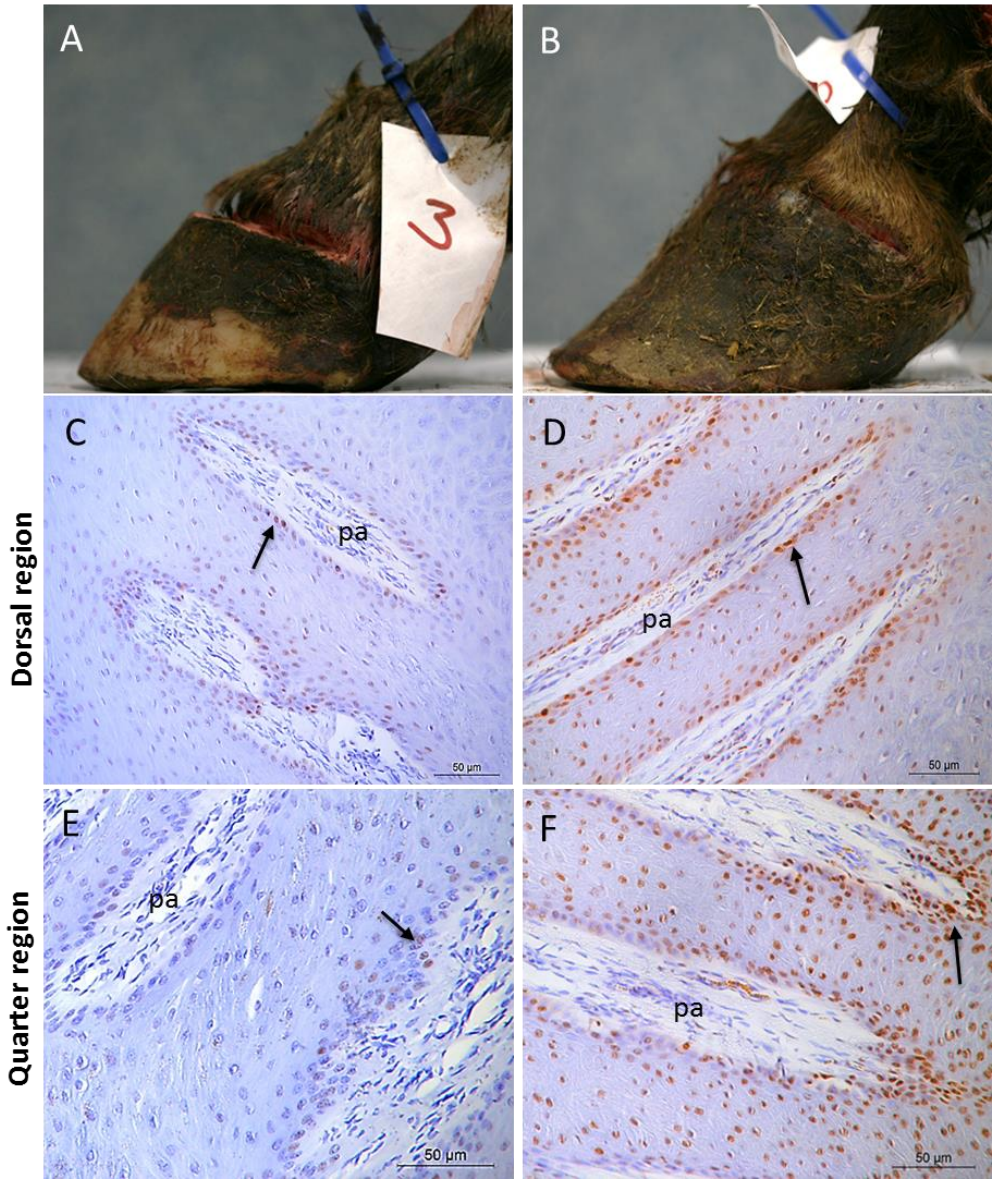


Figure 5-3: Localisation of PCNA +ve cells in coronary epidermis of equine foot

The PCNA stained cells between hooves samples and their hoof capsule shape illustrate a variation across the shape of the dorsal and quarter regions was considered with a percentage of proliferating cells (black arrows). A, B) show the variation in the dorsal shape of the hoof capsule. A variation in the expression of PCNA was also noted at dorsal (C, D) and quarters (E, F) dermal papillae (pa) suggesting that a normal dorsal hoof curvature (A) produce less PCNA positive cells at the dorsal (C) or quarter (E) region than a dished (or positively curved) hoof wall (see B, D/dorsal and F/quarters). Scale bar represents 50µm.

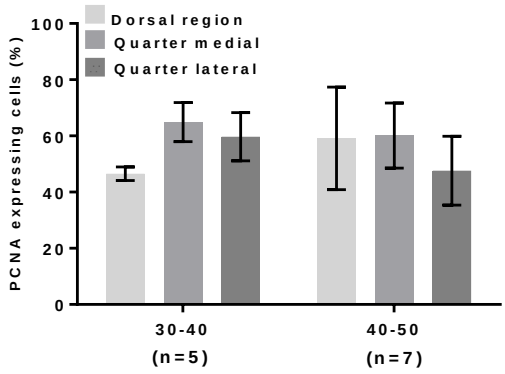


Figure 5-4: The percentage of PCNA in relation to hoof angle

No significant variations were recorded between the contact angle between the hoof and the ground and the percentage of PCNA positive cells in dorsal and quarter regions. Statistical comparisons between groups were analysed using Two Way ANOVA.

5.4.2 Assessment of the expression of Ki-67 proliferation antibody

The results from Ki-67 protein expression experiments using immunohistochemical staining indicated that Ki-67 was mostly expressed in the nuclei of cells in the basal germinal layer of epithelial dermal papillae, but cytoplasmic in the supra basal layer, or further away, of the dermal papillae as well as in both proximal basal or distal end of dermal papillae (Figure 5-5A+B). Similar to the coronary region, the basal cell layer of skin tissues was identified by Ki-67 expression in the nuclei of basal epidermal cells with less intensity further away from the basal layer and this was used as a control tissue to confirm the expression of Ki-67 in the epidermal tissue (Figure 5-5C).

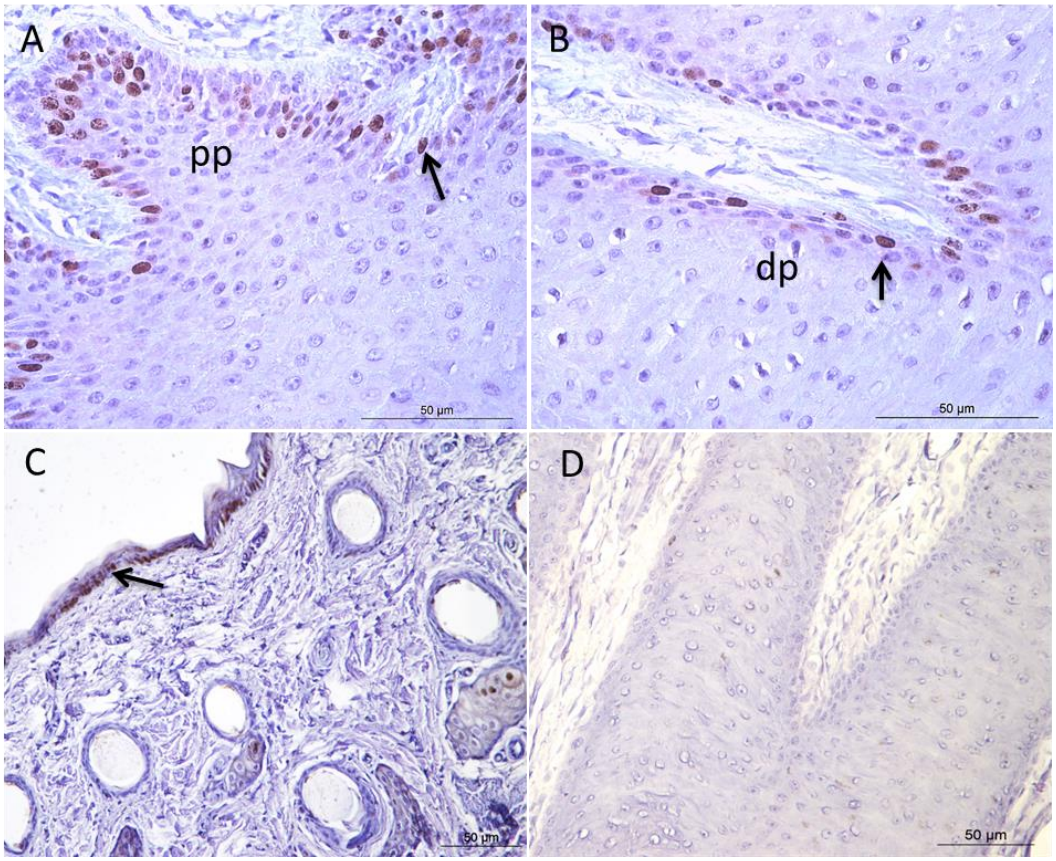


Figure 5-5: Localisation of Ki-67 +ve cells in the epithelium of coronary papillae and skin

Images of Ki-67 +ve cells in the coronary epithelium. A) Close to the basement membrane in proximal papillae (pp); B) around the dermal papillae in the distal papillae (dp); C) in equine skin epithelium (black arrow indicates the proliferating cells at the basal epidermal layer cells); D) negative control of the coronary region. Scale bar represents 50µm.

There were no significant differences between the contact hoof angle and the percentage of Ki-67 +ve cells in different hoof regions, or within group and between groups as defined in Figure 5-6.

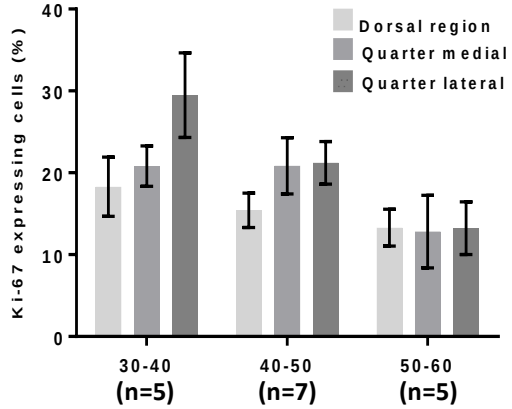


Figure 5-6: The correlation between expression of Ki-67 and hoof angle

Graph showing Ki-67 expression levels as a function of hoof angles. No significant variations were found between the hoof angle and percentage of proliferating cells at the three regions on the coronet: dorsal, quarter medial and quarter lateral regions. Statistical comparisons between groups were analysed using Two Way ANOVA.

A correlation between the dorsal hoof curvatures and the percentage of Ki-67 +ve cells was revealed (Figure 5-7) indicating that there may be a difference in the overall growth rate between the various capsular shapes. Further analysis showed that there was a regional variation in Ki-67 +ve cells along the epidermal dorsal and quarter coronary regions (Figure 5-7A2+B2 and A3+B3). The frequency of Ki-67 positive cells increased at the quarters as a function of the hoof curvature (i.e. for dished hooves) but no variations were noticed at the dorsal regions whatever the dorsal curvatures involved (Figure 5-7A2+B2). At the quarters the percentage of Ki-67 +ve cells in the basal epidermal papillae was 19.97%±3.32% for positively curved hooves (Figure 5-7A3) and 13.73%±3.87% for negatively curved hooves (Figure 5-7B3).

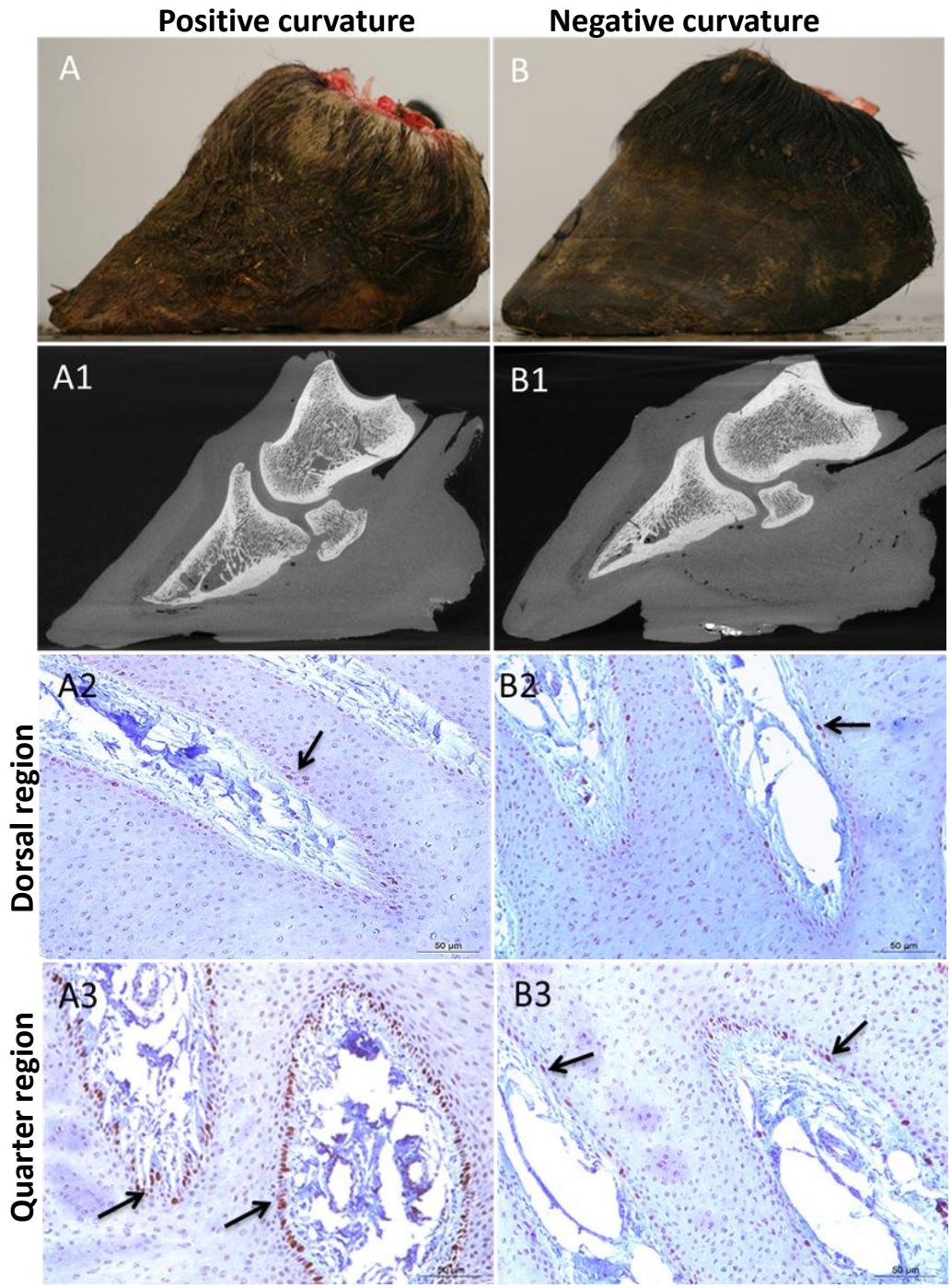


Figure 5-7: Correlation between the expression of Ki-67 and hoof curvature

Images (A, B) show the variation across the shape of the dorsal hoof wall, while A1, B1 illustrate the curvatures considered through micro CT- images (images A, A1 represents the positive hoof curvature, while B, B1 represents the negative hoof curvature). Photomicrographs (A2, A3 and B2, B3) showing the percentage of Ki-67 stained cells between hoof samples in relation to their curvature. A2, B2) Show representative views with no variation in the percentage of proliferating cells in the dorsal regions, whereas this difference appeared obvious in image A3, which showed an increasing expression of Ki-67 in the quarter region for positively curved hooves, in comparison negatively curved hooves with image B3. Scale bar represents 50µm.

It was also found that there was no correlation between Ki-67 positive cells at the dorsal region whatever the hoof curvature involved (Figure 5-8A). However, there was a strong correlation between Ki-67 +ve cells and the dorsal curvature of the hoof at the quarter regions (Figure 5-8B). From the non-linear regression analyses in Figure 5-8B, it is apparent that a clear regression in the percentage of Ki-67 +ve cells against the positive hoof curvature, as when the positive hoof curvature was small the mitotic index was smaller 8.67%, and when the hoof curvature was large the mitotic index was larger 29.29% (Figure 5-8B). These results revealed that lower positive hoof curvature had a lower Ki-67 proliferating cell proportion than larger hoof curvatures.

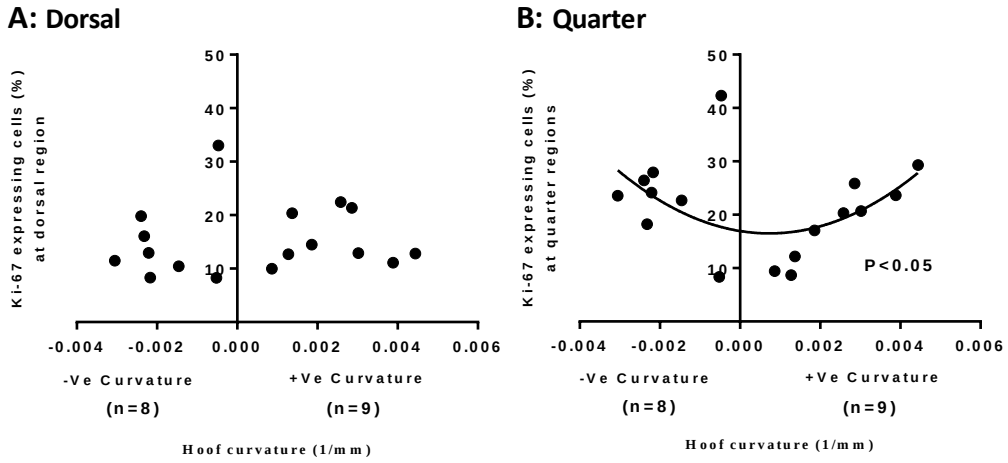


Figure 5-8: Percentage of Ki-67 +ve cells plotted against hoof curvature

A) No significant correlation between either the positive or negative hoof curvatures when compared against a percentage of Ki-67 +ve cells in the dorsal regions, however, (B) shows a significant correlation in quarter region when positive hoof curvatures is present. Statistical analysis was performed using non-linear regression.

Further analysis was carried out investigating the correlation between the dorsal curvatures of distal phalanx and the percentage of Ki-67 +ve cells was found during a comparison of Ki-67 +ve cells with bone curvatures. The results indicated that there may be a variance in the general growth rate between the

different capsular shapes. However, there was not shown any correlation with either positive and/or negative bone curvature (Figure 5-9A+B).

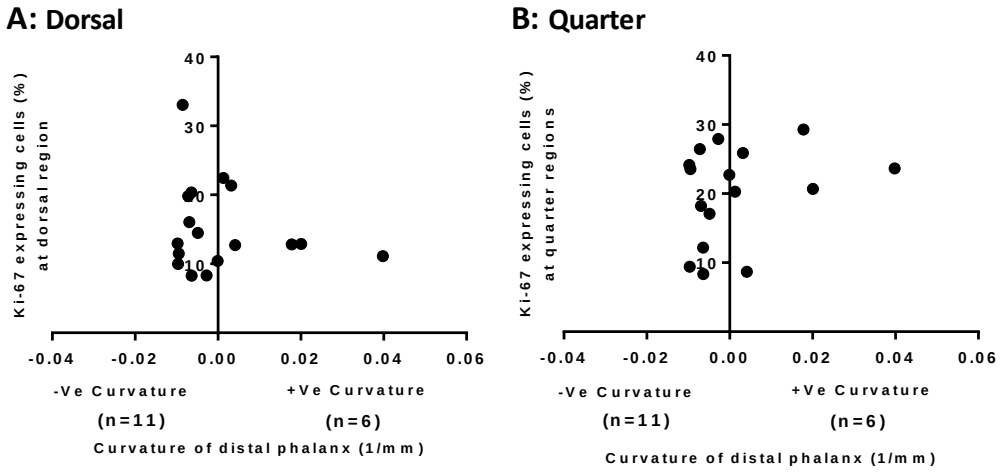


Figure 5-9: Percentage of Ki-67 +ve cells plotted against distal phalanx curvature

A, B) Shows no significant correlation between either positive/negative bone curvatures when compared against a percentage of proliferating cells in the dorsal/quarter regions. Statistical analysis was carried out using GraphPad software.

5.4.3 Assessment the localization of stem progenitor keratinocytes p63

Immunostaining was also carried out to show the levels of stem cells using the stem progenitor marker p63. Expression of p63 was observed in the nuclei of germinal basal and suprabasal cells in the coronary epidermal tissues of the equine hoof. The results of p63 expression levels were higher in the basal and suprabasal layers around the dermal papillae and the percentage of positive cells dropped progressively further away from the basal layers to become undetectable in fully differentiated keratinocytes (Figure 5-10). Statistical analysis showed there were no significant differences found between the contact hoof angle and the different hoof regions (Figure 5-11).

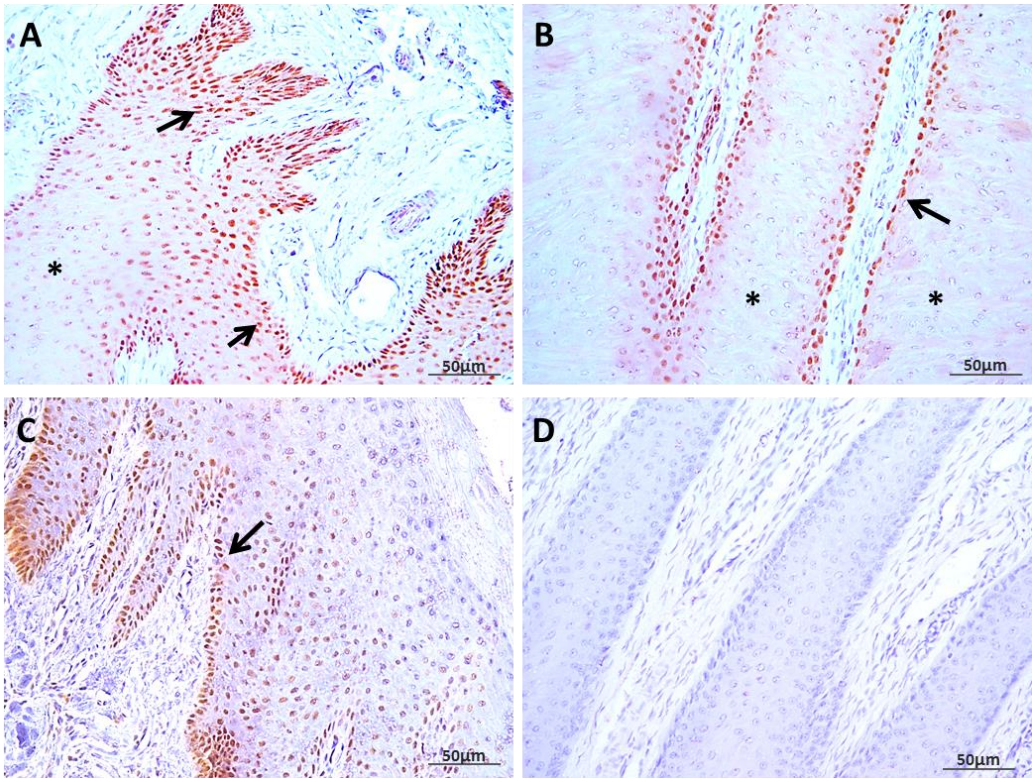


Figure 5-10: Expression of p63 in the epithelium of coronary papillae

Photomicrographs illustrating the frequency of p63 expressed in epidermal cells (in brown) apparent in A and B. A) Represents an image of p63 +ve cells at the proximal part of dermal papillae, the black arrows indicate high p63 +ve cells on the basal and supra-basal layer, while the asterisk indicates undetectable p63 +ve cells further away from the basal cells. B) Photomicrograph of dermal papillae further away from the proximo-basal dermal papillae; C) in equine skin epithelium (black arrow indicates p63 +ve cells at the basal epidermal layer cells); D) negative control of the coronary region. Scale bar represents 50µm.Scale bar represents 50µm.

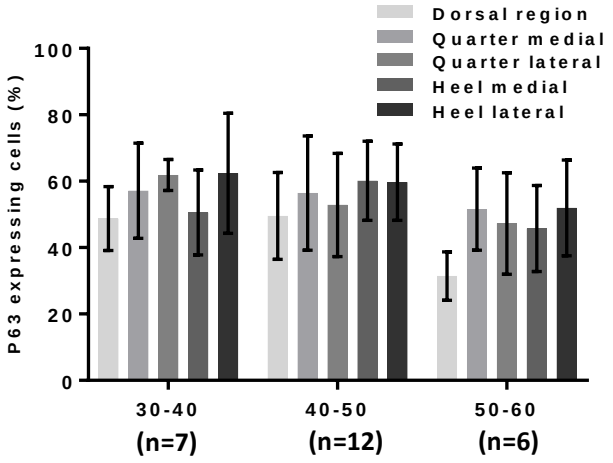


Figure 5-11: The correlation between expression of p63 and hoof angle

Graph showed no significant variation between the contact hoof angle and a percentage of p63 proliferating cells in the dorsal, quarter and heel regions. All comparisons of p63 +ve cells between groups or within groups were not significantly difference. Statistical comparisons between groups were analysed using Two Way ANOVA.

Similar to the relationships observed in the Ki-67 staining, the findings indicated that there was regional variation in p63 +ve cells between different regions across the coronary epidermal tissue in the dorsal, quarter and heel regions (Figure 5-12A2+B2, A3+B3 and A4+B4). The frequency of p63 positive cells in the dorsal region was 38.59%±5.85% in positively curved hooves in comparison with negative hoof curvature 51.44%±7.49% (Figure 5-12A2+B2). Whereas, the frequency of p63 +ve cells was similar between positive and negative curvatures in the quarter and heel regions, 45%±5.38% and 52.74%±3.73% respectively (Figure 5-12A3+B3 and A4+B4).

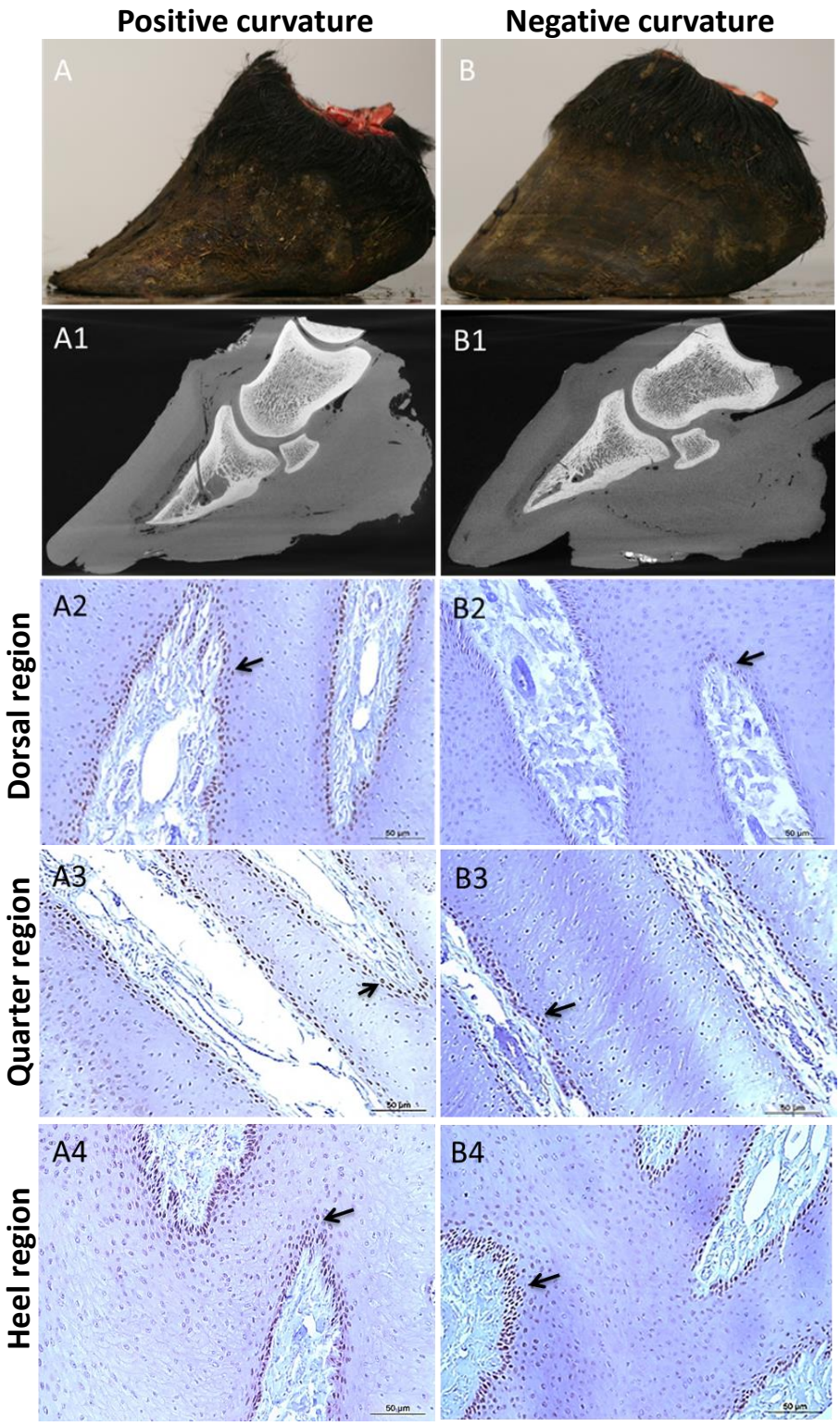


Figure 5-12: Correlation between the expression of p63 and hoof curvature

Images (A, B) show the variation of the shape of the dorsal hoof wall and (A1, B1) illustrate the curvatures considered through micro CT- images (images A, A1 represent the positive hoof curvature, while B, B1 represent the negative hoof curvature). Photomicrographs (A2-A4 and B2-B4) showing p63 +ve cells between hoof samples in relation to their curvature. A2, B2 show representative views showing a variation in the p63 +ve cells in the dorsal region, whereas there was no difference appeared in image A3, B3 in the quarter region and the same in images A4, B4 in the heel regions. Scale bar represents 50µm.

Further statistical tests were carried out using the non-linear regression which examined the average mitotic index of p63 +ve cells in dorsal, quarter and heel regions against the hoof curvature values. Results revealed that there was a significant correlation with positive hoof curvature but did not show a correlation with the negative hoof curvature. The results revealed that in the dorsal region when the hoof curvature was low the mitotic index was smaller at 37.58% and increased dramatically with the degree of curvature to reach the maximum 65.96%. Similar observations were performed at quarter regions (Figure 5-13B) with a minimum 27.31% and a maximum of 66%. In contrast, negative hoof curvatures did not show any correlation between the expression of p63 and the value of the curvature at dorsal regions, while at quarter region it appeared that there were higher expression of p63 as a function of the value of the curvature with a maximum 72.51% and a minimum of 29.75% (Figure 5-13B).

In comparison with the above analysis, the heel regions did not show much correlation with either negative or positive hoof curvatures (Figure 5-14).

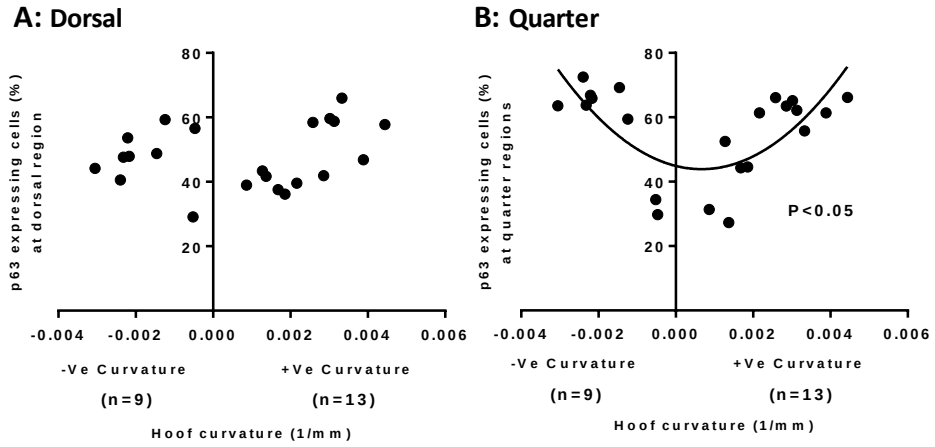


Figure 5-13: Percentage of p63 +ve cells plotted against hoof curvature

A) No significant correlation between either the positive or negative hoof curvatures when compared against a percentage of p63 +ve cells in the dorsal regions, however, (B) shows a significant correlation between in quarter region when positive hoof curvatures is present. Statistical analysis was performed using non-linear regression.

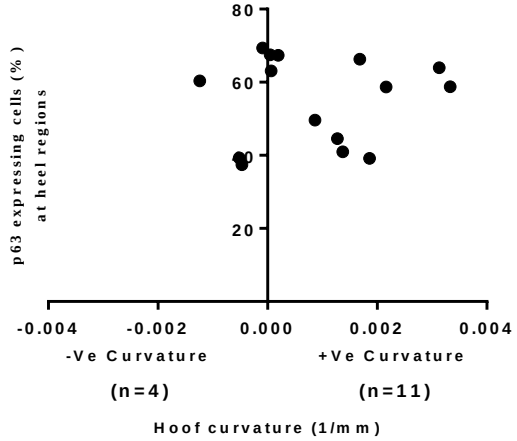


Figure 5-14: Percentage of p63 +ve cells plotted against hoof curvature at heel region

No regression was found between the percentage of p63 expressed and the positive or negative curvatures in the heel regions. Statistical analysis was carried using linear regression GraphPad software.

Further analysis was carried out investigating the correlation between the dorsal bone curvatures of distal phalanx and the percentage of p63 +ve cells. There may be a variance in the general growth rate between the different capsular shapes. The present study did not show a significant correlation between P63 +ve cells with either positive or negative bone curvatures (Figure 5-17A+B).

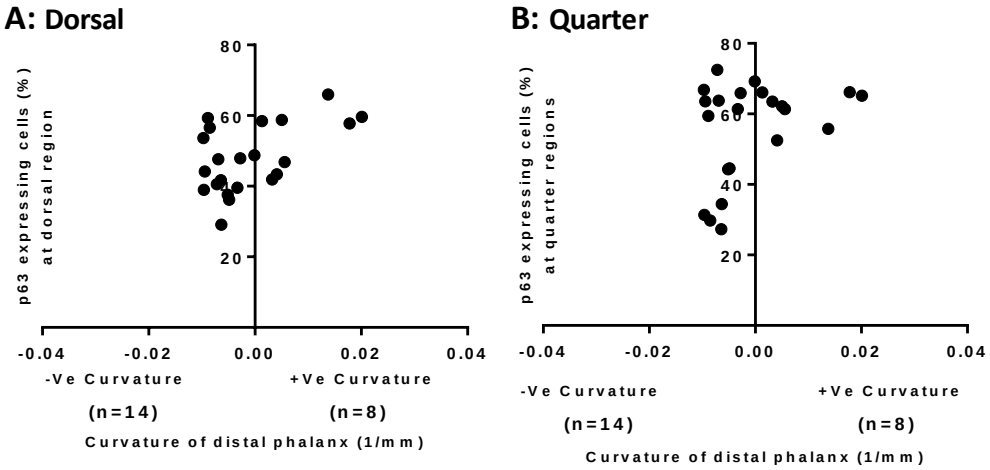


Figure 5-15: Percentage of p63 +ve cells plotted against distal phalanx curvature

A, B,) Show no significant correlation between the positive/negative dorsal distal phalanx curvatures when compared against a percentage of p63 +ve cells in the dorsal region or quarter region. Statistical analysis was carried using GraphPad software.

5.4.4 Variation between the percentage of p63 and Ki-67 +ve cells

Further analysis showed that there was a significant difference between the expression of p63 and Ki-67 in cells (Figure 5-16). This difference in expression levels suggests that the function of these two proteins is, as expected, dissimilar. p63 is expected to be expressed in progenitor keratinocyte stem cells, whereas Ki-67 is involved in the proliferation of cells (Table 5-1).

Table 5-1: Ki-67 and p63 proliferation technique

Antibody	Dorsal region	Quarter medial	Quarter lateral
Ki-67	15.20555±1.55	19.90896±2.43	22±2.26
P63	46.65314±2.06	56.54952±3.91	54.51154±3.80

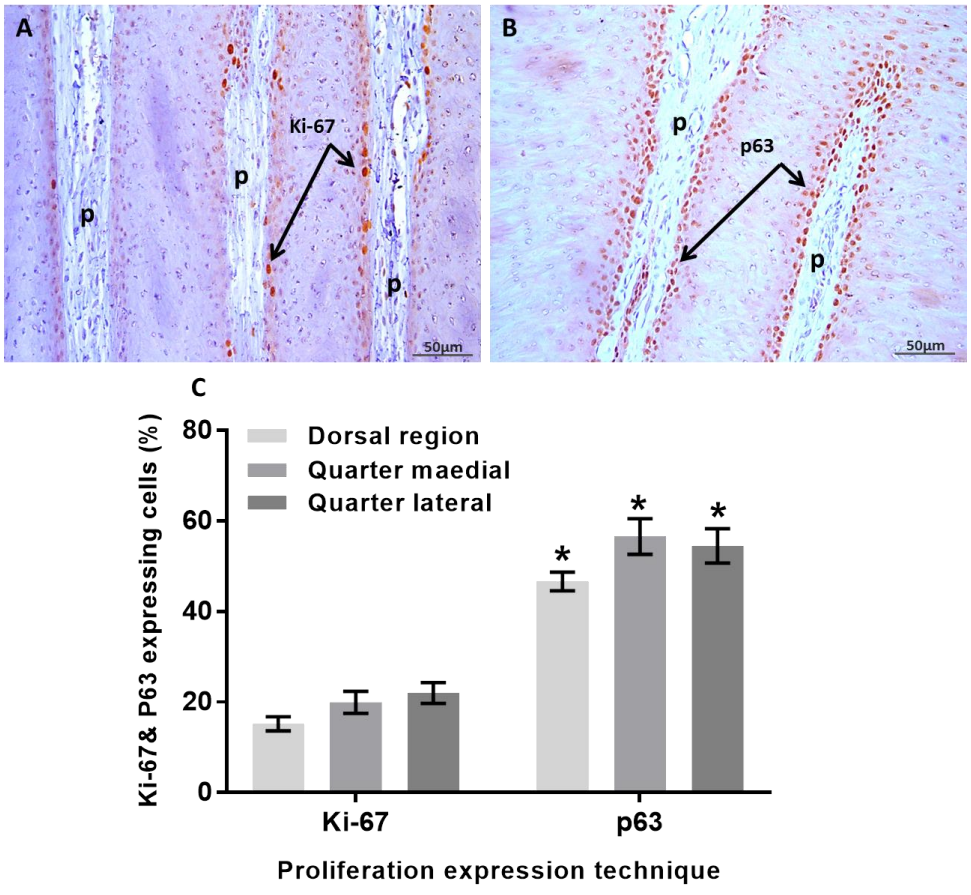


Figure 5-16: Difference between Ki-67 and p63 antibodies

A, B) Shows difference between Ki-67 (A) and p63 (B) +ve cells as indicated by black arrows lining dermal papillae (p). C) Significant variation across an anatomical region (dorsal, quarter medial, quarter lateral) of p63 and Ki67 expression levels. Statistical comparisons between groups were analysed using Two Way ANOVA (* indicates $P<0.05$ vs Ki-67 +ve cells). Scale bar represents 50µm. N= 17 per group.

5.4.5 Expression of K14 and p63 in epithelial coronary papillae

The results showed the overlay between p63 and K14 expression markers in subsets of basal and suprabasal layers with variable staining intensity (Figure 5-17). Particularly, these merged images demonstrated that the stem cell marker p63 expression was accompanied with the basal keratin K14 marker at the basal layer which was undetectable or present at very low levels at the suprabasal layer. Expression of p63 was also apparent along the basal and suprabasal epidermal layer cells, and was undetectable further away from the basement membrane. As a result, there was a clear correlation in the expressions of p63 and K14 in the same region around the dermal papillae (Figure 5-17D+H).

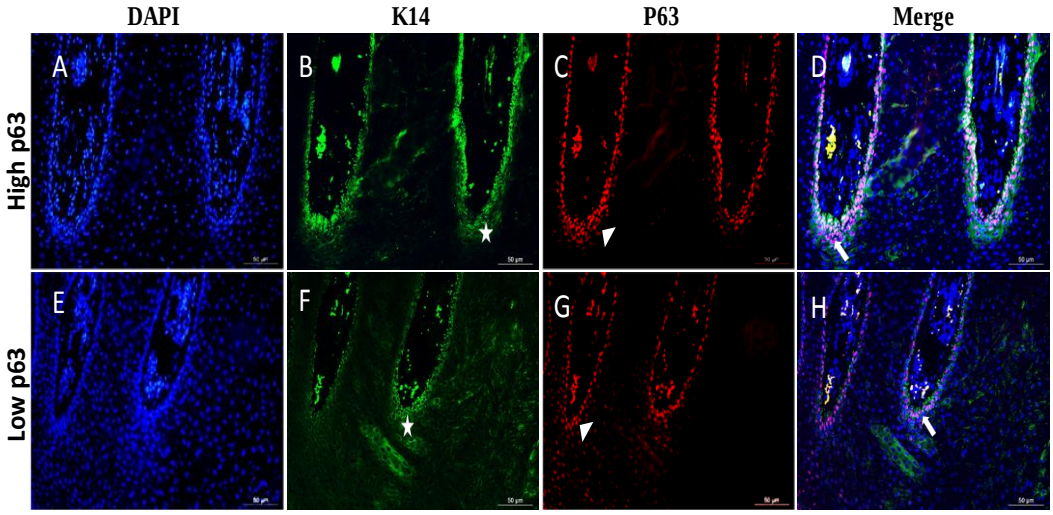


Figure 5-17: Expression of p63 and K14 in equine hoof papillae.

The first and the second rows represented dermal papillae specimens from equine hoof labelled with antibodies against K14 (B, F), p63 (C, G) and DAPI (A, E), whereas (D, H) represented the merged images of P63/K14/DAPI. The first row was carried out from a hoof with a high percentage of p63 +ve cells around papillae; while the second row was performed from a hoof with low percentage of p63 +ve cells around papillae. Scale bar represents 50µm. When merged, the pictures demonstrate a spatial correlation between the expressions of K14 and p63.

The current results indicated that the basal cell marker K14 was expressed in the cytoplasmic compartment of the basal and adjacent suprabasal layers of the epidermal coronary papillae (Figure 5-18). In particular, the expression was much higher in the basal layer compared to the suprabasal layer and almost inexistent distal from this area. Additionally, expression of K14 was detected in the basal and suprabasal layers of equine skin as a control (Figure 5-18I).

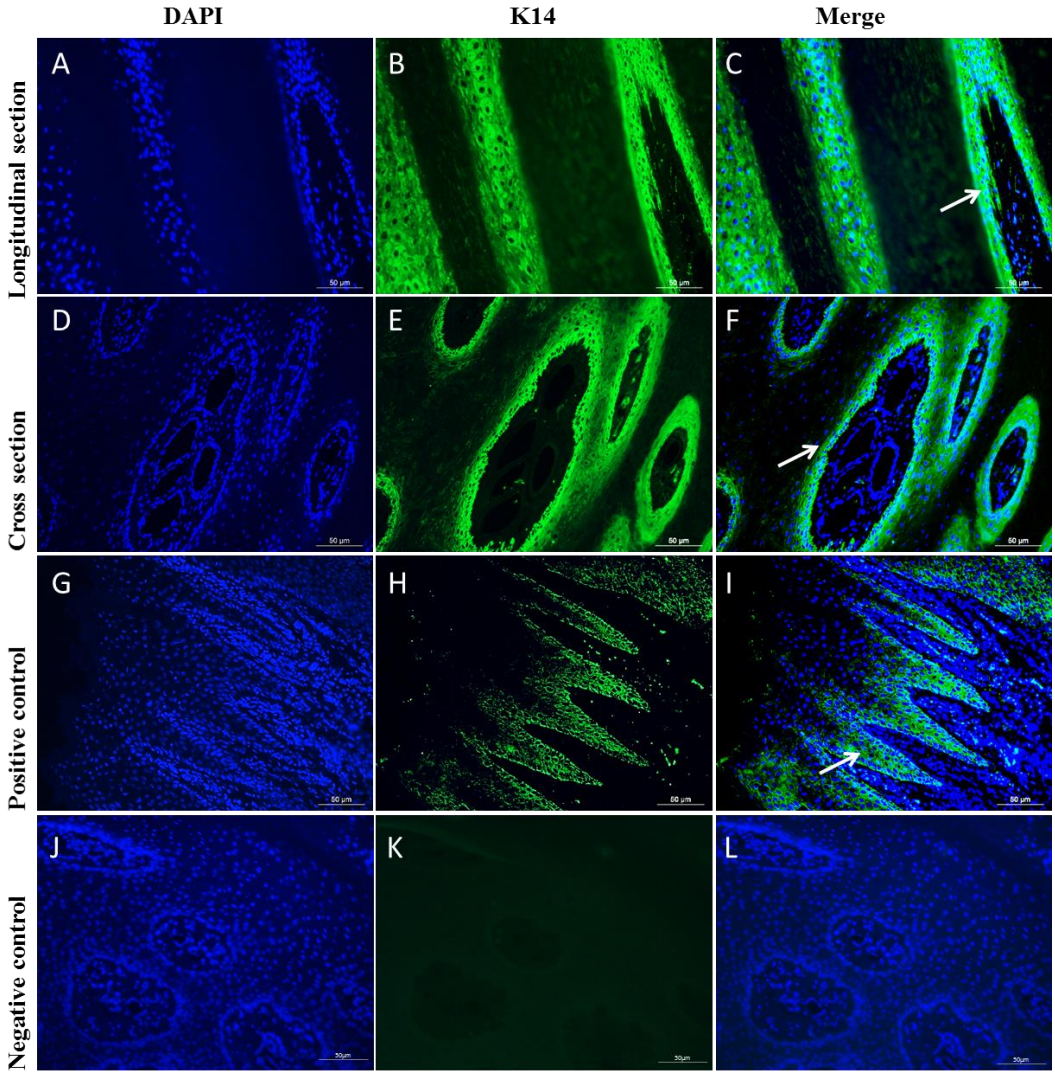


Figure 5-18: Expression of epithelial cell marker K14 in equine hoof papillae

The first (A, B, C) and second (D, E, F) rows represented longitudinal and cross sections respectively of dermal papillae stain with DAPI and K14 antibody. The last row (G, H, I) corresponds to the same labelling, but of a patch of horse skin. (C, F, I) Represented merged images with K14 and DAPI (white arrows indicate the keratin K14 expression in the basal and supra basal layer of the epidermal tissue. (J, K, L) show the negative control for the dermal papillae. Scale bar represents 50µm.

The results indicated that there was a significant correlation between K14 expression levels and the positive hoof curvatures in the quarter region (Figure 5-19). However, no correlations were found with the negative curvature on either dorsal or quarter regions.

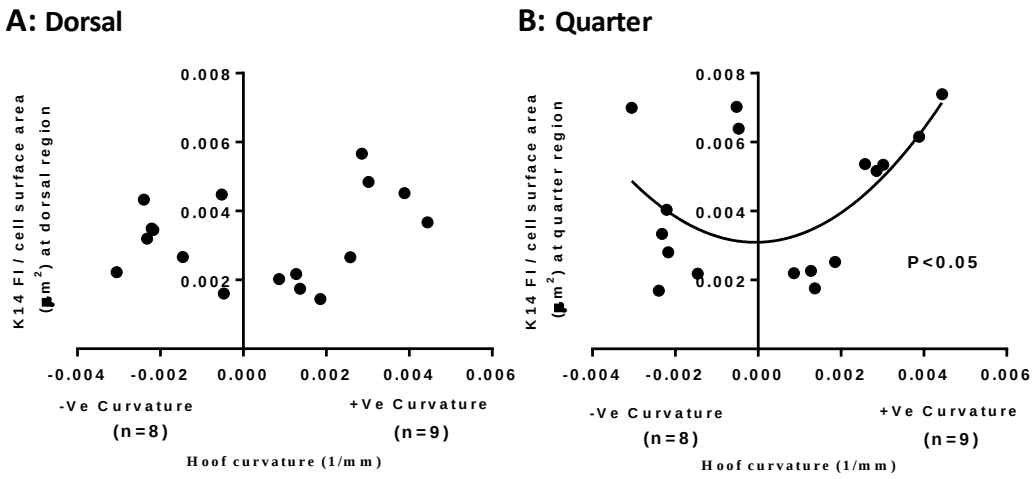


Figure 5-19: Correlation between K14 expression and hoof curvature

A, B) Show the relationship between K14 expression levels and the hoof curvatures. As (A), (B) show, there was a positive correlation between the level of K14 expressed and the value of positive hoof curvature in the quarter region, whereas no correlation were found with the negative curvatures. Statistical analysis was carried out using non-linear regression.

The comparisons between Ki-67 and K14 expression levels and the hoof curvatures did not show any strong regressions on either dorsal/quarter region (Figure 5-20A+B). However, there was a correlation between the ratio of K14 to p63 and hoof curvature at quarter but not dorsal region (Figure 5-21).

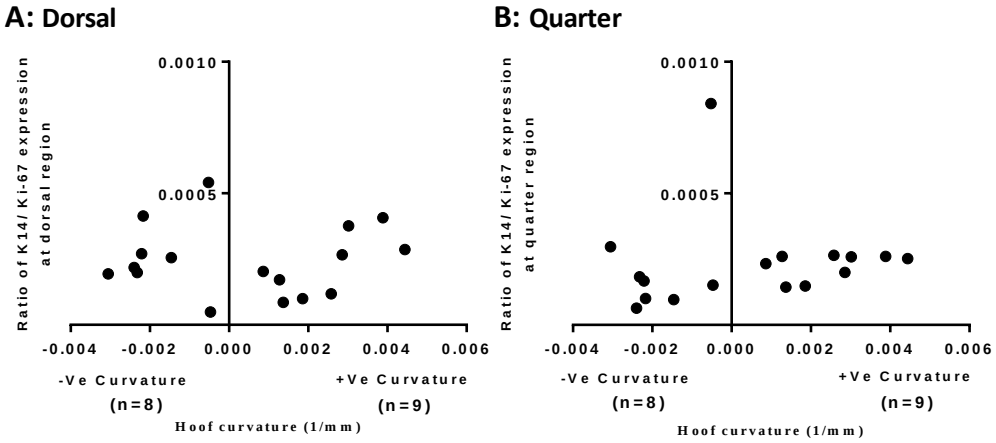


Figure 5-20: The ratio of K14 expression to Ki-67 +ve cells against hoof curvature

A, B) No correlation was found between the K14 expression to Ki-67 +ve and on either the dorsal or the quarter regions. Statistical analysis was carried using GraphPad software.

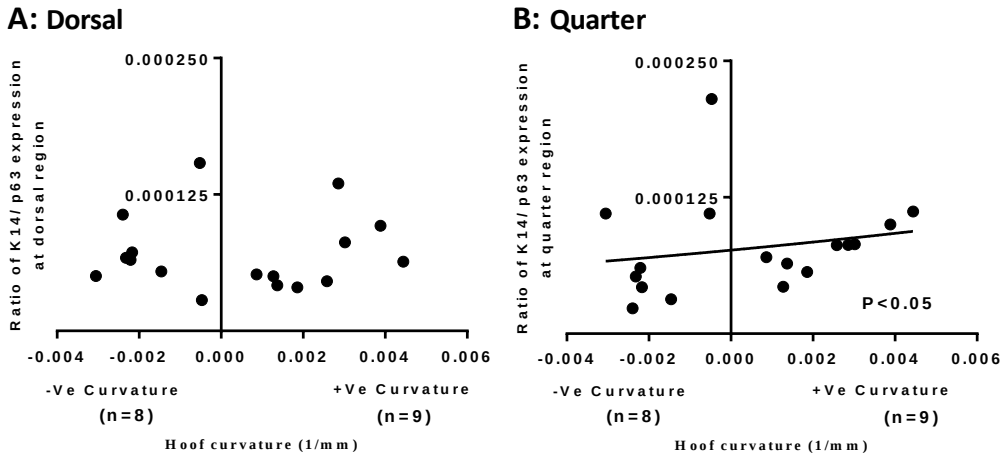


Figure 5-21: The ratio of K14 expression to p63 +ve cells plotted against hoof curvature

A) Shows no significant correlation between K14 expression to p63 and the hoof curvatures. B) A significant correlation was found between K14 expression to p63+ve cells and positive hoof curvature at the quarter region. Statistical analysis was carried using non-linear regression.

5.4.6 Assessment of apoptosis at the dermal coronary region

The results of the average percentage of TUNEL positive cells for each of the hoof sections presented a significant variation as a function of hoof shapes. The results revealed that TUNEL positive cells were present in the basal and suprabasal layer of dermal papillae but at very low numbers (Figure 5-22A+B). Similarly, TUNEL positive cells were found in the equine hair follicles as a control (Figure 5-22C) while the negative control of the same equine coronary tissue did not show the TUNEL positive cells (Figure 5-22D).

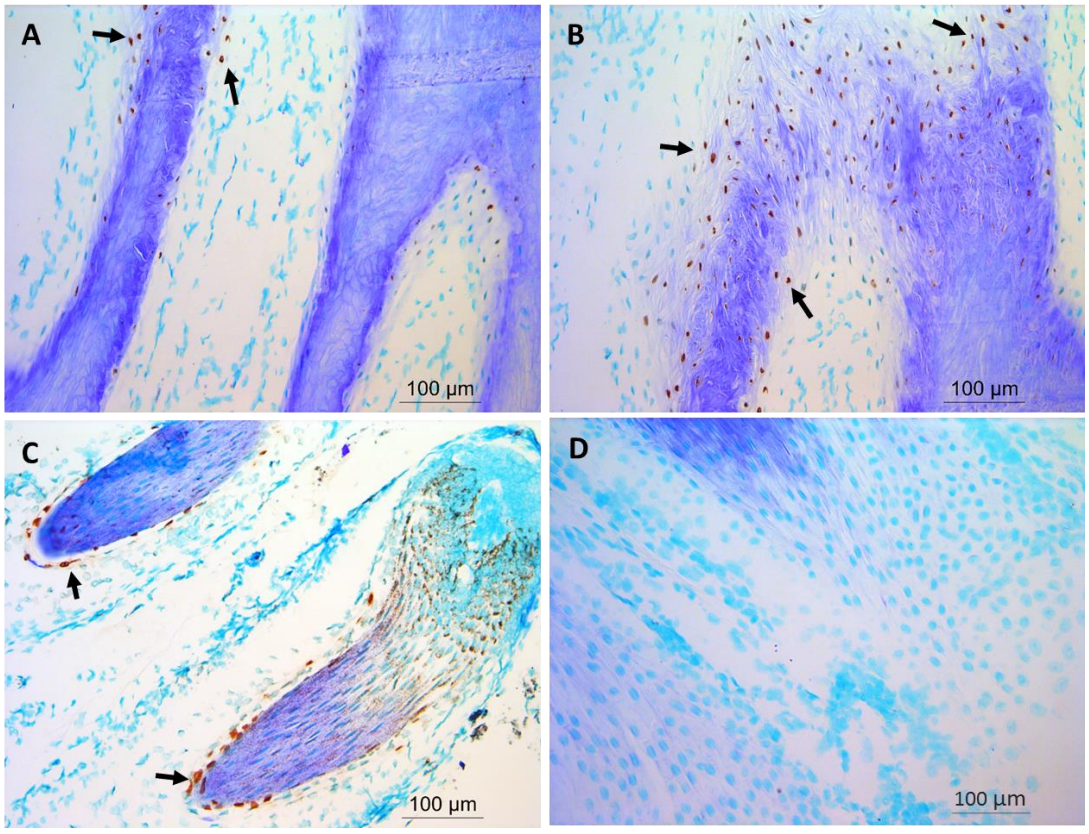


Figure 5-22: Apoptotic TUNEL positive cells

TUNEL positive cells were detected using the DNA fragmentation technique (TUNEL assay). (A, B) TUNEL positive cells in the equine epidermal coronary region. (C) Shows positive controls from hair follicles (black arrows indicate the site of apoptotic cells). D) Negative control equine epidermal coronary region showing no cell staining. Scale bar represents 100µm.

Results revealed a clear regression with positive hoof curvatures but did not show a correlation with the negative hoof curvatures. The results showed that in the quarter region when the positive hoof curvature was small the apoptotic index was high (24.81%) and decreased dramatically with the increasing the degree of hoof curvature to reach to minimum value (2.76%) (Figure 5-23). In contrast, negative hoof curvatures did not show a similar result at either dorsal or quarter regions (Figure 5-23).

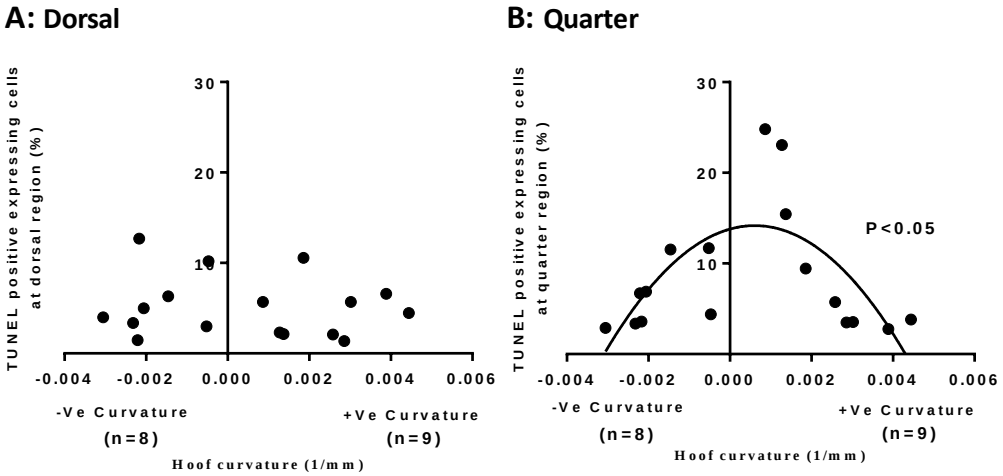


Figure 5-23: Percentage of TUNEL +ve cells plotted against hoof curvature

A) No significant correlation was found at the dorsal curvature. B) Shows, a clear correlation between the TUNEL positive cells and the hoof curvature at quarters. Statistical analysis was carried out using non-linear regression.

Additional analysis was carried out investigating the correlation between the ratio of Ki-67 or p63 to TUNEL positive cells at the dorsal and quarter region. The present study revealed a significant correlation between the ratio of Ki-67 or p63 to TUNEL positive cells with positive curvatures at the quarter regions (Figure 5-24), whereas, no significant correlations with either positive or negative curvature were found at dorsal regions (Figure 5-24).

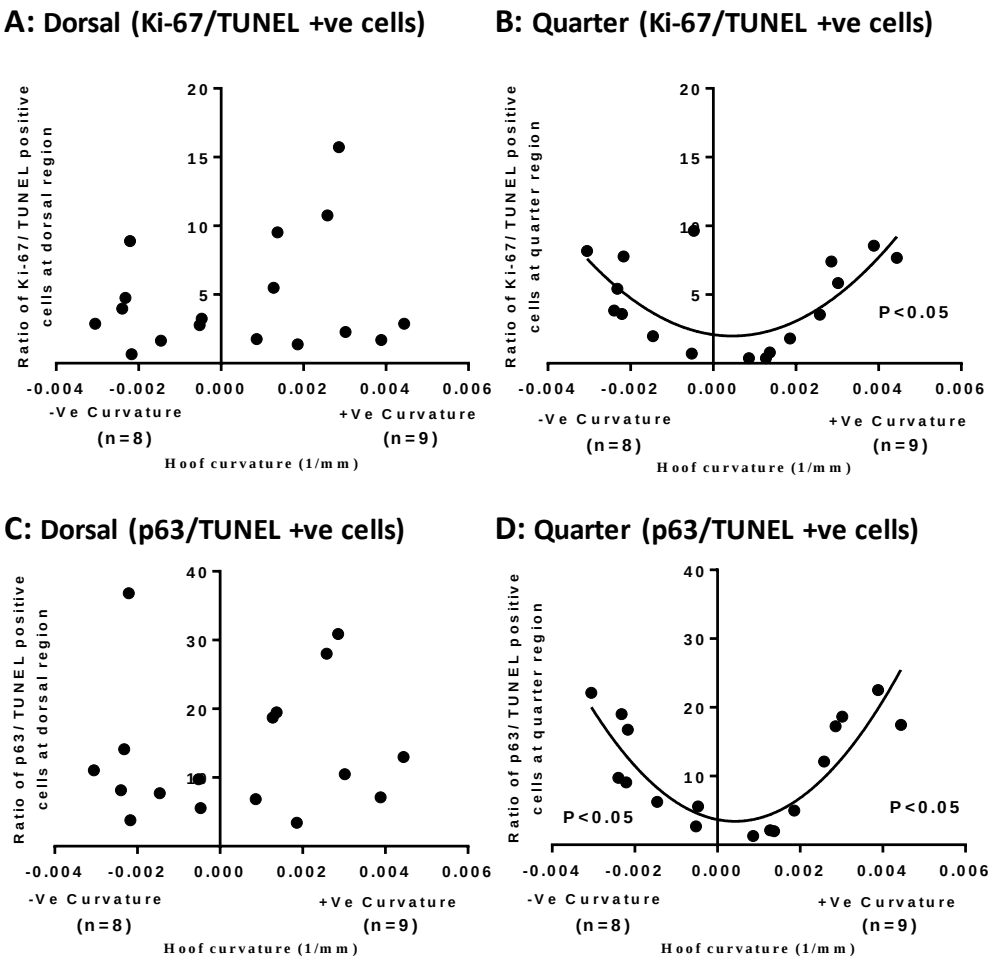


Figure 5-24: The ratio of Ki-67 or p63 to TUNEL +ve cells plotted against hoof curvature

Graphs presenting the ratio of Ki-67 or p63/ TUNEL positive cells and hoof curvature. A, C) Shows no significant correlation between the ratio of Ki-67or p63/ TUNEL with both negative and positive curvature at dorsal regions. (B, D) Represents a significant correlation between the ratio of Ki-67 or p63/ TUNEL and positive curvatures at the quarter regions. Statistical analysis was carried using linear regression.

5.4.7 The influence of the degree of hoof curvature on epithelium thickness

The current study revealed that there was a clear regression with positive hoof curvature at dorsal and more obvious at the quarter regions, whereas no correlations were found with the negative hoof curvatures. The results showed that in the dorsal region when the positive hoof curvature was low the ratio of epithelial thickness was high (0.75mm) and significantly decreased with the curvature value to reach the minimum (0.38mm) (Figure 5-25). Similarly results

were found at quarter regions with a maximal thickness (0.66mm) with low curvature and a minimum one (0.44mm) with high curvature (Figure 5-25B). In contrast, negative hoof curvatures did not show any trend at either dorsal or quarter regions (Figure 5-25).

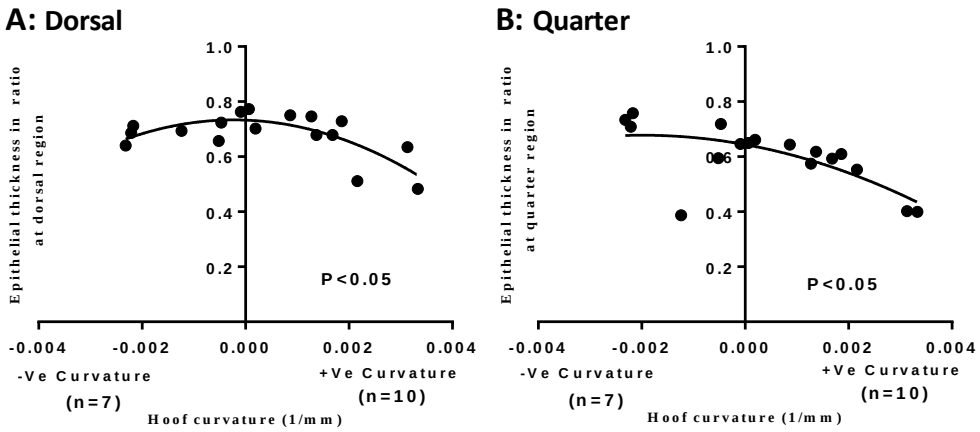


Figure 5-25: The ratio of epithelial thickness plotted against hoof curvature

A, B) Significant correlation between the tissue thickness and the value of hoof curvature in either dorsal or quarter regions for positively curved hooves only Statistical analysis was carried using non-linear regression.

5.5 Discussion

Equine epidermal basal cells play a vital role in epithelial remodelling (Pinto, 2012, Broeckx et al., 2013), and are considered to be active participants in pathological changes of equine laminitis (Leise et al., 2014, Wang et al., 2013). The current findings revealed that there is no correlation between PCNA proliferating cells and hoof curvatures and angles. A potential explanation for that is that PCNA has a long half-life of at least 20hrs, and this could lead to continuous labelling in some cells that are not actually proliferating (Muskhelishvili et al., 2003). In addition, PCNA could label cells even after ending the cell cycle or react to damaged DNA even when the cell is no longer active in the cell division (Bologna-Molina et al., 2013). This protein is essential for DNA repair by removal and replacement of the abnormal DNA and therefore appeared in non-proliferating cells (Liu et al., 2003).

However, p63 expression in equine hoof is a valid marker of stem cells in equine skin, eye, coronet and lamellae (Carter et al., 2011, Linardi et al., 2015) and also in human and mouse skin (Pellegrini et al., 2001, Yu et al., 2014, Senoo et al., 2007). The percentages of p63 +ve cells were calculated in the coronary region of the hoof wall where the hoof grows (Daradka and Pollitt, 2004, Carter et al., 2011). It is a commonly held view that p63 plays a vital role in the regenerative proliferation of epithelial tissues (Koster et al., 2004, Truong et al., 2006, Senoo et al., 2007). In the epidermal regions, p63 works as a key controlling element of cellular propagation and ultimately differentiation (Candi et al., 2008). Nuclear p63 is found in the germinal basal layer cells of the epidermal tissues (Pellegrini et al., 2001), as it is involved in the

proliferative ratio of stem cells in the epithelium (Pellegrini et al., 2001, Senoo et al., 2007).

The Ki-67 marker detects cells in active phases of the cell division and for that reason has been employed in our study as a marker to identify proliferating cells (Scholzen and Gerdes, 2000, Carter et al., 2010a). It was observed in this study that while a high expression of p63 is generally obtained with positive curvature; Ki-67 positive cells in the coronary quarter hoof wall were significantly correlated with hoof curvature, which may be indicative of cell proliferation (Scholzen and Gerdes, 2000, Liu et al., 2003). The role of epidermal stem cells in hoof growth, homeostasis and laminitis has been examined by Carter et al. (2011) who observed that laminitic horses has lower a percentage of proliferating epithelium cells +ve p63 than those of non-lame horses.

However, the present findings suggest that the relatively high p63 +ve cells for hooves which have positive curvature demonstrates the self-renewing of basal stem cells in those areas. In contrast, proliferating cells with high Ki-67 +ve cells were correlated with hoof curvature at quarter regions (Figure 5-8B), whereas there was no relationship between Ki-67 expression levels and the hoof curvature values at the level of dorsal regions (Figure 5-8A). This could be interpreted as the cell indexes of p63 around the dermal papillae constantly provide epidermis to produce quickly increasing capsular wall, whereas Ki-67 proliferating cells in the same region around dermal papillae express the active cell that shares in the repairs of tissue homeostasis as it is worked in skin (Blanpain and Fuchs, 2009, Carter et al., 2011). Furthermore, p63 is considered to be the initiator for the skin stratification pathway and for

sustaining the potential epidermal differentiation and absence of p63 could lead to a decrease in the population of the differentiated cells (Koster and Roop, 2007). This has also been confirmed in the equine hoof by Carter et al. (2011) who observed a decrease in p63 expression levels in laminitic horses in comparison to the non-laminitic horses.

Recently, in vitro studies of equine skin, eye and hooves have shown constant expression of p63 in the first two layers of all epithelial tissues (Linardi et al., 2015). This suggests that p63 performs a double pivotal role: one is through starting the developmental epithelial stratification and the second is by sustaining growth possibilities of germinal basal layers into mature epidermal tissues (Koster et al., 2004). From this, it seems that p63 is vital for both the proliferation and differentiation of developmental keratinocytes (Truong et al., 2006).

Remarkably, a recent study indicates that the expression levels of p63 appears to increase through differentiation of keratinocyte and participates to form outer epidermal layers (Kouwenhoven et al., 2015). A number of researchers have validated that K14 is a specific marker for labelling the cytoplasmic compartment of the basal cells of stratified epithelium in equine epithelium (Bragulla and Homberger, 2009, Carter et al., 2011, Linardi et al., 2015). Even though most of the cells in the basal layers are positive for the K14, there are a number of cells which are not basal stem cells (Linardi et al., 2015). In the current study the restricted expression of K14 in the basal layer or the adjacent suprabasal layer of the epidermal cells, Figure 5-22, might reflect the unique differentiation aspect of basal cells to form cornified tissue within the tubular horn of dermal papillae. These findings highlighted the relationship between

p63 and K14 (Figure 5-23) suggesting that p63 and keratin K14 are complementary markers as shown previously in Figure 5-23. The negative hoof curvature did not show any correlation between the expression of K14 and p63 markers within either the dorsal or the quarter regions. It can thus be suggested that the correlation between p63 and K14 could provide a signal for hoof wall regeneration, and differentiation of keratinocytes, which might contribute to the pathogenesis of the equine hoof.

5.5.1 Conclusion

In conclusion, the immunostaining and labelling of p63 or Ki-67 proliferating cells, in addition to K14 and TUNEL apoptotic cells localized along the dermal papillae in the coronary hoof region correlated with the hoof curvature when positive. These outcomes suggest that the two proteins (p63 and Ki-67) participate in hoof growth, and very probably to the differential growth of the hoof capsule as observed in chronic laminitis. This is probably through contribution towards a sustained level of epidermal basal cells. Even though more analysis is required over a varied range of the capsular wall deformities and their causes, these findings suggest that changing the hoof curvature can influence of hoof synthesis probably by changing the amount of proliferative cells via a feedback mechanism involving physical forces.

Chapter 6
General Discussion

6.1 General discussion

Equine foot diseases, in particular foot lameness and laminitis, remain worldwide issues (Pollitt, 2004b, Heymering, 2010, Belknap and Geor, 2017). To date, the mechanisms behind overgrowth and/or distortion of hoof capsule in response to mechanical stress have been poorly understood, as well as its potential involvement in equine laminitis. The main goal of this study was to provide novel evidence on the role of progenitor keratinocytes lining the dermal papillae in hoof pathology, in particular their responses to biophysical stimuli. These cellular responses were examined via evaluating the growth rate at the coronet. The biophysical data from this has provided unique insights into equine hoof growth, expands, and improves our knowledge as to how hoof grows.

The findings reported in Chapter 3 largely complement those of earlier studies (Leach, 1980, Bragulla, 2003, Daradka and Pollitt, 2004). However, this study has raised vital questions about the natural distribution of basal progenitor keratinocytes, as a high percentage of these cells were positively labelled with the stem cell marker p63 on the proximal basal dermal papillae and not the middle or basal dermal papillae, as shown by Senoo et al. (2007), on epithelial stratification. These findings suggest that progenitor keratinocytes at the coronet are exposed to different types of biomechanical/ biophysical stimuli, resulting in the expression of stem cell markers. These stimuli have been found to increase cell proliferation (Yano et al., 2004), cell orientation, differentiation (Saha et al., 2006, Gu et al., 2017), migration, apoptosis and/or hypertrophy of the epithelium (Tokuyama et al., 2015). Hence, the importance of tissue homeostasis is essential for self-renewal and initiation of new epidermal tissue via cell differentiation, and this

process is maintained due to the presence of progenitor keratinocytes that have the capability for continuing homeostatic regulation (Blanpain and Fuchs, 2009). It is well known that basal cells at the coronary region are the main constituent progenitors of the hoof wall (Daradka and Pollitt, 2004, Eurell and Frappier, 2013). This continuity in hoof growth is important in order to regenerate hoof wear at the ground border (Parks, 2003). Many studies have attempted to determine the requirements for the proliferation of the hoof epidermis, as it is one of the challenges in understanding the role of hoof growth in equine laminitis. Daradka and Pollitt (2004) demonstrated using bromohydroxiuridine (BrdU) that the coronet and proximal lamellae are the main sites of proliferation in the capsular wall. These results corroborate those reported by Castro (2015) who found a high proliferation index using 5-ethynil-2-deoxyuridine (EdU) in epidermal cells at the coronet (23.97±1.50%), with a lower proliferation indexes at the proximal (4.01±0.54%); middle (0.16 ±0.02%); distal lamellae (0.07 ±0.01%). Additionally, labelling with p63 showed a decrease in expression in laminitic horses in comparison to non-laminitic horses (Carter et al., 2011). Furthermore, De Laat et al. (2013b) revealed that the physio-pathological influence of insulin on horses induces laminitis via increasing cell proliferation, identified by the labelling of nuclear protein TPX2. However, in the epidermal hoof wall proliferation studies the dermal papillae were not fully investigated. In addition, our understanding of how the growth mechanism contributes to capsular wall deformity is inadequate. The findings reported here provide additional insights into cell behaviour at the coronet. This work centred around using a cell models to investigate the stimuli leading to the proliferation efficacy on the BM and along the papillae and within the interpapillary space as a function of the

distance from the basal layer of the coronary epidermis. The results from this study found that high percentages of proliferation index measured by the cell proliferation markers Ki-67 and p63 were observed at the proximal part of papillae compared to a low proliferation index at the distal end of papillae. These results are essential for comparing the growth rate between hooves. These findings also have important implications for understanding the potentiality of physical forces acting at the basal epidermal papillae that, as a consequence, might have an influence on the basal progenitor keratinocytes via cell proliferation. This agrees with the assumption that variations in cell proliferation may be affected by the impact of biomechanical stress and that may occur in acute laminitis (Collins et al., 2010).

A practical implication of these findings relate to hoof diseases, as these may help to define which parts may be causally involved in the weaknesses of the capsular wall.

The first step in cell differentiation starts when moving at the transition form (spinous form) migrating from basal to suprabasal cells (Blanpain and Fuchs, 2009). This is manifested by proliferation inhibition mediated by genes encoding K5 and 14, and K1 and 10 (Bragulla and Homberger, 2009). Expression of keratin increases cell stiffness against the mechanical forces at the external surface of the skin (Blanpain and Fuchs, 2009). The cells that line the dermal papillae and rest on the basement membrane constituent the mature hoof wall tissue (Leach, 1980, Bragulla and Hirschberg, 2003, Pollitt, 2004a). The method which maintains a constant number of basal epidermal cells in the coronet participating in renewing hoof tissue (Pollitt, 1998, Daradka and Pollitt, 2004). These are delivered through a physiological process called tissue homeostasis involving progenitor stem cells

possessing the capability for self-renewing and to differentiate into different cell lineages when specifically stimulated (Blanpain and Fuchs, 2009). This continuous proliferation of the basal epidermal cells, their differentiation and cornification correspond to that of most structural hard keratin, for instance hair, nail, wool, quills, hooves, horns and claws (Lynch et al., 1986, Marshall et al., 1991, Rouse and Van Dyke, 2010).

In the model presented in this study, TUNEL positive apoptotic cells were assessed. TUNEL positive cells were present at the transition which demarcates the stratum spinosium to the stratum corneum and were not shown further away/beyond the stratum spinosium. Results have revealed the structural importance of cell apoptosis along the dermal papillae as only few studies have investigated apoptosis in the hoof wall formation. In fact most were focused on the lamellae, demonstrating an increasing number of apoptotic cells in laminitic horse observed at the interconnection between the secondary and primary lamellae. This suggests that apoptosis might promote the structural failure of the hoof wall attachment (Faleiros et al., 2004).

Our study also showed a high nuclear expression of Ki-67 and p63 in cells in the proximal part of the papillae at the attachment between the dermal to epidermal tissues, whereas no apoptotic cells were present in this same region. In contrast, at the level where transition occurs between the stratum spinosium and the stratum corneum an obvious labelling was shown for the TUNEL positive cells without any proliferation markers being observed in cells. It can be hypothesized that the apoptosis and the cornification occurs to counterbalance the gravity and adhesion stresses allowing the hoof to grow. Nevertheless, the reason why cells do not die before the transition may partly be explained by the expression of p63 marker

inhibiting DNA damage (Alenzi, 2004, Li et al., 2012). P63 is also essential in controlling the proliferation and differentiation in epidermal keratinocytes (Romano et al., 2012, Botchkarev and Flores, 2014), in cell metabolism (Candi et al., 2017) and also participates in protecting keratinocytes from oxidative stress initiating apoptosis (Latina et al., 2016). Additionally, p63 contributes to gene regulation in particular adhesion molecules, cytokeratin, chromatin remodelling elements (Satb1, Brg1) and polycomb proteins/components of nuclear envelop (Rapisarda, 2015). In the skin, the transition layer is the main site of apoptosis in epidermal keratinocytes (Raj et al., 2006) generating a balance between apoptosis and proliferation that maintains the epidermal thickness (Raj et al., 2006). In the skin formation the first step of apoptosis is initiated via damage to mitochondria (Martinvalet et al., 2005). Three pathways, i.e. external, internal and granzyme participate in cell death, starting via the cleavage of caspase-3 and, as a consequence, leading to DNA fragmentation, degradation of cytoskeleton network and nuclear proteins, proteins cross-link and finally the generation apoptotic bodies (Martinvalet et al., 2005, Elmore, 2007). This thesis could help with understanding the clinical implications of new apoptosis based therapeutics and their impact on hoof growth (Faleiros et al., 2004).

In this thesis, a cellular model was achieved in Chapter 4 by the purification of a subculture of equine progenitor keratinocytes (EPKs) isolated from the dermal papillae at the coronet region. This allowed us to address the influence of biophysical or biological stimulations on cell proliferation and differentiation that may occur naturally. Knowledge of EPKs behaviour *in vitro* provides a distinctive method to examine hoof pathologies related to keratinocytes (Pollitt, 2004b, Belknap and Geor, 2017) without employing live horses (French and Pollitt,

2004c, Eps and Pollitt, 2006, Hurley et al., 2006, De Laat et al., 2010). Some studies have attributed biomechanical causes / uneven loading for the lamellae detachment and the onset of foot diseases (Thomason, 1998, Johnston and Back, 2006, Merritt et al., 2016). However, although a number of studies have examined the keratinocytes from the skin of horses (Dahm et al., 2002, Broeckx et al., 2013, Sharma et al., 2016) or hoof lamellae (Visser and Pollitt, 2010, Pinto, 2012), none considered EPKs from dermal papillae and whether those cells could have implications in the distortion of the capsule. Furthermore, the role of chemical, physical and biological stresses in keratinocytes has not been entirely characterised. This thesis demonstrates that EPKs can be efficiently isolated, purified and cultured growing initially as spheres and forming colonies of cobblestone-shaped cells +ve stem cell markers such as CD44 and K14. K14 confirmed the purity of EPKs, as observed in in human skin (Porter et al., 2000, Lloyd et al., 1995) or human nail (De Berker et al., 2000). These findings were consistent with other studies showing that equine keratinocytes isolated from hoof lamellae and/or skin have an typical cobblestone morphology producing different keratin filaments (Visser and Pollitt, 2010, Broeckx et al., 2013, Borena et al., 2014, Sharma et al., 2016). In the hoof lamellae, for instance Carter et al. (2010b) identified K124, K42 in addition to K14 and K5 at the basal and suprabasal layers.

Additionally the role of stress microfilaments F-actin in EPKs were investigated via the inhibition of non-muscle myosin (NMII) using blebbistatin causing the disassembling of stress microfilaments (Kovács et al., 2004, Shutova et al., 2012). The consequence of the treatment with blebbistatin was a clear modification and retraction of microfilaments F-actin and commitment to final differentiation. Zhang and Rao (2005) demonstrated in primary cultures of porcine eyes that

treatment with 10–200µM blebbistatin caused amendments in cellular morphology, reduced F-actin microfilament formation, decreased the level of focal adhesion and blocked differentiation (Straight et al., 2003). The action of blebbistatin on inhibiting F-actin filaments is also involved in cell migration and seemed not to be cytotoxic (Engler et al., 2006, Arora et al., 2015). F-actin is well known to be a critical regulator of vascular disease, tumour formation, and controls stem cell pluripotency and differentiation (Newell-Litwa et al., 2015). In this study, F-actin filament organization was labelled clearly at lamellipodia and stress fibres, while cells treated using blebbistatin did not show any clear staining patterns. Treatment with 100µM blebbistatin over two days causes cell enormous detachment (Shutova et al., 2012) which is in agreement with our current findings. However, no information was found on how the inhibition of actin filaments influences EPKs behaviour. The current investigation revealed that continuous incubation of EPK culture with blebbistatin reduced the proliferation potency of cells and increased the commitment of cells to terminal differentiation. The role of blebbistatin in the decreasing proliferation is in agreement with recent studies (Huang et al., 2011, Mih et al., 2012, Hirata et al., 2017). Decrease in cellular proliferation is critical for epithelial haemostasis as keratinocytes have a unique actomycin motor system that once inhibited has a consequence on cellular division in confluent keratinocytes as shown by Hirata et al. (2017). The main role of microfilaments F-actin or NMMII is in the cell adhesion/migration and tissue structure and its mutations cause monogenic disorder (Vicente-Manzanares et al., 2009). However and similar to the current results, Swailes et al. (2006) showed that the blocking NMMII in mouse myoblasts leads to an increase in their length of about 200% at day 2 in comparison to control cells. Similarly, Sarkar et al.

(2009) found that treatment with 30µM blebbistatin using human keratinocytes increased cell migration and altered cell morphology. These results are coherent with the fact that epithelial cell migration is involved in in wound healing, where their responses are controlled by the actomyosin systems (Sarkar et al., 2009) and that it can reverses epidermal thickening (Samuel et al., 2011). From this study, we can conclude that F-actin has an important role in cell commitment to differentiation and proliferation.

Other important findings were the impact of hydrostatic pressure (HP), stretch, oxygen levels and insulin incubation that may be involved in foot disease involving keratinocytes. HP applications represent a process of applying physical forces that mimic the compressive strength that could be generated by inflammation or mechanical loading on the basement membrane that may assist the initiation of equine laminitis (Moore et al., 2004). Studies have demonstrated that HP induces cellular division in a RhoA- and/or Rac1-dependent manner (Zhao et al., 2015) or differentiation in bone marrow mesenchymal stem cells (Liu et al., 2009). The current findings show that HP application on cultured keratinocytes with values 495 Pa and 990 Pa at days 3 and 5 promoted the expression of Ki-67, formed multinucleate cells and increased the expression of K14 and K10 at day 5. These observations in the cytokeratin expression suggested that cytoskeleton filaments may play a role in the mechanism of cell response to physical forces (Knight et al., 2006, Paluch et al., 2015). Therefore, the importance of HP application suggests that it might be used as an active method for encouraging the cellular activity of keratinocytes, and that Ki-67 and cytoskeletal keratin could be expressed to dynamically regulate the compressive strength response of keratinocytes.

It has already been reported that cells respond/react to different variety of physical forces such as compression, shear, tension, osmosis and/or gravity in their environment (Agha et al., 2011, Barnes et al., 2017). In this thesis, a significant result was found by applying a stretch on cultured keratinocytes as this imitates the stress borne from cells changing their size and applying a tension on the papillae. The results from applying stretch on EPKs incubated with 20µM blebbistatin mimicked response to tensile strength when their contractile system blocked. The obvious effect of applying cell stretch was the increase in K14 and K10 with little to no expression of nuclear protein Ki-67. By comparing the latter results to those following the treatment of EPKs with blebbistatin but without stretch and EPKs one found a clear impact of stretch on cytokeratin expression at day 3 while no response were observed in non-stretched cells. Based on these observations, it may be hypothesised that cell stretching is involved in controlling cell volume expanding EPKs, and this is translated by an increased amount of keratins expressed in cell. Furthermore, it was shown that stretching cells without blebbistatin lead to very strong expression patterns of K14 and K10 suggesting that while the increase in cell volume upon stretching can lead to keratin expression, maintaining intact F-actin elicits a much stronger response suggesting that stress filaments are involved in cytokeratin expression. This is aligned with keratin overexpression in cancer cells when they are stretched (Russell et al., 2004). However, the impacts of stretch were more visible just after EPKs isolation, culturing them too long in culture removed the cells ability to respond to stretch. While many stretch studies have been conducted on human/murine skin keratinocytes (Yano et al., 2004, Reichelt, 2007, Tokuyama et al., 2015, Bonakdar et al., 2015) non have performed on EPKs. Furthermore, it was confirmed that

stretching cells led to a modified patterns of F-actin filaments similar to what has been observed in human keratinocytes (Russell et al., 2004). This could support the idea that keratinocytes or cells in general are sensitive to physical/mechanical forces signals via a reorganization of their F-actin filaments (Rodgers et al., 2005, Lee et al., 2012). It has been reported that mechanical forces have an impact on wound healing (Lee et al., 2012), directing/reducing these forces in the wound environment and provides the potential to diminish the development of scar tissue (Barnes et al., 2017). Yano et al. (2004) reported that continuous stretching for 24hrs of human cultured keratinocytes inhibited the expression of K10 and promoted the expression of K6, which differed from the findings presented here. In conclusion, it is shown that in EPKs physical forces can promote/change in the expression pattern of cytoskeletal keratins. This model advances our molecular understanding of the biophysical stimuli of hoof growth induced by tensile stretch events such as lamellar wedge (Collins et al., 2010), chronic foot lameness or laminitis due to over growth rate (Pollitt, 2004b, Dyson et al., 2011b) and distortion of hoof capsule (Redden, 2003).

The modulation of oxygen concentration is also important in understanding the differentiation of keratinocytes as it is in humans. The 21% atmospheric oxygen level O_2 (Seinfeld and Pandis, 2016) can only diffuse over a thickness of ~0.4mm within the skin (Stücker et al., 2002) and that it is well acknowledged that tissues are usually perfused with low oxygen levels in comparison to the atmospheric level, for example oxygen levels range from 14% in the alveolar tissue to 1 to 5% in the brain (Studer et al., 2000). Furthermore it has been reported that oxygen levels on dermal papillae in human nails ranged between 5% at the dermal-epidermal junction to 21% at the end of papillae depending on the cell position

within the axis of dermal papillae (Wang et al., 2003). Regarding the equine hoof, recently published studies by Pawlak et al. (2013) showed a high concentration of HIF-1α in normal lamellae tissue that was grater in laminitic feet than non laminitic feet (Pawlak et al., 2013, Gardner, 2015). In the present study, 1% and 3% O_2 levels triggered HIF-1α expression but, only 1% O_2 up-regulated K14, K10 and Ki-67 expression. These findings agreement with Pawlak et al. (2013). HIF-1α has been showed to be involved in: (i) the differentiation of myeloid cells (Song et al., 2008); (ii) wound healing (Botusan et al., 2008); (iii) angiogenesis via increase vascular endothelial growth factor (VEGF) (Yip, 2015) and; (iv) inflammatory signalling in laminitis (Pawlak et al., 2013). Those observations suggested that the high concentration of HIF-1α in equine hoof tissue compared to that of integument and viscera tissues indicate the importance of oxygen level in hoof lamellar tissue and foot diseases (Stewart et al., 2009). Similar results found that HIF-1α is increased in equine skin once injured (Deschene et al., 2011). However, in contrast to our findings, it was also reported that 1% O_2 level suppresses the expression of human skin keratin K1 and K10; with no impact on the level of HIF-1α (Park et al., 2016). Altogether, our results point towards the possible role of low oxygen levels as being involved in the proliferation/differentiation process of EPKs. This is in agreement with the known roles of low oxygen levels in protecting adult stem cells from oxidative DNA damage (Cipolleschi et al., 1993, Eliasson and Jönsson, 2010). This can stimulate the cell cycle (Ortmann et al., 2014) or the cellular metabolism (Keith and Simon, 2007). Also, this could stimulate the proliferation/differentiation processes such as in mouse corneal epithelial progenitor cell (Dong et al., 2013), rat mesencephalic precursor cells of rat (Studer et al., 2000) or adipose stromal cells (Yamamoto et

al., 2013). Hence, those results support indirectly the role of ischaemia due to vasoconstriction in the hoof disease process (Pawlak et al., 2013, Gardner, 2015). Furthermore, our data indicate the potential role of vascular dysfunctions in laminitis induced by the release of vasoactive inflammatory mediators inside the dermis leading to post-capillary oedema as a severe low oxygen-initiating event (Peroni et al., 2005, Noschka et al., 2009a).

In the present study, investigation of insulin concentrations using EPK cells revealed strong nuclear location of Ki-67 and expression of K14 at a concentration of 0.1µg/ml (=2400µU/ml) similar to that needed to induce acute laminitis in live horse (1036µU/ml) (Asplin et al., 2007, De Laat et al., 2010). High insulin concentrations (>1000µU/ml) have been reported in the field in laminitic horses (Reeves et al., 2001), compared to healthy ones (5.4-36µU/ml) (McGowan et al., 2004). The role of insulin in inducing proliferation agrees with the study by Bailey and Chockalingham (2010) on cultured keratinocytes from the hoof lamellae where insulin was found to increase cell proliferation to 54%. Many studied have considered the specific role of insulin in inducing equine laminitis (McGowan, 2008, De Laat et al., 2010, Karikoski et al., 2011, Karikoski et al., 2015, Lane et al., 2017) as insulin promotes cell proliferation in the lamellae tissue assessed via the histopathology of insulin-induced laminitis (De Laat et al., 2011b, De Laat et al., 2013b). However, to date, the precise mechanism by which insulin promotes the pathophysiology of laminitis is unclear. If insulin increases Ki-67 expression hoof growth might be involved in laminitis via EPKs hyper-proliferative responses as observed in endocrinopathic and specific cases of equine laminitis (De Laat et al., 2011b, De Laat et al., 2013a, Castro, 2015). Further studies will assess what the intracellular signalling pathways are leading

to insulin-induced proliferation in EPKs or whether other receptors like IGF-R are involved.

In chapter 5, a significant linear correlation was found between the expression of Ki-67 and P63 and the positive hoof curvature at quarter regions. These findings can be related to those showing that positive dorsal curvature is associated with the re-orientation and/or rotation of the distal phalanx and with clear alterations in the physio-morphology of trabecular and/or cortical bone thickness (Paul, 2016). These data present strong evidence that positive curvature (dished-shaped hoof) could be related to cellular proliferation at the coronary region. Studies have shown such changes in the coronary band shape where ramified growth rings increase with increasing hoof angle in lame horses in comparison to non-laminitic horses (Dyson et al., 2011b). Additionally, connections between the nuclear expression of p63 in hoof growth/homeostasis and laminitis has been studied by Carter et al. (2011) who reported its low expression level in laminitic horses compared to non-lame horses. The highest expression of p63 in the quarters in positively curved hooves may be related to the self-renewal potential induced by p63 and its ability to oppose cell death (Senoo et al., 2007, Li et al., 2012). Additionally, the high expression of Ki-67 (and related proliferation) and its positive correlation with the dorsal curvature further suggests that hoof growth might be involved in the conformation/distortion of the hoof. So far only the dorsal contact angle with the ground or the geometry of the hoof were considered in hoof distortion (Thomason, 1998, Douglas, 1999, Thomason et al., 2002, Ramsey et al., 2013, Jansová et al., 2015) but we add here further information that connects the coronet region (EPKs proliferation/Ki-67 and p63) to the same angular parameter. It is reasonable to propose that such findings provide a

connection between hoof growth and the physical forces involved especially with regard to the ground reaction force linked to the angular parameter/dorsal curvature. So far, no one has examined the possibility of linking the coronet region, the physical forces and the hoof shape. However, a clear understanding of such connections can serve future clinical researches to control hoof growth.

6.2 Summary of integrated key findings

This thesis provides several noteworthy contributions to our understanding of the way hoof grows and responds to biophysical forces as well as the role of these forces in the development of equine lameness/laminitis. In Chapter 3 the data obtained from the changes in cell volume demonstrated the mechanism of hoof morphogenesis. As discussed in Chapter 3, studying the behaviour of progenitor keratinocytes (Chapter 4) enabled us to understand the behaviour of progenitor keratinocytes as shown in Chapter 3 regarding the increase in cell volume when moving away from the basement membrane. In Chapter 4 by blocking F-actin the role of microfilaments in the changes in cell size and commitment of cell for further differentiation were demonstrated. This was also confirmed by measuring the size of cells as a function of the distance from the basement membrane. These changes in the cell volume that may happen during the early stage of hoof morphogenesis, suggests a possible role of physical stresses and cell elongation in the development and movement of the interpapillary horn. Elasticity of F-actin across the keratinocyte would allow a force applied to the interpapillary space to be absorbed across the dermal papillae allowing hoof growth. In addition, in Chapter 3, it was identified that there were high percentages of proliferation/stem cells (measured by the cell proliferation Ki-67/stem p63 markers) at the proximal

part of papillae, in comparison to the distal end. Those results corroborate with the observation made in cultured cells when the hydrostatic pressure elicited an increase in cell proliferation and/or differentiation of cells. Furthermore, when the cells were stretched over a period of 10 days the change in cell size was similar to the ones observed in the interpapillary space in Chapter 3. These cells under stretch exhibited differentiation patterns similar to that generated by the interpapillary horn. The findings in Chapter 3 regarding the localization of TUNEL positive apoptotic cells indicated the presence of critical zone determining horn formation. Additionally, the significant correlation between apoptosis/cornification at the critical zone as a function of the distance from the basement membrane suggests that this arises due to a balance between the gravity, the adhesion and the growth stresses, allowing the hoof to grow as indicated in Chapter 5 when the proliferation index was compared with the dorsal curvature of the hoof. Additionally, knowledge gained from observations of progenitor keratinocyte behaviour *in vitro* provided a typical method to examine hoof pathologies related to keratinocytes proliferation and differentiation. Under low oxygen levels of 1% O_2, cultured keratinocytes increased their proliferation and differentiation levels. These experiments gave an insight into the potential role of HIF-1α on equine cultured keratinocytes. This in turn improves our understanding of the pathophysiology of equine laminitis, due to the roles that infection and ischaemia/vasoconstriction and/or hypoxia are supposed to have in the hoof disease process. The results found in Chapters 4 and 5 provided some insights into why equine laminitis occurs. For instance, in Chapter 4 it was observed that insulin increases Ki-67 expression in culture keratinocytes. This suggests that insulin-mediated increases in hoof growth might be involved in laminitis via the

response of EPKs, as found in endocrinopathic and cases of equine laminitis. In Chapter 5 the immunostaining and labelling of p63 (stem cell regulator) or Ki-67 (proliferating cells), in addition to K14 and TUNEL apoptotic cells were linked to the hoof curvature showed the correlation between the hoof shape and hoof growth. These are relevant in equine lameness/laminitis. Overgrowth of the hoof capsule as shown in positive hoof curvature at quarter regions shown in chapter 5 is relevant to previous observations of chronic lameness (Carter et al. 2011). Additionally, a significant non-linear correlation was found between the expression of Ki-67 and p63 and the positive hoof curvature at quarter region. This provides new insights into the mechanism of hoof growth in response to the ground reaction stress. Furthermore, in Chapter 5, the results regarding p63 positive cell suggested an increase in p63 positive cells with increasing hoof curvature which was inversely associated with the intensity of epidermal hyperplasia. This indicated the capability of the hoof capsule to counter balance potential distortion via the maintenance of progenitor stem keratinocytes proliferation and differentiation. Figure 6-1 summarises the biophysical forces involved in hoof growth.

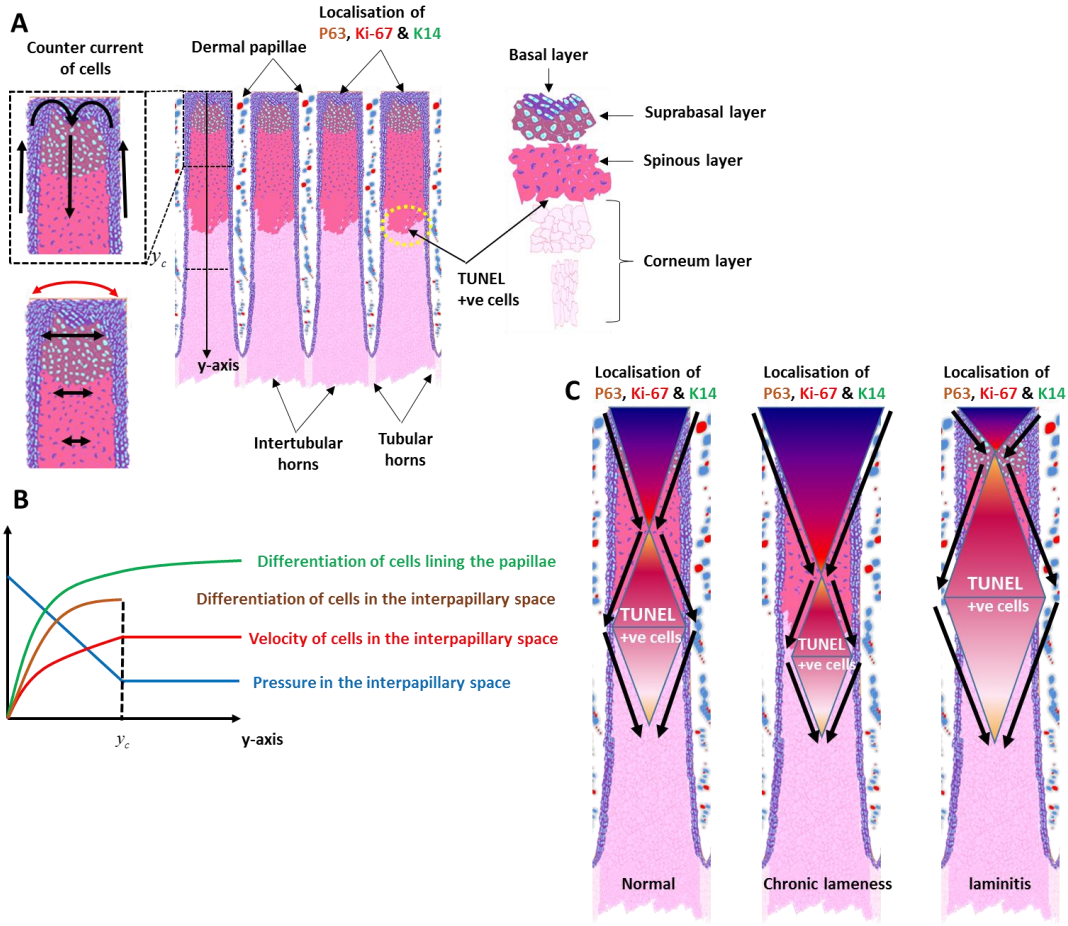


Figure 6-1: Schematic drawing shows the hoof growth and distortion

A) Shows the physical forces involves inside interpapillary spaces represented by black arrows. B) Illustrates the correlation between forces generation and hoof growth. C) Represents different faces of hoof growth occur in normal, chronic lameness and laminitis.

6.2.1 Conclusion and future work

Many studies have focused on biological factors in hoof growth, but very few have tried to understand the underlying physical and biological mechanisms of hoof growth and how these might influence foot disease. This thesis provides a description of the physiological and cellular properties of equine hoof growth at the coronary region, as well as the influence of physical factors on EPK cells. The morphometric data of keratinocytes along the dermal papillae and within the interpapillary space as a function of the distance from basement membrane provide new evidences regarding the development and movement of interpapillary horn. These data add further knowledge to the framework exploring the role of dermal papillae in hoof growth. However, the information provided is unique as it is the first attempt to connect physics and biology together to further explain hoof growth and its pathologies. As far as physics (or biophysics) is involved it is clear that EPKs respond to physical stimuli (stretch and pressure) and that those responses may be at play when the hoof grows, due to the inherent forces present in the hoof given its physiological function as a weight bearing element. These results, while still in their infancy, might explain the development of hoof diseases in the future such as chronic foot lameness. In particular, the connection between the dorsal curvature of the hoof and the ability of cells to proliferate from the quarters suggests that hoof deformities may be related to how cells proliferate from the coronet region. Such ability to proliferate may be related to the specific response that EPK cells develop when faced with a change in the ground reaction stress or physical forces (due to the hoof deformity) explaining the chronic aspect of hoof deformities. While the results described in this thesis are different from those found in human, they are nonetheless important to expand our

understanding of the pathophysiology of equine feet diseases and in particular equine laminitis. This thesis supports that the distortion patterns of the capsular wall are borne from the interplay between physics and biology.

6.2.2 Future work

It would be interesting to examine at a population level how the genotypes of horses influence hoof growth especially with regard to tissue renewal/regeneration. Further investigation should also concentrate on the relationship between insulin receptors (IR and IGF-1R) and the respective pathways triggered in EPK cells. The field of mechano-biology needs to be further developed in the field of equine hoof to demonstrate the importance of the relations between physics and biology at the cellular level and to up-scale those to the entire hoof. In line with the last suggestion, future studies should concentrate on the physical consequences of laminitis and its significance on the forces acting on the suspensory apparatus/laminar junction and; more efforts are needed to provide an accurate method enabling stress measurements at the dermal papillae to provide essential data about the impact of strain in this area. Finally, a study of epigenetic mechanisms affecting hoof growth could provide essential information with regard to the role of the environment in hoof diseases.

7 References

AGHA, R., OGAWA, R., PIETRAMAGGIORI, G. & ORGILL, D. P. 2011. A review of the role of mechanical forces in cutaneous wound healing. *Journal of Surgical Research,* 171**,** 700-708.

AGUIAR, C., THERRIEN, J., LEMIRE, P., SEGURA, M., SMITH, L. & THEORET, C. 2015. Differentiation of equine induced pluripotent stem cells into a keratinocyte lineage. *Equine Veterinary Journal,* 48, 338-345.

ALENZI, F. Q. 2004. Links between apoptosis, proliferation and the cell cycle. *British Journal of Biomedical Science,* 61**,** 99-102.

ALIBARDI, L. 2009. Ultrastructural characteristics of the process of cornification in developing claws of the brushtail possum (Trichosurus vulpecula). *Acta Zoologica,* 90**,** 285-300.

ALONSO, L. & FUCHS, E. 2003. Stem cells of the skin epithelium. *Proceedings of the National Academy of Sciences,* 100**,** 11830-11835.

ALVAREZ, C. B. G. 2007. *The biomechanical interaction between vertebral column and limbs in the horse: a kinematical study*. Ph. D. Thesis. Utrecht University Repository, 32-37.

AMORY, J., BARKER, Z., WRIGHT, J., MASON, S., BLOWEY, R. & GREEN, L. E. 2008. Associations between sole ulcer, white line disease and digital dermatitis and the milk yield of 1824 dairy cows on 30 dairy cow farms in England and Wales from February 2003–November 2004. *Preventive Veterinary Medicine,* 83**,** 381-391.

ARCHER, S., BELL, N. & HUXLEY, J. 2010. Foot lameness in UK dairy cows: a review of the current status. *In Practice,* 32**,** 492-504.

ARORA, S., SAHA, S., ROY, S., DAS, M., JANA, S. S. & TA, M. 2015. Role of nonmuscle myosin II in migration of wharton's jelly-derived mesenchymal stem cells. *Stem Cells and Development,* 24**,** 2065-2077.

ASPLIN, K., PATTERSON-KANE, J., SILLENCE, M., POLLITT, C. & MC GOWAN, C. 2010. Histopathology of insulin-induced laminitis in ponies. *Equine Veterinary Journal,* 42**,** 700-706.

ASPLIN, K. E., SILLENCE, M. N., POLLITT, C. C. & MCGOWAN, C. M. 2007. Induction of laminitis by prolonged hyperinsulinaemia in clinically normal ponies. *The Veterinary Journal,* 174**,** 530-535.

BAILEY, S. & CHOCKALINGHAM, S. 2010. Proliferative effects of insulin on equine lamellar epithelial cells mediated by the IGF-1 receptor. *Journal of Equine Veterinary Science,* 30**,** 96.

BAILEY, S. R., MARR, C. M. & ELLIOTT, J. 2004. Current research and theories on the pathogenesis of acute laminitis in the horse. *The Veterinary Journal,* 167**,** 129-142.

BALU, M., MAZHAR, A., HAYAKAWA, C. K., MITTAL, R., KRASIEVA, T. B., KONIG, K., VENUGOPALAN, V. & TROMBERG, B. J. 2013. In vivo multiphoton NADH fluorescence reveals depth-dependent keratinocyte metabolism in human skin. *Biophysics Journal,* 104**,** 258-67.

BANKS, W. J. 1993. *Applied Veterinary Histology*, Mosby-Year Book, Inc. 84-96

Murray, RD., Downham, DY., Clarkson, MJ., Faull, WB., Hughes, JW., Manson, FJ., Merritt, JB., Russell, WB., Sutherst, JE., Ward, WR. (1996) Epidemiology of lameness in dairy cattle: description and analysis of foot lesions. *Veterinary Record*, 138, 586-591.

BARNES, L. A., MARSHALL, C. D., LEAVITT, T., HU, M. S., MOORE, A. L., GONZALEZ, J. G., LONGAKER, M. T. & GURTNER, G. C. 2017. Mechanical forces in cutaneous wound healing: emerging therapies to minimize scar formation. *Advances in Wound Care*, 6, 342.

BARRANDON, Y. & GREEN, H. 1987. Three clonal types of keratinocyte with different capacities for multiplication. *Proceedings of the National Academy of Sciences,* 84**,** 2302-2306.

BARRETO-VIANNA, A. R., OLIVEIRA, L. S., LEONARDO, A. S., SANTANA, M. I., GODOY, R. F. & DE LIMA, E. M. 2013. Density of primary and secondary epidermal laminae of equine hoof. *Pesquisa Veterinária Brasileira,* 33**,** 543-548.

BARREY, E. 1990. Investigation of the vertical hoof force distribution in the equine forelimb with an instrumented horseboot. *Equine Veterinary Journal*, 22**,** 35-38.

BATH, C., YANG, S., MUTTUVELU, D., FINK, T., EMMERSEN, J., VORUM, H., HJORTDAL, J. & ZACHAR, V. 2013. Low oxygen is a key regulator of limbal epithelial stem cell growth and differentiation. *Stem Cell Research,* 10**,** 349-360.

BAXTER, G. M. 2011. *Adams and Stashak's foot lameness in horses*, John Wiley & Sons. Chapter 5, 516-520.

BELKNAP, J. K. & GEOR, R. J. 2017. *Equine Laminitis*, John Wiley & Sons. 421-426.

BELLENZANI, M. C., MERRITT, J. S., CLARKE, S. & DAVIES, H. M. 2012. Investigation of forelimb hoof wall strains and hoof shape in unshod horses exercised on a treadmill at various speeds and gaits. *American Journal of Veterinary Research,* 73**,** 1735-1741.

BENTLEY, V., SAMPLE, S., LIVESEY, M., SCOLLAY, M., RADTKE, C., FRANK, J., KALSCHEUR, V. & MUIR, P. 2007. Morphologic changes associated with

functional adaptation of the navicular bone of horses. *Journal of Anatomy,* 211**,** 662-672.

BERIAULT, D. R., HADDAD, O., MCCUAIG, J. V., ROBINSON, Z. J., RUSSELL, D., LANE, E. B. & FUDGE, D. S. 2012. The mechanical behavior of mutant K14-R125P keratin bundles and networks in NEB-1 keratinocytes. *PLoS One,* 7**,** e31320.

BERTRAM, J. & GOSLINE, J. 1987. Functional design of horse hoof keratin: the modulation of mechanical properties through hydration effects. *Journal of Experimental Biology,* 130**,** 121-136.

BICALHO, R. C. & OIKONOMOU, G. 2013. Control and prevention of foot lameness associated with claw lesions in dairy cows. *Livestock Science,* 156**,** 96-105.

BLACKING, T., WATERFALL, M. & ARGYLE, D. 2011. CD44 is associated with proliferation, rather than a specific cancer stem cell population, in cultured canine cancer cells. *Veterinary Immunology and Immunopathology,* 141**,** 46-57.

BLANPAIN, C. & FUCHS, E. 2009. Epidermal homeostasis: a balancing act of stem cells in the skin. *Nature reviews Molecular Cell Biology,* 10**,** 207-217.

BLANPAIN, C., LOWRY, W. E., GEOGHEGAN, A., POLAK, L. & FUCHS, E. 2004. Self-renewal, multipotency, and the existence of two cell populations within an epithelial stem cell niche. *Cell,* 118**,** 635-648.

BLAU, H. M., BRAZELTON, T. & WEIMANN, J. 2001. The evolving concept of a stem cell: entity or function? *Cell,* 105**,** 829-841.

BOLOGNA-MOLINA, R., MOSQUEDA-TAYLOR, A., MOLINA-FRECHERO, N., MORI-ESTEVEZ, A. D. & SÁNCHEZ-ACUÑA, G. 2013. Comparison of the value of PCNA and Ki-67 as markers of cell proliferation in ameloblastic tumor. *Medicina Oral, Patologia Oraly Cirugia Bucal,* 18**,** e174.

BONAKDAR, N., SCHILLING, A., SPÖRRER, M., LENNERT, P., MAINKA, A., WINTER, L., WALKO, G., WICHE, G., FABRY, B. & GOLDMANN, W. H. 2015. Determining the mechanical properties of plectin in mouse myoblasts and keratinocytes. *Experimental Cell Research,* 331**,** 331-337.

BORENA, B. M., MEYER, E., CHIERS, K., MARTENS, A., DEMEYERE, K., BROECKX, S. Y., DUCHATEAU, L. & SPAAS, J. H. 2014. Sphere-forming capacity as an enrichment strategy for epithelial-like stem cells from equine skin. *Cellular Physiology and Biochemistry,* 34**,** 1291-1303.

BOTCHKAREV, V. A. & FLORES, E. R. 2014. p53/p63/p73 in the epidermis in health and disease. *Cold Spring Harbor Perspectives in Medicine,* 4**,** a015248.

BOTUSAN, I. R., SUNKARI, V. G., SAVU, O., CATRINA, A. I., GRÜNLER, J., LINDBERG, S., PEREIRA, T., YLÄ-HERTTUALA, S., POELLINGER, L. &

BRISMAR, K. 2008. Stabilization of HIF-1α is critical to improve wound healing in diabetic mice. *Proceedings of the National Academy of Sciences,* 105**,** 19426-19431.

BOWDEN, P. E., HENDERSON, H. & REILLY, J. D. 2009. Defining the complex epithelia that comprise the canine claw with molecular markers of differentiation. *Veterinary Dermatology,* 20**,** 347-359.

BOWKER, R. 2003. The growth and adaptive capabilities of the hoof wall and sole: functional changes in response to stress. Proceedings of the 49th Annual Convention of the American Association of Equine Practitioners, New Orleans, Louisiana, 146-168.

BRAGULLA, H. 2003. Fetal development of the segment-specific papillary body in the equine hoof. *Journal of Morphology,* 258**,** 207-224.

BRAGULLA, H. & HIRSCHBERG, R. M. 2003. Horse hooves and bird feathers: Two model systems for studying the structure and development of highly adapted integumentary accessory organs—the role of the dermo-epidermal interface for the micro-architecture of complex epidermal structures. *Journal of Experimental Zoology Part B: Molecular and Developmental Evolution,* 298B**,** 140-151.

BRAGULLA, H., KÖNIG, H. E. & LIEBICH, H.-G. 2007. *Veterinary Anatomy of Domestic Mammals: Textbook and Colour Atlas,* Schattauer Verlag. 647-650.

BRAGULLA, H. H. & HOMBERGER, D. G. 2009. Structure and functions of keratin proteins in simple, stratified, keratinized and cornified epithelia. *Journal of Anatomy,* 214**,** 516-559.

BRAS, R. J. 2011. Management of distal displacement of P3 ("sinking") with foot casts. *Journal of Equine Veterinary Science,* 31**,** 573-577.

BROECKX, S. Y., MAES, S., MARTINELLO, T., AERTS, D., CHIERS, K., MARIËN, T., PATRUNO, M., FRANCO-OBREGÓN, A. & SPAAS, J. H. 2013. Equine epidermis: a source of epithelial-like stem/progenitor cells with in vitro and in vivo regenerative capacities. *Stem Cells and Development,* 23**,** 1134-1148.

BROSTER, C., BURN, C., BARR, A. & WHAY, H. 2009. The range and prevalence of pathological abnormalities associated with foot lameness in working horses from developing countries. *Equine Veterinary Journal,* 41**,** 474-481.

BUDRAS, K.-D., SACK, W. O. & ROCK, S. 2003. *Anatomy of the horse: an illustrated text,* Schlütersche. 24-26.

BUDRAS, K.-D., SACK, W. O. & RÖCK, S. 2012. *Anatomy of the Horse: with Aaron Horowitz and Rolf Berg,* Schlütersche. 10-12.

BUDRAS, K., MÜLLING, C. & HOROWITZ, A. 1996. Rate of keratinization of the wall segment of the hoof and its relation to width and structure of the zona alba

(white line) with respect to claw disease in cattle. *American Journal of Veterinary Research,* 57**,** 444-455.

BUDRAS, K. D. & SACK, W. O. 2012. *Anatomy of the Horse,* Manson Publishing.

BUTCHER, D. T., ALLISTON, T. & WEAVER, V. M. 2009. A tense situation: forcing tumour progression. *Nature Reviews Cancer,* 9**,** 108-122.

BYRNE, C., TAINSKY, M. & FUCHS, E. 1994. Programming gene expression in developing epidermis. *Development,* 120**,** 2369-2383.

CAI, P., MIZUTANI, Y., TSUCHIYA, M., MALONEY, J. M., FABRY, B., VAN VLIET, K. J. & OKAJIMA, T. 2013. Quantifying cell-to-cell variation in power-law rheology. *Biophysical Journal,* 105**,** 1093-1102.

CANDI, E., CIPOLLONE, R., DI VAL CERVO, P. R., GONFLONI, S., MELINO, G. & KNIGHT, R. 2008. p63 in epithelial development. *Cellular and Molecular Life Sciences,* 65**,** 3126-3133.

CANDI, E., SCHMIDT, R. & MELINO, G. 2005. The cornified envelope: a model of cell death in the skin. *Nature reviews. Molecular Cell Biology,* 6**,** 328.

CANDI, E., SMIRNOV, A., PANATTA, E., LENA, A. M., NOVELLI, F., MANCINI, M., VITICCHIÈ, G., PIRO, M. C., DI DANIELE, N. & ANNICCHIARICO-PETRUZZELLI, M. 2017. Metabolic pathways regulated by p63. *Biochemical and Biophysical Research Communications,* 482**,** 440-444.

CARTER, R., ENGILES, J., MEGEE, S., SENOO, M. & GALANTINO-HOMER, H. 2011. Decreased expression of p63, a regulator of epidermal stem cells, in the chronic laminitic equine hoof. *Equine Veterinary Journal,* 43**,** 543-551.

CARTER, R., MEGEE, S., ENGILES, J., SENOO, M. & GALANTINO-HOMER, H. 2010a. Cellular Proliferation Markers in Lamellar Tissue and Skin Measured by Indirect Immunofluorescence. *Journal of Equine Veterinary Science,* 30**,** 104.

CARTER, R. A., SHEKK, V., DE LAAT, M. A., POLLITT, C. C. & GALANTINO-HOMER, H. L. 2010b. Novel keratins identified by quantitative proteomic analysis as the major cytoskeletal proteins of equine (Equus caballus) hoof lamellar tissue. *Journal of Animal Science,* 88**,** 3843-3855.

CASTRO, M. 2015. *The effects of locally delivered insulin on equine hoof lamellar tissue.* Ph. D. Thesis, The University of Queensland. 61-72.

CHAN, Y.-M., ANTON-LAMPRECHT, I., YU, Q.-C., JÄCKEL, A., ZABEL, B., ERNST, J.-P. & FUCHS, E. 1994. A human keratin 14" knockout": the absence of K14 leads to severe epidermolysis bullosa simplex and a function for an intermediate filament protein. *Genes & Development,* 8**,** 2574-2587.

CHESTERTON, R., LAWRENCE, K. & LAVEN, R. 2008. A descriptive analysis of the foot lesions identified during veterinary treatment for foot lameness on dairy farms in north Taranaki. *New Zealand Veterinary Journal,* 56**,** 130-138.

CHRISTENSEN, A. P. & COREY, D. P. 2007. TRP channels in mechanosensation: direct or indirect activation? *Nature Reviews Neuroscience,* 8**,** 510-521.

CHRISTODOULOPOULOS, G. 2009. Foot foot lameness in dairy goats. *Research in Veterinary Science,* 86**,** 281-284.

CIPOLLESCHI, M. G., SBARBA, P. D. & OLIVOTTO, M. 1993. The role of low oxygen in the maintenance of hematopoietic stem cells. *Blood,* 82**,** 2031-2037.

CLARKSON, M. J., DOWNHAM, D. Y., FAULL, W. B., HUGHES, J. W., MANSON, F. J., MERRITT, J. B., MURRAY, R. D., RUSSELL, W. B., SUTHERST, J. E. & WARD, W. R. 1996. Incidence and prevalence of foot lameness in dairy cattle. *Veterinary Record,* 138**,** 563-567.

CLAYTON, E., DOUPÉ, D. P., KLEIN, A. M., WINTON, D. J., SIMONS, B. D. & JONES, P. H. 2007. A single type of progenitor cell maintains normal epidermis. *Nature,* 446**,** 185-189.

CLIFTON, R. & GREEN, L. 2016. Pathogenesis of ovine footrot disease: a complex picture. *Veterinary Record,* 179**,** 225-227.

COLLINS, J. N., GALUPPO, L. D., THOMAS, H. L., WISNER, E. R. & HORNOF, W. J. 2004. Use of computed tomography angiography to evaluate the vascular anatomy of the distal portion of the forelimb of horses. *American Journal of Veterinary Research,* 65**,** 1409-1420.

COLLINS, S. N., VAN EPS, A. W., POLLITT, C. C. & KUWANO, A. 2010. The lamellar wedge. *Veterinary Clinics of North America: Equine Practice,* 26**,** 179-195.

CRIPPS, P. & EUSTACE, R. 1999. Factors involved in the prognosis of equine laminitis in the UK. *Equine Veterinary Journal,* 31**,** 433-442.

CROSS, B. 2011. New survey reveals UK's current equine healthcare problems. Available from, http://www.bluecross.org.uk/2000-84227/new-survey-reveals-uks-current-equine-healthcare-problems-.html.

CRUZ, C., THOMASON, J., FARAMARZI, B., BIGNELL, W., SEARS, W., DOBSON, H. & KONYER, N. 2006. Changes in shape of the Standardbred distal phalanx and hoof capsule in response to exercise. *Equine and Comparative Exercise Physiology,* 3**,** 199-208.

DAHM, A., BRUIN, A., LIMAT, A., TSCHARNER, C., WYDER, M. & SUTER, M. 2002. Cultivation and characterisation of primary and subcultured equine keratinocytes. *Equine Veterinary Journal,* 34**,** 114-120.

DARADKA, M. & POLLITT, C. C. 2004. Epidermal cell proliferation in the equine hoof wall. *Equine Veterinary Journal,* 36**,** 236-41.

DAVIES, H., PHILIP, C. & MERRITT, J. S. 2007. Functional anatomy of the equine digit: determining function from structure. *Equine Podiatry. Saunders Elsevier, St. Louis***,** 25-41.

DE BERKER, D., WOJNAROWSKA, F., SVILAND, L., WESTGATE, G., DAWBER, R. & LEIGH, I. 2000. Keratin expression in the normal nail unit: markers of regional differentiation. *British Journal of Dermatology,* 142**,** 89-96.

DE LAAT, M., KYAW-TANNER, M., NOURIAN, A., MCGOWAN, C., SILLENCE, M. & POLLITT, C. 2011a. The developmental and acute phases of insulin-induced laminitis involve minimal metalloproteinase activity. *Veterinary Immunology and Immunopathology,* 140**,** 275-281.

DE LAAT, M., VAN EPS, A., MCGOWAN, C., SILLENCE, M. & POLLITT, C. 2011b. Equine laminitis: comparative histopathology 48 hours after experimental induction with insulin or alimentary oligofructose in standardbred horses. *Journal of Comparative Pathology,* 145**,** 399-409.

DE LAAT, M. A., MCGOWAN, C., SILLENCE, M. & POLLITT, C. 2010. Equine laminitis: induced by 48 h hyperinsulinaemia in Standardbred horses. *Equine Veterinary Journal,* 42**,** 129-135.

DE LAAT, M. A., PATTERSON-KANE, J. C., POLLITT, C. C., SILLENCE, M. N. & MCGOWAN, C. M. 2013a. Histological and morphometric lesions in the pre-clinical, developmental phase of insulin-induced laminitis in Standardbred horses. *The Veterinary Journal,* 195**,** 305-312.

DE LAAT, M. A., POLLITT, C. C., KYAW-TANNER, M. T., MCGOWAN, C. M. & SILLENCE, M. N. 2013b. A potential role for lamellar insulin-like growth factor-1 receptor in the pathogenesis of hyperinsulinaemic laminitis. *The Veterinary Journal,* 197**,** 302-306.

DELLMANN, H. & EURELL, J. 1998. Textbook of Veterinary Histology. 5th . *Ed. Baltimore, Philadelphia, London, Paris, Bangkok, Buenos Aires, Hong Kong, Munich, Sydney, Tokyo, Wroclaw: Williams & Wilkins A Waverly Company. p***,** 273-286.

DEPIANTO, D. & COULOMBE, P. A. 2004. Intermediate filaments and tissue repair. *Experimental Cell Research,* 301**,** 68-76.

DESCHENE, K., CÉLESTE, C., BOERBOOM, D. & THEORET, C. L. 2011. Constitutive expression of low oxygen-inducible factor-1 α in keratinocytes during the repair of skin wounds in horses. *Wound Repair and Regeneration,* 19**,** 250-259.

DI PALMA, F., DOUET, M., BOACHON, C., GUIGNANDON, A., PEYROCHE, S., FOREST, B., ALEXANDRE, C., CHAMSON, A. & RATTNER, A. 2003. Physiological strains induce differentiation in human osteoblasts cultured on orthopaedic biomaterial. *Biomaterials,* 24**,** 3139-3151.

DONG, N., QIN, W., XUE, Y., LI, C. & LIU, Z. 2013. Low oxygen affects in vitro proliferation and differentiation of mouse corneal epithelial progenitor cell. *In Vitro Cellular & Developmental Biology-Animal,* 49**,** 508-514.

DOUGLAS, J. 1999. *Morphological and material properties of the equine hoof wall and laminar junction*. Ph. D. Thesis, University of Guelph. P, 34-45.

DOUGLAS, J., BIDDICK, T., THOMASON, J. & JOFRIET, J. 1998. Stress/strain behaviour of the equine laminar junction. *Journal of Experimental Biology,* 201**,** 2287-2297.

DOUGLAS, J., MITTAL, C., THOMASON, J. & JOFRIET, J. 1996. The modulus of elasticity of equine hoof wall: implications for the mechanical function of the hoof. *The Journal of Experimental Biology,* 199**,** 1829-1836.

DOUGLAS, J. E. 1998. MORPHOLOGICAL AND MATERIAL PROPERTIES.

DOUGLAS, J. E. & THOMASON, J. J. 2000. Shape, orientation and spacing of the primary epidermal laminae in the hooves of neonatal and adult horses (Equus caballus). *Cells Tissues Organs,* 166**,** 304-318.

DRUMOND, B., GINELLI, A. M. G., FALEIROS, R. R., DE MAGALHÃES, J. F. & COELHO, C. S. 2016. Hoof capsule distortion and radiographic measurements of the front feet in Mangalarga Marchador horses subjected to athletic training. *Pferdeheilkunde,* 32**,** 110-118.

DUCRO, B., BOVENHUIS, H. & BACK, W. 2009. Heritability of foot conformation and its relationship to sports performance in a Dutch Warmblood horse population. *Equine Veterinary Journal,* 41**,** 139-143.

DYSON, S., TRANQUILLE, C., COLLINS, S., PARKIN, T. & MURRAY, R. 2011a. An investigation of the relationships between angles and shapes of the hoof capsule and the distal phalanx. *Equine Veterinary Journal,* 43**,** 295-301.

DYSON, S. J., TRANQUILLE, C. A., COLLINS, S. N., PARKIN, T. D. & MURRAY, R. C. 2011b. External characteristics of the lateral aspect of the hoof differ between non-lame and lame horses. *The Veterinary Journal,* 190**,** 364-371.

EADES, S. C. 2010. Overview of current laminitis research. *Veterinary Clinics of North America: Equine Practice,* 26**,** 51-63.

EADES, S. C., HOLM, A. M. & MOORE, R. M. A review of the pathophysiology and treatment of acute laminitis: pathophysiologic and therapeutic implications of

endothelin-1. Proceedings of the 48th Annual Convention of the American *Association of Equine Practitioners. Orlando, FL*, 2002. 353-361.

ECKHART, L., LIPPENS, S., TSCHACHLER, E. & DECLERCQ, W. 2013. Cell death by cornification. *Biochimica et Biophysica Acta (BBA)-Molecular Cell Research,* 1833**,** 3471-3480.

ELIASSON, P. & JÖNSSON, J. I. 2010. The hematopoietic stem cell niche: low in oxygen but a nice place to be. *Journal of Cellular Physiology,* 222**,** 17-22.

ELMORE, S. 2007. Apoptosis: a review of programmed cell death. *Toxicologic Pathology,* 35**,** 495-516.

ENGILES, J., GALANTINO-HOMER, H., BOSTON, R., MCDONALD, D., DISHOWITZ, M. & HANKENSON, K. 2015. Osteopathology in the equine distal phalanx associated with the development and progression of laminitis. *Veterinary Pathology,* 52**,** 928-944.

ENGILES, J. B. 2010. Pathology of the distal phalanx in equine laminitis: more than just skin deep. *Veterinary Clinics of North America: Equine Practice,* 26**,** 155-165.

ENGLER, A. J., SEN, S., SWEENEY, H. L. & DISCHER, D. E. 2006. Matrix elasticity directs stem cell lineage specification. *Cell,* 126**,** 677-689.

EPS, A. V. & POLLITT, C. 2006. Equine laminitis induced with oligofructose. *Equine Veterinary Journal,* 38**,** 203-208.

ETHIER, D. M., KYLE, C. J., KYSER, T. K. & NOCERA, J. J. 2010. Variability in the growth patterns of the cornified claw sheath among vertebrates: implications for using biogeochemistry to study animal movement. *Canadian Journal of Zoology,* 88**,** 1043-1051.

EURELL, J. A. & FRAPPIER, B. L. 2013. *Dellmann's textbook of veterinary histology*, 6th Ed. John Wiley & Sons. 343-347.

FALEIROS, R. R., STOKES, A. M., EADES, S. C., KIM, D. Y., PAULSEN, D. B. & MOORE, R. M. 2004. Assessment of apoptosis in epidermal lamellar cells in clinically normal horses and those with laminitis. *American Journal of Veterinary Research,* 65**,** 578-585.

FARAMARZI, B. 2011. Morphological spectrum of primary epidermal laminae in the forehoof of Thoroughbred horses. *Equine Veterinary Journal,* 43**,** 732-736.

FARAMARZI, B. 2014. Morphological and Biomechanical Properties of Equine Laminar Junction. *Journal of Equine Veterinary Science,* 34**,** 589-592.

FARAMARZI, B., CRUZ, A. M. & SEARS, W. C. 2011. Changes in hoof surface strain distribution in response to moderate exercise in Standardbreds. *American Journal of Veterinary Research,* 72**,** 484-490.

FARAMARZI, B., THOMASON, J. J. & SEARS, W. C. 2009. Changes in growth of the hoof wall and hoof morphology in response to regular periods of trotting exercise in Standardbreds. *American journal of Veterinary Research,* 70**,** 1354-1364.

FLINT, M. & MERRILEES, M. 1977. Relationship between the axial periodicity and staining of collagen by the Masson trichrome procedure. *The Histochemical Journal,* 9**,** 1-13.

FLINT, M. H., LYONS, M. F., MEANEY, M. & WILLIAMS, D. 1975. The Masson staining of collagen—an explanation of an apparent paradox. *The Histochemical Journal,* 7**,** 529-546.

FLORENCE, L. & MCDONNELL, S. 2006. Hoof growth and wear of semi-feral ponies during an annual summerself-trimming'period. *Equine Veterinary Journal,* 38**,** 642.

FLOYD, A. & MANSMANN, R. 2007. *Equine podiatry*, Elsevier Health Sciences.

FRACKOWIAK, H. & KOMOSA, M. 2006. The dynamics of hoof growth of the primitive Konik horses (Equus caballus gmelini Ant.) in an annual cycle. *Biological Rhythm Research,* 37**,** 223-232.

FRANCK, A., COCQUYT, G., SIMOENS, P. & DE BELIE, N. 2006. Biomechanical properties of bovine claw horn. *Biosystems Engineering,* 93**,** 459-467.

FRENCH, K. & POLLITT, C. 2004a. Equine laminitis: congenital, hemidesmosomal plectin deficiency in a Quarter Horse foal. *Equine Veterinary Journal,* 36**,** 299-303.

FRENCH, K. & POLLITT, C. 2004b. Equine laminitis: Glucose deprivation and MMP activation induce dermo-epidermal separation in vitro. *Equine Veterinary Journal,* 36**,** 261-266.

FRENCH, K. & POLLITT, C. 2004c. Equine laminitis: loss of hemidesmosomes in hoof secondary epidermal lamellae correlates to dose in an oligofructose induction model: an ultrastructural study. *Equine Veterinary Journal,* 36**,** 230-235.

FUCHS, E. & CLEVELAND, D. W. 1998. A structural scaffolding of intermediate filaments in health and disease. *Science,* 279**,** 514-519.

GARDNER, A. 2015. *Lamellar Mitogen-Activated Protein Kinase and Low oxygen Signaling in a Sepsis-Related Laminitis Model and a Novel Supporting Limb Laminitis Model.* Ph. D. Thesis, The Ohio State University.

GARDNER, A., VAN EPS, A., WATTS, M., BURNS, T. & BELKNAP, J. 2017. A novel model to assess lamellar signaling relevant to preferential weight bearing in the horse. *The Veterinary Journal,* 221**,** 62-67.

GLADE, M. & SALZMAN, R. 1985. Effects of toe angle on hoof growth and contraction in the horse. *Journal of Equine Veterinary Science,* 5**,** 45-50.

GOERMAR, F., BERND, A., BEREITER-HAHN, J. & HOLZMANN, H. 1993. Mechanical stimulation enhances human keratinocyte differentiation in culture: induction of cytokeratin 9 synthesis. *Cell and Tissue Culture Models in Dermatological Research.* Springer. 87-97.

GREEN, L., HEDGES, V., SCHUKKEN, Y., BLOWEY, R. & PACKINGTON, A. 2002. The impact of clinical foot lameness on the milk yield of dairy cows. *Journal of Dairy Science,* 85**,** 2250-2256.

GU, L.-H. & COULOMBE, P. A. 2007. Keratin function in skin epithelia: a broadening palette with surprising shades. *Current Opinion in Cell Biology,* 19**,** 13-23.

GU, S. R., KANG, Y. G., SHIN, J. W. & SHIN, J.-W. 2017. Simultaneous engagement of mechanical stretching and surface pattern promotes cardiomyogenic differentiation of human mesenchymal stem cells. *Journal of Bioscience and Bioengineering,* 123**,** 252-258.

GUILAK, F., COHEN, D. M., ESTES, B. T., GIMBLE, J. M., LIEDTKE, W. & CHEN, C. S. 2009. Control of stem cell fate by physical interactions with the extracellular matrix. *Cell Stem Cell,* 5**,** 17-26.

GUNNARSSON, V., STEFÁNSDÓTTIR, G., JANSSON, A. & ROEPSTORFF, L. 2017. The effect of rider weight and additional weight in Icelandic horses in tölt: part II. Stride parameters responses. *Animal***,** 1-6.

GUSTÅS, P., JOHNSTON, C., ROEPSTORFF, L. & DREVEMO, S. 2001. In vivo transmission of impact shock waves in the distal forelimb of the horse. *Equine Veterinary Journal,* 33**,** 11-15.

HAMPSON, B. 2011. The effects of environment on the horse's hoof. *Journal of Equine Veterinary Science,* 31**,** 609.

HAMPSON, B., LAAT, M., MILLS, P. & POLLITT, C. 2013. The feral horse foot. Part A: observational study of the effect of environment on the morphometrics of the feet of 100 Australian feral horses. *Australian Veterinary Journal,* 91**,** 14-22.

HAMRICK, M. W. 2001. Development and evolution of the mammalian limb: adaptive diversification of nails, hooves, and claws. *Evolution & Development,* 3**,** 355-363.

HAN, P. & BARTELS, D. M. 1996. Temperature dependence of oxygen diffusion in H2O and D2O. *Journal of Physical Chemistry,* 100**,** 5597-5602.

HARRISON, S. M., MONAHAN, F. J., ZAZZO, A., BAHAR, B., MOLONEY, A. P., SCRIMGEOUR, C. M. & SCHMIDT, O. 2007. Three-dimensional growth of bovine hoof as recorded by carbon stable isotope ratios. *Rapid Communications in Mass Spectrometry,* 21**,** 3971-3976.

HEDGES, J., BLOWEY, R., PACKINGTON, A., O'CALLAGHAN, C. & GREEN, L. 2001. A longitudinal field trial of the effect of biotin on foot lameness in dairy cows. *Journal of Dairy Science,* 84**,** 1969-1975.

HENDRY, K. A., MACCALLUM, A. J., KNIGHT, C. H. & WILDE, C. J. 2001. Synthesis and distribution of cytokeratins in healthy and ulcerated bovine claw epidermis. *Journal Dairy Research,* 68**,** 525-37.

HEYMERING, H. W. 2010. 80 causes, predispositions, and pathways of laminitis. *Veterinary Clinics of North America: Equine Practice,* 26**,** 13-19.

HILL, N., MURPHY, P., NELSON, A., MOUTTOTOU, N., GREEN, L. & MORGAN, K. 1997. Foot lameness and foot lesions in adult British dairy goats. *Veterinary Record,* 141**,** 412-416.

HINCKLEY, K., FEARN, S., HOWARD, B. & HENDERSON, I. 1996. Nitric oxide donors as treatment for grass induced acute laminitis in ponies. *Equine Veterinary Journal,* 28**,** 17-28.

HINCKLEY, K. & HENDERSON, I. 1996. The epidemiology of equine laminitis in the UK. *Proceedings of the 35th Congress of the British Equine Veterinary Congress, Warwick,*. 62-67.

HINTERHOFER, C., FERGUSON, J., APPRICH, V., HAIDER, H. & STANEK, C. 2006. Slatted floors and solid floors: Stress and strain on the bovine hoof capsule analyzed in finite element analysis. *Journal of Dairy Science,* 89**,** 155-162.

HINTERHOFER, C., STANEK, C. & HAIDER, H. 2000. The effect of flat horseshoes, raised heels and lowered heels on the biomechanics of the equine hoof assessed by finite element analysis (FEA). *Journal of Veterinary Medicine Series A,* 47**,** 73-82.

HIRATA, H., SAMSONOV, M. & SOKABE, M. 2017. Actomyosin contractility provokes contact inhibition in E-cadherin-ligated keratinocytes. *Scientific Reports,* 7.

HIRSCHBERG, R. M., MÜLLING, C. K. & BUDRAS, K. D. 2001. Pododermal angioarchitecture of the bovine claw in relation to form and function of the papillary body: a scanning electron microscopic study. *Microscopy Research and Technique,* 54**,** 375-385.

HOLROYD, K., DIXON, J. J., MAIR, T., BOLAS, N., BOLT, D. M., DAVID, F. & WELLER, R. 2013a. Variation in foot conformation in lame horses with different foot lesions. *The Veterinary Journal,* 195**,** 361-365.

HOLROYD, K., DIXON, J. J., MAIR, T., BOLAS, N. & WELLER, R. 2013b. Is there a relationship between foot conformation and foot lesions in lame horses? *Journal of Equine Veterinary Science,* 33**,** 858-859.

HOMBERGER, D. G., HAM, K., OGUNBAKIN, T., BONIN, J. A., HOPKINS, B. A., OSBORN, M. L., HOSSAIN, I., BARNETT, H. A., MATTHEWS, I. & KENNETH, L. 2009. The structure of the cornified claw sheath in the domesticated cat (Felis catus): implications for the claw-shedding mechanism and the evolution of cornified digital end organs. *Journal of Anatomy,* 214**,** 620-643.

HOOD, D. M., GROSENBAUGH, D. A., MOSTAFA, M. B., MORGAN, S. J. & THOMAS, B. C. 1993. The role of vascular mechanisms in the development of acute equine laminitis. *Journal of Veterinary Internal Medicine,* 7**,** 228-234.

HOOD, D. M., TAYLOR, D. & WAGNER, I. P. 2001. Effects of ground surface deformability, trimming, and shoeing on quasistatic hoof loading patterns in horses. *American Journal of Veterinary Research,* 62**,** 895-900.

HUANG, J., ZHANG, J., PATHAK, A., LI, J. & STOUFFER, G. A. 2011. Perivascular delivery of blebbistatin reduces neointimal hyperplasia after carotid injury in the mouse. *Journal of Pharmacology and Experimental Therapeutics,* 336**,** 116-126.

HUBBI, M. E. & SEMENZA, G. L. 2015. Regulation of cell proliferation by low oxygen-inducible factors. *American Journal of Physiology-Cell Physiology,* 309**,** C775-C782.

HURLEY, D. J., PARKS, R. J., REBER, A. J., DONOVAN, D. C., OKINAGA, T., VANDENPLAS, M. L., PERONI, J. F. & MOORE, J. N. 2006. Dynamic changes in circulating leukocytes during the induction of equine laminitis with black walnut extract. *Veterinary Immunology and Immunopathology,* 110**,** 195-206.

IRELAND, J., CLEGG, P., MCGOWAN, C., MCKANE, S., CHANDLER, K. & PINCHBECK, G. 2012. Disease prevalence in geriatric horses in the United Kingdom: veterinary clinical assessment of 200 cases. *Equine Veterinary Journal,* 44**,** 101-106.

JANČÍKOVÁ, P., HORKÝ, P. & ZEMAN, L. 2012. The effect of feed additive containing vitamins and trace elements on the elements profile and growth of skin derivatives in horses. *Annals of Animal Science,* 12**,** 381-391.

JANSOVÁ, M., ONDOKOVÁ, L., VYCHYTIL, J., KOCHOVÁ, P., WITTER, K. & TONAR, Z. 2015. A finite element model of an equine hoof. *Journal of Equine Veterinary Science,* 35**,** 60-69.

JOHNSON, P., KREEGER, J., KEELER, M., GANJAM, V. & MESSER, N. 2000. Serum markers of lamellar basement membrane degradation and lamellar histopathological changes in horses affected with laminitis. *Equine Veterinary Journal,* 32**,** 462-468.

JOHNSON, P. J. 2017. Endocrine and Metabolic Dysregulation in Laminitis: Role of Corticosteroids. *Equine Laminitis***,** 141-148.

JOHNSTON, C. & BACK, W. 2006. Hoof ground interaction: when biomechanical stimuli challenge the tissues of the distal limb. *Equine Veterinary Journal,* 38**,** 634-641.

JONES, C. L., MONAGHAN, P., FIELD, T. R., SMITH, A. J., WARD, P. N. & LEIGH, J. A. 2004. Localization of MtuA, an LraI homologue in Streptococcus uberis. *Journal of Applied Microbiology,* 97**,** 149-157.

KALER, J. & GREEN, L. E. 2008. Naming and recognition of six foot lesions of sheep using written and pictorial information: A study of 809 English sheep farmers. *Preventive Veterinary Medicine,* 83**,** 52-64.

KANEPS, A. J. & TURNER, T. A. 2004. Diseases of the foot. *Equine sports medicine and surgery: basic and clinical sciences of the equine athlete. Edinburgh: Saunders***,** 260-288.

KARIKOSKI, N., HORN, I., MCGOWAN, T. & MCGOWAN, C. 2011. The prevalence of endocrinopathic laminitis among horses presented for laminitis at a first-opinion/referral equine hospital. *Domestic Animal Endocrinology,* 41**,** 111-117.

KARIKOSKI, N., MCGOWAN, C., SINGER, E., ASPLIN, K., TULAMO, R.-M. & PATTERSON-KANE, J. 2015. Pathology of natural cases of equine endocrinopathic laminitis associated with hyperinsulinemia. *Veterinary Pathology,* 52**,** 945-956.

KARIKOSKI, N. P., PATTERSON-KANE, J. C., ASPLIN, K. E., MCGOWAN, T. W., MCNUTT, M., SINGER, E. R. & MCGOWAN, C. M. 2014. Morphological and cellular changes in secondary epidermal laminae of horses with insulin-induced laminitis. *American journal of Veterinary Research,* 75**,** 161-168.

KASAPI, M. A. & GOSLINE, J. M. 1997. Design complexity and fracture control in the equine hoof wall. *Journal of Experimental Biology,* 200**,** 1639-1659.

KASAPI, M. A. & GOSLINE, J. M. 1999. Micromechanics of the equine hoof wall: optimizing crack control and material stiffness through modulation of the properties of keratin. *Journal of Experimental Biology,* 202**,** 377-391.

KATZ, L. & BAILEY, S. 2012. A review of recent advances and current hypotheses on the pathogenesis of acute laminitis. *Equine Veterinary Journal,* 44**,** 752-761.

KATZ, L. M. 2004. *Equine acute laminitis: epidemiological and pathophysiological studies.* Ph. D., University of London. P, 35-45.

KAYA, G., RODRIGUEZ, I., JORCANO, J. L., VASSALLI, P. & STAMENKOVIC, I. 1997. Selective suppression of CD44 in keratinocytes of mice bearing an antisense CD44 transgene driven by a tissue-specific promoter disrupts

hyaluronate metabolism in the skin and impairs keratinocyte proliferation. *Genes & Development,* 11**,** 996-1007.

KEANE, M., PAUL, E., STURROCK, C. J., RAUCH, C. & RUTLAND, C. S. 2017. Computed tomography in veterinary medicine: currently published and tomorrow's vision. *Computed Tomography-Advanced Applications.* Intech, 273-276.

KEEGAN, K., DENT, E., WILSON, D., JANICEK, J., KRAMER, J., LACARRUBBA, A., WALSH, D., CASSELLS, M., ESTHER, T. & SCHILTZ, P. 2010. Repeatability of subjective evaluation of foot lameness in horses. *Equine Veterinary Journal,* 42**,** 92-97.

KEEGAN, K., PAI, P., WILSON, D. & SMITH, B. 2001. Signal decomposition method of evaluating head movement to measure induced forelimb foot lameness in horses trotting on a treadmill. *Equine Veterinary Journal,* 33**,** 446-451.

KEITH, B. & SIMON, M. C. 2007. Low oxygen-inducible factors, stem cells, and cancer. *Cell,* 129**,** 465-472.

KIM, S., WONG, P. & COULOMBE, P. A. 2006. A keratin cytoskeletal protein regulates protein synthesis and epithelial cell growth. *Nature,* 441**,** 362-365.

KNIGHT, M., TOYODA, T., LEE, D. & BADER, D. 2006. Mechanical compression and hydrostatic pressure induce reversible changes in actin cytoskeletal organisation in chondrocytes in agarose. *Journal of biomechanics,* 39**,** 1547-1551.

KONIG, H. E., LIEBICH, H.-G. & EDITORHORST ERICH KÖNIG, H.-G. L. 2007. *Veterinary anatomy of domestic mammals: textbook and color atlas*. P, 622-628.

KOSTER, M. I., DAI, D., MARINARI, B., SANO, Y., COSTANZO, A., KARIN, M. & ROOP, D. R. 2007. p63 induces key target genes required for epidermal morphogenesis. *Proceedings of the National Academy of Sciences,* 104**,** 3255-3260.

KOSTER, M. I., KIM, S., MILLS, A. A., DEMAYO, F. J. & ROOP, D. R. 2004. p63 is the molecular switch for initiation of an epithelial stratification program. *Genes & Development,* 18**,** 126-131.

KOSTER, M. I. & ROOP, D. R. 2007. Mechanisms regulating epithelial stratification. *Annual Review of Cell and Developmental Biology,* 23**,** 93-113.

KOUWENHOVEN, E. N., VAN BOKHOVEN, H. & ZHOU, H. 2015. Gene regulatory mechanisms orchestrated by p63 in epithelial development and related disorders. *Biochimica et Biophysica Acta (BBA)-Gene Regulatory Mechanisms,* 1849**,** 590-600.

KOVÁCS, M., TÓTH, J., HETÉNYI, C., MÁLNÁSI-CSIZMADIA, A. & SELLERS, J. R. 2004. Mechanism of blebbistatin inhibition of myosin II. *Journal of Biological Chemistry*, 279**,** 35557-35563.

KUMMER, M., GEYER, H., IMBODEN, I., AUER, J. & LISCHER, C. 2006. The effect of hoof trimming on radiographic measurements of the front feet of normal Warmblood horses. *The Veterinary Journal*, 172**,** 58-66.

KUWANO, A., KATAYAMA, Y., KASASHIMA, Y., OKADA, K. & REILLY, J. D. 2002. A gross and histopathological study of an ectopic white line development in equine laminitis. *The Journal of Veterinary Medical Science/the Japanese Society of Veterinary Science,* 64**,** 893-900.

KUWANO, A., UENO, T., KATAYAMA, Y., NISHIYAMA, T. & ARAI, K. 2005. Unilateral basement membrane zone alteration of the regenerated laminar region in equine chronic laminitis. *Journal of Veterinary Medical Science,* 67**,** 685.

KVEDAR, J. C., KUBILUS, J. & BADEN, H. P. 1986. Cytokeratins of the bovine hoof: classification and studies on expression. *Biochimica et Biophysica Acta (BBA)-General Subjects,* 884**,** 462-473.

KYAW-TANNER, M. & POLLITT, C. C. 2004. Equine laminitis: increased transcription of matrix metalloproteinase-2 (MMP-2) occurs during the developmental phase. *Equine Veterinary Journal,* 36**,** 221-225.

KYAW-TANNER, M., WATTLE, O., EPS, A. V. & POLLITT, C. 2008. Equine laminitis: Membrane type matrix metalloproteinase-1 (MMP-14) is involved in acute phase onset. *Equine Veterinary Journal,* 40**,** 482-487.

LANCASTER, L. 2011. Hoof capsule flares: gross and microscopic examination of the "normal" hoof wall. *Journal of Equine Veterinary Science,* 31**,** 572.

LANCASTER, L. S., BOWKER, R. M. & MAUER, W. A. 2013. Equine hoof wall tubule density and morphology. *Journal of Veterinary Medical Science,* 75**,** 773-778.

LANDMAN, M., DE BLAAUW, J., VAN WEEREN, P. & HOFLAND, L. 2004. Field study of the prevalence of foot lameness in horses with back problems. *The Veterinary Record,* 155**,** 165-168.

LANE, H., BURNS, T., HEGEDUS, O., WATTS, M., WEBER, P., WOLTMAN, K., GEOR, R., MCCUTCHEON, L., EADES, S. & MATHES, L. 2017. Lamellar events related to insulin-like growth factor-1 receptor signalling in two models relevant to endocrinopathic laminitis. *Equine Veterinary Journal,* 49, 643-654.

LATINA, A., VITICCHIÈ, G., LENA, A., PIRO, M., ANNICCHIARICO-PETRUZZELLI, M., MELINO, G. & CANDI, E. 2016. ΔNp63 targets

cytoglobin to inhibit oxidative stress-induced apoptosis in keratinocytes and lung cancer. *Oncogene,* 35**,** 1493-1504.

LEACH, D. H. 1980. *The structure and function of the equine hoof wall.* Ph. D. Thesis, University of Saskatchewan. P, 47-49.

LEBLEU, V. S., MACDONALD, B. & KALLURI, R. 2007. Structure and function of basement membranes. *Experimental Biology and Medicine,* 232**,** 1121-1129.

LEE, Y. S., WYSOCKI, A., WARBURTON, D. & TUAN, T. L. 2012. Wound healing in development. *Birth Defects Research Part C: Embryo Today: Reviews,* 96**,** 213-222.

LEISE, B., WATTS, M., ROY, S., YILMAZ, A., ALDER, H. & BELKNAP, J. 2014. Use of laser capture microdissection for the assessment of equine lamellar basal epithelial cell signalling in the early stages of laminitis. *Equine Veterinary Journal*.

LETHBRIDGE, L. A. 2009. *Foot lameness of dairy cattle: factors affecting the mechanical properties, haemorrhage levels, growth and wear rates of bovine claw horn: a thesis presented in partial fulfilment of the requirements of a doctoral degree in Animal Science.* Ph. D. Thesis, Massey University. P, 72-83.

LEWIS, C., NADEAU, J., HOAGLAND, T. & DARRE, M. 2014. Effect of season on travel patterns and hoof growth of domestic horses. *Journal of Equine Veterinary Science,* 34**,** 918-922.

LI, A., SIMMONS, P. J. & KAUR, P. 1998. Identification and isolation of candidate human keratinocyte stem cells based on cell surface phenotype. *Proceedings of the National Academy of Sciences,* 95**,** 3902-3907.

LI, X., CHEN, J., YI, Y., LI, C. & ZHANG, Y. 2012. DNA damage down-regulates ΔNp63α and induces apoptosis independent of wild type p53. *Biochemical and Biophysical Research Communications,* 423**,** 338-343.

LIMA, L. R. D., MENDES, H. M., SORIANI, F. M., SOUZA, D. G. D., ALVES, G. E. S., TEIXEIRA, M. M. & FALEIROS, R. R. 2016. Histologic and inflammatory lamellar changes in horses with oligofructose-induced laminitis treated with a CXCR1/2 antagonist. *Pesquisa Veterinária Brasileira,* 36**,** 13-18.

LIMOUZE, J., STRAIGHT, A. F., MITCHISON, T. & SELLERS, J. R. 2004. Specificity of blebbistatin, an inhibitor of myosin II. *Journal of Muscle Research and Cell Motility,* 25**,** 337-341.

LINARDI, R. L., MEGEE, S. O., MAINARDI, S. R., SENOO, M. & GALANTINO-HOMER, H. L. 2015. Expression and localization of epithelial stem cell and differentiation markers in equine skin, eye and hoof. *Veterinary Dermatology,* 26**,** 213.

LIU, J., ZHAO, Z., LI, J., ZOU, L., SHULER, C., ZOU, Y., HUANG, X., LI, M. & WANG, J. 2009. Hydrostatic pressures promote initial osteodifferentiation with ERK1/2 not p38 MAPK signaling involved. *Journal of Cellular Biochemistry,* 107**,** 224-232.

LIU, M., LAWSON, G., DELOS, M., JAMART, J., IDE, C., COCHE, E., WEYNAND, B., DESUTER, G., HAMOIR, M. & REMACLE, M. 2003. Predictive value of the fraction of cancer cells immunolabeled for proliferating cell nuclear antigen or Ki67 in biopsies of head and neck carcinomas to identify lymph node metastasis: comparison with clinical and radiologic examinations. *Head & neck,* 25**,** 280-288.

LLOYD, C., YU, Q.-C., CHENG, J., TURKSEN, K., DEGENSTEIN, L., HUTTON, E. & FUCHS, E. 1995. The basal keratin network of stratified squamous epithelia: defining K15 function in the absence of K14. *Journal of Cell Biology,* 129**,** 1329-1344.

LOFTUS, J. P., JOHNSON, P. J., BELKNAP, J. K., PETTIGREW, A. & BLACK, S. J. 2009. Leukocyte-derived and endogenous matrix metalloproteinases in the lamellae of horses with naturally acquired and experimentally induced laminitis. *Veterinary Immunology & Immunopathology,* 129**,** 221-230.

LULEVICH, V., YANG, H.-Y., ISSEROFF, R. R. & LIU, G.-Y. 2010. Single cell mechanics of keratinocyte cells. *Ultramicroscopy,* 110**,** 1435-1442.

LYNCH, M. H., O'GUIN, W. M., HARDY, C., MAK, L. & SUN, T.-T. 1986. Acidic and basic hair/nail ("hard") keratins: their colocalization in upper cortical and cuticle cells of the human hair follicle and their relationship to "soft" keratins. *Journal of Cell Biology,* 103**,** 2593-2606.

MACCALLUM, A., KNIGHT, C., HENDRY, K., WILDE, C., LOGUE, D. & OFFER, J. 2002. Effects of time of year and reproductive state on the proliferation and keratinisation of bovine hoof cells. *Veterinary Record,* 151**,** 285-289.

MAGIN, T. M., VIJAYARAJ, P. & LEUBE, R. E. 2007. Structural and regulatory functions of keratins. *Experimental Cell Research,* 313**,** 2021-2032.

MAIOLINO, S. A., KINGSTON, A. K. & LEMELIN, P. 2016. Comparative and Functional Morphology of the Primate Hand Integument. In: Kivell T., Lemelin P., Richmond B., Schmitt D. (eds) *The Evolution of the Primate Hand. Developments in Primatology: Progress and Prospects*. Springer, New York, P, 195-224.

MALIKIDES, N., MCGOWAN, T. & PEAD, M. 2007. Equine and canine foot lameness. *Animal Physiotherapy: Assessment, Treatment and Rehabilitation of Animals***,** 73-101.

MALIYE, S. & MARSHALL, J. F. 2016. Objective assessment of the compensatory effect of clinical hind limb foot lameness in horses: 37 cases (2011–2014). *Journal of the American Veterinary Medical Association,* 249**,** 940-944.

MANI, S. A., GUO, W., LIAO, M.-J., EATON, E. N., AYYANAN, A., ZHOU, A. Y., BROOKS, M., REINHARD, F., ZHANG, C. C. & SHIPITSIN, M. 2008. The epithelial-mesenchymal transition generates cells with properties of stem cells. *Cell,* 133**,** 704-715.

MARSHALL, R., ORWIN, D.-G. & GILLESPIE, J. 1991. Structure and biochemistry of mammalian hard keratin. *Electron microscopy reviews,* 4**,** 47-83.

MARTINVALET, D., ZHU, P. & LIEBERMAN, J. 2005. Granzyme A induces caspase-independent mitochondrial damage, a required first step for apoptosis. *Immunity,* 22**,** 355-370.

MCGOWAN, C. 2008. The role of insulin in endocrinopathic laminitis. *Journal of Equine Veterinary Science,* 28**,** 603-607.

MCGOWAN, C., FROST, R., PFEIFFER, D. & NEIGER, R. 2004. Serum insulin concentrations in horses with equine Cushing's syndrome: response to a cortisol inhibitor and prognostic value. *Equine Veterinary Journal,* 36**,** 295-298.

MCGOWAN, C. M. 2010. Endocrinopathic laminitis. *Veterinary Clinics of North America: Equine Practice,* 26**,** 233-237.

MCKITTRICK, J., CHEN, P.-Y., BODDE, S., YANG, W., NOVITSKAYA, E. & MEYERS, M. 2012. The structure, functions, and mechanical properties of keratin. *The Journal of The Minerals, Metals & Materials Society,* 64**,** 449-468.

MEDINA-TORRES, C. E., MASON, S. L., FLOYD, R. V., HARRIS, P. A. & MOBASHERI, A. 2011. Low oxygen and a low oxygen mimetic up-regulate matrix metalloproteinase 2 and 9 in equine laminar keratinocytes. *The Veterinary Journal,* 190**,** e54-e59.

MERRITT, J., DAVIES, H. & PARKS, A. H. 2016. Digital Biomechanics Relevant to Laminitis. *Equine Laminitis***,** 39-47.

MIH, J. D., MARINKOVIC, A., LIU, F., SHARIF, A. S. & TSCHUMPERLIN, D. J. 2012. Matrix stiffness reverses the effect of actomyosin tension on cell proliferation. *Journal of Cell Science,* 125**,** 5974-5983.

MILLS, J., ZARLENGA, D. & DYER, R. 2009. Bovine coronary region keratinocyte colony formation is supported by epidermal-dermal interactions. *Journal of Dairy Science,* 92**,** 1913-1923.

MISHRA, P. C. & LEACH, D. 1983. Extrinsic and intrinsic veins of the equine hoof wall. *Journal of Anatomy,* 136**,** 543.

MOLEMAN, M., HEEL, M., WEEREN, P. & BACK, W. 2006. Hoof growth between two shoeing sessions leads to a substantial increase of the moment about the distal, but not the proximal, interphalangeal joint. *Equine Veterinary Journal,* 38**,** 170-174.

MOORE, R., EADES, S. & STOKES, A. 2004. Evidence for vascular and enzymatic events in the pathophysiology of acute laminitis: which pathway is responsible for initiation of this process in horses? *Equine Veterinary Journal,* 36**,** 204-209.

MOORE, R. M. & JENNE, M. 2010. Vision 20/20–Conquer laminitis by 2020. *Journal of Equine Veterinary Science,* 30**,** 74-76.

MOORMAN, V. J., REISER II, R. F., PETERSON, M. L., MCILWRAITH, C. W. & KAWCAK, C. E. 2013. Effect of forelimb foot lameness on hoof kinematics of horses at a walk. *American Journal of Veterinary Research,* 74**,** 1192-1197.

MORDAK, R. & ANTHONY, P. S. 2007. The reaction of healthy hooves, claws and nails to a 3% solution of hydrogen peroxide. *Acta Scientiarum Polonorum***,** 33, 323-231.

MORGAN, R. A., KEEN, J. A., WALKER, B. R. & HADOKE, P. W. 2016. Vascular Dysfunction in Horses with Endocrinopathic Laminitis. *PloS One,* 11**,** e0163815.

MORRISON, S. 2010. Chronic laminitis: foot management. *Veterinary Clinics of North America: Equine Practice,* 26**,** 425-446.

MÜLLING, C. K., GREEN, L., BARKER, Z., SCAIFE, J., AMORY, J. & SPEIJERS, M. 2006. Risk factors associated with foot foot lameness in dairy cattle and a suggested approach for foot lameness reduction. *World Buiatrics Congress*.

MÜLLING, C. K. & GREENOUGH, P. R. 2006. Applied physiopathology of the foot. *World Buiatrics Congress,* 103-117.

MUNGALL, B. A. & POLLITT, C. C. 1999. Zymographic analysis of equine laminitis. *Histochemistry and Cell Biology,* 112**,** 467-472.

MURRAY, R. C., WALTERS, J. M., SNART, H., DYSON, S. J. & PARKIN, T. D. H. 2010. Identification of risk factors for foot lameness in dressage horses. *The Veterinary Journal,* 184**,** 27-36.

MUSKHELISHVILI, L., LATENDRESSE, J. R., KODELL, R. L. & HENDERSON, E. B. 2003. Evaluation of cell proliferation in rat tissues with BrdU, PCNA, Ki-67 (MIB-5) immunohistochemistry and in situ hybridization for histone mRNA. *Journal of Histochemistry & Cytochemistry,* 51**,** 1681-1688.

NANBA, D., TOKI, F., MATSUSHITA, N., MATSUSHITA, S., HIGASHIYAMA, S. & BARRANDON, Y. 2013. Actin filament dynamics impacts keratinocyte stem cell maintenance. *EMBO Molecular Medicine,* 5**,** 640-653.

NEWELL-LITWA, K. A., HORWITZ, R. & LAMERS, M. L. 2015. Non-muscle myosin II in disease: mechanisms and therapeutic opportunities. *Disease Models & Mechanisms,* 8**,** 1495-1515.

NIEUWHOF, G. & BISHOP, S. 2005. Costs of the major endemic diseases of sheep in Great Britain and the potential benefits of reduction in disease impact. *Animal Science,* 81**,** 23-29.

NISHIMURA, K., BLUME, P., OHGI, S. & SUMPIO, B. E. 2009. The effect of different frequencies of stretch on human dermal keratinocyte proliferation and survival. *Journal of Surgical Research,* 155**,** 125-131.

NONGA, H., MAKUNGU, M., BITTEGEKO, S. & MPANDUJI, D. 2009. Occurrences and management of foot lameness in goats: A case study of Magadu farm, Morogoro, Tanzania. *Small Ruminant Research,* 82**,** 149-151.

NOSCHKA, E., MOORE, J. N., PERONI, J. F., LEWIS, S. J., MORROW, J. D. & ROBERTSON, T. P. 2009a. Thromboxane and isoprostanes as inflammatory and vasoactive mediators in black walnut heartwood extract induced equine laminitis. *Veterinary Immunology and Immunopathology,* 129**,** 200-210.

NOSCHKA, E., VANDENPLAS, M. L., HURLEY, D. J. & MOORE, J. N. 2009b. Temporal aspects of laminar gene expression during the developmental stages of equine laminitis. *Veterinary Immunology and Immunopathology,* 129**,** 242-253.

O'CALLAGHAN, K. 2002. Lamneness and associated pain in cattle-challenging traditional perceptions. *In Practice,* 24**,** 212-219.

O'CONNOR, S., SOLAZZO, C. & COLLINS, M. 2015. Advances in identifying archaeological traces of horn and other keratinous hard tissues. *Studies in Conservation,* 60**,** 393-417.

O'GRADY, S. 2011. A fresh look at white line disease. *Equine Veterinary Education,* 23**,** 517-522.

O'GRADY, S. & CASTELIJNS, H. 2011. Sheared heels and the correlation to spontaneous quarter cracks. *Equine Veterinary Education,* 23**,** 262-269.

O'GRADY, S. E. 2012. Farriery for the Hoof with a Sheared Heel. *Veterinary Clinics of North America: Equine Practice,* 28**,** 381-392.

ORSINI, J. A. 2011. A Fresh Look at the Process of Arriving at a Clinical Prognosis Part 1: Laminitis. *Journal of Equine Veterinary Science,* 31**,** 194-201.

ORSINI, J. A., WRIGLEY, J. & RILEY, P. 2010. Home care for horses with chronic laminitis. *Veterinary Clinics of North America: Equine Practice,* 26**,** 215-223.

ORTMANN, B., DRUKER, J. & ROCHA, S. 2014. Cell cycle progression in response to oxygen levels. *Cellular and Molecular Life Sciences,* 71**,** 3569-3582.

OTIS, J. S., BURKHOLDER, T. J. & PAVLATH, G. K. 2005. Stretch-induced myoblast proliferation is dependent on the COX2 pathway. *Experimental Cell Research,* 310**,** 417-425.

OTT, E. & JOHNSON, E. 2001. Effect of trace mineral proteinates on growth and skeletal and hoof development in yearling horses. *Journal of Equine Veterinary Science,* 21**,** 287-291.

PALUCH, E. K., NELSON, C. M., BIAIS, N., FABRY, B., MOELLER, J., PRUITT, B. L., WOLLNIK, C., KUDRYASHEVA, G., REHFELDT, F. & FEDERLE, W. 2015. Mechanotransduction: use the force (s). *BMC Biology,* 13**,** 47.

PARK, J.-Y., JUNG, J.-Y., KIM, H.-J., BAE, I.-H., KIM, D.-Y., LEE, T. R. & SHIN, D. W. 2016. Low oxygen leads to abnormal epidermal differentiation via HIF-independent pathways. *Biochemical and Biophysical Research Communications,* 469**,** 251-256.

PARKS, A. 2003. Form and function of the equine digit. *Veterinary Clinics of North America: Equine Practice,* 19**,** 285-307.

PARKS, A. & O'GRADY, S. E. 2003. Chronic laminitis: current treatment strategies. *Veterinary Clinics of North America: Equine Practice,* 19**,** 393-416.

PARKS, A. H. 2016. Structural Dynamics of Displacement of the Distal Phalanx. *Equine Laminitis***,** 176-180.

PASS, M., POLLITT, S. & POLLITT, C. 1998. Decreased glucose metabolism causes separation of hoof lamellae in vitro: a trigger for laminitis? *Equine Veterinary Journal,* 30**,** 133-138.

PAUL, E. K. 2016. *The utilisation of µ-computed tomography for the investigation of equine papilla/lamella-associated foot foot lameness.* MSc, Thesis. The University of Nottingham. 56-60.

PAVLIN, D., DOVE, S., ZADRO, R. & GLUHAK-HEINRICH, J. 2000. Mechanical loading stimulates differentiation of periodontal osteoblasts in a mouse osteoinduction model: effect on type I collagen and alkaline phosphatase genes. *Calcified Tissue International,* 67**,** 163-172.

PAWLAK, E., GEOR, R., WATTS, M., BLACK, S., JOHNSON, P. & BELKNAP, J. 2013. Regulation of low oxygen-inducible factor-1a and related genes in equine digital lamellae and in cultured keratinocytes. *Equine Veteterinary Journal,* 46**,** 203-209.

PEDERSEN, S. F. & NILIUS, B. 2007. Chapter Ten-Transient Receptor Potential Channels in Mechanosensing and Cell Volume Regulation. *Methods in Enzymology,* 428**,** 183-207.

PEKNY, M. & LANE, E. B. 2007. Intermediate filaments and stress. *Experimental Cell Research,* 313**,** 2244-2254.

PELLEGRINI, G., DELLAMBRA, E., GOLISANO, O., MARTINELLI, E., FANTOZZI, I., BONDANZA, S., PONZIN, D., MCKEON, F. & DE LUCA, M. 2001. p63 identifies keratinocyte stem cells. *Proceedings of the National Academy of Sciences,* 98**,** 3156-3161.

PERONI, J., HARRISON, W., MOORE, J., GRAVES, J., LEWIS, S., KRUNKOSKY, T. & ROBERTSON, T. 2005. Black walnut extract-induced laminitis in horses is associated with heterogeneous dysfunction of the laminar microvasculature. *Equine Veterinary Journal,* 37**,** 546-551.

PFAFFL, M. W. 2001. A new mathematical model for relative quantification in real-time RT–PCR. *Nucleic Acids Research,* 29**,** e45-e45.

PINTO, V. M. R. 2012. *Isolation and Characterization of Adult Progenitor Cells From Healthy and Laminitic Hoof Tissue.* MSc., Thesis. Louisiana State University , P, 78-89.

POLLITT, C. 1990. An autoradiographic study of equine hoof growth. *Equine Veteterinry Journal,* 22**,** 366-368.

POLLITT, C. 1994. The basement membrane at the equine hoof dermal epidermal junction. *Equine Veterinary Journal,* 26**,** 399-407.

POLLITT, C. 1996. Basement membrane pathology: a feature of acute equine laminitis. *Equine Veterinary Journal,* 28**,** 38-46.

POLLITT, C. 1998. The anatomy and physiology of the hoof wall. *Equine Veterinary Education,* 10**,** 318-325.

POLLITT, C. & BLAKE-CADDEL, L. 1991. The role of arteriovenous anastomoses in the pathophysiology of equine laminitis. *Proceedings of the Annual Convention of the American Association of Equine Practitioners,*. 711-720.

POLLITT, C. & COLLINS, S. 2013. The suspensory apparatus of the distal phalanx (SADP). *Journal of Equine Veterinary Science,* 33**,** 874-876.

POLLITT, C. & COLLINS, S. 2016. The suspensory apparatus of the distal phalanx in normal horses. *Equine Veterinary Journal,* 48**,** 496-501.

POLLITT, C. C. 2004a. Anatomy and physiology of the inner hoof wall. *Clinical Techniques in Equine Practice,* 3**,** 3-21.

POLLITT, C. C. 2004b. Equine laminitis. *Clinical Techniques in Equine Practice,* 3**,** 34-44.

POLLITT, C. C. 2010. The Anatomy and Physiology of the Suspensory Apparatus of the Distal Phalanx. *Veterinary Clinics of North America: Equine Practice,* 26**,** 29-49.

POLLITT, C. C. 2016. Dysregulation of the Lamellar Basal Epithelial Cell in Laminitis: Role of the Cytoskeleton and Cell Junctions. *Equine Laminitis***,** 43, 167-172.

POLLITT, C. C. & VISSER, M. B. 2010. Carbohydrate Alimentary Overload Laminitis. *Veterinary Clinics of North America: Equine Practice,* 26**,** 65-78.

PONTA, H., SHERMAN, L. & HERRLICH, P. A. 2003. CD44: from adhesion molecules to signalling regulators. *Nature reviews Molecular Cell Biology,* 4**,** 33-45.

PORTER, R. M. & LANE, E. B. 2003. Phenotypes, genotypes and their contribution to understanding keratin function. *Trends in Genetics,* 19**,** 278-285.

PORTER, R. M., LUNNY, D. P., OGDEN, P. H., MORLEY, S. M., MCLEAN, W. I., EVANS, A., HARRISON, D. L., RUGG, E. L. & LANE, E. B. 2000. K15 expression implies lateral differentiation within stratified epithelial basal cells. *Laboratory Lnvestigation,* 80**,** 1701-1710.

POUMAY, Y. & PITTELKOW, M. R. 1995. Cell density and culture factors regulate keratinocyte commitment to differentiation and expression of suprabasal K1/K10 keratins. *Journal of Investigative Dermatology,* 104**,** 271-276.

RAJ, D., BRASH, D. E. & GROSSMAN, D. 2006. Keratinocyte apoptosis in epidermal development and disease. *Journal of Investigative Dermatology,* 126**,** 243-257.

RAMMS, L., FABRIS, G., WINDOFFER, R., SCHWARZ, N., SPRINGER, R., ZHOU, C., LAZAR, J., STIEFEL, S., HERSCH, N. & SCHNAKENBERG, U. 2013. Keratins as the main component for the mechanical integrity of keratinocytes. *Proceedings of the National Academy of Sciences,* 110**,** 18513-18518.

RAMSEY, G. 2011. *Equine hoof biomechanics.* Ph. D. Thesis. The University of Auckland, P, 56-74.

RAMSEY, G., HUNTER, P. & NASH, M. 2011. The effect of hoof angle variations on dorsal lamellar load in the equine hoof. *Equine Veterinary Journal,* 43**,** 536-542.

RAMSEY, G. D., HUNTER, P. J. & NASH, M. P. 2012. The influence of tissue hydration on equine hoof capsule deformation and energy storage assessed using finite element methods. *Biosystems Engineering,* 111**,** 175-185.

RAMSEY, G. D., HUNTER, P. J. & NASH, M. P. 2013. The influence of loading conditions on equine hoof capsule deflections and stored energy assessed by finite element analysis. *Biosystems Engineering,* 115**,** 283-290.

RANGARAJAN, A., TALORA, C., OKUYAMA, R., NICOLAS, M., MAMMUCARI, C., OH, H., ASTER, J. C., KRISHNA, S., METZGER, D. & CHAMBON, P. 2001. Notch signaling is a direct determinant of keratinocyte growth arrest and entry into differentiation. *The European Molecular Biology Organization Journal,* 20**,** 3427-3436.

RAPISARDA, V. 2015. *Mechanisms of epigenetic regulation in epidermal keratinocytes during skin development. Role of p63 transcription factor in the establishment of lineage-specific gene expression programs in keratinocytes via regulation of nuclear envelope-associated genes and Polycomb chromatin remodelling factors.* Ph. D. Thesis. University of Bradford, P, 79-88.

RAUCH, C. & CHERKAOUI-RBATI, M. 2014. Physics of nail conditions: why do ingrown nails always happen in the big toes? *Physical Biology,* 11**,** 066004.

REDDEN, R. F. 2003. Hoof capsule distortion: understanding the mechanisms as a basis for rational management. *Veterinary Clinics of North America: Equine Practice,* 19**,** 443-462.

REEVES, H., LEES, R. & MCGOWAN, C. 2001. Measurement of basal serum insulin concentration in the diagnosis of Cushing's disease in ponies. *The Veterinary Record,* 149**,** 449-452.

REICHELT, J. 2007. Mechanotransduction of keratinocytes in culture and in the epidermis. *European journal of Cell Biology,* 86**,** 807-816.

REILLY, J., COLLINS, S., COPE, B., HOPEGOOD, L. & LATHAM, R. 1998a. Tubule density of the stratum medium of horse hoof. *Equine Veterinary Journal,* 30**,** 4-9.

REILLY, J., COTTRELL, D., MARTIN, R. & CUDDEFORD, D. 1996. Tubule density in equine hoof horn. *Biomimetics,* 4**,** 23-36.

REILLY, J., COTTRELL, D., MARTIN, R. & CUDDEFORD, D. 1998b. Effect of supplementary dietary biotin on hoof growth and hoof growth rate in ponies: a controlled trial. *Equine Veterinary Journal,* 30**,** 51-57.

RITMEESTER, A., BLEVINS, W., FERGUSON, D. & ADAMS, S. 1998. Digital perfusion, evaluated scintigraphically, and hoof wall growth in horses with chronic laminitis treated with egg bar-heart bar shoeing and coronary grooving. *Equine Veterinary Journal,* 30**,** 111-118.

ROBERTSON, D., SAVAGE, K., REIS-FILHO, J. S. & ISACKE, C. M. 2008. Multiple immunofluorescence labelling of formalin-fixed paraffin-embedded (FFPE) tissue. *BMC Cell Biology,* 9**,** 13.

RODGERS, K. E., ELLEFSON, D. D., ESPINOZA, T., RODA, N., MALDONADO, S. & DIZEREGA, G. S. 2005. Effect of NorLeu3-A (1-7) on scar formation over time after full-thickness incision injury in the rat. *Wound Repair and Regeneration,* 13**,** 309-317.

RODRIGUEZ, P. G., FELIX, F. N., WOODLEY, D. T. & SHIM, E. K. 2008. The role of oxygen in wound healing: a review of the literature. *Dermatologic Surgery,* 34**,** 1159-1169.

ROMANO, R.-A., ORTT, K., BIRKAYA, B., SMALLEY, K. & SINHA, S. 2009. An active role of the ΔN isoform of p63 in regulating basal keratin genes K5 and K14 and directing epidermal cell fate. *PloS One,* 4**,** e5623.

ROMANO, R.-A., SMALLEY, K., MAGRAW, C., SERNA, V. A., KURITA, T., RAGHAVAN, S. & SINHA, S. 2012. ΔNp63 knockout mice reveal its indispensable role as a master regulator of epithelial development and differentiation. *Development,* 139**,** 772-782.

ROSS, M. W. & DYSON, S. J. 2010. Diagnosis and Management of Foot lameness in the Horse. *Health Sciences*, 36, 549-554.

ROUSE, J. G. & VAN DYKE, M. E. 2010. A review of keratin-based biomaterials for biomedical applications. *Materials,* 3**,** 999-1014.

RUSSELL, D., ANDREWS, P. D., JAMES, J. & LANE, E. B. 2004. Mechanical stress induces profound remodelling of keratin filaments and cell junctions in epidermolysis bullosa simplex keratinocytes. *Journal of Cell Science,* 117**,** 5233-5243.

RYAN, T. 2013. Dorsal hoof wall grooving for the treatment of acute laminitis. *Journal of Equine Veterinary Science,* 33**,** 877.

SAHA, S., JI, L., DE PABLO, J. J. & PALECEK, S. P. 2006. Inhibition of human embryonic stem cell differentiation by mechanical strain. *Journal of Cellular Physiology,* 206**,** 126-137.

SALO, Z., THOMASON, J. & RUNCIMAN, R. 2010. Analysis of strain and stress in the equine hoof using finite element analysis: comparison with minimum principal strains recorded in vivo. *Biosystems Engineering,* 107**,** 262-270.

SAMUEL, M. S., LOPEZ, J. I., MCGHEE, E. J., CROFT, D. R., STRACHAN, D., TIMPSON, P., MUNRO, J., SCHRÖDER, E., ZHOU, J. & BRUNTON, V. G. 2011. Actomyosin-mediated cellular tension drives increased tissue stiffness and β-catenin activation to induce epidermal hyperplasia and tumor growth. *Cancer Cell,* 19**,** 776-791.

SANCHEZ-ESTEBAN, J., CICCHIELLO, L. A., WANG, Y., TSAI, S.-W., WILLIAMS, L. K., TORDAY, J. S. & RUBIN, L. P. 2001. Mechanical stretch promotes alveolar epithelial type II cell differentiation. *Journal of Applied Physiology,* 91**,** 589-595.

SANDER, R. 2015. Compilation of Henry's law constants (version 4.0) for water as solvent. *Atmospheric Chemistry & Physics,* 15 4399–4981.

SARKAR, S., EGELHOFF, T. & BASKARAN, H. 2009. Insights into the roles of non-muscle myosin IIA in human keratinocyte migration. *Cellular and Molecular Bioengineering,* 2**,** 486.

SARRATT, S. M. & HOOD, D. M. 2005. Evaluation of architectural changes along the proximal to distal regions of the dorsal laminar interface in the equine hoof. *American journal of Veterinary Research,* 66**,** 277-283.

SCHOLZEN, T. & GERDES, J. 2000. The Ki-67 protein: from the known and the unknown. *Journal of Cellular Physiology,* 182**,** 311-322.

SCHÖPKE, K., WEIDLING, S., PIJL, R. & SWALVE, H. 2013. Relationships between bovine hoof disorders, body condition traits, and test-day yields. *Journal of Dairy Science,* 96**,** 679-689.

SEINFELD, J. H. & PANDIS, S. N. 2016. *Atmospheric chemistry and physics: from air pollution to climate change*, John Wiley & Sons, P, 763-767.

SEITZINGER, A. H., TRAUB-DARGATZ, J., KANE, A., KOPRAL, C., MORLEY, P., GARBER, L., LOSINGER, W. & HILL, G. A comparison of the economic costs of equine foot lameness, colic, and equine protozoal myeloencephalitis (EPM). *Proceedings,* 2000. 1048-1050.

SELTMANN, K., FRITSCH, A. W., KÄS, J. A. & MAGIN, T. M. 2013. Keratins significantly contribute to cell stiffness and impact invasive behavior. *Proceedings of the National Academy of Sciences,* 110**,** 18507-18512.

SENOO, M., PINTO, F., CRUM, C. P. & MCKEON, F. 2007. p63 Is essential for the proliferative potential of stem cells in stratified epithelia. *Cell,* 129**,** 523-536.

SHARMA, R., BARAKZAI, S. Z., TAYLOR, S. E. & DONADEU, F. X. 2016. Epidermal-like architecture obtained from equine keratinocytes in three-dimensional cultures. *Journal of Tissue Engineering and Regenerative Medicine,* 10**,** 627-636.

SHERLOCK, C. & PARKS, A. 2013. Radiographic and radiological assessment of laminitis. *Equine Veterinary Education,* 25**,** 524-535.

SHUTOVA, M., YANG, C., VASILIEV, J. M. & SVITKINA, T. 2012. Functions of nonmuscle myosin II in assembly of the cellular contractile system. *PloS One,* 7**,** e40814.

SIMS, J. R., KARP, S. & INGBER, D. E. 1992. Altering the cellular mechanical force balance results in integrated changes in cell, cytoskeletal and nuclear shape. *Journal of Cell Science,* 103**,** 1215-1222.

SINGH, S., MURRAY, R. & WARD, W. 1992. Histopathological and morphometric studies on the hooves of dairy and beef cattle in relation to overgrown sole and laminitis. *Journal of Comparative Pathology,* 107**,** 319-328.

SIRGHI, L., PONTI, J., BROGGI, F. & ROSSI, F. 2008. Probing elasticity and adhesion of live cells by atomic force microscopy indentation. *European Biophysics Journal with Biophysics Letters,* 37**,** 935-945.

SONG, L., ZHANG, J., WU, S., HUANG, Y., ZHAO, Q., CAO, J., WU, Y., WANG, L. & CHEN, G. 2008. Low oxygen-inducible factor-1α-induced differentiation of myeloid leukemic cells is its transcriptional activity independent. *Oncogene,* 27**,** 519.

SPEDDEN, E., WHITE, J. D., NAUMOVA, E. N., KAPLAN, D. L. & STAII, C. 2012. Elasticity Maps of Living Neurons Measured by Combined Fluorescence and Atomic Force Microscopy. *Biophysical Journal,* 103**,** 868-877.

STEWART, A. J., PETTIGREW, A., COCHRAN, A. M. & BELKNAP, J. K. 2009. Indices of inflammation in the lung and liver in the early stages of the black walnut extract model of equine laminitis. *Veterinary Immunology and Immunopathology,* 129**,** 254-260.

STEWART, J. 2013. *Understanding the Horse's Feet*, The Crowood Press.Wiltshire, P, 32-45.

STRAIGHT, A. F., CHEUNG, A., LIMOUZE, J., CHEN, I., WESTWOOD, N. J., SELLERS, J. R. & MITCHISON, T. J. 2003. Dissecting temporal and spatial control of cytokinesis with a myosin II Inhibitor. *Science,* 299**,** 1743-1747.

STÜCKER, M., STRUK, A., ALTMEYER, P., HERDE, M., BAUMGÄRTL, H. & LÜBBERS, D. W. 2002. The cutaneous uptake of atmospheric oxygen contributes significantly to the oxygen supply of human dermis and epidermis. *The Journal of Physiology,* 538**,** 985-994.

STUDER, L., CSETE, M., LEE, S.-H., KABBANI, N., WALIKONIS, J., WOLD, B. & MCKAY, R. 2000. Enhanced proliferation, survival, and dopaminergic differentiation of CNS precursors in lowered oxygen. *Journal of Neuroscience,* 20**,** 7377-7383.

SWAILES, N. T., COLEGRAVE, M., KNIGHT, P. J. & PECKHAM, M. 2006. Non-muscle myosins 2A and 2B drive changes in cell morphology that occur as myoblasts align and fuse. *Journal Cell Science,* 119**,** 3561-3570.

TANI, H., MORRIS, R. J. & KAUR, P. 2000. Enrichment for murine keratinocyte stem cells based on cell surface phenotype. *Proceedings of the National Academy of Sciences,* 97**,** 10960-10965.

TAYLOR, G., LEHRER, M. S., JENSEN, P. J., SUN, T.-T. & LAVKER, R. M. 2000. Involvement of follicular stem cells in forming not only the follicle but also the epidermis. *Cell,* 102**,** 451-461.

THIEME, K., EHRLE, A. & LISCHER, C. 2015. Radiographic measurements of the hooves of normal ponies. *The Veterinary Journal,* 206**,** 332-337.

THOMASON, J. 1998. Variation in surface strain on the equine hoof wall at the midstep with shoeing, gait, substrate, direction of travel, and hoof shape. *Equine Veterinary Journal,* 30**,** 86-95.

THOMASON, J., BIEWENER, A. & BERTRAM, J. 1992. Surface strain on the equine hoof wall in vivo: implications for the material design and functional morphology of the wall. *Journal of Experimental Biology,* 166**,** 145-168.

THOMASON, J., BIGNELL, W., BATISTE, D. & SEARS, W. 2004. Effects of hoof shape, body mass and velocity on surface strain in the wall of the unshod forehoof of Standardbreds trotting on a treadmill. *Equine and Comparative Exercise Physiology,* 1**,** 87-97.

THOMASON, J., FARAMARZI, B., REVILL, M. A. & SEARS, W. 2008. Quantitative morphology of the equine laminar junction in relation to capsule shape in the forehoof of Standardbreds and Thoroughbreds. *Equine Veterinary Journal,* 40**,** 473-480.

THOMASON, J., MCCLINCHEY, H. & JOFRIET, J. 2002. Analysis of strain and stress in the equine hoof capsule using finite element methods: comparison with principal strains recorded in vivo. *Equine Veterinary Journal,* 34**,** 719-725.

THOMASON, J. J., MCCLINCHEY, H. L., FARAMARZI, B. & JOFRIET, J. C. 2005. Mechanical behavior and quantitative morphology of the equine laminar junction. *The Anatomical Record Part A: Discoveries in Molecular, Cellular, and Evolutionary Biology,* 283A**,** 366-379.

THOMASON, J. J. & PETERSON, M. L. 2008. Biomechanical and mechanical investigations of the hoof-track interface in racing horses. *Veterinary Clinics of North America: Equine Practice,* 24**,** 53-77.

TOKUYAMA, E., NAGAI, Y., TAKAHASHI, K., KIMATA, Y. & NARUSE, K. 2015. Mechanical stretch on human skin equivalents increases the epidermal thickness and develops the basement membrane. *PloS One,* 10**,** e0141989.

TOMBOLATO, L., NOVITSKAYA, E. E., CHEN, P.-Y., SHEPPARD, F. A. & MCKITTRICK, J. 2010. Microstructure, elastic properties and deformation mechanisms of horn keratin. *Acta Biomaterialia,* 6**,** 319-330.

TOMIC-CANIC, M., KOMINE, M., FREEDBERG, I. M. & BLUMENBERG, M. 1998. Epidermal signal transduction and transcription factor activation in activated keratinocytes. *Journal of Dermatological Science,* 17**,** 167-181.

TOMLINSON, D., MÜLLING, C. & FAKLER, T. 2004. Formation of Keratins in the Bovine Claw: Roles of Hormones, Minerals, and Vitamins in Functional Claw Integrity. *Journal of Dairy Science,* 87**,** 797-809.

TROTTER, G. W. 2004. Hoof balance in equine foot lameness. *Journal of Equine Veterinary Science,* 24**,** 494-495.

TRUONG, A. B., KRETZ, M., RIDKY, T. W., KIMMEL, R. & KHAVARI, P. A. 2006. p63 regulates proliferation and differentiation of developmentally mature keratinocytes. *Genes & Development,* 20**,** 3185-3197.

TUMBAR, T., GUASCH, G., GRECO, V., BLANPAIN, C., LOWRY, W. E., RENDL, M. & FUCHS, E. 2004. Defining the epithelial stem cell niche in skin. *Science,* 303**,** 359-363.

UHLIR, C., LICA, T., KÜBBER, P., PEHAM, C., SCHEIDL, M. & GIRTLER, D. 1997. Compensatory movements of horses with a stance phase foot lameness. *Equine Veterinary Journal,* 29**,** 102-105.

UPRICHARD, K., BODEN, L. & MARSHALL, J. 2014. An Online Survey to Characterise Spending Patterns of Horse Owners and to Quantify the Impact of Equine Foot lameness on a Pleasure Horse Population. *Equine Veterinary Journal,* 46**,** 4-4.

UYEDA, T. Q., IWADATE, Y., UMEKI, N., NAGASAKI, A. & YUMURA, S. 2011. Stretching actin filaments within cells enhances their affinity for the myosin II motor domain. *PloS One,* 6**,** e26200.

VAN ASPEREN, E. N. 2010. Ecomorphological adaptations to climate and substrate in late Middle Pleistocene caballoid horses. *Palaeogeography, Palaeoclimatology, Palaeoecology,* 297**,** 584-596.

VAN ASPEREN, E. N. 2012. Late Middle Pleistocene horse fossils from northWestern Europe as biostratigraphic indicators. *Journal of Archaeological Science,* 39**,** 1974-1983.

VAN HEEL, M. C., VAN WEEREN, P. R. & BACK, W. 2006. Compensation for changes in hoof conformation between shoeing sessions through the adaptation of angular kinematics of the distal segments of the limbs of horses. *American Journal of Veterinary Research,* 67**,** 1199-1203.

VAN HEMERT, C., HANDEL, C. M., BLAKE, J. E., SWOR, R. M. & O'HARA, T. M. 2012. Microanatomy of passerine hard-cornified tissues: Beak and claw structure of the black-capped chickadee (Poecile atricapillus). *Journal of Morphology,* 273**,** 226-240.

VERMUNT, J. 1992. Subclinical laminitis in dairy cattle. *New Zealand Veterinary Journal,* 40**,** 133-138.

VERMUNT, J. & GREENOUGH, P. 1994. Predisposing factors of laminitis in cattle. *British Veterinary Journal,* 150**,** 151-164.

VERMUNT, J. & GREENOUGH, P. 1995. Structural characteristics of the bovine claw: horn growth and wear, horn hardness and claw conformation. *British Veterinary Journal,* 151**,** 157-180.

VICENTE-MANZANARES, M., MA, X., ADELSTEIN, R. S. & HORWITZ, A. R. 2009. Non-muscle myosin II takes centre stage in cell adhesion and migration. *Nature reviews. Molecular Cell Biology,* 10**,** 778.

VISSER, M. & POLLITT, C. 2011. The timeline of lamellar basement membrane changes during equine laminitis development. *Equine Veterinary Journal,* 43**,** 471-477.

VISSER, M. B. & POLLITT, C. C. 2010. Characterization of extracellular matrix macromolecules in primary cultures of equine keratinocytes. *BMC Veterinary Research,* 6**,** 16.

WAGNER, A. E. 2010. Effects of stress on pain in horses and incorporating pain scales for equine practice. *Veterinary Clinics of North America: Equine Practice,* 26**,** 481-492.

WAGNER, B. A., VENKATARAMAN, S. & BUETTNER, G. R. 2011. The rate of oxygen utilization by cells. *Free Radic Biolological Mededicine,* 51**,** 700-12.

WALTER, N., BUSCH, T., SEUFFERLEIN, T. & SPATZ, J. P. 2011. Elastic moduli of living epithelial pancreatic cancer cells and their skeletonized keratin intermediate filament network. *Biointerphases,* 6**,** 79-85.

WANG, B. 2016. *Structural and Functional Design Strategies of Biological Keratinous Materials*. Ph. D., Thesis. University of California. P, 36-73.

WANG, C., SHAN, S., WANG, C., WANG, J., LI, J., HU, G., DAI, K., LI, Q. & ZHANG, X. 2017. Mechanical stimulation promote the osteogenic differentiation of bone marrow stromal cells through epigenetic regulation of Sonic Hedgehog. *Experimental Cell Research,* 352**,** 346-356.

WANG, L., PAWLAK, E. A., JOHNSON, P. J., BELKNAP, J. K., EADES, S., STACK, S., COUSIN, H. & BLACK, S. J. 2013. Impact of laminitis on the canonical Wnt signaling pathway in basal epithelial cells of the equine digital laminae. Plos One, 8, e56025.

WANG, W., WINLOVE, C. & MICHEL, C. 2003. Oxygen partial pressure in outer layers of skin of human finger nail folds. *The Journal of Physiology,* 549**,** 855-863.

WASEEM, A., ALAM, Y., LALLI, A., DOGAN, B., TIDMAN, N., PURKIS, P., JACKSON, S., MACHESNEY, M. & LEIGH, I. M. 1999. Keratin 15 expression in stratified epithelia: downregulation in activated keratinocytes. *Journal of Investigative Dermatology,* 112**,** 362-369.

WEBB, A., LI, A. & KAUR, P. 2004. Location and phenotype of human adult keratinocyte stem cells of the skin. *Differentiation,* 72**,** 387-395.

WEISHAUPT, M., WIESTNER, T., HOGG, H., JORDAN, P. & AUER, J. 2004. Compensatory load redistribution of horses with induced weightbearing hindlimb foot lameness trotting on a treadmill. *Equine Veterinary Journal,* 36**,** 727-733.

WEISHAUPT, M. A. 2008. Adaptation strategies of horses with foot lameness. *Veterinary Clinics of North America: Equine Practice,* 24**,** 79-100.

WHITE, S. D., AFFOLTER, V. K., BANNASCH, D. L., SCHULTHEISS, P. C., HAMAR, D. W., CHAPMAN, P. L., NAYDAN, D., SPIER, S. J., ROSYCHUK, R. A. & REES, C. 2004. Hereditary equine regional dermal asthenia (‘hyperelastosis cutis’) in 50 horses: clinical, histological, immunohistological and ultrastructural findings. *Veterinary Dermatology,* 15**,** 207-217.

WHITTON, C. 2016. Equine foot lameness. *Animal Physiotherapy: Assessment, Treatment and Rehabilitation of Animals*. *Ed*. McGowan, C. M. Blackwell Publishing, P, 73-84.

WIGGERS, N., NAUWELAERTS, S. L., HOBBS, S. J., BOOL, S., WOLSCHRIJN, C. F. & BACK, W. 2015. Functional locomotor consequences of uneven forefeet for trot symmetry in individual riding horses. *PloS One,* 10**,** e0114836.

WILLIAMS, K., MOTIANI, K., GIRIDHAR, P. V. & KASPER, S. 2013. CD44 integrates signaling in normal stem cell, cancer stem cell and (pre) metastatic niches. *Experimental Biology and Medicine,* 238**,** 324-338.

WINTER, A. 2008. Foot lameness in sheep. *Small Ruminant Research,* 76**,** 149-153.

WU, P., HOU, L., PLIKUS, M., HUGHES, M., SCEHNET, J., SUKSAWEANG, S., WIDELITZ, R. B., JIANG, T.-X. & CHUONG, C.-M. 2004. Evo-Devo of amniote integuments and appendages. *The International Journal of Developmental Biology,* 48**,** 249.

WYLIE, C. E., COLLINS, S. N., VERHEYEN, K. L. & NEWTON, J. R. 2011. Frequency of equine laminitis: a systematic review with quality appraisal of published evidence. *The Veterinary Journal,* 189**,** 248-256.

YAMAMOTO, Y., FUJITA, M., TANAKA, Y., KOJIMA, I., KANATANI, Y., ISHIHARA, M. & TACHIBANA, S. 2013. Low Oxygen Tension Enhances Proliferation and Maintains Stemness of Adipose Tissue–Derived Stromal Cells. *Biological Research,* 2**,** 199-205.

YANO, S., KOMINE, M., FUJIMOTO, M., OKOCHI, H. & TAMAKI, K. 2004. Mechanical stretching in vitro regulates signal transduction pathways and cellular proliferation in human epidermal keratinocytes. *Journal of Investigative Dermatology,* 122**,** 783-790.

YIP, W. L. 2015. Influence of oxygen on wound healing. *International Wound Journal,* 12**,** 620-624.

YU, X. M., LI, C. W., CHAO, S. S., LI, Y. Y., YAN, Y., ZHAO, X. N., YU, F. G., LIU, J., SHEN, L. & PAN, X. L. 2014. Reduced growth and proliferation dynamics of nasal epithelial stem/progenitor cells in nasal polyps in vitro. *Scientific Reports,* 4, 4619.

ZHANG, H., ZHANG, S., ZHAO, H., QIAO, J., LIU, S., DENG, Z., LEI, X., NING, L., CAO, Y. & ZHAO, Y. 2015. Ovine hair follicle stem cells derived from single vibrissae reconstitute haired skin. *International Journal of Molecular Sciences,* 16**,** 17779-17797.

ZHANG, M. & RAO, P. V. 2005. Blebbistatin, a novel inhibitor of myosin II ATPase activity, increases aqueous humor outflow facility in perfused enucleated porcine eyes. *Investigative Ophthalmology & Visual Science,* 46**,** 4130-4138.

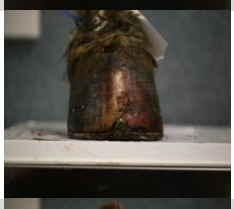
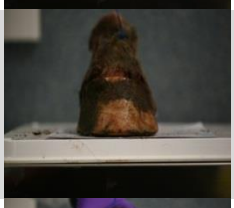
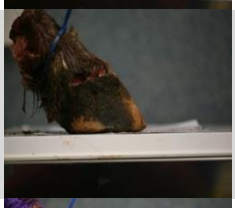
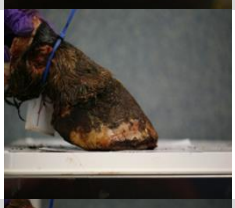
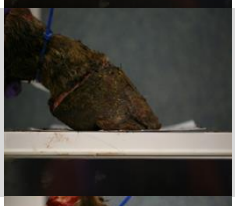
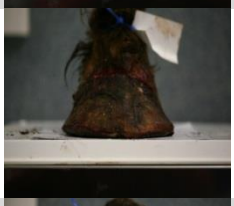
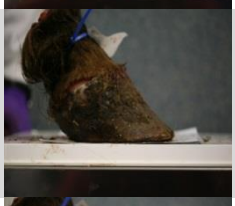
ZHAO, Y.-H., LV, X., LIU, Y.-L., ZHAO, Y., LI, Q., CHEN, Y.-J. & ZHANG, M. 2015. Hydrostatic pressure promotes the proliferation and osteogenic/chondrogenic differentiation of mesenchymal stem cells: The roles of RhoA and Rac1. *Stem Cell Research,* 14**,** 283-296.

ZHOU, J., WANG, J., ZHANG, N., ZHANG, Y. & LI, Q. 2015. Identification of biomechanical force as a novel inducer of epithelial-mesenchymal transition features in mechanical stretched skin. *American Journal of Translational Research,* 7**,** 2187.

ZHOU, Z. L., NGAN, A. H. W., TANG, B. & WANG, A. X. 2012. Reliable measurement of elastic modulus of cells by nanoindentation in an atomic force microscope. *Journal of the Mechanical Behavior of Biomedical Materials,* 8**,** 134-142.

8 Appendices

8.1 An example of equine feet images

Hoof name	Dorsal view	Lateral view	Medial view
Hoof 1			
Hoof 2			
Hoof 3			
Hoof 4			
Hoof 5			
Hoof 6			
Hoof 7			
Hoof 8			

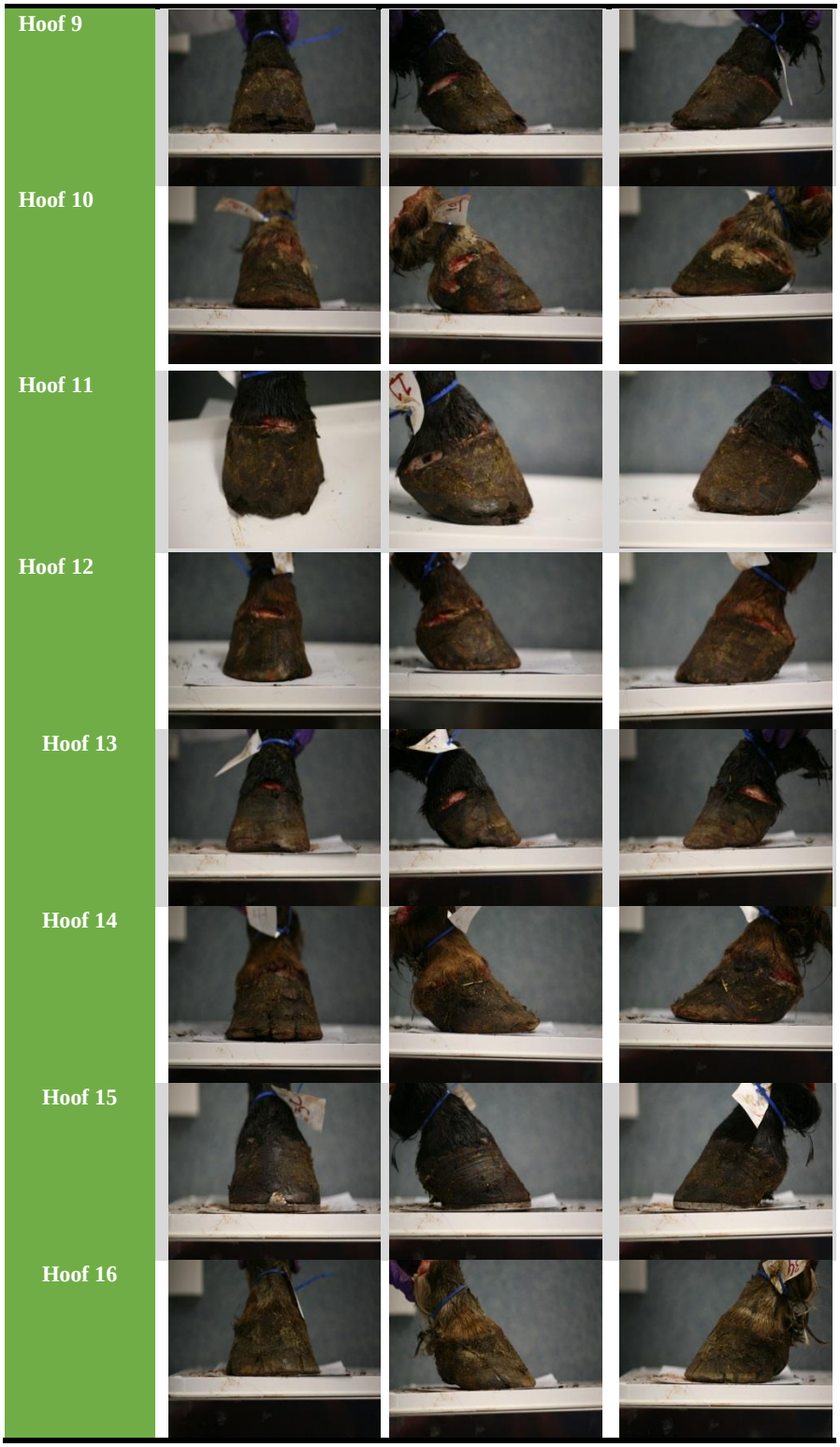


Figure 8-1: Photographs of equine feet

Photographs illustrating the different hoof capsule shape taken from the dorsal, medial, and lateral views.

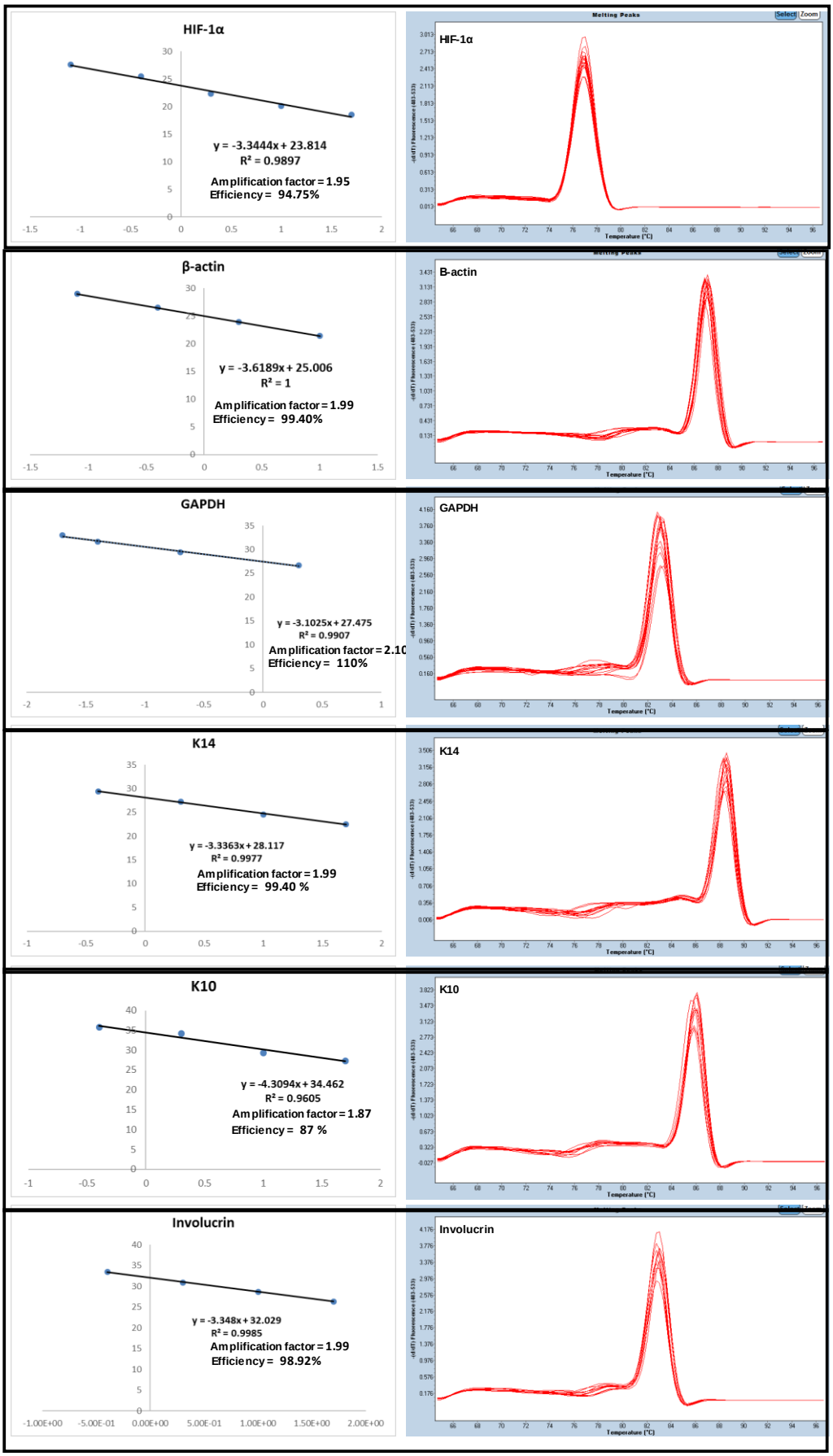
8.2 Experimental design

Experimental name	Number of the hooves were used in each experiment
Chapter 3	
Counting the number of dermal papillae	15
Measure the diameter of dermal papillae	3
Measure the changes in cell size	3
Measure epithelial thickness	16
Measure hoof wall thickness	13
Basement membrane thickness	11
The amount of collagen fibres	12
The frequency of p63 +ve cells against papillae length	7
The frequency of Ki-67 +ve cells against papillae length	7
The frequency of TUNEL apoptotic +ve cells against papillae length	7
Chapter 4	
Assessment of the influence of blebbistatin on cytoskeletal EPKs	3, each in triplicate
Assessment of EPKs pluripotency during cell passages	3, each in triplicate
Osteogenesis of EPKs	3, each in triplicate
The influence of hydrostatic pressure on EPKs	3, each in triplicate
Stretch of EPKs after incubation for 24hrs with blebbistatin	3, each in triplicate
Stretch of EPKs incubated with blebbistatin	3, each in triplicate
Stretch of EPKs without blebbistatin	3, each in triplicate
Stretch of EPKs after 10 days of culture	3, each in triplicate
EKPs assessment under 1% oxygen levels	3, each in triplicate
EKPs assessment under 3% oxygen levels	3, each in triplicate
EKPs assessment under 5% oxygen levels	3, each in triplicate
Assessment gene expression under 5% O2	3, each in triplicate
Assessment the impact of insulin on equine hoof culture keratinocytes	3, each in triplicate
Assessment the PI3k/Akt pathway in cultured keratinocytes treated with Insulin	3, each in triplicate
Chapter 5	
Evaluation of staining patterns of PCNA +ve cells	12
Assessment of the expression of Ki-67 proliferation antibody	17
Assessment the localization of stem progenitor keratinocytes p63	22
Variation between the percentage p63 and Ki-67 +ve cells	17
Expression of epithelial cell marker K14 in equine hoof papillae	17
The comparisons between Ki-67 and K14 expression levels and the hoof curvatures	17
The comparisons between p63 and K14 expression levels and the hoof curvatures	17
Assessment of TUNEL apoptotic +ve cells at the dermal coronary region	17
The correlation between the ratio of Ki-67 or p63 to TUNEL positive cells	17
The influence of the degree of hoof curvature on epithelium thickness	17
Contact hoof angle	25
CT scan image for hoof curvature	22
CT scan image for hoof curvature	22

8.3 Collagenase digest

Collagenase digest was previously prepared from 1% Bovine Serum Albumin (BSA, Fisher Scientific, UK). BSA was prepared by mixing 0.5gm BSA/ 50ml DMEM-F-12 (w/v) and filtered using 50ml Falcon tube, 50ml syringe and 0.22µm filter unit) and 0.1% collagenase type-1 (collagenase from Clostridium histolyticum Type I, Sigma, USA) in 50ml DMEM-F-12 (Dulbecco's Modified Eagle's Medium/Nutrient Mixture F-12 Ham with L-glutamine, 15 mM HEPES, sodium bicarbonate, Sigma-Aldrichand, Uk, and 2% antibiotic/antimycotic Gibco, UK).

8.4 The efficiency of the primers



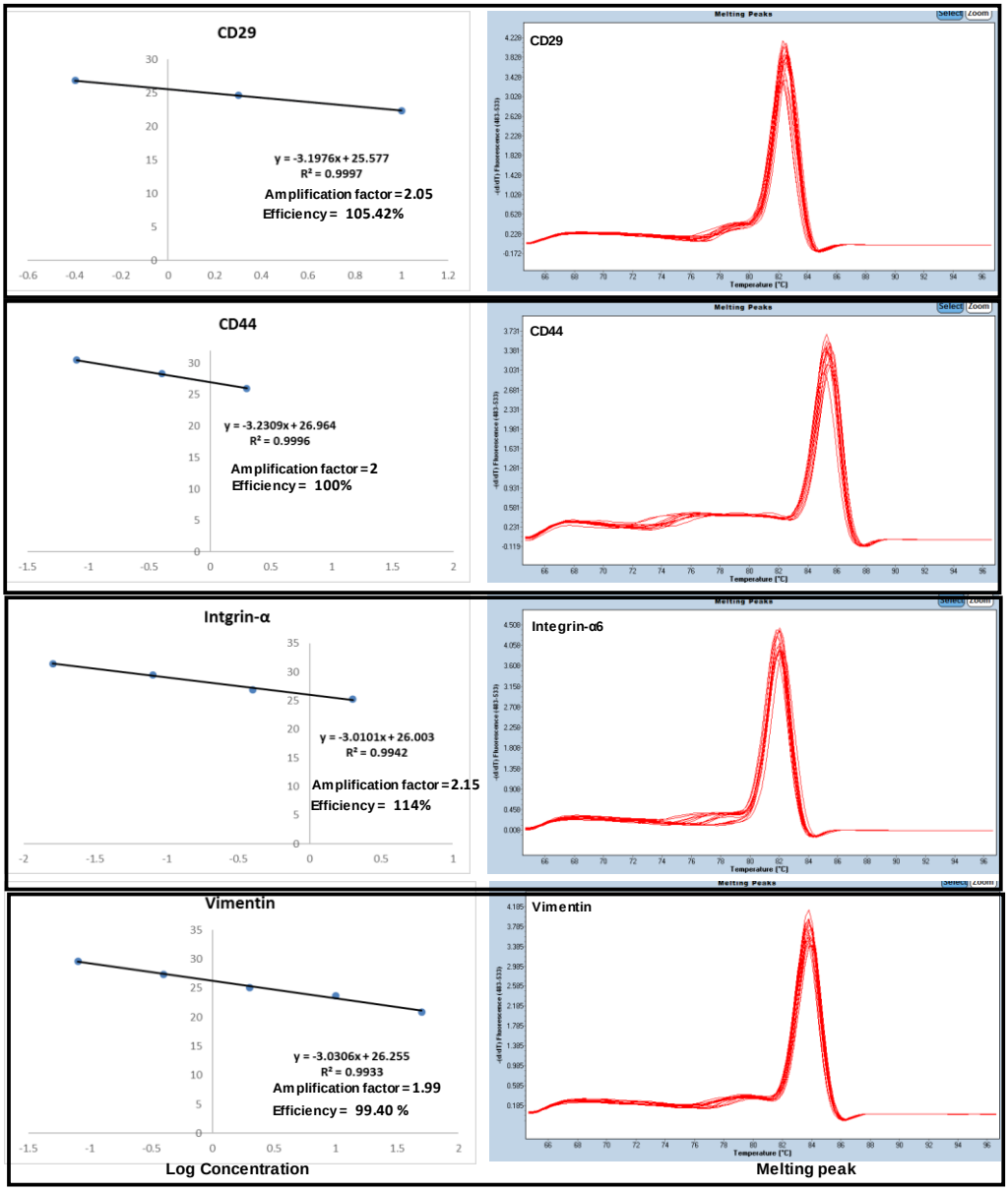


Figure 8-2: Standard cure calculation of equine keratinocytes genes copy number

Schematic diagram illustrates the calculation of standard curve; X-axis shows keratinocytes genes copy number that can be plotted using the mean of Ct values crossing points on Y-axis

8.5 Relation between hydrostatic pressure and oxygen concentration

This calculation has been performed by Dr. Cyril Rauch. The oxygen concentration profile over time can be estimated using a diffusion equation with specific boundary conditions. To do this consider the diffusion equation of the oxygen concentration, C, i.e. $\partial C/\partial t = D\partial^2 C/\partial x^2$, where the x-axis is the longitudinal axis of the tube (that is also the axis of symmetry) and D the diffusion coefficient of oxygen in water. Given the two different extremities of the tube, one includes two boundary conditions, the first boundary condition is related to the open part of the tube (see figure 1A-SM3) in contact with air. If one assumes that oxygen dissolution is done sufficiently rapidly to consider the thermodynamic balance, then the concentration of oxygen in the top layer of fluid, i.e. at $x = h$, of the culture medium is constant and shall be noted C_0. In contact with the cells, the amount of oxygen available that is consumed per unit of cell surface area and time is a function of the oxygen concentration near the cells, i.e. at $x = 0$. Assume a condition where oxygen saturation prevails, individual cells will consume: $j_0 = D[\partial C/\partial x]_{x=0}$. However, oxygen saturation may not necessarily prevail and a new term needs to be introduced. To this end one adds a Michaelis-Menten term (or absorption probability term) stating that the variation of oxygen concentration at the cell level varies as: $[\partial C/\partial x]_{x=0} = j_0/D[C/(C^* + C)]_{x=0}$. The later relation suggests that the flow of oxygen inside cells is also a function of the ability of cells to capture (i.e. adsorb) oxygen. As a result when oxygen is in excess, i.e. when $C >> C^*$, the oxygen disappears as $[\partial C/\partial x]_{x=0} \sim j_0/D$; whereas when it is at low concentration, i.e.

when $C \ll C^*$, oxygen clearance follows a first order kinetic $[\partial C/\partial x]_{x=0} \sim j_0/D[C/C^*]_{x=0}$. The Michaelis-Menten (or adsorption) term provides then the second boundary condition at $x=0$. Finally we also assume that initially the concentration of oxygen is constant across the tube and of value C_0. Posing $\tilde{C}=C/C_0$ (and $\tilde{C}^*=C^*/C_0$), $\tilde{t}=h^2/D$ and $\tilde{x}=x/h$, the diffusion equation and initial and the two boundary conditions become, respectively, $\partial\tilde{C}/\partial\tilde{t}=\partial^2\tilde{C}/\partial\tilde{x}^2$, $\tilde{C}(\tilde{x},\tilde{t}=0)=1$, $\tilde{C}(\tilde{x}=1,\tilde{t})=1$ and $\left[\partial\tilde{C}/\partial\tilde{x}\right]_{\tilde{x}=0}=\Omega\left[\tilde{C}/\left(\tilde{C}^*+\tilde{C}\right)\right]_{\tilde{x}=0}$ with $\Omega=j_0h/C_0D$. In order to resolve the diffusion equation we pose a new reduced variable that is $\eta=\tilde{x}/\sqrt{\tilde{t}}$. Inserting this new variable in the diffusion equation, using the chain rule method gives, $\eta\partial\tilde{C}/\partial\eta=-2\partial^2\tilde{C}/\partial\eta^2$, which can be integrated simply as: $\tilde{C}(\eta)=A\int_0^{\eta}\exp\left(-u^2/4\right)du+B$. The first boundary condition gives: $1=A\int_0^{1/\sqrt{\tilde{t}}}\exp\left(-u^2/4\right)du+B$; or equivalently: $\tilde{C}(\eta)=1+A\int_{1/\sqrt{\tilde{t}}}^{\eta}\exp\left(-u^2/4\right)du$. As a result the flow at $x=0$, i.e. $\left[\partial\tilde{C}/\partial\tilde{x}\right]_{\tilde{x}=0}$, can be determined using Leibniz formula namely $\left[\partial\tilde{C}/\partial\tilde{x}\right]_{\tilde{x}=0}=A/\sqrt{\tilde{t}}$. Finally, using the second boundary condition at $x=0$, the parameter 'A' can be determined as the result of a quadratic equation leading to:

$$\tilde{C}(\eta)=1+\frac{1}{2}\frac{\int_{1/\sqrt{\tilde{t}}}^{\eta}\exp\left(-u^2/4\right)du}{\int_{1/\sqrt{\tilde{t}}}^{0}\exp\left(-u^2/4\right)du}\left[-V+\sqrt{\left(V+2\Omega\sqrt{\tilde{t}}\int_{1/\sqrt{\tilde{t}}}^{0}\exp\left(-u^2/4\right)du\right)^2}\right]$$

$$V=1+\tilde{C}^*-\Omega\sqrt{\tilde{t}}\int_{1/\sqrt{\tilde{t}}}^{0}\exp\left(-u^2/4\right)du$$

Note that the later relation is the only physical solution we were looking for. Indeed, in the case where oxygen was diffusing much faster than any other kinetics involved, i.e. $\Omega \sim 0$, the oxygen concentration everywhere in the tube should be given by the initial concentration, namely $\tilde{C}(0)=1$. Similarly, the same solution can be deduced from the fact that $\tilde{C}(0)=1$ when $\tilde{t} \sim 0$. It is worth noting the presence of two characteristic times, i.e. $\tilde{t}_1 \sim 1$ (diffusion time) and $\tilde{t}_2 \sim 1/\Omega^2$ (oxygen consumption kinetic) providing insights into the temporal evolution of the system. To determine the impact of the hydrostatic pressure on those previous characteristic times one recalls that the hydrostatic pressure, P, is given by $P = \rho g h$ where ρ and g are, respectively, the density of the culture solution and the gravitational constant. Let us note, P_0 and h_0 the control pressure and the height of fluid in control conditions, it follows simply that for any new value of h, the corresponding hydrostatic pressure, P, is $P/P_0 = h/h_0$. As the characteristic times defined above are also function of h, their values are expected to be modulated by the pressure. In particular by noting $(\tilde{t}_1)_0$ the initial diffusion time for h_0 one finds naturally: $\tilde{t}_1 \sim (\tilde{t}_1)_0 (P/P_0)^2 \sim (P/P_0)^2$, as by definition $(\tilde{t}_1)_0 \sim 1$ (see above). Regarding the second characteristic time corresponding to the oxygen consumption kinetic, as both $\tilde{t}_2 \sim 1/h^2$ and $1/\Omega^2 \sim 1/h^2$ the hydrostatic pressure will not impact on this second kinetic. Naturally, we also assume that the mechanical pressure itself does not impact on the biology of oxygen consumption. It is now possible to compare the temporal

evolution of different systems under different hydrostatic pressures, and by posing $\tilde{P} = P / P_0$ one finds:

$$\tilde{C}(0) = 1 + \frac{1}{2}\left[-V + \sqrt{\left(V + 2\Omega\sqrt{\tilde{t}} \int_{\tilde{P}/\sqrt{\tilde{t}}}^{0} \exp\left(-u^2/4\right) du \right)^2} \right]$$

$$V = 1 + \tilde{C}^* - \Omega\sqrt{\tilde{t}} \int_{\tilde{P}/\sqrt{\tilde{t}}}^{0} \exp\left(-u^2/4\right) du$$

The previous relation relies on two parameters, Ω and $\tilde{C}^*$, that need to be estimated. To allow us to surmise the aqueous solubility of oxygen under atmospheric pressure we must first use Henry's law which states that at a set temperature, the amount of a given gas dissolved in a homogenous aqueous solution is proportional to the partial pressure of the gas in equilibrium with the liquid (Sander, 2015). This can be summarised using Henry's coefficient which is described mathematically as $H = C/P$ where, H, C and P are the Henry's coefficient, the oxygen concentration in aqueous medium and the partial atmospheric pressure of oxygen, respectively. The coefficient is a constant at a given temperature, which equates to $1.3 \cdot 10^{-5} mol/J$ at 20^{o}C (Sander, 2015). However, the temperature in culture condition is 37 ^{o}C, which using van t Hoff's equation changes the coefficient (Sander, 2015). As a result, at 37 ^{o}C the coefficient is $1.6 \cdot 10^{-5} mol/J$. Using Dalton's law which states that the total partial pressure of gases is equal to the sum of the individual partial pressure exerted by each gas, the partial pressure of oxygen being 21%, the concentration of oxygen in the culture medium can be estimated as $C_0 \sim 3.3 \cdot 10^{-7} mol/cm^3$. Oxygen consumptions vary across cells (Wagner et al., 2011) however experiments performed based on combined hemodynamic and two-photon excited

fluorescence data, the oxygen consumption rate in the stratum basale in human is estimated to be $\sim 0.035 \cdot 10^{-12} mol/cell/h$ (Balu et al., 2013). Assuming a similar value in equids, with a cell surface area $\sim 100 \mu m^2$ one finds $j_0 \sim 7.7 \cdot 10^{-14} mol \cdot cm^{-2} \cdot s^{-1}$. Consider now the diffusion rate of oxygen in aqueous medium $D \sim 2.6 \cdot 10^{-5} cm^2 \cdot s^{-1}$ (Han and Bartels, 1996) one obtains $\Omega = j_0 h / C_0 D \sim 9 \cdot 10^{-3} h / h_0$ where $h_0 \sim 1cm$. As a result, $\tilde{t}_2 >> \tilde{t}_1$ that is to say that only oxygen diffusion is the limiting physical phenomenon in the process of oxygen exchange between cells and the culture medium and that cells will be in contact with a reservoir of oxygen, namely that their consumption will not impact on the oxygen concentration in solution. Regarding $\tilde{C}^*$, a cell culture with a 21% partial pressure of oxygen is way beyond high oxygen condition. In this context, it is expected that $\tilde{C}^* = C^* / C_0 << 1$ namely that cells in tissue do not rely on an excessively large oxygen concentration to function optimally and be in saturating condition. A plot of oxygen consumption as a function of time is given in Figure 8.2 demonstrating that whatever the pressure applied, the cells will always be in saturating conditions regarding oxygen.

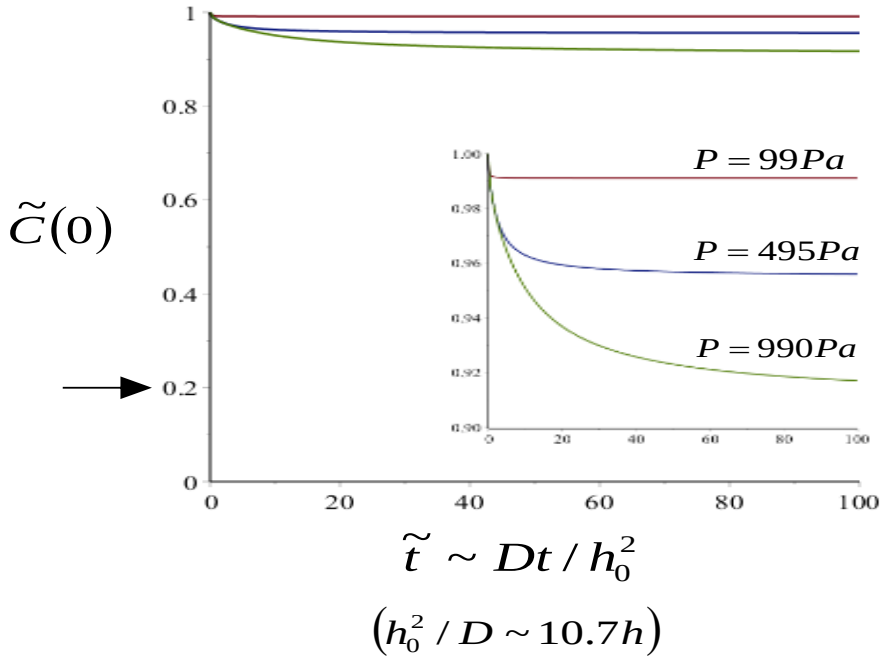


Figure 8-3: Schematic diagram showing the calculation of oxygen concentration

8.6 Specificity of antibody

NCBI Blast: Protein Sequence

β-actin

NCBI Blast:Protein Sequence (375 letters)

Descriptions

Sequences producing significant alignments:

Description	Max score	Total score	Query cover	E value	Ident	Accession
actin, cytoplasmic 1 [Equus caballus]	785	785	100%	0.0	100%	NP_001075307.1

Alignments

actin, cytoplasmic 1 [Equus caballus]
Sequence ID: **NP_001075307.1** Length: 375 Number of Matches: 1
Range 1: 1 to 375

Score	Expect	Method	Identities	Positives	Gaps	Frame
785 bits(2028)	0.0()	Compositional matrix adjust.	375/375(100%)	375/375(100%)	0/375(0%)	

Features:

```
Query  1    MDDDIAALVVDNGSGMCKAGFAGDDAPRAVFPSIVGRPRHQGVMVGMGQKDSYVGDEAQS  60
            MDDDIAALVVDNGSGMCKAGFAGDDAPRAVFPSIVGRPRHQGVMVGMGQKDSYVGDEAQS
Sbjct  1    MDDDIAALVVDNGSGMCKAGFAGDDAPRAVFPSIVGRPRHQGVMVGMGQKDSYVGDEAQS  60

Query  61   KRGILTLKYPIEHGIVTNWDDMEKIWHHTFYNELRVAPEEHPVLLTEAPLNPKANREKMT  120
            KRGILTLKYPIEHGIVTNWDDMEKIWHHTFYNELRVAPEEHPVLLTEAPLNPKANREKMT
Sbjct  61   KRGILTLKYPIEHGIVTNWDDMEKIWHHTFYNELRVAPEEHPVLLTEAPLNPKANREKMT  120

Query  121  QIMFETFNTPAMYVAIQAVLSLYASGRTTGIVMDSGDGVTHTVPIYEGYALPHAILRLDL  180
            QIMFETFNTPAMYVAIQAVLSLYASGRTTGIVMDSGDGVTHTVPIYEGYALPHAILRLDL
Sbjct  121  QIMFETFNTPAMYVAIQAVLSLYASGRTTGIVMDSGDGVTHTVPIYEGYALPHAILRLDL  180

Query  181  AGRDLTDYLMKILTERGYSFTTTAEREIVRDIKEKLCYVALDFEQEMATAASSSSLEKSY  240
            AGRDLTDYLMKILTERGYSFTTTAEREIVRDIKEKLCYVALDFEQEMATAASSSSLEKSY
Sbjct  181  AGRDLTDYLMKILTERGYSFTTTAEREIVRDIKEKLCYVALDFEQEMATAASSSSLEKSY  240

Query  241  ELPDGQVITIGNERFRCPEALFQPSFLGMESCGIHETTFNSIMKCDVDIRKDLYANTVLS  300
            ELPDGQVITIGNERFRCPEALFQPSFLGMESCGIHETTFNSIMKCDVDIRKDLYANTVLS
Sbjct  241  ELPDGQVITIGNERFRCPEALFQPSFLGMESCGIHETTFNSIMKCDVDIRKDLYANTVLS  300

Query  301  GGTTMYPGIADRMQKEITALAPSTMKIKIIAPPERKYSVWIGGSILASLSTFQQMWISKQ  360
            GGTTMYPGIADRMQKEITALAPSTMKIKIIAPPERKYSVWIGGSILASLSTFQQMWISKQ
Sbjct  301  GGTTMYPGIADRMQKEITALAPSTMKIKIIAPPERKYSVWIGGSILASLSTFQQMWISKQ  360

Query  361  EYDESGPSIVHRKCF  375
            EYDESGPSIVHRKCF
Sbjct  361  EYDESGPSIVHRKCF  375
```

CD44

NCBI Blast:Protein Sequence (51 letters)

Descriptions

Sequences producing significant alignments:

Description	Max score	Total score	Query cover	E value	Ident	Accession
PREDICTED: CD44 antigen isoform X9 [Equus caballus]	97.8	97.8	100%	4e-26	92%	gi|545180840|XP_005598080.1

Alignments

PREDICTED: CD44 antigen isoform X9 [Equus caballus]

Sequence ID: **gi|545180840|XP_005598080.1** Length: 428 Number of Matches: 1

Range 1: 378 to 428

Score	Expect	Method	Identities	Positives	Gaps	Frame
97.8 bits(242)	4e-26()	Compositional matrix adjust.	47/51(92%)	49/51(96%)	0/51(0%)	

Features:

```
Query  1    EDRKPSGLNGEASKSQEMVHLVNKESSETPDQFMTADETRNLQNVDMKIGV  51
            +DRK SGLNGEAS+SQEMVHLVNKESSET DQFMTADETRNLQNVDMKIGV
Sbjct  378  DDRKASGLNGEASRSQEMVHLVNKESSETQDQFMTADETRNLQNVDMKIGV  428
```

HIF-1α

NCBI Blast:Protein Sequence (200 letters)

Descriptions

Sequences producing significant alignments:

Description	Max score	Total score	Query cover	E value	Ident	Accession
PREDICTED: hypoxia-inducible factor 1-alpha [Equus caballus]	389	389	100%	2e-130	95%	gi|953886374|XP_014591308.1

Alignments

PREDICTED: hypoxia-inducible factor 1-alpha [Equus caballus]

Sequence ID: **gi|953886374|XP_014591308.1** Length: 974 Number of Matches: 1

Range 1: 452 to 651

Score	Expect	Method	Identities	Positives	Gaps	Frame
389 bits(1000)	2e-130()	Compositional matrix adjust.	190/200(95%)	195/200(97%)	0/200(0%)	

Features:

```
Query  1    TTGQVRMLAKRGGVVWVETQATVIYNTKNSQPQCIVCVNYVVSGIIQHDLIFSLQQTECV  60
            TTGQVRMLAKRGGVVWVETQATVIYNTKNSQPQCIVCVNYVVSGIIQHDLIFSLQQTECV
Sbjct  452  TTGQVRMLAKRGGVVWVETQATVIYNTKNSQPQCIVCVNYVVSGIIQHDLIFSLQQTECV  511

Query  61   LKPVESSDMKMTQLFTKVESEDTSSLFDKLKKEPDALTLLAPAAGDTIISLDFGSNDTET  120
            LKPVESSDMK++QLFTKVESEDTSSLFDKLKKEPDALTLLAPAAGDTIISLDFGSNDT+T
Sbjct  512  LKPVESSDMKISQLFTKVESEDTSSLFDKLKKEPDALTLLAPAAGDTIISLDFGSNDTDT  571

Query  121  DDQQLEEVPLYNDVMLPSPNEKLQNINLAMSPLPTAETPKPLRSSADPALNQEVALKLEP  180
            DDQQLEEVPLYNDVMLP  NEK+QNINLAMSPLP +ETPKPLRSSADPALNQEVALKLEP
Sbjct  572  DDQQLEEVPLYNDVMLPLSNEKIQNINLAMSPLPASETPKPLRSSADPALNQEVALKLEP  631

Query  181  NPESLELSFTMPQIQDQTPS  200
            NPESLELSFTMPQIQDQ  S
Sbjct  632  NPESLELSFTMPQIQDQPAS  651
```

K10

NCBI Blast:NP_000412.3 keratin, type I cytoskeletal 10...

Descriptions

Sequences producing significant alignments:

Description	Max score	Total score	Query cover	E value	Ident	Accession
PREDICTED: keratin, type I cytoskeletal 10 isoform X1 [Equus caballus]	611	611	52%	0.0	92%	XP_005597479.1
keratin 10 [Equus caballus]	608	608	52%	0.0	92%	NP_001333005.1

Alignments

keratin 10 [Equus caballus]

Sequence ID: **NP_001333005.1** Length: 559 Number of Matches: 1

Range 1: 135 to 443

Score	Expect	Method	Identities	Positives	Gaps	Frame
608 bits(1569)	0.0()	Compositional matrix adjust.	285/309(92%)	302/309(97%)	0/309(0%)	

Features:

```
Query  145  NEKVTMQNLNDRLASYLDKVRALEESNYELEGKIKEWYEKHGNSHQGEPRDYSKYYKTID  204
            NEKVTMQNLNDRLASYLDKVRALEESNYELEGKIKEWYEKHGN+ Q EPRDYSKYY+ I+
Sbjct  135  NEKVTMQNLNDRLASYLDKVRALEESNYELEGKIKEWYEKHGNAGQREPRDYSKYYQIIE  194

Query  205  DLKNQILNLTTDNANILLQIDNARLAADDFRLKYENEVALRQSVEADINGLRRVLDELTL  264
            DLKNQI+NLT DNAN++LQIDNARLAADDFRLKYENE+ALRQSVEADINGLRRVLDELTL
Sbjct  195  DLKNQIINLTNDNANVVLQIDNARLAADDFRLKYENELALRQSVEADINGLRRVLDELTL  254

Query  265  TKADLEMQIESLTEELAYLKKNHEEEMKDLRNVSTGDVNVEMNAAPGVDLTQLLNNMRSQ  324
            TKADLEMQIESLTEELAYLKKNHEEEM+DL+NVSTGDVNVEMNAAPGVDLT+LLNNMR+Q
Sbjct  255  TKADLEMQIESLTEELAYLKKNHEEEMRDLQNVSTGDVNVEMNAAPGVDLTELLNNMRNQ  314

Query  325  YEQLAEQNRKDAEAWFNEKSKELTTEIDNNIEQISSYKSEITELRRNVQALEIELQSQLA  384
            YEQLAEQNRKDAEAWFNEKS+ELTTEI++NIEQ+SS+KSEITELRR VQ LEIELQSQLA
Sbjct  315  YEQLAEQNRKDAEAWFNEKSQELTTEINSNIEQMSSHKSEITELRRTVQGLEIELQSQLA  374

Query  385  LKQSLEASLAETEGRYCVQLSQIQAQISALEEQLQQIRAETECQNTEYQQLLDIKIRLEN  444
            LKQSLEASLAETEGRYCVQLSQIQAQIS+LEEQLQQIRAETECQN EYQQLLDIKIRLEN
Sbjct  375  LKQSLEASLAETEGRYCVQLSQIQAQISSLEEQLQQIRAETECQNAEYQQLLDIKIRLEN  434

Query  445  EIQTYRSLL  453
            EIQTYRSLL
Sbjct  435  EIQTYRSLL  443
```

K14

NCBI Blast:NP_001300886.1 keratin, type I cytoskeletal...

Descriptions

Sequences producing significant alignments:

Description	Max score	Total score	Query cover	E value	Ident	Accession
keratin, type I cytoskeletal 14 [Equus caballus]	474	474	100%	4e-168	93%	NP_001333127.1

Alignments

keratin, type I cytoskeletal 14 [Equus caballus]

Sequence ID: **NP_001333127.1** Length: 478 Number of Matches: 1

Range 1: 218 to 478

Score	Expect	Method	Identities	Positives	Gaps	Frame
474 bits(1219)	4e-168()	Compositional matrix adjust.	247/267(93%)	256/267(95%)	6/267(2%)	

Features:

```
Query  1    MSVEADINGLRRVLDELTLARADLEMQIESLKEELAYLKKNHEEEMASMRGQVGGDVNVE  60
            +SVEADINGLRRVLDELTLAR DLEMQIESLKEELAYL+KNHEEEM S+RGQV GDVNVE
Sbjct  218  LSVEADINGLRRVLDELTLARTDLEMQIESLKEELAYLRKNHEEEMNSLRGQVSGDVNVE  277

Query  61   MDAAPGVDLSRILNEMRDQYEKMAEKNRKDAEEWFFSKTEELNREVATNSELVQSGKSEI  120
            MDAAPGVDLSRILNEMRDQYEKMAEKNRKDAE+WFFSKTEELNREVATNSELVQSGKSEI
Sbjct  278  MDAAPGVDLSRILNEMRDQYEKMAEKNRKDAEDWFFSKTEELNREVATNSELVQSGKSEI  337

Query  121  SELRRTMQNLEIELQSQLSMKASLENNLEETKGRYCMQLAQIQEMIGSVEEQLAQLRCEM  180
            SELRRT+QNLEIELQSQLSMKASLEN+LEETKGRYCMQLAQIQE+I SVEEQLAQLRCEM
Sbjct  338  SELRRTVQNLEIELQSQLSMKASLENSLEETKGRYCMQLAQIQELISSVEEQLAQLRCEM  397

Query  181  EQQNQEYKILLDVKTRLEQEIATYRRLLEGEDAHLSSSQFSSSSQFSSGSQSSRDVTSTN  240
            EQQNQEYKILLDVKTRLEQEIATYRRLLEGEDAHLS+QFSS        SQSSRDVTST+
Sbjct  398  EQQNQEYKILLDVKTRLEQEIATYRRLLEGEDAHLSTQFSSG------SQSSRDVTSTS  451

Query  241  RQIRTKVMDVHDGKVVSTHEQVLRTKN  267
            RQIRTKVMDVHDGKVVSTHEQVLRTKN
Sbjct  452  RQIRTKVMDVHDGKVVSTHEQVLRTKN  478
```

PCNA

NCBI Blast:Protein Sequence (261 letters)

Descriptions

Sequences producing significant alignments:

Description	Max score	Total score	Query cover	E value	Ident	Accession
PREDICTED: proliferating cell nuclear antigen [Equus caballus]	528	528	100%	0.0	98%	XP_001494771.1

Alignments

PREDICTED: proliferating cell nuclear antigen [Equus caballus]
Sequence ID: **XP_001494771.1** Length: 261 Number of Matches: 1
Range 1: 1 to 261

Score	Expect	Method	Identities	Positives	Gaps	Frame
528 bits(1359)	0.0()	Compositional matrix adjust.	257/261(98%)	258/261(98%)	0/261(0%)	

Features:

```
Query  1    MFEARLVQGSILKKVLEALKDLINEACWDISSSGVNLQSMDSSHVSLVQLTLRSEGFDTY  60
            MFEARLVQGSILKKVLEALKDLINEACWDISSSGVNLQSMDSSHVSLVQLTLRSEGFDTY
Sbjct  1    MFEARLVQGSILKKVLEALKDLINEACWDISSSGVNLQSMDSSHVSLVQLTLRSEGFDTY  60

Query  61   RCDRNLAMGVNLTSMSKILKCAGNEDIITLRAEDNADTLALVFEAPNQEKVSDYEMKLMD  120
            RCDRNLAMGVNLTSMSKILKCAGNEDIITLRAEDNADTLALVFEAPNQEKVSDYEMKLMD
Sbjct  61   RCDRNLAMGVNLTSMSKILKCAGNEDIITLRAEDNADTLALVFEAPNQEKVSDYEMKLMD  120

Query  121  LDVEQLGIPEQEYSCVVKMPSGEFACICRDLSHIGDAVVISCAKDGVKFSASGELGNGNI  180
            LDVEQLGIPEQEYSCVVKMPSGEFA ICRDLSHIGDAVVISCAKDGVKFSASGELGNGNI
Sbjct  121  LDVEQLGIPEQEYSCVVKMPSGEFARICRDLSHIGDAVVISCAKDGVKFSASGELGNGNI  180

Query  181  KLSQTSNVDKEEEAVTIEMNEPVQLTFALRYLNFFTKATPLSSTVTLSMSADVPLVVEYK  240
            KLSQTSNVDKEEEAVTIEMNEPVQLTFALRYLNFFTKATPLS TVTLSMSADVPLVVEYK
Sbjct  181  KLSQTSNVDKEEEAVTIEMNEPVQLTFALRYLNFFTKATPLSPTVTLSMSADVPLVVEYK  240

Query  241  IADMGHLKYYLAPKIEDEEGS  261
            IADMGHLKYYLAPKIEDE+ S
Sbjct  241  IADMGHLKYYLAPKIEDEDAS  261
```

p63

NCBI Blast:NP_001316074.1 tumor protein 63 isoform 8...

Descriptions

Sequences producing significant alignments:

Description	Max score	Total score	Query cover	E value	Ident	Accession
PREDICTED: tumor protein 63 isoform X4 [Equus caballus]	842	842	98%	0.0	99%	XP_003363405.1

Alignments

PREDICTED: tumor protein 63 isoform X4 [Equus caballus]
Sequence ID: **XP_003363405.1** Length: 586 Number of Matches: 1
Range 1: 1 to 408

Score	Expect	Method	Identities	Positives	Gaps	Frame
842 bits(2174)	0.0()	Compositional matrix adjust.	408/408(99%)	407/408(99%)	0/408(0%)	

Features:

```
Query  1    MLYLENNAQTQFSEPQYTNLGLLNSMDQQIQNGSSSTSPYNTDHAQNSVTAPSPYAQPSS  60
            MLYLENNAQTQFSEPQYTNLGLLNSMDQQIQNGSSSTSPYNTDHAQNSVTAPSPYAQPSS
Sbjct  1    MLYLENNAQTQFSEPQYTNLGLLNSMDQQIQNGSSSTSPYNTDHAQNSVTAPSPYAQPSS  60

Query  61   TFDALSPSPAIPSNTDYPGPHSFDVSFQQSSTAKSATWTYSTELKKLYCQIAKTCPIQIK  120
            TFDALSPSPAIPSNTDYPGPHSFDVSFQQSSTAKSATWTYSTELKKLYCQIAKTCPIQIK
Sbjct  61   TFDALSPSPAIPSNTDYPGPHSFDVSFQQSSTAKSATWTYSTELKKLYCQIAKTCPIQIK  120

Query  121  VMTPPPQGAVIRAMPVYKKAEHVTEVVKRCPNHELSREFNEGQIAPPSHLIRVEGNSHAQ  180
            VMTPPPQGAVIRAMPVYKKAEHVTEVVKRCPNHELSREFNEGQIAPPSHLIRVEGNSHAQ
Sbjct  121  VMTPPPQGAVIRAMPVYKKAEHVTEVVKRCPNHELSREFNEGQIAPPSHLIRVEGNSHAQ  180

Query  181  YVEDPITGRQSVLVPYEPPQVGTEFTTVLYNFMCNSSCVGGMNRRPILIIVTLETRDGQV  240
            YVEDPITGRQSVLVPYEPPQVGTEFTTVLYNFMCNSSCVGGMNRRPILIIVTLETRDGQV
Sbjct  181  YVEDPITGRQSVLVPYEPPQVGTEFTTVLYNFMCNSSCVGGMNRRPILIIVTLETRDGQV  240

Query  241  LGRRCFEARICACPGRDRKADEDSIRKQQVSDSTKNGDGTKRPFRQNTHGIQMTSIKKRR  300
            LGRRCFEARICACPGRDRKADEDSIRKQQVSDSTKNGDGTKRPFRQNTHGIQMTSIKKRR
Sbjct  241  LGRRCFEARICACPGRDRKADEDSIRKQQVSDSTKNGDGTKRPFRQNTHGIQMTSIKKRR  300

Query  301  SPDDELLYLPVRGRETYEMLLKIKESLELMQYLPQHTIETYRQQQQQQHQHLLQKQTSIQ  360
            SPDDELLYLPVRGRETYEMLLKIKESLELMQYLPQHTIETYRQQQQQQHQHLLQKQTS+Q
Sbjct  301  SPDDELLYLPVRGRETYEMLLKIKESLELMQYLPQHTIETYRQQQQQQHQHLLQKQTSMQ  360

Query  361  SPSSYGNSSPPLNKMNSMNKLPSVSQLINPQQRNALTPTTIPDGMGAN  408
            S SSYGNSSPPLNKMNSMNKLPSVSQLINPQQRNALTPTTIPDGMGAN
Sbjct  361  SQSSYGNSSPPLNKMNSMNKLPSVSQLINPQQRNALTPTTIPDGMGAN  408
```

Ki-67

NCBI Blast:Protein Sequence (2896 letters)

Descriptions

Sequences producing significant alignments:

Description	Max score	Total score	Query cover	E value	Ident	Accession
PREDICTED: antigen KI-67 isoform X1 [Equus caballus]	1387	3362	100%	0.0	52%	XP_005602210.1
PREDICTED: antigen KI-67 isoform X2 [Equus caballus]	1131	3224	100%	0.0	53%	XP_014588817.1

Alignments

PREDICTED: antigen KI-67 isoform X1 [Equus caballus]
Sequence ID: **XP_005602210.1** Length: 2418 Number of Matches: 4

See 1 more title(s)
Range 1: 487 to 2110

Score	Expect	Method	Identities	Positives	Gaps	Frame
1387 bits(3589)	0.0()	Compositional matrix adjust.	848/1633(52%)	1076/1633(65%)	24/1633(1%)	

Features:

```
Query  124   VSRSSFSSDPDESDGIPLKRRVSFGGHLRPELFDENLPPNTPLKRGEAPTKRKSLVMHT  183
             V    F     ++ +G+ LKRRVSFGGHLRPELFDENLPPNTPLKRGE P KR+SL  HT
Sbjct  487   VDVGKFGDSINKVEGMSLKRRVSFGGHLRPELFDENLPPNTPLKRGETPMKRRSLATHT  546

Query  184   PPVLKKIIKEQPQPSGKQESGSEIHVEVKAQSLVISPPAPSPRKT-PVASDQRRRSCKTA  242
             P VLKKIIKEQ QPS K++S S+IH+EV  Q++V S PA +P KT PVA+DQRR S K +
Sbjct  547   PTVLKKIIKEQSQPSRKEDSPSKIHLEVTTQNVVKSSPAQNPTKTSPVANDQRRTSSKAS  606

Query  243   PASSSKS---QTEVPKRGGRKSGNLPSKRVSISRSQHDILQMICSKRRSGASEANLIVAK  299
               SS      QT+ PKRGGR+S +LPSKR+S  RSQH+ILQMI SKRRSGASEANLIVAK
Sbjct  607   SVSSGSKSPCQTDTPKRGGRRSSSLPSKRMSTDRSQHEILQMISYKRRSGASEANLIVAK  666

Query  300   SWADVVKLGAKQTQTKVIKHGPQRSMNKRQRRPATPKKPVGEVHSQFSTGHANSPCTIII  359
             SWADVVKLGAKQTQTKV+K GPQR +NKRQ+R  TPKKP G VH+QFSTGHANSPCTI+I
Sbjct  667   SWADVVKLGAKQTQTKVVKRGPQRQLNKRQKRINTPKKPTGSVHNQFSTGHANSPCTIVI  726

Query  360   GKAHTEKVHVPARPVRVLNNFISNQKMDFKEDLSGIAEMFKTPVKEQPQLTSTCHIAISN  419
             GKAH EKV+VPARPVR+LNNF+ N+KMDF EDLSG+ EMFKTP KE+PQ  S C I  SN
Sbjct  727   GKAHIEKVNVPARPVRMLNNFVFNKKMDFNEDLSGLTEMFKTPAKERPQRRSVCPITFSN  786

Query  420   SENLLGKQFQGTDSGEEPLLPTSESFGGNVFFSAQNAAKQPSDKCSASPP-LRRQCIREN  478
             SE+LLGK+FQ  +S E PLL  SE+FG ++F S QNA K+ SDK SASP   ++Q ++ N
Sbjct  787   SEDLLGKKFQVPNSEENPLLCASENFGESMFPSTQNAPKELSDKISASPASSKQQNMKVN  846

Query  479   GNVAKTPRNTYKMTSLETKTSDTETEPSKTVSTANRSGRSTEFRNIQKLPVESKSEETNT  538
              ++ KTPRN +KMT  E KT  +E EP + V++AN S RS   RN      E K++E  T
Sbjct  847   EDMEKTPRNMHKMTGAEMKTPVSEAEPMQAVASANTSRRSVGLRNRLTPGTEGKNQEMET  906

Query  539   EIVECILKRGQKATLLQ-QRREGEMKEIERPFETYKENIELKENDEKMKAMKRSRTWGQ-  596
                 IL R  + T LQ Q+ EGEM+E ER FE  K+ IE KEN EKM A++RSR   +
Sbjct  907   GTTGNILGRRLRKTPLQEQKLEGEMQESERSFELCKKIIESKENSEKMVAVRRSRRSSEL  966
```

Akt

NCBI Blast:P31750.2 RecName: Full=RAC-alpha serine/threonine-protein...

Descriptions

Sequences producing significant alignments:

Description	Max score	Total score	Query cover	E value	Ident	Accession
PREDICTED: RAC-alpha serine/threonine-protein kinase [Equus caballus]	980	980	100%	0.0	98%	XP_001492763.1

Alignments

PREDICTED: RAC-alpha serine/threonine-protein kinase [Equus caballus]
Sequence ID: **XP_001492763.1** Length: 479 Number of Matches: 1
Range 1: 1 to 479

Score	Expect	Method	Identities	Positives	Gaps	Frame
980 bits(2533)	0.0()	Compositional matrix adjust.	470/480(98%)	474/480(98%)	1/480(0%)	

/blast.ncbi.nlm.nih.gov/Blast.cgi

```
Query  1    MNDVAIVKEGWLHKRGEYIKTWRPRYFLLKNDGTFIGYKERPQDVDQRESPLNNFSVAQC  60
            MNDVAIVKEGWLHKRGEYIKTWRPRYFLLKNDGTFIGYKERPQDV+QRESPLNNFSVAQC
Sbjct  1    MNDVAIVKEGWLHKRGEYIKTWRPRYFLLKNDGTFIGYKERPQDVEQRESPLNNFSVAQC  60

Query  61   QLMKTERPRPNTFIIRCLQWTTVIERTFHVETPEEREEWATAIQTVADGLKRQEEETMDF  120
            QLMKTERPRPNTFIIRCLQWTTVIERTFHVETPEEREEW TAIQTVADGLKRQEEE MDF
Sbjct  61   QLMKTERPRPNTFIIRCLQWTTVIERTFHVETPEEREEWTTAIQTVADGLKRQEEE-MDF  119

Query  121  RSGSPSDNSGAEEMEVSLAKPKHRVTMNEFEYLKLLGKGTFGKVILVKEKATGRYYAMKI  180
            RSGSPSDNSGAEEMEVSLAKPKHRVTMNEFEYLKLLGKGTFGKVILVKEKATGRYYAMKI
Sbjct  120  RSGSPSDNSGAEEMEVSLAKPKHRVTMNEFEYLKLLGKGTFGKVILVKEKATGRYYAMKI  179

Query  181  LKKEVIVAKDEVAHTLTENRVLQNSRHPFLTALKYSFQTHDRLCFVMEYANGGELFFHLS  240
            LKKEVIVAKDEVAHTLTENRVLQNSRHPFLTALKYSFQTHDRLCFVMEYANGGELFFHLS
Sbjct  180  LKKEVIVAKDEVAHTLTENRVLQNSRHPFLTALKYSFQTHDRLCFVMEYANGGELFFHLS  239

Query  241  RERVFSEDRARFYGAEIVSALDYLHSEKNVVYRDLKLENLMLDKDGHIKITDFGLCKEGI  300
            RERVF EDRARFYGAEIVSALDYLHSEKNVVYRDLKLENLMLDKDGHIKITDFGLCKEGI
Sbjct  240  RERVFPEDRARFYGAEIVSALDYLHSEKNVVYRDLKLENLMLDKDGHIKITDFGLCKEGI  299

Query  301  KDGATMKTFCGTPEYLAPEVLEDNDYGRAVDWWGLGVVMYEMMCGRLPFYNQDHEKLFEL  360
            KDGATMKTFCGTPEYLAPEVLEDNDYGRAVDWWGLGVVMYEM+CGRLPFYNQDHEKLFEL
Sbjct  300  KDGATMKTFCGTPEYLAPEVLEDNDYGRAVDWWGLGVVMYEMVCGRLPFYNQDHEKLFEL  359

Query  361  ILMEEIRFPRTLGPEAKSLLSGLLKKDPTQRLGGGSEDAKEIMQHRFFANIVWQDVYEKK  420
            ILMEEIRFPRTL PEAKSLLSGLLKKDP QRLGGGSEDAKEIMQHRFFA+IVWQDVYEKK
Sbjct  360  ILMEEIRFPRTLSPEAKSLLSGLLKKDPKQRLGGGSEDAKEIMQHRFFASIVWQDVYEKK  419

Query  421  LSPPFKPQVTSETDTRYFDEEFTAQMITITPPDQDDSMECVDSERRPHFPQFSYSASGTA  480
            LSPPFKPQVTSETDTRYFDEEFTAQMITITPPDQDD+ME VDSERRPHFPQFSYSASGTA
Sbjct  420  LSPPFKPQVTSETDTRYFDEEFTAQMITITPPDQDDTMEGVDSERRPHFPQFSYSASGTA  479
```